The scope and limitations of novel NMR techniques to characterise and quantify biologically active compounds in the *Stratum corneum*

THESIS

Submitted for the degree of

DOCTOR OF PHILOSOPHY

in

Chemistry

at

Kingston University London

In collaboration with

GSK

by

Cameron Robertson

School of Life Sciences, Pharmacy and Chemistry,

Kingston University, Penrhyn Road,

Kingston-upon-Thames, Surrey, KT1 2EE

DECLARATION

This thesis entitled “The scope and limitation of novel NMR techniques to characterise and quantify biologically active compounds in the Stratum corneum” is based upon work conducted by the author in the School of Life Sciences, Pharmacy and Chemistry at Kingston University London between October 2016 and December 2019. All of the work described herein is original unless otherwise acknowledged in the text or by references. None of the work has been submitted for another degree in this or any other universities.

_____

Cameron Robertson

Acknowledgements

The most important person during the duration of my PhD has been my supervisor and mentor Dr. Adam Le Gresley, who from the moment we met made me feel a part of the team. I am so thankful for his continued confidence in me and my work. His confidence in my ability and his willingness to open platforms for me to display my work makes me so grateful for our supervisor-student relationship. I only hope that our continued work together will bring great discoveries and opportunities for both of us in the future. I know that his energy and faultless commitment will continue to be rewarded. My second supervisor, Dr Neil Williams, provided me with a natural networking platform with academics at the University. I truly appreciated this small gesture which allowed me to build relationships with senior academics at the University. This platform allowed me to understand the work/life balance to a greater degree. Invitations to additional events highlighted to me that it is not always about sharing ideas in meetings and the lab but that some solutions to scientific problems need to be found outside of the office.

I must also acknowledge my GSK supervisor Dr. Robert Lucas who, alongside Dr Nidhin Raj, provided priceless theoretical and technical insights on consumer health in the skin. Alongside this, the promotion of publication and time spared for feedback on work while balancing their own work will not be forgotten. I also could not have finished my PhD without the NMR support of Dr Jean-Marie Peron and Dr Mahboub Merzouk who dutifully answered questions on the subject and gave guidance on how to set up new experiments and implement novel pulse sequences that had not been run at Kingston University previously.

A special person who I need to acknowledge is my fiancé Tomris Coban. Tomris has become a pillar of my life and provided me with greater motivation, confidence and most importantly the ability to not take myself so seriously. Especially in lock down during this unprecedented year her companionship made a possibly very lonely and arduous period of my life one of joy and enlightenment. I also need to acknowledge my family for supporting me emotionally and financially during my time in Academia. I am truly grateful for their constant love and support, while trusting that I will come out a more complete and rounded person.

Finally I would like to thank Kingston University for the supply and servicing of all NMR equipment and continued support for external training opportunities to expand and build my technical knowledge with Bruker and the University of Manchester NMR methodology group.

Abstract

The accurate determination of biologically active compounds in the skin is of considerable importance when evaluating the penetration of skin health products through different layers of the skin. This thesis reports on the characterisation and quantitation of biologically active compounds in simple model mixtures and complex mixtures which mimic that of a typical skin product, through the use of qNMR, pure shift NMR and DOSY techniques complemented by semi-automated software packages. Characterisation and quantitation conditions were acquired over several heterogeneous samples allowing for analysis of how dynamic range and complexity of different sample mixtures affect the Limits of Detection (LOD) and Limits of Quantitation (LOQ) of biologically active compounds. NMR is of particular value in this task, as it is non-destructive, uses a primary ratio method for quantification, and tolerates a wide variety of hydrophilic and hydrophobic components within a given matrix. In this investigation we have attained a trueness level <10%, repeatability values of <1% and brought the limit of quantitation down to 100nM (˜limit of baseline range of several key biomarkers in the skin per litre seen in vivo), while commenting on the limitations observed, such as peak overlap and sensitivity limits. Pure shift optimised sequences allow us to reduce peak overlapping, allowing further characterisation of individual compounds and the separation of complex mixtures using NMR. These validated methodologies are then all brought together to develop a new methodology for ex-vivo analysis of skin layers. This analysis allowed for characterisation and quantitation of natural moisturising factors (NMF), biomarkers of hydration and skin health alongside construction of permeation profiles for common topical components in different formulations. Data analysis demonstrates results corroborate with results seen in previous validated methodologies which have more complex and time-consuming preparation and data processing than the proof of concept study presented here.

Abbreviations

AI	Physiogel AI lipid formulation
AMPs	Antimicrobial peptides
ATR-FTIR	Attenuated Total Reflectance Fourier Transform Infrafred
BIRD	Bilinear rotation decoupling
BW	Bluewater formulation
BW70	Bluewater formulation heat treated at 70^{o}C
CASE	Computer Assisted Structure Elucidation
CNS	Central Nervous System
COSY	Correlation Spectroscopy
CTP	Coherence transfer pathway
D1	Relaxation delay
D_2O	Deuterium Oxide
D20	Diffusion delay
DART	Direct Analysis in real time
DLS	Dynamic Light Scattering
DMSO-d6	Deuterated Dimethyl Sulfoxide
DOSY	Diffusion Ordered Spectroscopy
EM	Cryo electron microscopy
ESR	Electron spin resonance
FCF	Full cream formulation
FID	Free Induction Decay
FLIM	Fluorescence lifetime imaging
HMBC	Hetero multiple quantum coherence
HSQC	Hetero single quantum coherence
IR	Infrared
LED	Longitudinal eddy-current delay
LOD	Limit of detection
LOQ	Limit of quantitation
MALDI	Matrix assisted laser desorption ionization
MeOD	Deuterated Methanol
MPT	Multiphoton laser tomography
MS	Mass Spectrometry
NMF	Natural moisturising factor

NMR	Nuclear Magnetic Resonance
NOE	Nuclear Overhauser Effect
NOESY	Nuclear Overhauser effect spectroscopy
NS	Number of scans
OTTER	Opto-thermal transient emission radiometry
P	Physiogel
P30	Gradient Pulse duration for diffusion
PCA	Pyrollidone Carboxylate
PCA	Principal Component Analysis
PFG-NMR	Pulsed Field Gradient NMR
pH	Potential of hydrogen
PPM	Parts per million
PSYCHE	Pure shift yielded by chirp excitation
qNMR	Quantitative NMR
RF	Radio frequency
RG	Receiver gain
ROESY	Rotating-frame Overhauser Spectroscopy
RT-PCR	Real time Polymerase chain reaction
S/N	Signal to noise
SW	Sweep width
T1	Spin-lattice relaxation time
T2	Spin-spin relaxation time
TEWL	Trans Epidermal Water Loss
TOCSY	Total Correlation Spectroscopy
TLR	Toll like receptors
TSE	Triple spin echo
TSP	Trimethylsilylpropanoic acid
V	Bluewater Vehicle
XRC	X-Ray Crystallography
ZS	Zangger and Sterk

Contents

Figure list

Tables

Chapter 1 Introduction

1.1 The Skin: function, structure and pathologies

1.1.1 Basic structure of the skin

Skin is unique as an organ in that it has great heterogeneity depending on site, ethnicity, gender and age. Where such large variations in other organs would be considered diseased or in an abnormal state. For example, on the head, there is an abundance of pilosebaceous structures relative to skin on the palms and soles of feet which have a distinct lack of pilosebaceous structures. Despite the great differences seen between different sites of the body the skin has some universal features in its structure.

The skin has a surface, which is slightly acidic, with an average pH value of 5.5. This allows a resident skin biome to exist that resists the colonisation by pathogenic microorganisms. This 'Acid Mantle' is made acidic by the presence of acidic compounds present in perspiration and sebum. Below this surface of the skin there is the epidermis which is the outermost layer of skin, with the dermis below. This is where nerve endings exist, so that heat, cold, pain, and itching sensations can be felt. The dermis also holds the sebaceous glands, which produce sweat and oils providing protective and homeostatic functions for the skin. It also has a reservoir of immune cells present, with a larger role in the active immune system. Below the dermis there is subcutaneous fat, which is the most variable layer between individuals, and has a role in temperature management. It also supports the connection between the dermis, muscle and bone. These three areas of the skin show a high degree of differentiation between hairy skin, which covers more than 90% of the body and glabrous skin, which is hair free and exists on the soles of feet and palms of hand. The differentiation between these areas is for the specialised function of each type of skin. Hairy skin is specialised in response to tactile sensations that involve social exchanges and its ability to detect foreign objects before they cause harm or injury to the skin surface. Glabrous skin on the other hand has a large abundance of specialised nerves that better understand tactile details alongside being generally thicker (1).

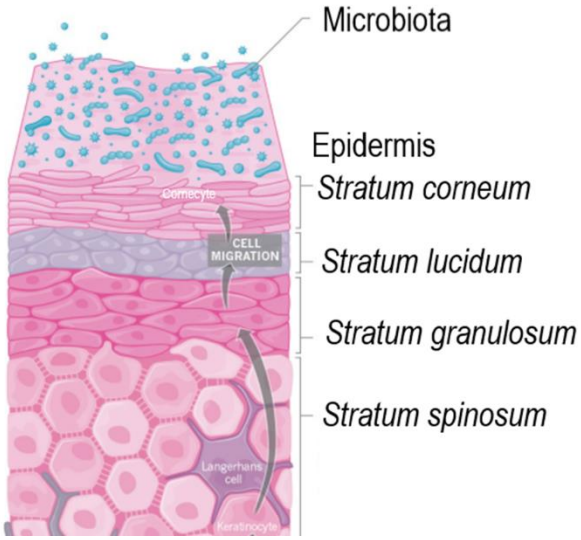

Figure 1 Structure of the epidermis; adapted from Gould J. 2018 (1)

The epidermis ranges from flat anucleated cells at the surface in the *Stratum corneum*, to continuously dividing basal cells at the *Stratum basale* layer. From a functional point of view the epidermis acts as the mechanical and antimicrobial barrier of the skin. The outermost layer of the skin is sometimes considered the natural microbiota of the skin, rather than the *Stratum corneum*. Because of the unique environment of the skin surface (dry, acidic and nutrient poor) an individually unique mixture of bacteria, fungi and virus reside. This mixture then acts as a first line of defence to fend off invading species by competing for nutrients and moisture. Alongside this, it also helps to communicate with immune cells in deeper layers of the skin through a chemical response to attack. The *Stratum corneum* is designated the role of protector from physical, rather than biological infarction. This is through the composition of the *Stratum corneum* being predominantly of dead, flattened cells that will protect the body from friction effects and also control water loss through the skin. A unique layer to glabrous skin is the *Stratum lucidum* which like the *Stratum corneum* is composed of dead cells but is also packed with lipid-rich eleiden, a water proofing component. In hairy skin the role of waterproofing is fulfilled by the *Stratum granulosum*, which consists predominantly of mature keratinocytes that are moving from the *Stratum basale* to the *Stratum corneum*. This is followed by the *Stratum spinosum*, which produces the protein keratin for the keratinization of skin cells at the surface of the skin. It also has active immune cells called Langerhan cells that help to inform the immune system when microbes are attacking the skin. The bottom layer of the epidermis is the *Stratum basale*. This layer is where continually dividing basal

cells will start pushing older cells upward to the skin surface. This layer, being the start point of epidermis cell differentiation, also contains malanocytes which controls the pigmentation of the skin. This makes the *Stratum basale* important when considering exposure to ultraviolet radiation and potential cancer risks.

As the cells are moved from the *Stratum basale* through the stratum spinosum and *Stratum granulosum* to the *Stratum corneum* the basale cells transform into keratinocytes and become increasingly keratinized as they progress before finally becoming corneocytes and leaving the skin surface through desquamation. The keratinization involves the elimination of organelles and formation of corneodesmosomes from cadherins, desmosomes and desmocollins. Around 95% of the skin surface is made up of keratinocytes cells and these are normally cycled through every 15 to 30 days. An aspect of keratinocyte movement towards the surface is the rate of differentiation of keratinocytes towards the surface of the skin, which is an indicator of cell age and pathology.

1.1.2 Stratum corneum

The *Stratum corneum* is composed of corneocytes that move towards the surface of the skin from the base of the *Stratum corneum* over 14 days. At the base, corneocytes have adherent cell membranes with an abundance of corneodesmosomes, desmoglein 1 and desmocollin 1. As the cells move to the surface they loosen and fall off with an increase in the abundance of corneodesmosomes, cornified cell envelope and desmosomal plates between corneocytes. The formation of corneodesmosomes in the upper cells is from complete reorganization of the intracellular space. This involves the cell organelles being completely dismantled and its keratin filaments forming into dense macrofibrils, which are held together by filaggrin (filament aggregating protein). This change gives an opportunity for analysis of the depth of the *Stratum corneum*, where depth of cornified layers can be correlated to the relative abundances of filaggrin and corneodesmosome break down components. The deeper layers of the epidermis: *Stratum granulosum; Stratum spinosum and Stratum basale*, in comparison, have a wide range of

desmogleins, desmosomes, tight junctions and cadherins with a complete lack of keratin present in *Stratum basale* cells.

When considering the corneocytes of the *Stratum corneum* as the bricks that build the wall that is our cornified layer of the skin, then intercellular lipids are the glue. This complex lipid mixture is a combination of cholesterol, cholesterol sulphates, ceramides and free fatty acids. These intercellular lipids are crucial to the correct functioning of the skin and to understanding of the trans-dermal delivery of drugs and topical components as this is the predominant pathway for delivery.

1.1.3 Keratinocytes, corneocytes and keratin in the epidermis

Keratinocytes are cells that produce the protein keratin. Keratin forms ropelike bundles in the cytoplasm, which crisscross with one another. These bundles are connected to other keratin bundles in adjacent cells via desmosome junctions that gives groups of these cells very high tensile strength and explains why the *Stratum corneum*, where desmosome and keratin abundance is highest, has resistance against friction and physical infarction. What causes differentiation of keratinocytes to corneocytes, is the process of anucleation, corneodesmosome formation, and formation of the horny layer. Focus from the change at the basal layer to the surface layer on how the fibrinogen forms and breaks down is a key factor in this. As described previously, keratinocytes start to differentiate from basal cells once they have left the *Stratum basale*. Once basal cells have left the *Stratum basale* they come into contact with a much greater number of keratinocytes and begin forming extensive inter-cell contacts and produce keratin. In the *Stratum spinosome* these contacts form spinous extensions which terminate at desmosome junctions. Once these contacts have formed and keratinocytes are moved into the *Stratum granulosum*, the cells still contain all organelles but are differentiated with the appearance of basophilic, keratohyalin granules which contain the filaggrin progenitor pre-filaggrin. Once cells transition between the *Stratum granulosum* and *Stratum corneum*, there is an elimination of nuclei and organelles within and their structures subsequently changing to a flattened polyhedron shape. This stage is where the cells

change from keratinocytes to corneocytes, which are connected by desmosome junctions called corneodesmosomes. These are simply modified desmosomes, which contain corneodesmosin. Corneocytes are unique in that they contain a densely packed network of keratin filaments which is surrounded by an envelope consisting of cross-linked, by transglutaminases, structural proteins. Shedding of skin from the *Stratum corneum* is accomplished by the disruption of cohesion between corneocytes through proteolysis of the corneodesmosome junction proteins that is tightly regulated, to process the desquamation of cells (2).

1.1.4 Filaggrin and its role in keratin binding, Natural Moisturisiing Factor (NMF), acidification of acid mantle and genetic studies

Filaggrin is an intermediate filament associated protein whose primary role is binding to intermediate keratin fibers in keratinocytes to form macrofibrils. It has also been demonstrated to have a role in the cornified envelope, and corneocytes of the epidermis. Filaggrin however is not synthesised in the outer cells but in the deeper layers and transported to the surface layers in keratohyalin granules in a progenitor form. The keratohyalin granules present in the *Stratum granulosum* of the epidermis is made up of profilaggrin, a highly phosphorylated protein that contains 10-12 tandemly repeated filaggrin monomers. The processing of profilaggrin to filaggrin monomers commences through dephosphorylation at specific points along the repeats and subsequent proteolysis during terminal differentiation of epidermal cells to corneocytes at the *Stratum granulosum* to *Stratum corneum* boundary.

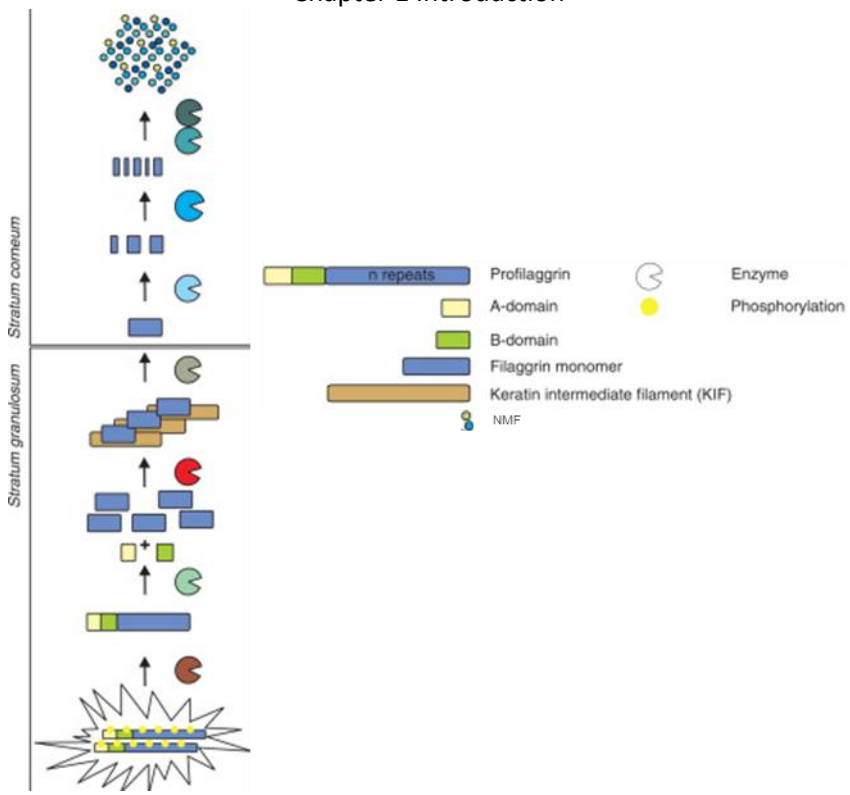

Figure 2 Breakdown process of profilaggrin to NMF, adapted from Hoste E et al 2011 (3)

Once in the surface layers of the *Stratum corneum,* filaggrin is itself broken down into its constituent free amino acids that function as mediators of epidermal flexibility. Some free amino acids are also modified to become more hygroscopic, specifically histidine to urocanate and glutamic acid to pyrrolidone carboxylic acid. These amino acids alongside chloride, sodium, lactate and urate are the compounds that are commonly grouped together to describe the natural moisturizing factors (NMFs) of the skin. The NMFs have been shown to be important in determining the hydration of the *Stratum corneum* under normal circumstances (4).

Early studies of skin, focusing on filaggrin, identified that the breakdown of filaggrin to NMF through proteolysis in the upper layers of the *Stratum corneum* is induced by a water gradient present in the *Stratum corneum*. This finding is very interesting as it can directly correlate NMF values to the water gradient within the *Stratum corneum* (5).

1.1.5 Innate immune responses of the *Stratum corneum*

The immune system of the skin consists of two distinct systems, namely the innate immune system and the adaptive immune system. The innate immune system covers the immune responses, at the onset of physical, chemical or biological attack to the skin, from agents already present in the skin. It also signals the activation of the adaptive immune system through release of signalling agents and receptor responses such as toll-like receptors (TLRs), mannose receptors and helicases, which activate production of antimicrobial peptides (AMPs). TLRs are activated specifically by the lipopolysaccharides of gram-negative bacteria, the lipoteichoic acid and peptidoglycans from gram-positive bacteria, alongside mannans from yeast and fungi, and nucleic acids produced from our own cells. Smaller compounds within the skin, in particular the extracellular matrix, can have their levels affected by the disruption to microbiota homeostasis. For example, infection by pathogenic microorganisms or infarction of external agents through physical damage from the environment, with tetanus as a specific example demonstrates this response in the way that tissue damage can create an anaerobic environment. This environmental change of the skin prevents the normal functioning of small immune system compounds and allows the colonisation by *Clostridium tetani* which releases the neurotoxin tetanospasmin and gives the characteristic symptoms of Tetanus (Trismus and reflex spasms) (6). Colonisation of the skin by non-native biota can further affect the homeostasis of the skin and can be measured either through biopsy or screening methodologies. A crucial protective aspect of the innate immune system is the presence of antimicrobial agents synthesized in the *Stratum granulosum*, which are packed into lamellar bodies and transported to the *Stratum corneum*. AMPs are also produced by sebocytes, mast cells and neutrophils in healthy human skin with sebocytes being the proposed source of the AMPs present in the sebum of sweat.

Keratinocytes of the epidermis have also been shown to induce inflammatory responses within the skin. When allergens, ultraviolet light or physical insult impacts the skin, keratinocytes act as signal transducers which converts these external stimuli into the production of pro-inflammatory cytokines, adhesion molecules and autocrine/paracrine chemotactic factors.

1.2 Biomarkers of the skin and topical formulation design

Biomarkers which have been measured and identified to evaluate the health and functions of layers of the skin include genes, enzymes and their respective activities, proteins and smaller molecules such as vitamins, NMFs and ions (Cl^-. Na^+, K^+, Ca^{2+}, Mg^{2+}, PO_4^{3-}). Studies on genetic biomarkers are widespread and heavily researched in the investigation of skin ageing, disease states and water retention potential. It has been shown that genome affecting biomarkers of the skin correlate to endogenous ageing, while also highlighting the Wnt signaling transduction pathways (7). In the ageing process. It has also been suggested to use these genetic biomarkers as an alternative to CNS sampling when investigating ageing (8). Techniques for analysing genetic biomarkers testing are undertaken in a high throughput fashion, for example with the use of quantitative real time polymerase chain reaction (RT-PCR), which has been used to verify nine genetic biomarkers out of 158 characterised human skin cell genes of the skin which attempted to identify molecular targets for drugs and therapeutic treatments (9). Enzymes and proteins as biomarkers have also been evaluated to monitor skin ageing and the appearance of senescent cells, which have been suggested to be indicative of premature cell ageing and deterioration of the skin through thickening of the skin layers and loss of desquamation function which leads to the observed structure of ageing skin and increased susceptibility to dryness and damage (10).

Table 1 Summary of common biomarkers of interest for consumer health products research

Class	Biomarker
Vitamins	E
	C
	D
Ions	Cl-
	Ca2+
	Na+
	Mg2+
	PO43-
	K+
Natural moisturizing factors	Free amino acids
	Pyrollidone Carboxylic acid
	Lactate
	Sugars
	Urea
	Citrate
	Formate
	Ammonia
	Uric Acid
	Glucosamine
	Creatine
Reactive Oxygen species	PM2.5
	Cytochrome c oxidase
	Fe2+
	Xanthine Oxidase
	Cytochrome P450
Antioxidants	Glutathione
	Carotene
	Ferritin
	Coenzyme Q

Specific proteins of interest are proteases that have a crucial role in desquamation of skin; these can be monitored through measurement of their activity in the skin. Smaller peptides, specifically AMPs, are also an important biomarker to determine the functioning of the skin, immune system and wound healing responses. Smaller molecule biomarkers have been studied, which include NMFs, free amino acids, metabolic breakdown products and ions. Ions and charged metabolic products have an effect on the physiological conditions of the skin, such as pH, which can be measured as a biomarker. One study has used these biomarkers to compare between infants and adults and showed significant differences between infant skin and adult skin. The results showed that the biomarkers measured which had roles in filaggrin processing, protease inhibition and

innate immune system function were upregulated during physiological transitions after birth that drove changes in skin pH and increased water-binding NMF components, while suppressing desquamation of skin through downregulation of protease activity. This study highlights the significance of biomarker characterisation and quantitation in the skin (11). A specific protease that is showing significant importance in the processing of filaggrin to NMF is that of Kallikrein (KLK), which is mainly functional through the actions of KLK5 and KLK7. KLK5 and KLK7 play crucial roles in the maintenance of the epidermal barrier and are heavily imlicatied in inflammatory skin diseases. Measurement of Kallikrein activity versus NMF levels could help to elucidate the specific steps and interactions of compounds leading to the development of novel treatments for inflammatory diseases (12).

1.2.1 Vitamin D

In the skin, vitamin D has a role in regulating the formation of the skin barrier through processing of the long chain glycosylceramides in the extracellular lipid mixture. The photo-production of vitamin D all takes place in the skin. Once in the epidermis, it diffuses to the dermal capillary bed, where it is transported to the liver by the vitamin D binding protein (13). Once in the liver vitamin D is hydroxylated to the active form 25-(OH) vitamin D and then oxidized in the kidneys to give the active form $1\alpha,25(OH)_2$vitamin D which alongside calcium function, helps to regulate skin differentiation, apoptosis and inhibition of cell proliferation (14).

It has been shown that an induction effect of Toll like receptor 2 and its co-receptor CDl4 is induced by vitamin D, therefore initiating the innate immune response in the skin, leading to CYP27B1 and cathelicidin production (15,16). Furthermore, the induction, of cathelicidin (LL-37) production by $1,25\text{-}(OH)_2D$ highlights another role of vitamin D in facilitating wound healing and tissue repair. This is demonstrated by the up regulation of cathelicidin during wound healing (17), modulation of inflammation (18), induction of angiogenesis (19) and improving re-epitheliasation (20).

1.2.2 Main targets for analysis in skin

The integrity of the skin and its ability to retain water has been shown to correlate to levels of NMF in the *Stratum corneum*, with disease states demonstrated to have different NMF values to healthy states. NMF compounds are breakdown products of Filaggrin that exist in the extracellular lipid matrix. The NMF compounds exist at varying concentrations with free amino acids being the most abundant at 40% w/w, Pyrollidone carboxylic acid at 12% w/w, lactate at 12% w/w, Ammonia, Uric acid, glucosamine and creatine at 1.5% w/w, with the least abundant compounds Citrate and Formate at 0.5% w/w (20).

Lactate has been suggested, together with potassium, to have a role in supporting the barrier effectiveness of the *Stratum corneum* in healthy skin. A study, using tape stripping of the skin, quantified lactate and correlated levels of lactate with potassium, however the exact relationship between keratinocyte proliferation and lactate is still uncertain. Despite this, lactate is known as an end product of glycolysis which is the main energy source in the epidermis, so is a promising marker for monitoring of skin health and function (21).

Pyrollidone carboxylate (PCA) is a cyclized derivative of glutamate and is included with glutamate in the calculation of NMF levels and can be used to investigate further by ratio correlation measurements with ratio studies in the skin of glutamate from proteolysed filaggrin to PCA to better understand the metabolism of amino acids in the different layers of the skin. PCA has been heavily studied as it has been shown that PCA concentration correlates to the functioning of the filaggrin genotype. This has led to several tape stripping papers, where the method of adhesive tapes being pressed onto the sampling site of the skin and subsequently abruptly removed to collect the stratum corneum layer of the skin at the sampling site for analysis is employed. that utilise this relationship to monitor not only its relationship to genetic variants of the FLG gene but also correlations to hydration, variation in ethnicity and anatomical site, and damage to the skin (22) (23).

The amino acids, which are most abundant in the NMF consist predominantly of amino acids from the proteolysis of filaggrin. A consequence of investigating the composition of filaggrin is it will help guide researchers to amino acid selection for analysis in the terminal layers of the *Stratum corneum*. The Uniprot data base for filaggrin (24) shows a compositional bias in the filaggrin repeats of serine, histidine and alanine. This marks these amino acids as compounds of interest in the analysis of the skin, especially serine which highlights the role of serine proteases in the management of the skin. (25). In the skin it has been illustrated that there is further specific processing of amino acids after proteolysis of filaggrin. This includes the conversion of histidine to urocanate via the elimination of ammonium through the action of histidine ammonialyase (26). Arginine is also converted to citrulline through the deamination during the post translational modification of residues on several locations along the profilaggrin structure (27). These two modified amino acids are present in the *Stratum corneum* and have been correlated to filaggrin status in disease states (26).

NMF compounds related to the energy cycles of the skin include formate, citrate and creatine. Formate is indicative of cellular and whole-body metabolism, which can cross the bridge between nutrition and toxicology measurements. Formate is a promising marker for analysis of human physiology and disease as a whole. (28). Citrate is known as the end product of the citric acid cycle, which has been classed as the most important metabolic pathway for energy in the body, functioning in the oxidation of carbohydrates, fats and amino acids from proteins. Measurement of citrate in the skin could give a measure of the metabolism in different layers of the skin (29). Creatine is normally only investigated as an energy precursor however it has been shown that cells that are exposed to higher levels of creatine has been shown to have increased protection from stress. Specifically oxidative stress and UV stress, which are pertinent areas of interest in skin research. Creatine has also been used in topical formulations for enhancement of skin protection. Analysis of the creatine-kinase system in the skin has therefore garnered quite a bit of interest (30).

1.2.3 Topical formulation design and active ingredient encapsulation and drug delivery

Topical treatments made for the skin are primarily evaluated for the potential to improve water retention and strength of the barrier of the skin towards irritants, be they physical or chemical. The design of topical treatments for the skin looks to include compounds which show an ability to decrease Trans Epidermal Water Loss (TEWL) and therefore increase the moisture level of the skin. One of the best-known moisturising compounds is glycerol/glycerin. It is known that glycerol acts through the drawing of water to the surface of the skin, through regulation of osmosis within the intracellular milieu, alongside a role in the maintenance of the fluid structure of cell membranes and intercellular lipids (ICLs) (31). Panthenol, has demonstrated significant decreases in TEWL through 30 day application of down to 1% solutions. It was also shown that panthenol containing formulations showed immediate reduction of TEWL after application when compared to controls and vehicle formulations (32).

Permeation of active compounds in topical creams can be enhanced through several methods, from varying the formulation composition to chemical and physical effects applied upon the *Stratum corneum* during application. When formulation vehicle design does not give the permeation desired of a certain compound, permeation enhancers have been added to the formulations. The most common of these permeation enhancers used in dermal treatments is that of glycols, specifically propylene glycol. However this is not the only 1,2-alkane diol that has been evaluated for this purpose. Pentylene glycol has also been shown to demonstrate anti-microbial activity alongside the desired moisturizing effects. Analysis of permeation profiles has shown that glycol-containing vehicles give a 100% increase in penetration to viable skin layers after 30 minutes. This analysis also gave an insight into the comparative effects of longer chain glycols which makes the method of permeation enhancement of glycols better understood (33). It has been shown that a relatively longer chain glycol, 1,2-pentanediol, at a low 5% proportion of formulation, showed a faster and greater penetration of caffeine in pig skin models., much like the permeation increase seen in dihydroavenanthramide D in the previous study (34). Further to vehicle design and the addition

of permeation enhancers, it has also been demonstrated through the work of McAuley *et al*, the potential of using heat alongside chemical enhancers to increase delivery of topical compounds. Through heating of scalp skin by around 12 kelvin over a 24 hour period of short duration heating pulses, it was shown that finasteride penetration into the human scalp and targeted hair follicles was significantly increased. This research also showed that particular combinations of penetration enhancers were used for targeting of permeation with heat application as adjunct to increased and faster permeation to the target area(35 - 37). These studies were, however, limited to showing increased permeation via the hair follicles to deeper skin layers rather than permeation through the extracellular lipid matrix of the *Stratum corneum*. It has been demonstrated that for binary systems composed of propylene glycol and fatty acids that permeation of the active Niacinamide in the human skin can be enhanced (38).

1.3 Analytical Chemistry techniques for investigation of the skin

Measured variation of certain biomarkers abundances throughout layers of the *Stratum corneum* can be indicative of how filaggrin forms and breaks down. It can also detail the NMF compound variability throughout the outer layers of the skin. This information can give insight into the filaggrin formation and breakdown in healthy skin. It also allows for correlation of NMF compounds with skin changes from the inner layers to outer layers.

1.3.1 Sampling models

Various experimental models are employed in dermal and transdermal research. These are categorized as *in vitro*, *ex vivo* and *in vivo*, which covers the use of culture skin models, excised human or animal skin and whole animal models respectively. It has been shown that measurements of NMF levels correlate between *in vitro* and *in vivo* samples from animal and human models have been validated, however many of the models and suggested correlations between biomarkers still show large deviations in results between *in vitro* and *ex/in vivo*. There is a limitation in the number of reported correlations that have been validated which researchers suggest is mainly through the

active nature of *in vivo* skin, which has a circulatory system that introduces unknown variables into the system being investigated. Despite the limitations of in vitro experiments, research has highlighted the potential of porcine skin as a comparable model to human skin. Which alongside the benefits of acquisition and ethical considerations, has a functional benefit through more similar barrier properties to *in vivo* skin than that of *in vitro* human skin interestingly. This however does mean that human culture studies are limited to studies on irritation and metabolism (39).

In vitro modelling is classically achieved through the development of keratinocyte cultures, either as monolayers of cells or as layers of keratinocytes with selective differentiation of keratinocytes which gives a much more complex model. The use of keratinocyte monolayers is restricted to investigation of the structural and functional features of keratinocytes by its simplistic nature, whereas full epidermal reconstructions can be used to interrogate differentiation of keratinocytes and formation of the cornified barrier. The epidermal reconstruction can also be designed in a way to compare how specific layer changes can affect the characteristics of the skin and is a very useful model for disease state investigations (40).

The use of *ex vivo* tissue for analysis has been shown to give reliable results as the layers of the skin have been defined *in vivo* processes and keratinocyte characteristics are correct. The difficulty with *ex vivo* use is in making sure that extraction, storage and acquisition of results is consistent between studies as reproducibility of results could suffer greatly despite the seemingly simple method of extraction. Studies using *ex vivo* samples from humans are ethically sounder than those from animal samples as informed consent can be given after cosmetic procedures and amputations as done in this study. These reasons make *ex vivo* tissue sampling a fruitful area for interrogation of not only skin features but also permeation profiling of formulations used for topical or cosmetic applications (41).

In vivo sampling of the skin is the most reliable model for investigation of the skin, as it is not limited by assumptions made about skin and lack of a microcirculatory system. However, *in vivo* skin is limited by researcher control, in the way that unknowns and their effects on treatments have to be elucidated as much as possible before conclusions can be made from findings. *In vivo* studies have also been predominantly undertaken on animal models rather than human models as these can be designed to an extent and are also a lot cheaper and controllable than human *in vivo* studies. Rodents are the animal of choice as they are relatively inexpensive, have validated methods of handling and are also small, so large sample based studies can be readily set up (42). One issue of animal modelling in *in vivo* studies is that the composition of free fatty acids, triglycerides and hair follicles must be considered when comparing the skin barriers of rodents compared to humans. This has more value in permeation models as these components are part of the main transdermal delivery pathway, with structural characterisation of keratinocytes and genetic effects being more comparable in animal models to human models as genes related to specific functions are commonly conserved in species (43).

Correlations between the different modelling methodologies and validation of *in vitro*/*ex vivo* findings and *in vivo* findings have been studied through the implementation of mathematical methods. Looking at mathematical laws can help us to better explain findings and discover correlations which may have been hidden before. Fick's Diffusion law which has been implemented in describing transport of permeable solutes through the non-viable layer of the *Stratum corneum*. Fick's law helps us to determine partition coefficients, diffusion coefficient, and thickness of barrier with consideration of *in vivo Stratum corneum* conditions such as viable epidermis, interfacial resistance and receptor removal rates.

Equation 1

$$\frac{dC}{dt} = K \times D \times \frac{C_0}{h}$$

C_0 is the donor concentration; K is the partition coefficient (measures the ratio of concentration of compound between two areas, here it is used for each side of membrane; D is the diffusion

coefficient (rate of diffusion for compounds through membrane being used); and h is the thickness of the barrier (44). Mathematical methods have been exploited to build several databases detailing compound permeation of the skin through *in vitro* studies and also in analyses of permeability of different species and anatomical sites of the skin, comparing their functional properties for different modelling types. One of the most comprehensive databases was made by Flynn which details the permeability coefficients of 94 compounds (45).

1.3.1.1 Tape stripping

Characterisation and quantification of active compounds allows us to follow the response of the skin elicited by topical or prescription application. A validated way of doing this is through tape stripping of the skin, where layers of keratinocyte cells are removed via the application of cellulose acetate strips to the chosen skin site and removed in a manner to keep the layer's depth, volume and mass as consistent as possible. Once removed, several analytical techniques can be used to evaluate the concentrations of specific active compounds within the skin. Squame Scans, a colorimetrical determination technique which indirectly measures the total *Stratum corneum* (SC) protein content on tape strips through measuring optical absorption at 850nm (infrared) can be used followed by further separation and analytical tests to determine the mass of specific compounds, peptides, proteins per mass of total protein removed to give normalized values between tape strips. Sonication tests have shown that sonication for a minimum of 10 minutes is sufficient to remove 85-90% of total protein from the tape strip, and a low rpm centrifugation removes any cell debris from the supernatant containing proteins, peptides and active compounds of the cells and extracellular matrix extracted which gives a reliable method of extraction.

The methodology of tape stripping has been used to analyse SC protein, enzyme activities and TEWL (46). Further studies measuring SC proteins from tape stripping have shown clear variation in the biochemistry of sensitive skin individuals (47). Tape stripping has also been used to measure NMF levels derived from filaggrin. These levels indicate changes in the development of the epidermis from basal layer to outer layers. Regional Tape stripping has been used to show regional and

temporal differences in NMF levels, alongside protease activities which is suggested as a prediction tool for atopic dermatitis in early childhood (48).

The use of tape stripping, where removal of uniform complete cell layers of corneocytes is achieved non-invasively, has been validated in the comparison of skin properties between different anatomical sites and ethnic groups. It was shown that the *Stratum corneum* of the face is structurally distinguishable from the *Stratum corneum* of the forearm, through measurement of *Stratum corneum* removed per tape strip. Differences in the furrowing of skin and relative layer thickness can begin to explain these differences, but function and exposure of these different skin types gives an interesting angle to these findings. It was also demonstrated that the regression between different anatomical sites and ethnicity was similar which suggests a reliable measurement and good reproducibility between groups. They also showed that the correlations between site and *Stratum corneum* matched those shown in previously published data on body sites not investigated in this study. They also generated calibration curves on the acquired data which paves the way for a potential rapid indirect protein assessment method (49).

The wealth and variety of the use of tape stripping in the analysis of skin exemplifies its robust and simple methodology. This assumption however must be taken with a grain of salt and caution must be practiced before tape stripping is employed. Tape stripping must have several parameters considered before and during implementation to make sure that the *Stratum corneum* is extracted in a homogenous way to avoid issues with repeatability and reproducibility. It has also been recommended to determine the amount of *Stratum corneum* removed for all tape strips to increase validity of conclusions. With these considerations in place the potential of tape stripping is huge, especially in the field of dermatological and pharmacological studies. Combination of this technique with skin biopsies and further developing imaging methodologies can also help to validate and compare correlations seen between different modeling systems (50).

1.3.2 Detection techniques; Spectroscopic methodologies

Vibrational spectroscopic methods, most commonly infrared (IR) spectroscopy, have been widely used in the analysis of the skin. Mid-infrared pulsed photoacoustic spectroscopy has also shown an ability to monitor glucose in the human epidermis (51).

IR is routinely used to measure the CH symmetric and asymmetric stretch (2850-2920cm^{-1}), carbonyl stretch, amide 1 and 2 bands in the skin as this give information about the lipid and protein conformation within *in vitro* models of the skin and ex/*in vivo* extracts/areas of the skin. Most IR studies use attenuated total reflectance Fourier transform IR (ATR-FTIR) and study the skin of the forearm, but there have been studies on other areas of the body such as the face. A study using skin tape strip samples from the face demonstrated the use of ATR-FTIR to monitor the composition and organization of SC lipids *in vivo*. (52).

An important finding by several studies using IR methodologies was through measuring permeation of different topical additives, such as octadecanoic acids and oleic acid, was that hydrated skin was more permeable (53, 54). The exact reasons are unclear, but research showed that phase separated pools can be formed in the *Stratum corneum* by permeation enhancers (55). Alongside this it was evidenced that the extracellular lipid pathway was the primary permeation route as studies on water diffusion through porcine skin showed water permeability being highly correlated to the –CH stretch of lipids within the pathway (56). ATR-FTIR has also been implemented in combination with in vivo tape stripping to assess the delivery and availability of drugs within the *Stratum corneum* (57). IR methods have shown potential in analysis of the skin however is very limited for screening as complex mixtures are almost impossible to distinguish and non-broadband irradiation is used for targeting of specific functional groups of compounds.

Electronic spectroscopic methods include UV, Fluorescence and NMR, with NMR addressed later on. The surface of the skin has been analyzed by diffuse reflectance UV spectroscopy however any deeper analysis is limited by the natural barrier of the skin to UV radiation. Despite this limitation

it has been observed that researchers moved the UV range closer to visible radiation to prevent cell damage through irradiation. To get around shorter transmission distance of visible light through skin, fibre optics are employed to apply the radiation source deeper in the skin. A study has used these techniques to measure penetration time of aminolevulinic acid in the forearm (58). This work is promising in the development of electronic monitors which persist in the skin and characterize skin properties (59).

Fluorescence methods are much more common when compared to UV methods. This is predominantly through the exploitation of fluorescence probes. The membrane fluorophore 1,6-diphenyl-1,3,5-hexatriene has been exploited to measure the effects of oleic acid on the skin and the transport of benzoic acid using fluorescence lifetime and limiting anisotropy methodologies (60). Transfer from *ex vivo* to *in vivo* fluorescence imaging has also been demonstrated for the investigation of skin lesions (61). MPT/FLIM studies on excised lesions corroborated with results from conventional dermatological techniques and histological techniques (62). Fluorescence is limited however by the predominant need for probes which limit the range of applications to predominantly larger tissue effects and cell area affects on skin and not the biomolecular changes that occur in the skin after chemical or physical infarction.

The use of mass spectrometry in the analysis of skin samples and extracts has predominantly been done using matrix assisted laser desorption ionization mass spectrometry (MALDI-MS) (63). The use of MALDI-MS has been demonstrated to measure levels of ketoconazole in porcine skin, the absorption profile of imipramine with an artificial model of the epidermis, and characterisation of lipid species present in *ex vivo* samples of the human skin. (64 - 66). A more recent MS method that has potential in the analysis of skin hydration and disease state is 'Direct analysis in real time mass spectrometry' (DART-MS). This technique has been used to directly quantify amino acids present in the *Stratum corneum* and is a very exciting technique for future analysis of NMF compounds and their correlations to varying *Stratum corneum* conditions (67).

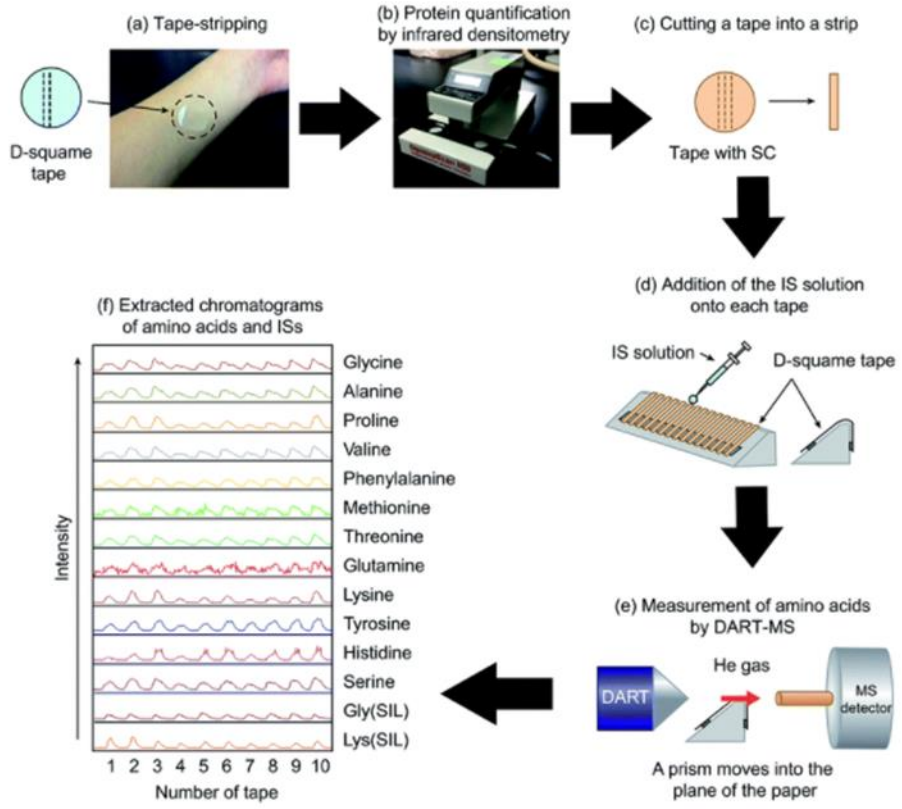

Figure 3 Flow chart of DART MS methodology for us in NMF determination, adapted from Maeno K et al. 2017 (100)

Other spectroscopic techniques used in the analysis of skin include Opto-Thermal Transient Emission Radiometry (OTTER) (68), Impedance Spectroscopy (69), Laser-Induced Breakdown Spectroscopy (zinc absorption *in vivo)* (70, 71) and Photoacoustic Spectroscopy (72). These techniques have predominantly been utilized to measure the permeation of actives, with OTTER being used to measure hydration of the skin *in vitro* and *in vivo* (73)(74) . Impedance spectroscopy has also been used for studies on the effects of mechanical and chemical damage to cadaver skin which gives some fascinating insights into possibilities of spectroscopic techniques on the skin from a different focus point (75)(76).

Use of HPLC for analysis of tape strip extractions is extensively used, with extraction procedures for studies investigating physiology and biochemistry of the stratum corneum (101), NMFs (102) and penetration of ferulic acid and UV filters (103) detailed in figure 4.

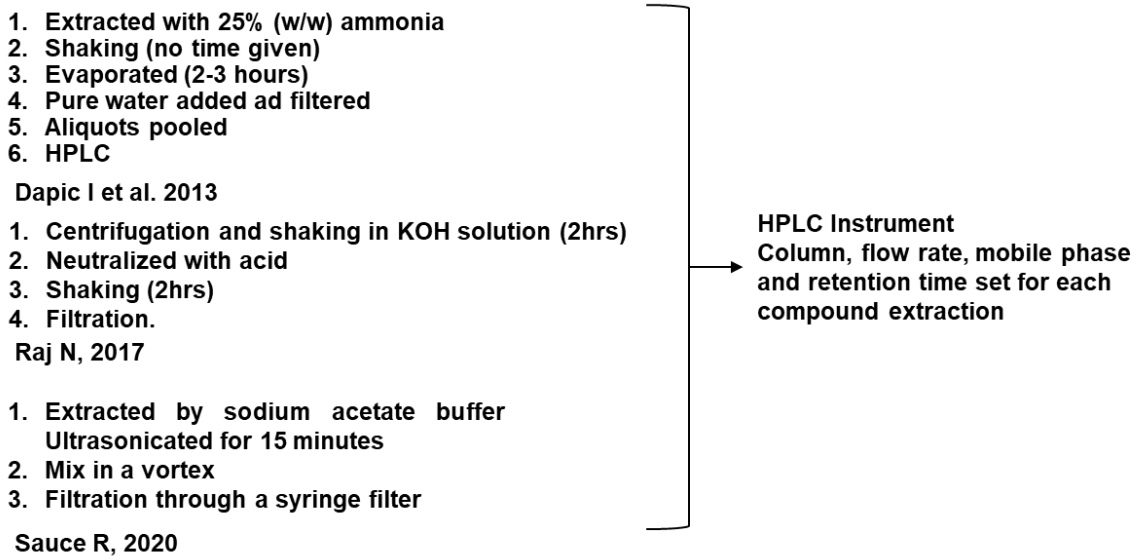

Figure 4 HPLC extraction procedures used in tape strip based studies (101 – 103)

Electron Spin Resonance (ESR), a technique based on the same principles as NMR, exploits unpaired electrons present in paramagnetic molecules which can absorb energy when in an applied magnetic field. It has been employed in skin research through measurements of diffusion of oxygen in the *Stratum corneum* (77), and measuring degree of disorder in lipid bilayers of the *Stratum corneum* caused by n-decymethyl sulphoxide application (78). Most interestingly for this work it was used in collaboration with tape stripping techniques to evaluate the effectiveness of different vesicle types (core multishell nanotransporter and invasomes) in delivering 3-carboxy-2,2,5,5-tetramethyl-1-pyrrolidinyloxy to layers of the *Stratum corneum* (79).

1.3.3 Nuclear Magnetic Resonance (NMR)

NMR is unique as an analytical technique in that it takes two very distinct forms, spectrometry (solid or liquid state, *in vitro*) and imaging which has the potential to image skin *in vitro*, *ex vivo* and even *in vivo*. Firstly the use of NMR as a spectrometric technique, predominantly used technique in *in vitro* models of the skin, will be reviewed.

NMR metabolomics is a useful tool for greater understanding of the metabolism that occurs in the human epidermis. A demonstrated use in determining nanotoxicology effects upon the skin was

demonstrated by a study of silver nanoparticles incident on keratinocytes. In this study keratinocytes of the epidermis were exposed to 48hrs of 30nm citrate-stabilized silver nanoparticles, at concentrations of 10 and 40 μg/mL. NMR was able to analyse specific metabolite concentration variations from intracellular and organic extracts, and extracellular culture media, which, in combination with multivariate analysis demonstrated that the keratinocytes exposed to the silver nanoparticles had upregulation in antioxidant protectors, and downregulation of energy depletion and cell membrane modification. This study also underlined the sensitivity of NMR metabolomics to be able to detect early biochemical events which change metabolite levels at lower concentrations of silver nano particles (80).

Alongside toxicological studies of the skin in response to formulation treatment there are a larger number of studies utilizing NMR methods to interrogate the permeation effects of excipients and actives. One such active is Azone® which is shown to induce structural disorder of the intercellular lamellar lipid structure in the *Stratum corneum* through the use of ^{2}H NMR. It was also suggested that fluid domains within the *Stratum corneum* are created in the lipid pathway which could explain the penetration enhancement effect (81). This early work led onto the use of other NMR methodologies for the analysis of formulation composition and respective effects on transdermal delivery of drug actives and topical compounds. PFG-NMR which determines self-diffusion coefficients of single molecules or groups of molecules was shown to be useful in optimizing microemulsions for transdermal delivery evaluating irritation to the skin (82). The demonstrated dependence of increased transdermal drug delivery on solubility and mobility within vehicle formulation through PFG-NMR was used in further studies for specific drugs including vinpocetine. (83).

Proton NMR spectroscopy has been extensively employed in the study of animal skin with self-diffusion, t1 and t2 values being measured to interrogate the hydration of water mobility in guinea

pig skin models (94)(95). Measurements of free and bound water in the human *Stratum corneum* has also been demonstrated through the application of proton NMR (96).

Using other isotopes apart from ^{1}H with NMR spectroscopy has also been utilized in the analysis of human, rat and porcine skin. The use of ^{19}F has predominantly been used in combination with fluorine containing probes to measure permeation and develop formulations with greater drug encapsulation and increased transdermal delivery of actives. *In vivo* Human and rat skin has been used to measure flurbiprofen absorption in the skin (91). Tape stripping of the viable epidermis has also been used in combination with 19F NMR spectroscopy to measure the effectiveness of natural micro emulsions. (92).

The heavy isotope of hydrogen, deuterium, has also been used in NMR spectroscopy to characterize polymorphism of *Stratum corneum* lipids and the lamellar structures that are formed by the extracellular lipid matrix that exists between the corneocytes and keratinocytes of the *Stratum corneum* (97 - 99).The use of ^{31}P NMR spectroscopy has been employed in the monitoring of disease state in people suffering from psoriasis. It showed potential as a non-invasive *in vivo* tool which allowed for the monitoring of treatment options and the characterisation of skin when in a diseased state (93).

Magnetic resonance imaging (MRI) has started to see more studies moving into *ex vivo* and *in vivo* areas, which is an exciting prospect for understanding of the skin layers and further increasing the resolution of imaging for smaller tissues. One such study which investigated nanoparticles and the skin looked at how semi-solid formulations could affect the skin penetration of iron oxide nanoparticles. This however used *in vitro* human epidermis/isolated *Stratum corneum*, to demonstrate that low-field pulsed NMR, which measured the t2 changes in the skin layers, gives a greater discrimination between permeation levels than the more commonly applied dynamic light scattering (DLS) methodology (84).

An imaging technique called stray field NMR which uses the natural magnetic inhomogeneity of the applied magnetic field to give spatial resolution has been used in several studies of the skin. *In vitro* studies have used stray field NMR to measure skin hydration through detection of water in the skin (87), it has also been used in the following study to measure both water levels and monitor how cosmetic formulations interact with the skin (88). Its use *in vivo* has been reported by Ciampi et al to profile the permeation of a model moisturizer formulation into human skin (89). The use of stray field NMR has also determined self-diffusion values for water in both models of the *Stratum corneum* and in viable epidermis models (90).

Transition from *ex vivo* skin layer discrimination to *in vivo* layer discrimination has led to construction of devices that can profile human skin *in vivo*. These devices are low-field pulsed NMR machines that are placed around the skin, commonly the arms or legs. These machines can then give contrast on the different skin layers through resolving the variation in relaxation times and diffusion coefficients in a specific direction, namely depth (85). These devices have then been shown to correlate dermal alterations to ageing and suggest the potential for a skin age assessment methodology through fingerprinting analysis of dermal alterations (86).

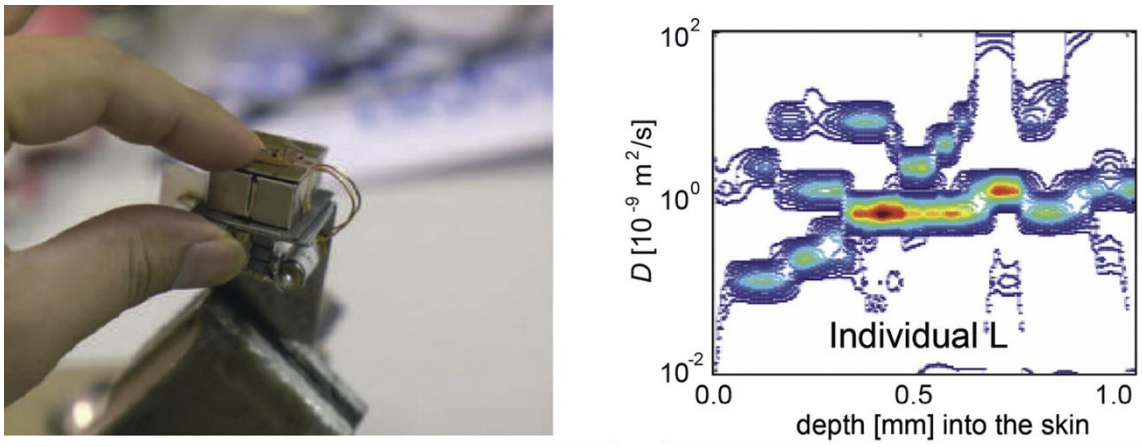

Figure 5 (Left) Example prototype low field NMR device for in-vivo diffusion measurements and (right) Depth resolved distributions of diffusion coefficients of palm skin (85).

1.4 NMR

The beginning of NMR research was sparked by the discovery in 1945 by Purcell, Torrey and Pound of weak radiofrequency signals generated by the nuclei of atoms in 1kg of paraffin wax (109), alongside the discovery of this same phenomenon in water by Bloch, Hansen and Packard (110). The potential of NMR in early experiments was not properly exploited until Fourier Transformed (FT) NMR where the conversion of signal as a function of time to a function of spatial or temporal frequency gave much easier interpretation and clearer results , started appearing in 1966 through work by Richard R. Ernst and co-workers (111). The basic anatomy of a NMR spectrometer contains a NMR sample tube space surrounded by shim coils and radio frequency coils for transmission and receiving with tuning capacitors present, all within a removable probe. This probe is then surrounded by a superconducting solenoid, which is cooled by liquid helium and a further cooling jacket of liquid nitrogen with a vacuum in place around the elements. The removable probe is connected to a console which controls the transmission and receiving switch, signal pre-amplifier, RF detector, analog / digital converter, which sends the data to a workstation computer. The workstation, through user control, determines the pulse programming through script selection and parameter set choice, alongside the pulse amplification through calibration of receiver gain (RG). NMR spectrometers can also contain additional elements to increase sensitivity and resolution with a few detailed as followed. Cryogenically cooled electronics and samples reduces the Johnson-Nyquist noise and increases sensitivity by reducing the distribution of spin states in the Boltzmann distribution. ($Mo \approx \gamma^2 h^2 Ns Bo / 4kT$, where γ is the gyromagnetic ratio, h is Planck's constant, Ns is the number of spins, Bo is magnetic field strength, k is the Boltzmann constant, and T is absolute temperature). Through the Boltzmann distribution it is observed that if the magnetic field strength is increased through the use of larger superconducting magnets the sensitivity will also increase by $B^{3/2}$. This increase however is very expensive as demonstrated by the recent 1.2GHz magnet installed at the University of Florence for $17.8 million in 2020. More commonly used and less costly techniques take advantage of the quantum mechanical properties of magnetic spin. These include dynamic nuclear polarisation, algorithmic cooling which increases the polarization of certain spins

and Quantum optimal control which shows significant sensitivity enhancement at the edge of spectra with reduced rf energy and pulse duration (112).

In general NMR spectra represent a set of Hamiltonian eigenvalue differences which correspond to the energies of the allowed transitions, in response to electromagnetic irradiation. Information about the chemical environment is given by the line position, with details of inter-atomic distances, bond angles and bond types given by specific line splitting. Another powerful aspect of NMR spectra is that integrals of specific lines is proportional to the concentration of the respective compound that produces the spectra lines.

The versatility of NMR is demonstrated by the ease of sample preparation, alongside the short experiment time required to acquire spectral data. NMR is a non-destructive process so samples can be reclaimed for analytes that are intermediates or have been synthesised in very small amounts. NMR is not affected by non-detectable impurities, like that of High Performance Liquid Chromatography (HPLC), Differential scanning calorimetry (DSC) and Capillary Electrophoresis (CE). It is observed that NMR when compared to HPLC has a benefit in its functionality as a primary method of quantification through integral ratio between target analyte and internal reference when deciding on a method for quantitative analysis.

These reasons help to explain why its implementation in research is increasing with further investment in Instrumentation advancement, primarily to overcome sensitivity drawbacks (113)(114) and pulse program development, with great progress in improving resolution(115). These progressive steps are fast making NMR one of the most advantageous analytical techniques, alongside that of the ‘gold standard’ GC-MS.

For 1D 1H qNMR acquisitions,, investigations on the limit of detection and quantitation is predominantly done with simple mixtures where the conditions for accurate quantitation can be met.This is because the calculation of peak areas for quantitation is impaired through overlapping peaks in more complex mixtures.

1.4.1 Quantitative NMR

Quantitative NMR has progressed at a slower rate than that of qualitative NMR (Structural Elucidation) because of the further steps required to interpret results. The disparity between the use of qualitative NMR and quantitative NMR can be recognized in the literature for pharmaceutical development and drug discovery. This helps us to understand why new software advances for qNMR, which cannot keep up with hardware advances, are about 10 years behind that of qualitative NMR.

Quantitation requires that the analyte of interest be completely dissolved in solvent for accurate quantitation. Another requirement is that the relaxation time (D1) between pulses be at least 5x-7x the T1 of the longest T1 in the sample; therefore leading to comparatively longer experiments than qualitative experiments, unless novel techniques are implemented by a skilled user. This consideration for D1 allows complete relaxation to take place; therefore accurate integrals taken on complete signal decays. A 90-degree pulse is also preferred to a 30-degree pulse to allow maximum signal acquired in the transverse direction.

With complex mixtures, there are other considerations, which must also be highlighted before a qNMR experiment can take place. These considerations fall mainly into two areas: Dynamic Range of the sample (concentration differences between analytes and other constituent parts); the number of constituents, which make up the sample (much greater chance of overlapping and mischaracterised spectra; leading to improper quantification). With these considerations in place for complex mixtures, several conclusions regarding S/N, RG values (Receiver Gain, ratio of output to input of a receiver, the higher this is, the greater the signal) and processing methods are come to. A suitable S/N is required for low concentration analytes to be quantified, for accurate integrals to be placed over them where the bias and slope is not significantly affected by the noise level. For accurate quantitation it is demonstrated that >50 S/N is required (107). Hand in hand with this there is a need to evaluate the RG value used; to allow for the certified reference materials concentration to be constant throughout the experiments, as in some it will be comparable to analyte but in other experiments it will be in the magnitude of 100,000x greater. This means a large RG is needed;

however, consideration of baseline distortion with increased RG values must be given. Most NMR scanners do however have an automated RG value function, which starts at max RG then drops the value until spectral overload is no longer a factor in the transformation of the free induction decay.

Even with the slower progress of qNMR compared to qualitative NMR techniques there has been a great deal of progress in qNMR research as its potential is being realised, especially in metabolomics, purity testing, counterfeit detection, and as a pharmaceutical tool (116). With greater automation being introduced by software manufacturers (MestreNova), qNMR is being exploited by more researchers as the Malz and Jancke equation is no longer required for personal calculations of concentrations through manual integral setting and peak characterisation to determine proton number,Equation 1.1 shows how the the determination of Concentration (M) from determined integrals and a known concentration of internal standard is achieved. This saves a lot of processing and analysis time as phase correction, baseline correction, peak picking and integral analysis all have to be done manually to allow for accurate quantitation whereas software such as MestreNova will use in built algorithms to determine concentration of known analyte peaks from the entering of a few details on internal standard and volume of solvent 1 step.

Equation 2

$$\frac{M_x}{M_y} = \frac{I_x}{I_y} \times \frac{N_y}{N_x}$$

I and N are the integral area and number of nuclei for the compounds respectively, with the resultant molar ratio given M.

1D ^{1}H qNMR is set up to allow for accurate quantitation of simple mixtures with very little overlap between signals. Internal standardisation can be set up with a certified reference material, which is at a specified concentration alongside an unknown concentration of analyte; this is the most common method for determining the absolute amount of substances in qNMR. In mixtures that are more complex however peaks will overlap with one another therefore not allowing accurate integrals of peaks to be calculated, this can be resolved to a degree with deconvolution, as this will separate peaks from two similarly concentrated compounds, which do not overlap/underlie one

another. When a peak of interest is underlying a solvent or more concentrated compound, a second dimension can be added to the acquisition to resolve this unresolved peak or addition of suppression techniques if the larger peak is not of interest to the researcher.

2D qNMR is suited to complex mixtures, as it allows for the resolving of peaks that are lost through underlying peaks or are crowded by other more concentrated peaks. The issue with 2D qNMR is that for 2D NMR sequences a lot more variability to the relaxation of the protons is introduced. This means that the integral of a cross peak will not be quantifiable without a large degree of error and uncertainty present. One sequence that has demonstrated a way around this $HSQC_0$ which takes repeats of HSQC scans. This sees an attenuation effect seen in the signal intensity from 1 scan to repeated scans through the effects of T2 relaxation, J coupling effects etc. However from these values the constant k value that is imposed at each repetition can be calculated and linearly back tracked to an imaginary number zero scan that has none of the effects of the repeated HSQC scans and therefore can be directly quantified with a certified reference material (117). Speeding-up of HSQC data acquisition can be achieved through implementation of the ASAP-HSQC (Acceleration by sharing adjacent polarization) Experiments and non-uniform sampled Ultrafast HSQC techniques which reduce the long recycle delay needed to achieve a pre-equilibrium proton polarization and the number of variable linearly sampled t1 increments required for optimum resolution in the indirect F1 dimension (118).

qNMR has also demonstrated its potential to quantify larger molecules such as peptides and proteins since it can provide direct traceability to the SI and impurity standards are not required unlike other techniques. Routinely however MS, LC, x-ray crystallography (XRC) and cryo electron microscopy (EM) are used for the analysis of protein structure. The gold standard technique XRC has limitations which may be resolved by NMR analysis, this include the necessity for samples in XRC to be in a solid crystalline state which is challenging for the peptides of interest in this project considering they interact with membranes and are intrinsically disordered native unfolded peptides (119) .This is not an issue with NMR techniques which allow for a similar atomic resolution but

avoids solid state sample requirements; be that as it may an isotopically labelled protein is often required.

qNMR has also been shown to be a useful quantitative tool when used in tandem with other NMR techniques used primarily for characterisation. The combination of DOSY experiments and qNMR experiments has been used to characterise and quantify natural products within a complex mixture of compounds and shows great promise in this area of research (120). It is also shown that qNMR techniques have developed to allow determination of the quantitative structural and affinity information of interacting ligands. Saturation Transfer Difference NMR (STD NMR) is currently one of the most powerful NMR techniques for detection and subsequent characterization of transient receptor-ligand interaction in liquid state analysis. STD NMR has become a basic method in drug discovery, design and optimization (121 – 124). Quantitative analysis of STD NMR intensities has been developed, upon the modification of the complete relaxation and conformational exchange matrix (CORCEMA) from transferred NOE experiments (125)(126).

1.4.1.1 Chenomx^{tm}

Chenomx is a NMR spectra metabolite identifier and quantification tool. It works through automatic identification of compounds in a sample mixture by means of NMR spectroscopy. The sample mixture to be analysed has its measured conditions input into the system, where the system can pick a set of reference spectra of database compounds which may be present in the sample mixture. This allows the production of a test spectrum from unique sample mixtures with different measured conditions, which alongside the selected sets of reference spectra produce composite spectra containing peaks of suspected compounds within the sample mixture. Detailed pathway of action and processing methodology is illustrated in the patent application (127).

1.4.2 Broadband 1H homonuclear decoupled NMR Spectroscopy

In the last decade, interest in increasing the resolution of NMR spectra for use in complex and biological mixtures of small molecules for metabolite analysis has greatly increased (115)(128). This had led to a race for researchers to develop novel and innovative broadband ^{1}H homonuclear

decoupled methods that allow for high S/N, low number of artefacts and non-time consuming simplified J^{HH} multiplet pattern for proton resonances. From newly developed methodologies, highly resolved ^{1}H NMR spectra are beginning to be seen for mixtures, with clean, minimally overlapped spectra through collapsing of multiplets to singlets. These techniques show great potential in not only improving spectra analysis but also making it simpler, faster and easier for researchers to come to conclusions.

The potential of decoupling through bond interactions for proton NMR is exemplified by the universal use of broadband heteronuclear ^{1}H decoupling in ^{13}C spectrum acquisition which shows substantial benefits through simplification of analysis (129 - 132). 1D ^{1}H NMR however suffers much more from signal overlap and thus lower signal resolution. Even with the use of high magnetic fields for acquisition of 1D^{1}H NMR spectra the resolution improvements do not counteract the limited range seen for ^{1}H chemical shifts. Additional J^{HH} couplings for individual protons also means further splitting that further exasperates the issue of overlapping peaks. Many researchers will however point to the structural information given by proton multiplet structure which correspond to specific bond relationships between atoms, such as their dihedral angle constraints or spin systems. These points however are mitigated again by signal overlap which prevents accurate elucidation of independent peak multiplets and can lead to improper characterisation. It has also been demonstrated by the development of multidimensional techniques that most J information, which is primarily analysed to determine peak correlations are shown more clearly in 2D techniques e.g. COSY, TOCSY, HSQC, HMBC, with even dihedral angles constraints being made less needed as ROESY and NOESY experiments demonstrate through space correlations between protons which will give greater understanding of molecular structure. It has also been seen that pure shift experiments benefit the use of Computer-assisted Structure Elucidation (CASE) software as more complex multiplet structures than expected can confuse the CASE calculation and give erroneous results. In figure 6, the collapsing of multiplets in the aliphatic region of Cholecalciferol is demonstrated, which

in a standard 1D^{1}H acquisition is very hard to determine the number of individual proton environments but is clear when observing singlet peaks in the pure shift acquired spectra.

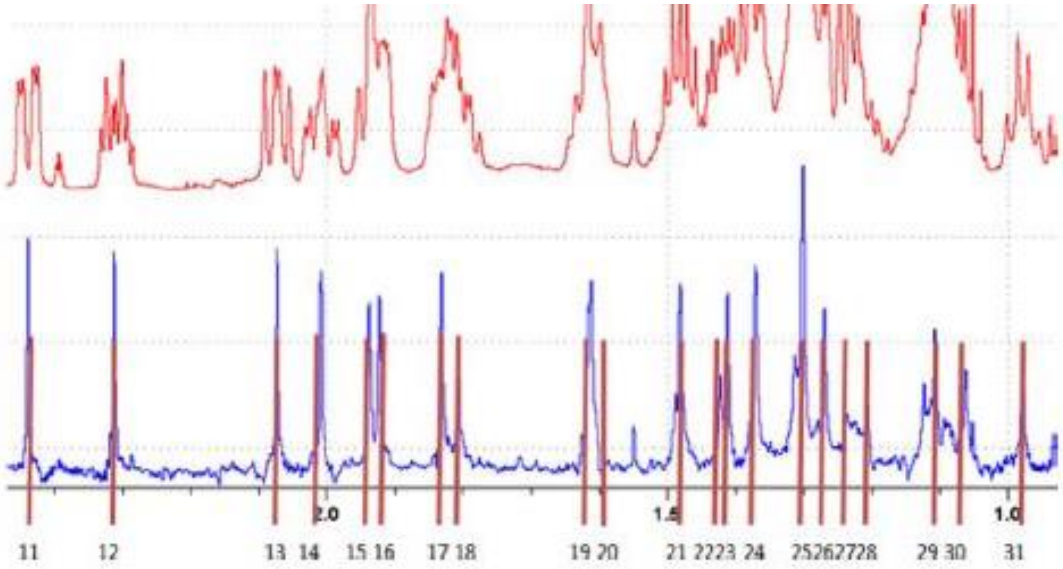

Figure 6 (Top) 1D1H spectra acquired using standard pulse sequence, (Bottom) 1D1H spectra acquired using PSYCHE pulse sequence (219)

1.4.2.1 Pure shift methodology and principles

Despite the promise of pure shift methodology to improve NMR spectra resolution, it is not new and there are reasons, such as experiment time and inconsistent coupling suppression, which have previously hindered the use of pure shift NMR in complex mixture analysis (133-137). Recent research has however demonstrated the versatility of pure shift methodologies and how changes to pulse sequence building has improved artefact suppression, S/N and time required for acquisition. The new pulse sequences, with large investments of time and work into optimization and simplification of these techniques has led to subsequent concatenation of Pure shift methodologies with more commonly used 1D and 2D NMR pulse sequences which has opened the door for wider use of pure shift methodologies (115).

Pure shift pulse sequences are built to manipulate spins, where the acquired signal only presents average evolution with effects from chemical shift, therefore giving it the name pure shift, this means that signals do not split due to coupling and present as a single peak for each proton environment. This is achieved most routinely through the use of two main pulse sequence types.

Pulse sequences where evolution affected by scaler coupling is refocused, called J-refocusing experiments and pulse sequences where the evolution affected by scalar couplings is kept constant, named constant time experiments.

J-refocusing experiments utilise RF pulses to suppress scalar coupling (J) at a given evolution time. Several pulse sequences can be employed to apply this suppression of scalar couplings, where they group available spins either as active or passive. The signal seen at the end of acquisition is a product of the active spins, whereas passive spins are free to be manipulated to remove influence of scalar couplings. Manipulation of passive spins is achieved by inversion of spins by J -refocussing elements, which not only refocuses effect from couplings but beneficially leaves the phases of the active spin coherences unchanged for ease of processing. This action leaves the active spins decoupled and measured through processing of signal, while passive spins being the actively manipulated element are not present in the observable signal. Pulse sequences that employ J-refocussing elements are based on the initial experiment by J.R. Garbow et al (135) called Bilinear Rotation Decoupling of homonuclear scalar interactions (BIRD), include the Zangger and Sterk method (ZS) (136), anti z-COSY experiments (138) and time reversal methods (139). ZS uses frequency and spatially selective refocusing whereas the anti-z COSY and time-reversal experiments utilise low-flip-angle pulse pairs to refocus J couplings. Despite the differences in how these experiments acquire data they all reverse the effects of J-coupling by suppression at specific evolution times. The first BIRD experiment mapped out signal evolution with suppression of J coupling point by point, however it took a relatively great amount of time to acquire the data. A benefit that has been shown is that slow evolution of spins under the effects of J-coupling means that measurements do not need to be taken at the instant of J-refocusing, rather a chunk of acquired data can be taken before and after the instant of J-refocusing. This ‘chunk’ of data is acquired over a time <<2/J where it is observed that the instance of J refocusing occurs at the midpoint of this ‘chunk’. When collecting a succession of these ‘chunks’ together with evolution times incremented by t1 (relaxation times) of individual molecules in a pseudo 2D way, this allows

for subsequent combination of these results to build a composite signal where chemical shift evolution continues seamlessly between chunks with J coupling refocused at the center of each individual ‘chunk’. The combination of these ‘chunks’ together into one element is called an interferogram which is processed in the same way as a normal Free Induction Decay (FID), through Fourier transformation, filtering, phase correction and baseline correction, with the only real difference being that scalar couplings of peaks are suppressed and collapsed to purely the chemical shift element of the peak. Further spectral resolution improvements can be achieved through selection of a larger number of chunks which alongside giving a longer FID, leads to narrower line widths. Alongside number of chunks, the duration of chunks also affects the quality of spectra as there is less chance that J-refocusing will deviate between the exact centres of chunks if chunks are made shorter in the acquisition parameters. The acquisition methodology classically used for the pseudo-2D interferogram originally detailed by Zangger and Sterks work (140), acquires chunks of data independently of each other in a way determined by pulse script. Once the individual chunks have been acquired, a separate script within Bruker Topspin software can be used to build a 1D FID from the pseudo 2D FID chunks. A more complex method which several pure shift pulse sequences have been written with is ‘real-time’ acquisition, where one excitation pulse can be utilised to produce the whole interferogram instead of acquiring the data in chunks. The advantages of this technique means that there is no pseudo 2D acquisition meaning experimental time is only a matter of seconds longer than conventionally acquired 1D ^{1}H spectra. It has been demonstrated that the most time-efficient way is to acquire chunks rather than acquisition on a point-by-point basis, which despite acquiring data without residual J-modulation is a lot slower than acquiring data in chunks (135). Acquisition of a pure shift interferogram with N number of points requires N number of experiments, this factor means that there is a large sensitivity penalty associated with pure shift interferogram acquisitions. This penalty can be avoided if whole Free Induction Decays (FID) are acquired and a 2D spectrum with decoupling in the second dimension is constructed.

It has been observed that with some of the earliest pure shift methods, that projection of integrals from 2D J-resolved spectra at 45 degrees to the frequency space, where self-correlations are taken, can be used to produce a 1D pure shift spectra. This method is however limited by reduced resolution and quantification potential. The new method Pure Shift Yielded by CHirp Excitation (PSYCHE) is based upon a technique called the anti z-COSY experiment which uses a 45 degree projection of integrals with a selective method allowing for exclusion of the cross-peak resonances producing a absorbance mode spectra (141).

1.4.2.2 PSYCHE

Pure Shift Yielded by Chirp Excitation (PSYCHE) uses two small flip angle swept-frequency pulses which are used in combination with a weak pulsed field gradient to achieve homonuclear decoupling. PSYCHE NMR was chosen for this research as it is seen to be the most tolerant of strong coupling effects as well as being very easy to implement.

1.4.2.3 Methodology

The acquisition of a spectra with PSYCHE based homodecoupling requires the implementation of several key aspects for pulse sequence design and spin manipulation. These include the use of low flip angle pulses for homodecoupling, artefact suppression using spatio-temporal averaging, pulse sequences being swept frequency and saltire chirp pulses in design and the selection of the coherence transfer pathway (CTP) during these saltire chirp pulses. To describe the pulse sequence for a PSYCHE experiment, first the pulse sequence that predicated the PSYCHE pulse sequence, the Anti z-COSY experiment needs to be described.

The Anti z-COSY experiment Is built upon a 2D exchange experiment of NOESY, where the flip angles of the 2 pulses between mixing time are reduced in angle. Oschkinat et al, suggested the use of 20 degrees which did not allow exchange to happen and was simply implemented to eliminate CTPs in the different quantum coherences (single, multiple and zero), with retention of transfer processes through longitudinal magnetization like that given by z-filters, therefore the name anti z-COSY. The

experiment was used with resolved J-coupling systems where cross relaxation and exchange could be clearly observed (142).

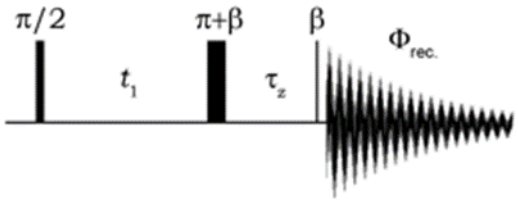

Figure 7 Anti z-COSY pulse sequence

This experiment then allows the effect of low-flip angle pulses on the diagonal signals in the correlation spectra to be harnessed to achieve pure shift spectra from projection. When comparing a simplified version of the PSYCHE pulse sequences with the anti z-COSY pulse sequence a close resemblance between these pulse sequences is observed in figure 7 and 8.

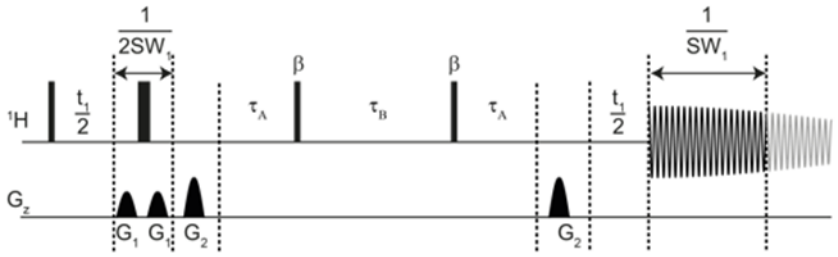

Figure 8 Simplified PSYCHE pulse sequence

This resemblance allows us to determine the best flip angle to minimise the signal intensities of off diagonal cross peaks and keep sensitivity of on diagonal cross peaks high which represent the pure shift spectra, as the same 2D correlation spectroscopy model is used for PSYCHE as used for anti z-COSY. This relationship between flip angle and relative intensities of cross peaks can be determined through charting of relative intensities of groups of cross peaks relative to flip angle degree.

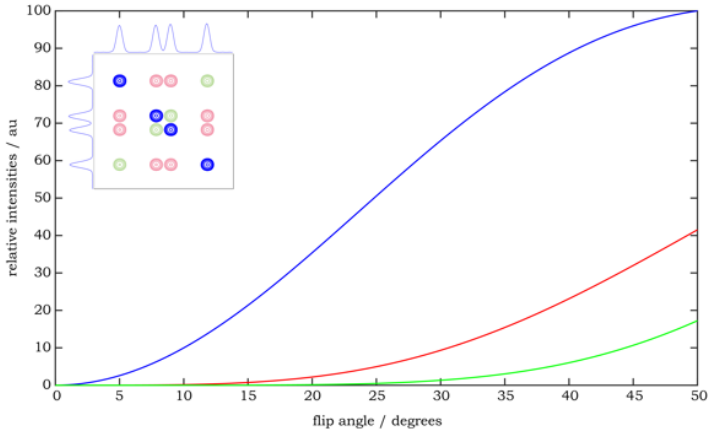

Figure 9 Anti z-COSY spectra and respective peak intensity depending on pulse angle, (Adapted from workshop on pure shift by the University of Manchester)

The acquisition of PSYCHE sequences is hampered through acquisition of not only wanted decoupled signals, but also unwanted signals, including recoupling, zero-quantum and strong coupling signals alongside the COSY type responses from the pulse sequence used. Thankfully all of these unwanted signals have time-dependent phases which gives the opportunity to remove these signals through averaging of a number of transients of experiments with variations between coherence evolution times which allows for suppression when averaged together. This technique is what PSYCHE uses to minimise effects from these unwanted signals. The spatio-temporal averaging is determined by incrementing τA and decrementing τB as seen in the simplified PSYCHE pulse sequence above. When these variable delayed experiments are summed together the unwanted time-invariant phase signals are suppressed with wanted singlets remaining and amplified.

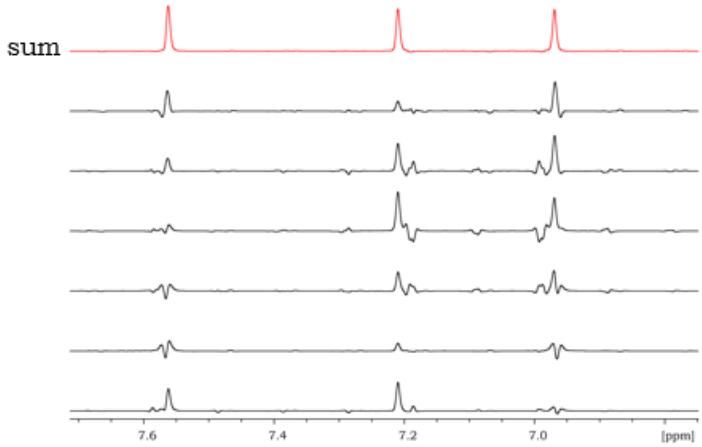

Figure 10 Sum of pulse cycled spectra and individual pulse cycled spectra

Additional acquisition artefacts exist for PSYCHE through the construction of the data interferogram which is subsequently processed to produce the pure shift spectra. These artefacts include chunking artefacts that can arise through improper selection of chunk number and duration within the acquisition time. These occur by loss of acquisition of whole chunks as the acquisition time cuts them short. Fast pulsing artefacts can arise when single quantum magnetisation is rephrased between transients that have reduced relaxation delay and effects on spins are not reset. Digital filter artefacts, also described as ringing artefacts, can arise from the large changes of single intensities between constructed interferograms between chunks, the main methods to remove this is to drop data points at the start of each acquisition chunk to minimise the large change digital filter effects between chunks.

The main difference of course seen in PSYCHE is detailed in its name through the implementation of saltire chirp pulses with swept frequency. Swept frequency pulses have been primarily used in the use of broadband inversion and refocusing of spins. They sweep the frequency across the spectral window determined by the user in a linear frequency, whereas in PSYCHE, swept-frequency low-flip angle pulses are used. Below, a normal (unidirectional) chirp pulse is illustrated, where the frequency sweeps from low-to-high with the equation determining the shape of pulse given by frequency range ΔF (Hz) from $-\Delta F/2$ to $+\Delta F/2$, during time τp (sec), and r.f. amplitude of A (Hz).

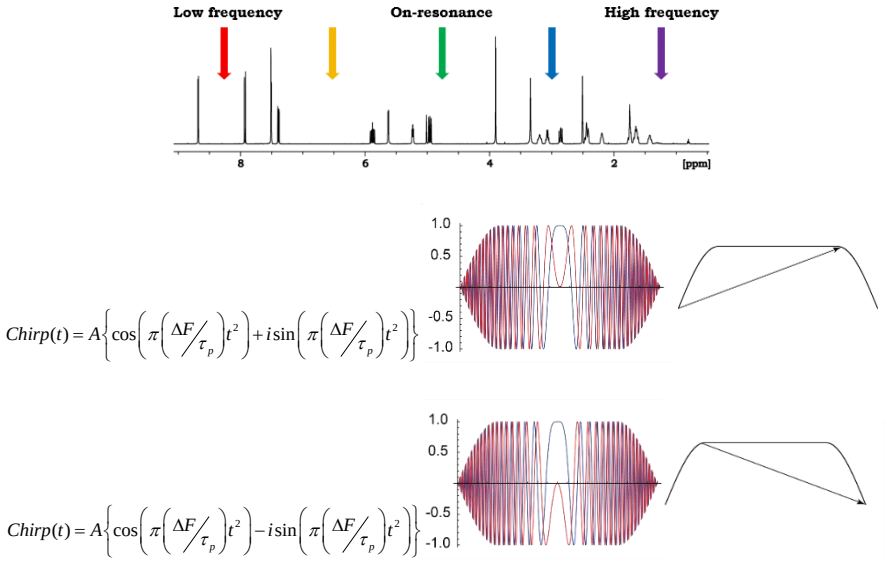

Figure 11 (Top) Spectra annotated detailing swept frequency ranges from low to high, (Middle) Chirp Low to High frequency equation, wave form and simplified wave form, (Bottom) Chirp High to Low frequency equation, Pulse shape and simplified pulse shape

PSYCHE pulses use both High-to-Low and Low-to-High chirp pulses where frequency range is swept; ΔF (Hz) is from +ΔF/2 to –ΔF/2. When averaging these chirp pulses together, a pure real waveform, named a saltire chirp pulse is acquired. The saltire chirp pulse is an amplitude modulated pulse with constant phase through an absence of an imaginary part in its respective waveform.

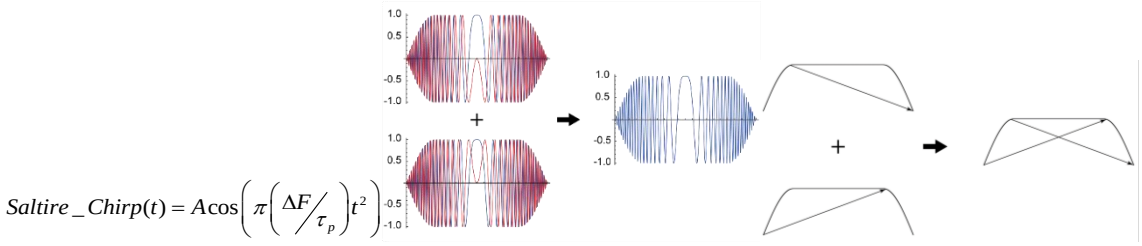

Figure 12 Average of low to high and high to low chirp pulses, Saltire Chirp pulse equation, Waveform and simplified waveform

The design of the waveform means that the respective flip angle of pulses is representative of the integral of the amplitude envelope in respect to time. This is illustrated by the following equation, where amplitude is calculated from the r.f. amplitude of a saltire chirp pulse with a sweep-width of ΔF Hz, duration of τp sec, and flip angle of β°.

Equation 3

$$A = \left[\frac{\beta}{360}\right] \times \sqrt{\frac{2\Delta F}{\tau_p}}$$

Further saltire chirp pulse optimization for use in the PSYCHE pulse sequence was done through averaging of two pairs of inversed sweeping unidirectional chirps to create a double saltire pulse

element. This gives advantages for saltire pulses through its linear dependence of r.f on flip angle which is greatly beneficial for PSYCHE low flip angle pulses, where very small r.f. amplitudes are needed. It also gives greater signal to noise relative to unidirectional sweeped chirp pulses.

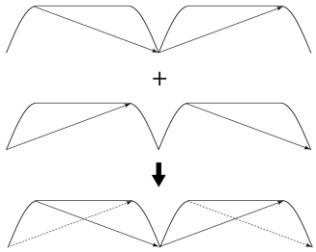

Figure 13 Simplified wave forms of averaging of inversed sweeping unidirectional chirp pulses to double saltire pulse used in PSYCHE pulse sequence

The elimination of coherences with the PSYCHE pulse sequence has been accomplished not through elimination but through manipulation of the coherence transfer pathway during the saltire pulses. Using the double saltire PSYCHE element introduces two CTPS which are manipulated by encoding gradients during the pulses. The evolution of coherences during a saltire PSYCHE element can be represented as the superposition of two independent CTPs being enforced by the presence of the encoding gradient during the pulses. Where the encoding gradient affects the Saltire PSYCHE elements at different points, specifically at the low frequency part of the pulse where coherences are affected. These effects are illustrated below.

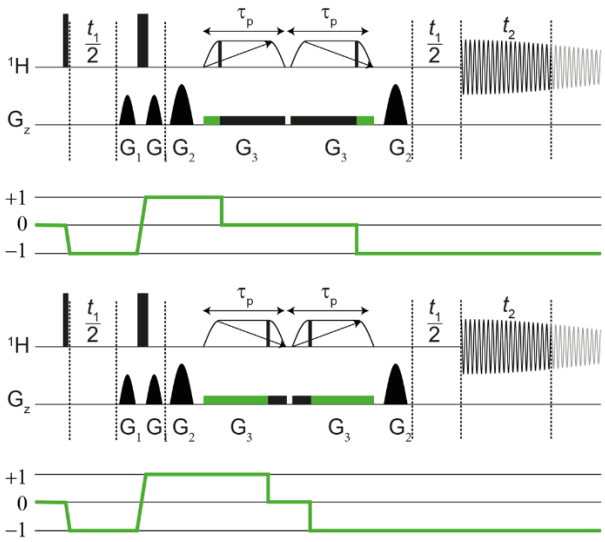

Figure 14 Highlighted Coherence transfer pathways for PSYCHE pulse sequence separated into separate pairs of chirp pulses

This means that the final pulse sequence for 1D ^{1}H PSYCHE experiments, with features detailed above is as follows.

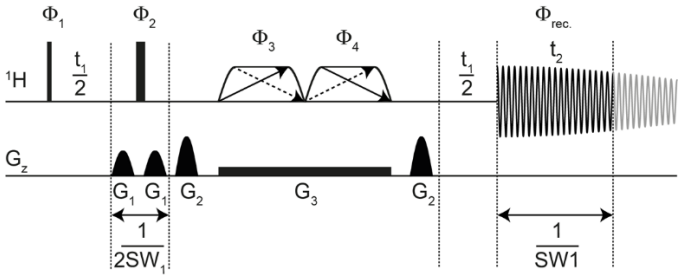

Figure 15 Full PSYCHE pulse sequence

When implementing the PSYCHE pulse sequences it becomes clear that several considerations must be taken to ensure good quality spectra are acquired. These included deciding upon how to compromise between maximizing sensitivity while still minimizing recoupling signals from evolving. The sweep-rate of the pulse, ΔF/τp, needs to be optimised so as to keep spectral purity as high as possible, but prevent misinterpretation through signal loss by relaxation and diffusion effects on spins. For spatial averaging of acquired data, gradient pulses are used, which means that attention needs to be paid to the time, shape and power of gradient, where values should be matched with the set bandwidth of the PSYCHE pulse for highest spectral quality.

1.4.2.4 Application

Pure shift yielded by chirp excitation (PSYCHE) is one of the most extensively used recent 1D ^{1}H pure shift experiments as it has been shown to demonstrate superior sensitivity and artefact suppression when compared to other techniques. Its implementation is also assisted by tutorials on pulse sequence, parameters, processing and optimization given by the founders of the experiment at the University of Manchester NMR methodology group. Its use in complex mixtures has been demonstrated in a variety of studies ranging from organic chemistry applications to materials and metabolomics applications. In organic chemistry the use of PSYCHE has demonstrated an ability to improve the measurement of relaxation times within complex mixtures of organic chemical systems (143). PSYCHE has also been used in the study of soft corals, where comparative studies showed the potential of PSYCHE in materials science compared to classical proton NMR analysis (144).

Further analysis of a geographical materials nature has also been seen in studies where PSYCHE NMR is used in combination with selective excitation filters for improved analysis of waste-water (145). The main area that PSYCHE pulse sequences have been exploited is in the study of metabolomics, including in food quality analysis (146), metabolomics profiling (147) and metabolites (148).

1.4.2.5 PSYCHE-Diffusion NMR

The simple application of PSYCHE has led to its use in conjunction with other NMR techniques including PSYCHE-iTOCSY (Total Correlation SpectroscopY) and PSYCHE-iCOSY (Correlation Spectroscopy). In this study, PSYCHE is combined with the previously introduced DOSY NMR in a method known as PSYCHE-iDOSY (149). PSYCHE-iDOSY is a unique pseudo 3D method involving the combination of a diffusion encoded dimension within the PSYCHE pure shift pulse sequence.

1.4.3 Diffusion Ordered Spectroscopy (DOSY)

The use of DOSY allows for the resolution of compounds through elucidation of their diffusion constants. DOSY is predominantly used in a qualitative manner but has also been shown to give quantitative results through measurement of self-diffusion coefficients. Resolution through diffusion coefficients determination can be correlated with chemical shifts of compounds to give a 2D DOSY spectra. Since all diffusion coefficients of nuclei present in a single molecule will be the same, molecules can be separated from one another in complex mixtures. Alongside mixture separation, measured self-diffusion coefficients can give molecular size information, monomer/dimer status and also encapsulation information through construction of an external calibration curve with normalized diffusion coefficients which takes molecular shape into account (As always though several things must be considered when interpreting the results, including the strength of field gradient in the probe, and the limitations inherent in the application of the Stokes-Einstein equation.

The pulse sequences used in DOSY are built upon a foundation where a pair of gradient pulses effect spins to the effect they are made to precess in one direction during the first gradient pulse followed by a reverse in direction at the second pulse. A non-uniform magnetic field is induced by a "gradient pulse" which creates inhomogeneity linearly along the z direction of the NMR sample. Spins will diffuse at different rates, so spins that diffuse at a greater rate during the set time period, (diffusion delay (D20)), between gradients experience a larger variability in magnetic field to spins that diffuse at a slower rate. This principle means that the intensity of different spins will be refocused at different degrees at the end of the second gradient pulse. This means that the final intensity shown by the NMR signal is affected, with variability in the reduction of individual molecule intensity dependent on diffusion properties. When translating these initial diffusion measurements into quantifiable measurements the diffusion constant of individual molecules (D) correlates to its characteristics. This is achieved through the use of the Stokes-Einstein equation shown below.

Equation 4

$$D = \frac{k_B T}{6\pi\eta R_H}$$

T = Temperature; η = Viscosity; R_H = hydrodynamic radius of the molecule; k_B = Boltzmann constant

Initial DOSY pulse sequences were designed with a spin echo (90-t-180-t-acquire) pulse sequence, where the gradients were used with the same sign. This works as the 180 degree pulse inverts the magnetisation which means that the second gradient refocuses the spins. Modifications were however needed for this experiment as the magnetization decayed with the time constant T2, not T1, which meant that the sensitivity of the experiment was very low. One of the classically used DOSY experiments now is the stimulated echo sequence which makes the magnetization stored along the z-axis, meaning that decay of magnetization is dependent on T1, giving larger signal intensity potential. The addition of a spoil gradient is needed to eliminate magnetization that does not return to the z-axis, therefore T2 effects are ameliorated. Longitudinal Eddy current Delay (LED) sequence DOSY experiments are essentially the same as a STE sequence but they have an additional dephasing of magnetization in the transverse plane which is followed by an additional delay. These additional elements are to allow for dephasing and rephasing of magnetization, with return to the

z direction, with the additional delay allowing for eddy currents, generated by large changes in magnetic field in coil, to decay before magnetization is translated into the transverse plane for acquisition of signal. The addition of a pair of gradient pulses with opposite polarity in lieu of the two individual gradient pulses can refocus static gradient terms, which consequently minimises the effects seen by eddy currents. It must however be considered that if the 180-degree pulse is not perfect, as it usually is through magnetic inhomogeneity, there will be signal left at the end of the sequence that is not diffusion encoded as there will be rephasing of magnetization unaffected by the 180 degree pulse by the second pair of gradient pulses. This is one of the factors of error seen when calculating self-diffusion coefficients as the final signal will have an error term. The use of spoil gradients reduces these effects but not completely, to remove this effect completely sixteen steps of phase cycling for each step would be required in the absence of bipolar gradients as this has been shown to average out the artefacts that present through the rephasing of magnetization.

All the above reasons identify LED sequences with bipolar gradients as the most suitable experiments to use in DOSY acquisitions. This is demonstrated by their ability to deal with gradient eddy currents and imperfections seen in gradient pulses in an inexpensive manner when considering signal to noise as loss of signal is low since the additional delay is milliseconds and T1 is the magnetization determining factor which is in the range of seconds so maximum signal is minimally affected.

When optimizing DOSY pulse sequences, the main parameters to select for target compounds range of self-diffusion coefficients is the duration of time between pulse gradients and the delay between gradients which determines the time that molecules are allowed to diffuse through magnetic inhomogeneity before refocusing (D20; Δ) and the time that pulse gradients that creates the inhomogeneity in the magnetic field are applied (P30; δ). When selecting D20 and P30 values the aim is to see a significant reduction in signal when the gradient power is at 95%, compared to a small reduction in signal when the gradient power is at 5%. If these values are selected

appropriately then the decay curve of signals will be well described throughout the ranges of gradient strengths applied during the experiment and allow for a reduced error when fitting curves to a diffusion coefficient as illustrated in figure 16.

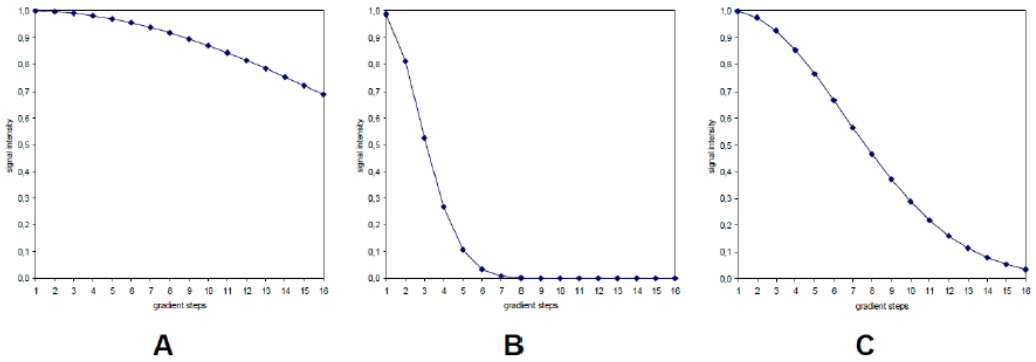

Figure 16 A) in this Δ and δ are too small, B) Δ and δ are too big and in C) Δ and δ are at proper values for sampling across the whole decay curve

Researchers must also be aware that the lock phase is set correctly, improper setting can result in lineshapes which are highly distorted and unphaseable in all gradient experiments. This problem however can be easily resolved through correction of lock phase manually or automatically before acquisition. An issue that is less about pulse design and more an intrinsic problem with the experiment itself is convection effects induced by rapid changes in magnetic fields through turning on and off gradients, which cause uneven temperatures in the samples. To try and avoid convection effects, stabilisation of temperature can be mediated through using a stable gas flow between 400 and 535 L/h in the NMR probe. Also it is crucial that locking onto solvent is stabilised appropriately after rapid switching on and off of gradients.

Translational diffusion of molecules in liquid states is a fundamental property of mass transport *in-vivo* and *in-vitro* mixtures and determines the characteristics of most chemical processes. The ability of NMR to easily measure and exploit the translational diffusion of individual molecular species makes it a powerful tool in the analysis of mixtures and how changes in emulsion properties affect the properties of individual molecular species. This technique was demonstrated as early as 1981 by Peter Stilbs through the assignment of self- diffusion coefficients in complex mixtures using Fourier-transformed pulsed-gradient spin-echo measurements which showed errors in diffusion

coefficients of just a few percent (150). These initial findings demonstrated the possible power of NMR as an analytical tool for separation of molecular species within complex mixtures. This experiment also built the basis for following pulse sequences which exploit the translational diffusion of molecular species through the design of pulse sequence. The most commonly used pulse sequences are described previously, with time where species are exposed to the linearly inhomogeneous magnetic field being different for different molecular species. This means that attenuation profiles for peaks of the same molecular species will match but profiles of different molecular species will be different and therefore give different calculated diffusion coefficients.

The spectra produced through the determination of diffusion coefficients of peaks produces a pseudo-2D spectra that displays diffusion coefficient values against chemical shift values (ppm). The size of the 2D contours in a DOSY spectrum reflects the standard error in the calculation of the diffusion coefficients of respective peaks. In complex mixtures with poorly resolved proton spectrum, the DOSY spectrum can have multiple overlapping signals making separation poor in highly concentrated areas such as the aliphatic region of emulsion mixtures. This means that calculated diffusion coefficients for molecular species will have a larger error as the attenuation profiles will be calculated collectively of the overlapping peaks.

Application of diffusion ordered spectroscopy in complex mixtures has seen recent advances, which make this technique more advantageous and promising for accurate separation of single molecules. These include selective DOSY through the use of excitation sculpting which has been primarily used for water suppression and the more interesting technique of exploiting property changes through the use of diffusography (151). DOSY has also been implemented in the characterization of complex mixtures through the detailing of structures present or formed by diffusing materials within a diverse range of samples and biological systems (152). Importantly to formulation and cell membrane modelling, DOSY has been used to characterize bicelle size and morphology alongside how different mixtures of lipids and detergents interact with one another (153).

1.4.3.1 PSYCHEiDOSY

Since PSYCHE incorporates a stimulated echo in it pulse sequence it was exploited to design PSYCHEiDOSY where the PSYCHE pulse sequence plays a dual role in not only collapsing multiplets but also diffusion encoding the NMR sample. With diffusion encoding being internalized in the PSYCHE pulse sequence with a diffusion delay being inserted between the two saltire pulses and gradients either side of the elements being made incremented. This way of introducing diffusion encoding is superior to concatenating the pure shift sequence with diffusion encoding sequences through an increase in signal as transient number can be higher in a smaller amount of time through absence of a second stimulated echo. It also makes the pulse sequence relatively simple which reduces the chance of pulse imperfections and the requirement for phase cycling. This internal diffusion encoding creates a pseudo-3D experiment where the amplitude of incremented gradients creates a dimension and a third dimension is created by the PSYCHE element with time between gradient pulses being incremented separately. Data acquisition is done in the same way as the PSYCHE experiment through the construction of an interferogram where chunks have a duration of 1/SW1. An interferogram is generated for each increment of the incremented gradient which is processed by a top-spin macro provided by Manchester University. The generated interferograms are then processed via normal 2D processing techniques to form a diffusion coefficient versus chemical shift spectra with coupling suppressed. The pulse sequence is the same as the PSYCHE pulse, however the incremented open half-sine shapes (G_2) indicate gradient levels that are changed to give diffusion encoding.

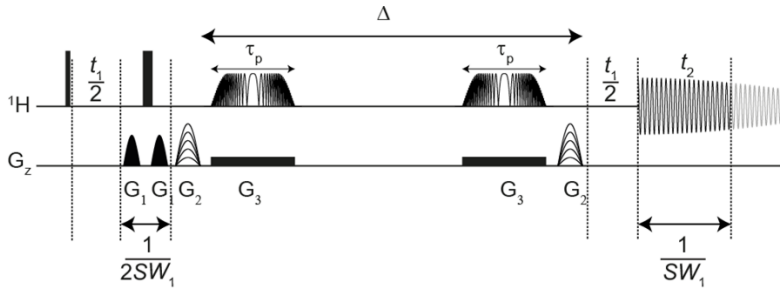

Figure 17 PSYCHEiDOSY pulse sequence

This addition to the pulse sequence requires the Stejskal-Tanner equation used for determination of diffusion coefficients to be modified to account for diffusion encoding within the PSYCHE pulse

element. The corrected equation, once simplified shows a close resemblance to the classic Stejskal-Tanner equation, where the difference is a gradient offset added to the listed diffusion gradients used in setting up the incremented gradients.

$$A\left(g_d^2\right) = \exp\left(-\gamma^2 D\left(g_d + \Delta g\right)^2\left(\Delta - \frac{\delta}{3}\right)\right)$$

$$\Delta g = \frac{\pi\tau_p g_p\left(2\delta - 2\Delta + 4\tau_s + \tau_p\right)}{2\delta\left(\delta - 4\Delta\right)}$$

Figure 18 Modified Stejskal-Tanner equation for Diffusion coefficient determination when using diffusion encoded PSYCHE experiments with added gradient offset in red

The potential of PSYCHEiDOSY in improving diffusion coefficient error is extensive for biological mixture analysis as seen by the below spectra produced in the original paper (149).

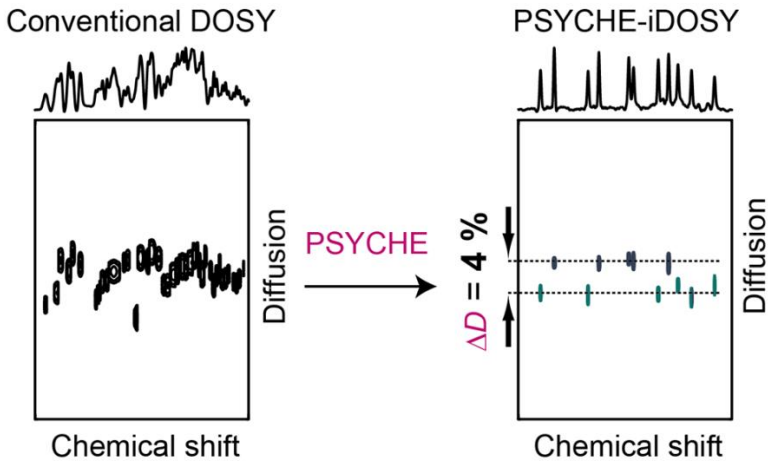

Figure 19 Diffusion resolution differences seen vitamin D3 and provitamin D3 for standard DOSY experiments compared to diffusion encoded PSYCHE experiments (149)

It is yet to be studied extensively in complex mixture analysis as of yet but recently published papers from our group have used this methodology for investigations of a variety of complex mixtures in the field of Chemical Engineering and Dermatology demonstrating the versatility of the technique and relative ease of use between disciplines (Papers in appendix).

1.4.4 Processing methodologies

1.4.4.1 Covariance Processing

Covariance processing provides a measure of the strength of the correlation between two or more sets of random variates within a data matrix. This has been implemented in NMR to produce increased resolution indirect data values for correlation spectroscopy experiments.

Covariance processing for indirect dimension resolution and reducing the required experiment time has been shown to be used in conjunction with PSYCHE methodologies for characterisation of complex mixtures. Interestingly covariance processing has demonstrated the ability to illustrate novel synthetic NMR spectral representations of small molecules through correlation of features of individual spectra in a fast, inexpensive way post acquisition e.g. HSQC-COSY acquisition.

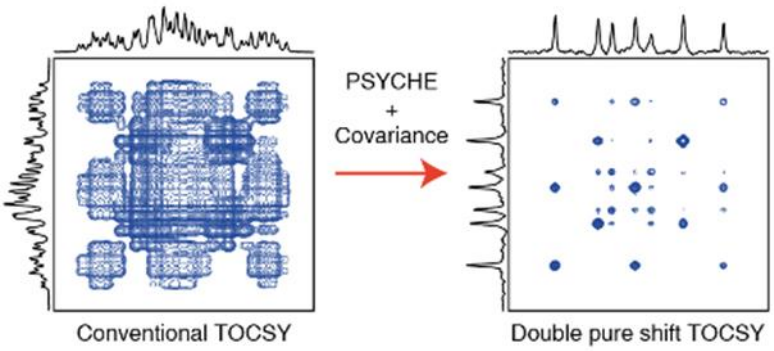

Figure 20 Use of Covariance processing with PSYCHE to acquire greater resolution spectra and improve interpretation of complex samples (154)

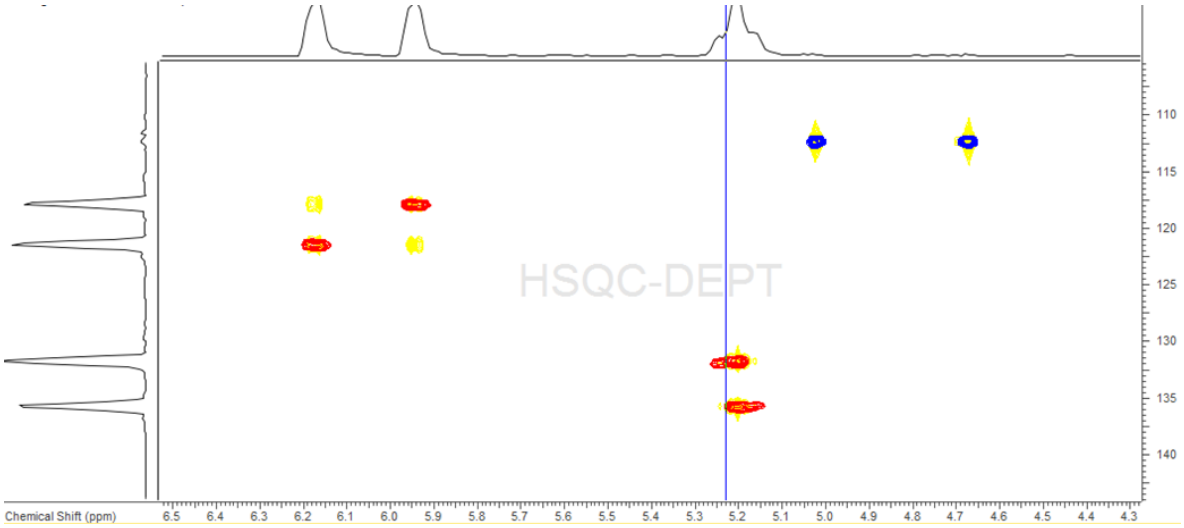

Figure 21 Covariance processing of HSQC and COSY spectra of Vitamin D_2 demonstrating an ability to show correlations between HSQC cross peaks (Red) through calculation from COSY coupling data (Yellow) using Mestrenova.

1.4.4.2 Non-Uniform Sampling (NUS)

Sampling of 2D NMR experiments requires uniform sampling of data in the indirect dimension that allows for processing by discrete Fourier transformation. This number of increments in the f1 and f2 dimension determines the duration of the experiment. Non-uniform sampling aims to reduce the number of data points collected in the indirect dimensions to reduce experiment time. The use of NUS has been driven by the use of 3D experiments in biomolecular NMR but can also be exploited for use in 2D experiments (155) (156). NUS experiments classically acquire a subset of indirect data traces, with usually 50-25% of data points being sampled. This can lead to a time saving of two to four times which allows for increases in sensitivity and resolution of more complex mixtures and acquisition of PSYCHE concatenated experiments in a reasonable time scale.

1.5 Summary

Features probed at the molecular level include bilayer packing, molecular interactions, diffusion rates, permeation of actives and formulation components within the epidermis. One of the most significant developments has been the move from in vitro techniques to ex and in vivo studies and here we aim to investigate how NMR can be utilised to improve sensitivity and resolution of these studies.

The real time characterisation and monitoring of biologically active compounds and formulation components in models and *ex vivo* samples of the *Stratum corneum* is becoming more possible and accessible to researchers. Despite this progress, the lack of *in vivo* studies, limits these methodologies and further studies need to be done. Validation of *in vivo* studies with *in vitro* and *ex vivo* studies using mathematical models helps to develop a deeper understanding of the skin and how formulation design affects the permeation of biologically active compounds and the irritation levels of specific formulation components.

1.5.1 Aims of Research

Skin is the first line barrier that protects the body from infection, attack by chemicals, photochemical effects and physical stimulus. In its defence role the skin produces vitamins,

regulates temperature and has the ability to sense harm and indicate that visually; this constitutes an effective warning mechanism. The physical appearance of skin disorders however, can also be a double-edged sword when it comes to the emotional and social aspects of a visible pathology. In an ever more connected world, the stigma attached to skin disorders is increasing and has led to increased pressure on medicine and industry to produce diagnostic tools and quick remedies to minimise any permanent effects on the individual. The accurate and rapid diagnosis of skin conditions and the evaluation of treatments for specific pathologies is crucial as delays in either of these steps can lead to temporary or permanent disabilities for the individual. This will mean the skin as a barrier can be permanently compromised.

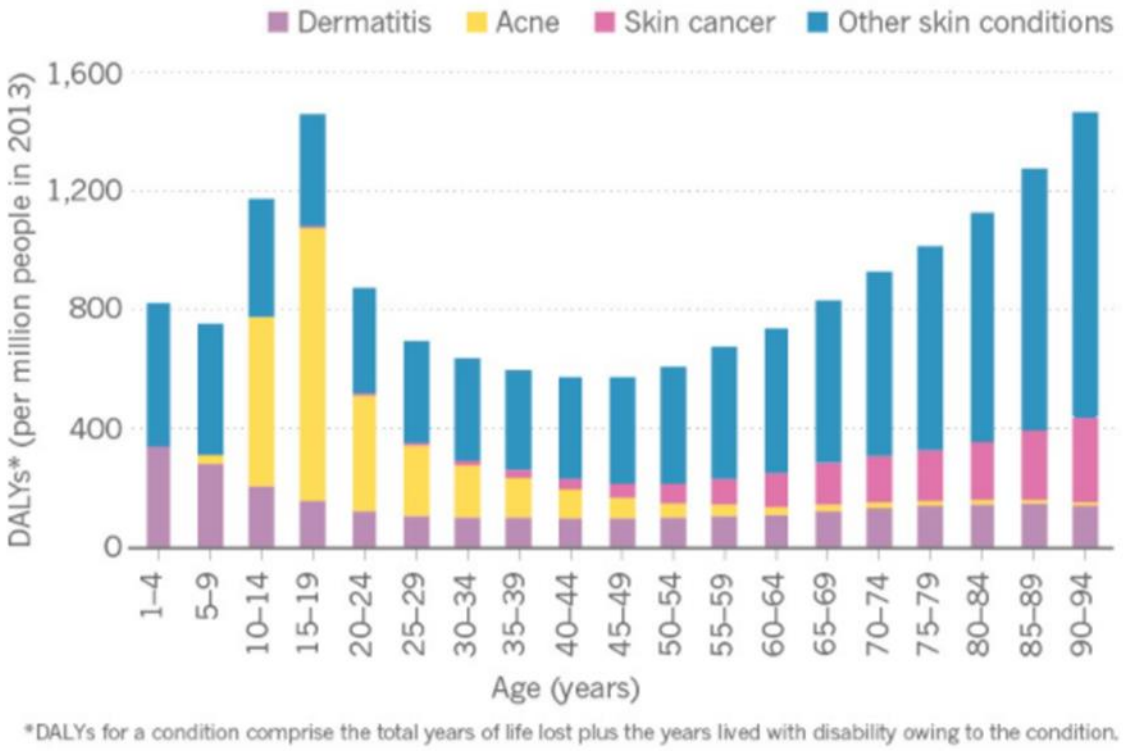

Figure 22 Skin conditions and their relative effects in different age group, measured by the disability-adjusted life year (DALY), which reflects a lost year of healthy life. Figure adapted from Gould J. 2018. Source: Inst. Health Metrics/Univ. Washington (2)

Understanding what compounds enable the correct functioning and maintenance of the skin, be they proteins, peptides, vitamins or small biologically active compounds is important when evaluating skin health and state of any diagnosed disease condition. The determination of the concentrations of these compounds required for optimal skin function can give insight to clinicians, researchers and the general population for skin health and care. If it is known that certain

biomarkers are present at higher levels in the *Stratum corneum,* compared with other layers of the skin, it allows for targeting of these biomarkers with tape strip extraction for evaluation of skin health. Knowing what these biomarkers are and whether they are specific to individuals or groups of people, can improve the specificity and selectivity of diagnostic testing. Alongside this, effectiveness of drug delivery can be enhanced when considering specific biomarkers at targeted locations within the skin.

General understanding of biomarkers within the skin is predicated on reliable quantitative data, produced by the specific analytical technique used for monitoring. When a stimulus is applied to warrant an effect, the incorrect characterisation or quantitation of a compound can lead to false positives or false negatives, which can lead to the misdiagnosis and subsequently improper medical or topical prescription. This would then require the use of further screening methods to identify the underlying problem. These complications can lead to long waiting times and increased cost to the patient and clinic respectively. The most common current diagnostic techniques for many deficiencies, which are relevant for the *Stratum corneum,* are biopsies with histological staining or a blood test, such as for vitamin D deficiency which measures the serum level of 25-hydroxyvitamin D (active form of vitamin D).

1.5.2 Project aims

In this thesis the scope and limitation of NMR methodologies for dermatological analysis will be evaluated. From separation, characterisation and quantitative reliability of actives and formulation components of topical treatments in model cream emulsions to implementation of the determined optimised experimental parameters in real world applications. Once I have successfully shown analysis of model mixtures and real word cream emulsions I aim to evaluate the effectiveness of these creams in a clinical application through analysis of *ex vivo* skin sample tape strip extracts. The versatility of these techniques is also investigated through application to other modalities such as quantitation of actives in commercial formulations, investigation of squalenes role in comeodonegenesis, protocol development for native antimicrobial peptides evaluation and also

highlighting its potential in fields outside of dermatology with work done in a chemical engineering environment on pyrolysis oils. These studies however are beyond the scope of this thesis so are included in the appendix for reader's reference.

The experimental strategy involves the implementation, testing and evaluation of novel techniques previously mentioned for novel use in skin research and whether these techniques can lead innovation in the commercial sphere. Using a variety of techniques this research aims to elucidate molecular interactions in complex mixtures, and provide support pathways for formulation design, reverse engineering, formulation stability and delivery of actives with in-vitro and in-vivo models. The focus will be on qNMR, Diffusion ordered Spectroscopy and the growing area of ultrahigh resolution NMR for these aims while adhering to IUPAC methods as outlined in IUPAC recommendations 2019 (218).

The Industry goals (GSK) of this research are to determine LOD and LOQ of NMR techniques for actives in their commercial products with RSD <1% (Chapter 3). Alongside this primary goal, evaluation of the novel techniques to determine whether actives of interest for their dermatological products can be characterised in-situ without destruction of samples and within a reasonable time scale leading to demonstration of practical applications on topical formulations in the bottle (Appendix 6.2.1), to application on the skin (Chapter 4) with corroboration seen to other gold standard methods currently used in this area such as HPLC and MS-DART for validation of proposed novel NMR techniques in this area. These main aims from GSK were supplemented are supplemented with additional aims to see the scope of our NMR instrumentation for monitoring skin health biomarker squalene (Appendix 6.2.3) and also developing knowledge of antimicrobial peptide interaction for subsequent drug discovery applications and drug delivery platforms (Appendix 6.2.2).

1.5.2.1 NMR

NMR is of particular value as a non-destructive analytical method. Its value as an analytical method is exemplified by its capacity to be used as a primary method for quantification, tolerance of a wide

variety of hydrophilic and hydrophobic elements within a given matrix alongside its large sample throughput by automation (104). In this study steps were taken to attain a trueness level of <10%, repeatability RSD values of <1% and the LOQ down to 100nM (≈ limit of baseline range of Vitamin D_2 and D_3 per litre seen in vivo) (105). To get near this LOQ in complex mixtures some key limitations need to be addressed that are not present in idealised samples. These limitations affect both assignment and quantitation of analytes of interest which may be present at low concentrations compared to formulation components.

1.5.2.2 Mixture Model Analysis

The accurate determination of the respective concentrations of biologically active compounds in the skin is becoming an increasingly important factor in the evaluation of key issues in policy making, health care and cosmetics. The scope and limitations for characterisation and quantitation of two biologically relevant compounds, which are currently garnering great interest in supplementation via dermal delivery mechanisms alongside oral supplementation, Vitamin D_2 (Ergocalciferol) and Vitamin D_3 (Cholecalciferol), in different cream formulations using 1D ^{1}H qNMR, 2D NMR techniques (HSQC and DOSY) and pure shift acquisitions are investigated. When quantifying biologically active compounds in a model system for the *Stratum corneum* or topical creams, the aim is to evaluate the respective solubilities of different biologically active compounds within different formulation mixtures. As Vitamin D is not soluble in polar solvents, it is assumed there is micellation by a surfactant present in the formulation, much like that of ergosterol or cholesterol in the membrane of a cell. Analysis of the solubility of Vitamin D in differing cream formulations can inform how vitamin D is best encapsulated. The characterisation and quantitation of vitamin D is applied over several heterogeneous model formulations with varying composition of elements, thus allowing for analysis of, for example, the dynamic range, complexity and quantitative composition of the different compounds within our mixtures. This allows for subsequent analyse of how different formulations affect the Limits of Detection (LOD) and Limits of Quantitation (LOQ) of smaller analytes (106) (107).

In summary; this investigation needs to be aware of factors which influence the trueness of our results: Solubility, peak integration issues such as resolution (overlapping of signals) and sensitivity (S/N), Dynamic Range (Receiver gain), when quantitatively analysing our samples.

1.5.2.3 Ex vivo skin analysis

These methodologies will then be used to analyse tape strips used for ex vivo extraction of skin with topical application of Physiogel Hypoallergenic Calming Relief A.I. Body Lotion (AI), Physiogel Hypoallergenic Daily Moisture Therapy Body Lotion (P), Bluewater vehicle formulation excluding lower abundance actives (V), Bluewater formulation (BW) and Bluewater formulation with skin heated to 70 degrees Celsius before tape stripping (BW70). 12 tape strips per treatment group will be acquired to avoid extraction of nucleated cells, which would cause greater ethical concerns and be less indicative of the horny layer of the skin. With the knowledge of furrows in the skin and expected variability between individual layers due to skin furrows, grouping of tape strip extractions into 3 groups, from extraction 1-4, 5-8, and 9-12 is done. The aim is to acquire data on the NMF abundances of the skin using the semi-automated metabolite quantitation software Chenomx^{tm} and calculate permeation profiles of formulation components using NMR methodology employed in previous model formulations and formulations from the bottle. Statistical analysis is then used to elucidate whether formulation permeation and abundance of certain components in skin tape extracts is affected by formulation design and application design. How individual or groups of formulation compounds may affect the variability of other topical components and/or NMF abundances in the skin is also investigated. Subsequent determination of how the results seen corroborate with previous findings on the skin will allow us to evaluate reliability and comment on the potential of NMR as an adjunct or replacement to other more commonly used dermatological methodologies.

1.5.3 The impact it will have on skin research

In this project, biologically active compounds in the *Stratum corneum* are investigated using novel NMR techniques. This will allow for determination of the strengths and limitations of validated NMR

techniques in complex *Stratum corneum* models with concentrations of key compounds at *in vivo* ranges from µM to nM concentrations. The limitations expected will include the limit of detection and quantitation of these techniques as the sensitivity of NMR is less than ideal for these models, unless many scans are run (n >1024). A further complication is resolution of unseparated and unpurified formulations, e.g. Metabolite mixtures, where many different compounds have a large dynamic range and overlapping signals. There are also limitations seen with 2D NMR sensitivity, despite its ability to improve the resolution of spectra, required to characterise key peaks in a complex model mixture. For 2D techniques, which require a multiple of the number of scans depending on the number of transients in the indirect dimension that is added, take a lot more time to acquire which means that increasing the scan number is a less favourable option for overcoming sensitivity issues when analysing complex mixtures as experiment time will become untenable. The implementation of novel ultra-fast 2D scans using NMR pulse sequences which allow an increase in scan number with an acceptable increase in acquisition time has been investigated to attempt to remedy this limitation (108). Determination of factors that increase the LOD and LOQ with novel techniques is a major contribution to the validation of NMR in characterisation and quantitation of complex mixtures with large dynamic ranges of abundances.

The real impact will however be shown the presentation of a novel proof of concept tape strip extraction method used in conjunction with NMR analysis on ex-vivo human skin samples which has not been observed in the literature up to 2020. The analysis will also bring together diffusion NMR to separate biological mixtures based on respective compound tumbling properties and subsequent generation of permeation profiles of multiple bioactive compounds from several topically applied treatments all from one instrument using automated acquisition of data. Partner this with semi-automatic characterisation and quantitation of NMFs using Chenomx™ and Statistical analysis (PCA) of tape strips and the potential of NMR for this application seen.

The novelty of this work is clearly demonstrated through NMR spectrometry not being used before to measure biologically active compounds from in-vivo tissue and this study demonstrates the great potential of these techniques for improving diagnostic speed and specificity for biomarkers relevant to understanding dermatological health.

Chapter 2 Materials and Methods

2.1 Vitamin D_2, D_3 and cream formulation analysis

2.1.1 Sample preparation

The compounds used for this project were all ordered through SIGMA and provided by GSK. Quantification targets: Vitamin D_2 (Cas Number: 50-14-6); Vitamin D_3 (Cas number: 67-97-0) ordered from SIGMA ALDRICH. Cream formulation componenets: Glycerol (CAS number: 56-81-5); Caprylic triglyceride (CAS number: 73398-61-5); Isostearyl Isoterate (CAS number: 41669-36-1); Niacinamide (CAS number: 98-92-0); Phospholipon (CAS number 92128-87-5); Vegetable Oil/Corn Oil (CAS number: 8001-30-7); Panthenol (CAS number: 81-13-0); Pentylene Glycol (CAS number: 111-29-5) provided by GSK.

Sample preparation was done using VWR pipettes (2-20µL, 20-200µL and 100-1000µL) for liquid state mass measurements, alongside a Mettler MT5 used for solid state mass measurements.

To prevent the observed separation of more lipophilic compounds from hydrophilic compounds that are included in the formulation a high shear mixer was employed for emulsification of all samples

2.1.2 NMR

NMR tubes used were Wilmad 5mm, thin-walled tubes (Product No: 535-pp-7); throughout the experiments run during the project. Only one NMR instrument, Bruker Avance III 600MHz FT-NMR, will be used throughout the project, so as to not add variance, introduced due to inter instrument inhomogeneity for validation. This however does limit the work in measurements of reproducibility on different instruments but for this stage of optimisation we did want confuse power level settings etc in the parameter sets that can be automatically optimised on different instruments. An example of this was from implementation of University of Manchester experiment parameters that had to be extensively optimised for use on our instrument despite same magnetic power (600MHz). This changes included shape pulse lengths and powers, pulse program delays and the gradients that are used for specific broadband acquisitions, specifically in pure shift acquisitions. Each sample was run

in triplicate to allow for repeatability analysis. All scans were run in batch automation, interleaved to prevent the effects from time dependence of each sample.

Quantitation was done through the primary ratio method analysis of integrals. Internal standard, TSP, with concentration set relative to that of the gravimetrically determined concentration of the target analyte Vitamin $D_{2/3}$. LOQ is when the required S/N for quantitation is no longer achieved in an idealised, separated sample, where reported values for this range from 15 to 150 S/N values, the value set as limit for S/N to determine if LOQ has been reached is 50 as this was predominantly used in previous studies (107)(157)(158).

Top-Spin was used for assignment of peaks (1D ^{1}H, COSY and HSQC) to identify which peak is best for integral selection when running integration. Automation of the quantitation process was done on the software plugin qNMR for MestReNova.

2.1.3 Statistics

Statistical analysis is automatically done by MestReNova to give RSD values for each sample; however these values were added to excel for further statistical interpretation: repeat sample variation; inter sample variation, in regards to sample complexity, analyte concentration and experimental parameter variation.

A Cole-Parmer LabGEN high shear homogenizer (UY-04727-89) was used to prepare the full cream formulations to allow for emulsification of the different components within the mixture.

2.1.4 Fatty acid

All seven fatty acid compositions (Lauric Acid, Myristic Acid, Caprylic Acid, Capric Acid, Caproic Acid, Palmitic Acid and Stearic Acid) were purchased from Fisher-Scientific (Loughborough UK). Deuterated chloroform containing 0.03 % (v/v) TMS of analytical grade, 99% purity purchased from Sigma-Aldrich (Dorset, UK).

All seven single sample analysis were prepared up to 100mM of sample dissolved with 1ml of $CDCL_3$ with 0.1ml added to 0.9ml of deuterated chloroform. 0.6mL of sample was transferred into 5mm NMR tube for acquisition. Two component mixtures were prepared by dissolving 2mg/µl in 1ml of $CDCl_3$ in separate 5ml vials, 0.05ml from each was extracted into 0.9ml $CDCl_3$ to make up 100mM of total fatty acid. Preparation of three fatty acid samples was achieved through addition of 32µl of each fatty acid into 1ml of $CDCl_3$. For complete mixtures with 6 and 7 compounds, samples were made up in CDCl3 with a final fatty acid concentration of 100mM.

2.2 Ex vivo skin analysis

2.2.1 General

Volumetric measurements were done using VWR single-channel pipettes, mechanical, variable volume, Ergonomic High Performance (EHP). A Mettler MT5 scale was used for solid state mass measurements.

2.2.2 Tape Stripping

Normal human skin samples were collected by Genoskin from donors who underwent abdominoplasty procedures and had given informed consent. Pathological skin biopsy was obtained by Genoskin for unused material from dermatology department of hospital with informed consent of the patient. Full ethical approval for the study protocol was obtained from local research ethics committee, and authorization given from the French Ministry of Research (AC-2011-1443) following Human Tissue Authority codes and practices for research on excised anucleated tissue samples for transport, storage and use. All studies were conducted according to the Declaration of Helsinki protocols. The experiments in this study were conducted on samples collected from a single donor women aged 42 years. Skin samples were collected immediately after surgery and processed immediately as nativeskin®. Upon receipt of the nativeskin®, the culture dish was incubated for at least 1 hour at 37 °C, 5 % CO_2, and 95% relative humidity before performing the first experiment. Skin samples were subsequently separated into 6 groups and treated respectively; Native skin with

no topical treatment applied (Ctrl), Physiogel AI lipid formulation (AI), Physiogel formulaton (P), BlueWater formulation vehicle (V), BlueWater formulation (BW) and BlueWater formulation heat treated at 70C^{o} (BW70). The skin was gently cleaned by swabbing with a cotton pad soaked in distilled water at ambient temperature and allowed to dry at room temperature. Skin sites are marked with a surgical marker to ensure tapes were consistently applied to the same area. Twelve consecutive standard D-Squame® tapes were taken from each nativeskin® sample. A standardised pressure device was used to apply 225 g cm-2 of pressure for 5s. Tapes were subsequently removed by a single rapid stroke. Tapes were stored in Eppendorf vials at -80^{o}C until further analysis (4). SquameScan® densitometer was used to measure the total protein content present within the tape strip.

2.2.3 Extraction

The tapes, alongside native deuterated PBS buffer as control, were sonicated in a solution of deuterated PBS buffer 0.1mM, pH5.5 for a minimum of 10 minutes in order to remove 85-90% of total protein from the tape strip. Low rpm centrifugation removes any cell debris from supernatant containing proteins, peptides and active compounds of cells and extracellular matrix.

2.2.4 NMR

A Bruker Avance III 600MHz FT-NMR Spectrometer at 300 K was used for all NMR acquisitions. NMR tubes used were 5 mm, Ultra-Thin Wall Precision NMR Sample Tubes 7" L, 600MHz, (545-PPT-7), from GPE-Scientific. Extracted deuterated PBS supernatant was added to NMR tube at a volume of 594µL, followed by the addition of 6µL TSP D_2O solution (10mM). TopSpin 3.5pl7 was used for acquisition preparation and processing of raw data. Quantitative data was acquired with the pulse program noesygppr1d, with a scan number of 1024. D1 = 4-10s after initial T1 relaxation experiments. Automatic Fourier transformation, phasing and baseline correction were applied followed by manual phase correction and manual integration of peaks with bias and slope manually corrected.

Quantitation was achieved through the use of the primary ratio method of integrals with an internal standard being spiked in samples, Trimethylsilylpropanoic acid (TSP), at a consistent concentration (100µM). Triplicate and interleaved experiments for each sample were acquired.

DOSY D20 and P30 values were calibrated through the acquisition of 1D experiments (ledbpgppr1d). Pulse sequence ledbpgppr2s was used with ns=64, d1 = 5s, D20 = 0.1s and P30 = 0.75ms, with 16 transients in the diffusion dimension (F1) for acquisition of 2D DOSY spectra. The software package Dynamics centre (Bruker UK Ltd) was used to determine the diffusion coefficients using the diffusion fit function (f(g)=I0*e-y^2*g^2*δ^2*(Δ-δ/3)*D).

2.2.5 Data Analysis

12 sample data sets for each treatment were used (Physiogel, Physiogel AI, BlueWater, BlueWater 70^{o} and BlueWater Vehicle) with 8 control samples, where no topical treatment was applied, were extracted. Controls were used to evaluate whether formulation had effects on extraction of uniform layers and first 4 samples were used for optimisation of extraction therefore only 8 samples that were extracted in the same way as treatments were analysed.

Tape strip samples were subsequently grouped into layers 1-4, 5-8 and 9-12 (Group 1, 2 and 3 respectively) to mitigate effects previously seen from skin furrows and variability in number of corneocytes extracted per layer of stratum corneum.

2.2.6 Chenomx^{tm}

Metabolite detection software ChenomxTMused to identify and quantify compounds through reference spectral database fitting of database spectra to acquired spectra for databased compounds(11).

The use of reference deconvolution as the fitting algorithm allows for overlapped peaks to be distinguished, matching to Spectral Reference Libraries which allows for subsequent identification

and quantitation of compounds visible in aqueous samples. The Spectral Reference libraries are built upon thousands of reference spectra acquired via single compound NMR analysis and are available from pH4 to pH 9. Alongside their own libraries, libraries can be imported for use from the HMDB however these libraries are not certified but can be used for characterisation from reference deconvolution.

2.2.7 Statistical Analysis

Statistical analysis was performed using Unscrambler X. Grouped NMF data averages were input into 11x15 matrix and normalised with area normalisation. The Principal component analysis model has a maximum of 7 components with mean centred data. Each variable was weighted equally with cross validation and calculated using the singular value decomposition (SVD) algorithm. Model warnings were set with ratio of calibrated to validated residual variance of 0.5, validated to calibrated residual variance of 0.75 and residual variance increase limit of 6%. Outlier limits were set with warnings at >5% and alarms at 0.5% F-residuals and hotelling T2. PCA overviews were produced displaying PC-1 against PC-2 with explained variance up to 95%.

Chapter 3 Characterisation and quantitation of Vitamin D_2/D_3

3.1 Importance of Vitamin D in the *Stratum corneum*

The effects of vitamin D deficiency have been highlighted since the turn of the 20th century. Decreased sun exposure through pollution and mass movement to industrial cities led to the rickets epidemic in industrialised western countries. At the height of the industrial revolution it was estimated that 80-90% of children in certain industrial cities suffered from rickets (162). The main reason that the deficiency of Vitamin D got to this point in the industrial revolution was through the lack of vitamin D synthesis in the skin due to insufficient photo-production.

The photo-production of Vitamin D takes place in the skin. Once in the epidermis, it diffuses to the dermal capillary bed, where it is transported to the liver by the vitamin D binding protein (163) (164). Sufficient UVB proton (255-350nm) levels, to produce Vitamin D_3 in the skin are only available during a small portion of the day. Absorption of UVB by ozone in the Earth's stratosphere, which varies depending on latitude, decreases the amount of UVB that the skin is exposed to. Compounding this fact is that the relationship between skin cancer and sun exposure has inadvertently caused a large decrease in Vitamin D production because of UVB being absorbed by sun screens and sun exposure being generally avoided. There is also a large effect from the effects of skin pigmentation, which leads to a much greater incident rate of vitamin D deficiency in dark skinned people living in higher latitudes as a Sun Protection Factor (SPF) of 15 will absorb 99% of UVB, therefore the natural melanin SPF of dark skinned people of 13.4 will reduce Vitamin D production compared to light skinned people with natural SPF of 3.4 (165) (166) (167) Ageing has also been shown to decrease the amount of 7-dehydrocholesterol in the skin (168).

This means that a large number of people do not have sufficient levels of the active form of vitamin D; 1,25-(OH)2D (>75nmol/L) for all the physiological functions of 1,25-(OH)2D to function appropriately.1,25-(OH)2D has been demonstrated to have a role in the regulation of skin differentiation, apoptosis and inhibition of cell proliferation (169) (170). In the skin specifically it has been found to regulate the formation of the skin barrier through processing of long chain glycosylceramides. Furthermore, it has an induction effect on Toll like receptor 2 and its co-receptor

CDl4 which initiates the innate immune response in the skin which induces CYP27B1 and cathelicidin production (171) (172). Furthermore the induction of cathelicidin (LL-37) production by 1,25-(OH)2D highlights another role of vitamin D in facilitating wound healing and tissue repair.. Unfortunately studies on whether topical administration of Vitamin D or its analogues can improve wound healing or tissue repair are yet to be widely produced. Studies on Vitamin D have also suggested roles in mental disorders, infections, autoimmune diseases, cancer, malabsorption, liver disorders, obesity, lung function and innate immunity but these are in the early stage of understanding with more research required to underpin methods of action (173).

In the advent of studies linking Vitamin D, its active metabolites and respective receptors to roles other than the formation and health of bone osteoclasts, there has been a new wave of health policy developments informed by these findings. From population based projects, such as in Finland which successfully raised the average Vitamin D levels to around 65nmol/l over a ten year program from mandatory fortification of dairy products in 2003 followed by a further increase in fortification and advisement of supplementation in 2007 which doubled vitamin D levels between 2007 and 2012 (174), to recommendations for broad nutritional policy (175), and specific nutrition guidance for Performance Athletes (176); and Older adults (177).

With more awareness of the detrimental effects of Vitamin D deficiency it is more important than ever to be able to correctly diagnose the estimated 1 Billion people worldwide who are deficient in Vitamin D.

3.1.1 Scope and Limitation of Vitamin D quantitation using NMR techniques

Validated novel qNMR techniques can be used to diagnose Vitamin D deficiency at a faster sample rate than other methods, due to easy sample preparation and relatively fast measurement of all analytes of interest at detectable concentrations (178). Because of the non-destructive and simple sample preparation of NMR, samples can be prepared which mimic the composition of the *Stratum*

corneum extracellular matrix capillary beds which vitamin D_3 diffuses to in the skin (179) (180). Alongside this it is shown that the LOD and LOQ for Vitamin D_2 and D_3 down to in vivo skin levels can be achieved with the implemented NMR techniques.

Alongside this characterisation of Vitamin D formulation using these techniques helps the innovation of consumer healthcare companies specifically on how they provide dermal delivery of Vitamin D for direct supplementation to the skin. Accurate determination of amount that can be delivered effectively, stability in bottle and how much is delivered to layers of the skin is therefore crucial for formulation chemists and manufacturers of consumer health products.

First experiments were run with controls of Vitamin D_2 and D_3 were run independently of cream formulation samples for assignment and determining the maximum potential LOD and LOQ. The cream formulation samples include simple mixtures, of only one or two of the cream formulation compounds which showed encapsulation potential and more complex mixtures which consist of all cream formulation components with blank controls of each included. This was to ensure the integrals being quantified are not that of artefacts, or peaks of the cream formulations that the vitamin D is being prepared in. Samples were also prepared in different NMR solvents e.g. D_2O and DMSO-d6, so that any effects of the solvent system can be determined. The data of samples in cream formulations ranging from simple mixtures to complex mixtures have been acquired, alongside relevant controls and a range of Vitamin D concentrations from 10mM to 100nM with concentration changes in increments of a dilution factor of 10. Data-sets with Experimental variation have also been acquired to analyse the effects upon our datasets: Number of scans (ns); Receiver Gain (RG); 1D and 2D techniques and Pure-shift techniques. A lower LOD and LOQ through implementation of novel NMR sequences and calibration of experimental parameters for resolution and sensitivity enhancement can be reached. More complex sample preparation methods are also implemented to allow for greater solubility of target analyte in cream samples.

3.2 Results

3.2.1 Assignment of Vitamin D_2 and D_3

The first step in analysing how reliable quantitation of Vitamin D2 and D3 in samples is to fully characterise Vitamin D2 and D3 by NMR . This was achieved with 10mM Vitamin D2 and D3 dissolved in DMSO-d6 and acquisition of 1D 1H proton experiments with large D1 values were acquired so that all peaks were relaxed appropriately before acquisition of subsequent transients of data.

These spectra were then assigned in comparison to the vitamin D2 and D3 spectra from the HMDB. The assignment reported by HMDB (181) is accurate and useful however some of the

multipletsidentified are assigned to more than one proton in the structure through overlapping of multiplet peaks.

This makes it harder to identify derivative changes and possible breakdown products once in a topical formulation or in a biological mixture. To improve characterization the acquisition

3.2.1.1 1D Proton Experiments

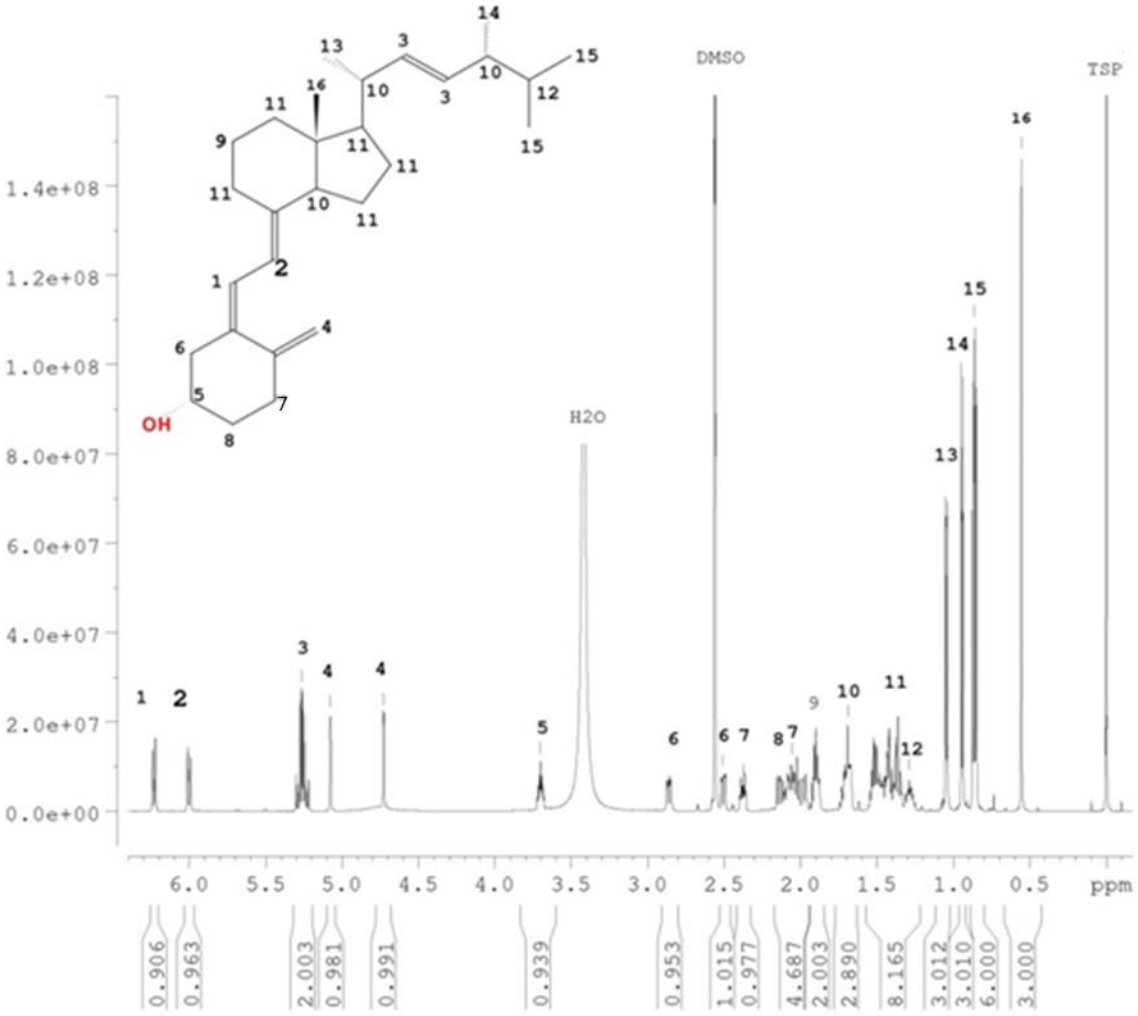

Figure 23 1D Proton, 256 scan spectra of D_2 10mM, with Vitamin D_2 and solvent peaks assigned as best as resolution allows.

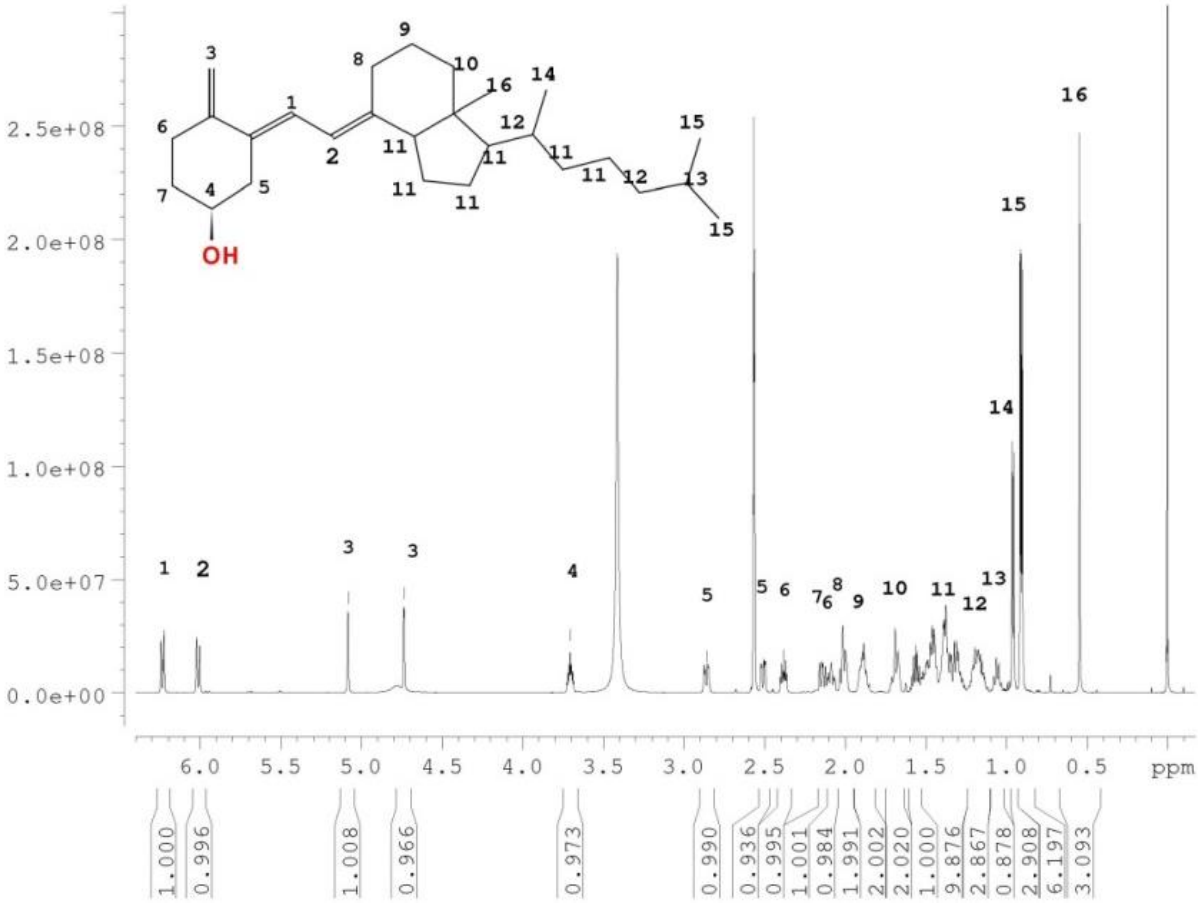

Figure 24 1D Proton, 256 scan spectra, Vitamin D_3 peaks assigned, solvent peaks of HDO (3.33ppm) and DMSO (2.5ppm) left unlabelled

The spectra of D_2 and D_3 corroborated the previous assignments in the human metabolome database and also assigned the spectra for D_3 which has very slight changes to that of the D_2 spectra but there is a clear difference seen at the peak assigned 3 in the D_2 spectra which is not seen for D_3 representing the addition of an alkene group to D_2. This differentiation will greatly facilitate the use of NMR in determining ratios of D_2 and D_3 in mixtures.

3.2.1.2 HSQC experiments for C13 and H1 assignment

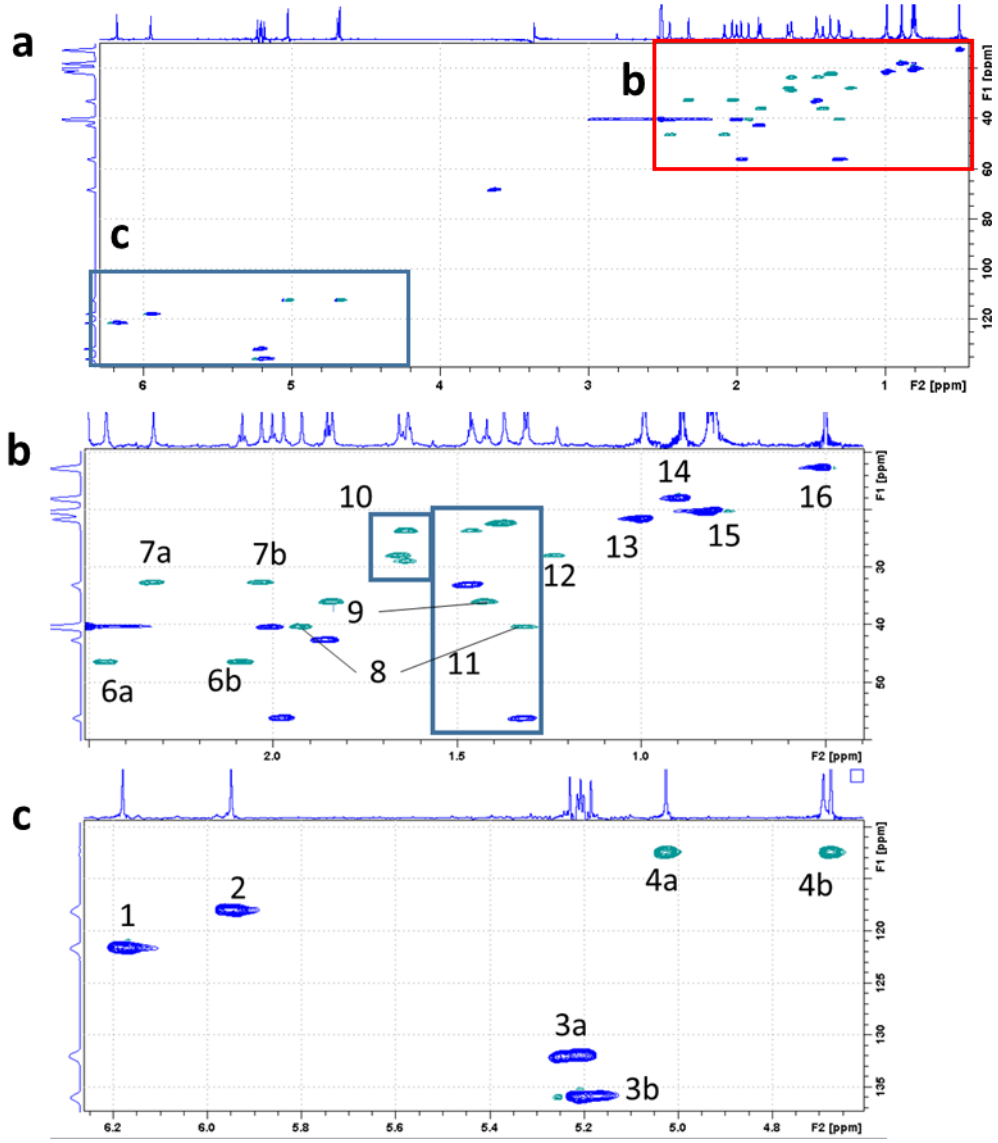

Figure 25 Vitamin D_2 10mM HSQC covering whole range of chemical shifts, a = whole HSQC spectral range for D_2, b = Aliphatic region of HSQC of D_2, c = zoomed in region from 4.6 to 6.2ppm of HSQC for D_2

Exploiting the transition into the second dimension through acquisition of HSQC spectra shows cross peaks correlating ^{13}C signals to ^{1}H signals. This allowed for further assignment of peaks that were overlapping and also shows that several peaks which shared ^{13}C resonances were protons in CH_2 aliphatic forms. HSQC experiments are however a lot more time expensive than proton experiments but since coherence is transferred back to the proton the sensitivity is acceptable. To gain the same assignment potential, a pure shift methodology is demonstrated that exploits proton acquisition but reduces overlap by multiplet suppression and includes proton peaks from amines, alcohols, carbonyls and phosphates etc. that are not bonded to carbon which is very useful particularly in biological mixture applications.

3.2.1.3 PSYCHE experiment implantation on instrument and optimization of settings

The most problematic artefacts seen during initial implementation of PSYCHE pulse sequence came from the water, however the addition of excitation sculpting elements to the pulse sequence reduced these. Artefacts were also observed from strong coupling effects, which can be reduced by the triple-spin-echo version of the sequence however these artefacts were quite small for acquired data sets. The default shapes for the parameter set were 10kHz sweep pulses of 40ms length (low->high and high->low frequency sweep). This means an additional 80ms delay in the sequence, which could cause T2 losses. Changing these to 20ms equivalents and P52 and P53 (Weak gradient and double-chirp PSYCHE pulse element durations) set to 20ms, and CNST51 (rf field for the shapes) to 630 reduced the T2 losses. After acquisition and processing of initial PSYCHE experiments severe artefacts were observed which prevented interpretation of spectra. These artefacts were identified as chunking artefacts that appeared for signals off resonance to the center of acquisition. Modification of sweep width and chunk sweep width to make the number of chunks a whole integer removed these effects as shown in figure 28.

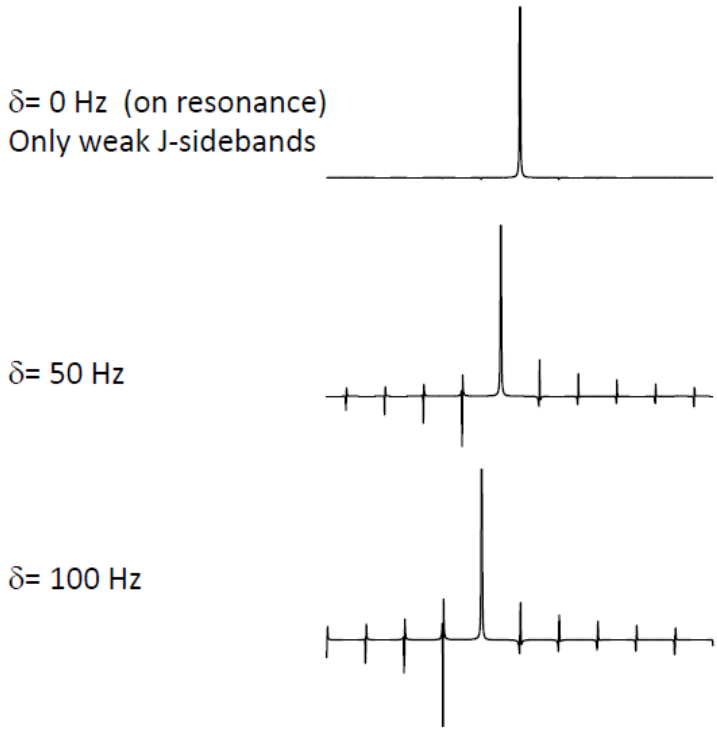

Figure 26 Visualisation of chunking artefacts at different resonance frequencies, adapted from University of Manchester Pure Shift workshop (https://www.nmr.chemistry.manchester.ac.uk/?q=node/421)

It is observed in figure 26 where sweep width has not been optimised that large artefacts appear at a greater intensity for peaks which are more off resonance to the centre of acquisition.

	F2	F1
Sw (ppm)	20.57	0.125
Sw (Hz)	8223.69	50

Figure 27 (Top) PSYCHE Spectra with chunking artefact (Middle) Zoomed in Spectra at 0ppm (Bottom) Sw2 and Sw1 values for experiment showing non whole integer difference between F1 and F2 sweep width which causes chunking artefacts

The total sweep width frequency in the direct dimension / total sweep width in the indirect dimensionequals 164.4737 which is not a whole integer therefore it is expected that artefacts are created. After correction of this to make SWH2/SWH1 a whole integer a pure shift spectra with no chunking artefacts is produced with no other effects seen.

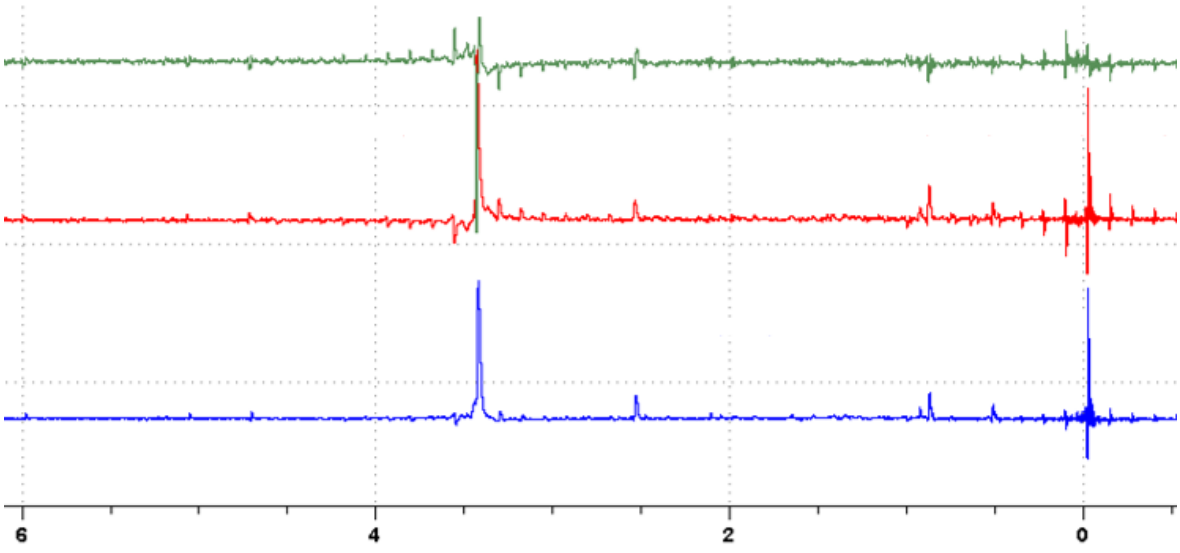

Figure 28 (Blue) Corrected Sw2/Sw1 PSYCHE spectra, (Red) Non-corrected PSYCHE Spectra with chunking artefacts present (Green) Difference Spectra between corrected and non-corrected spectra showing only chunking artefacts are removed and not signal

The difference spectra in figure 28 highlights that the only peaks that are changed are the chunking artefacts with pure shift peaks unaffected. This showed how crucial the proper setting of acquisitions are for artefact suppression.

An optimised PSYCHE experiment which uses a triple spin echo to reduce coupling artefacts for strong coupling binds which can improve the pure shift spectra acquired. However using the acquisition parameters for PSYCHE the chunking artefacts arose again even with SWH2/SWH1 optimised to make a whole integer for number of chunks in the whole sw.

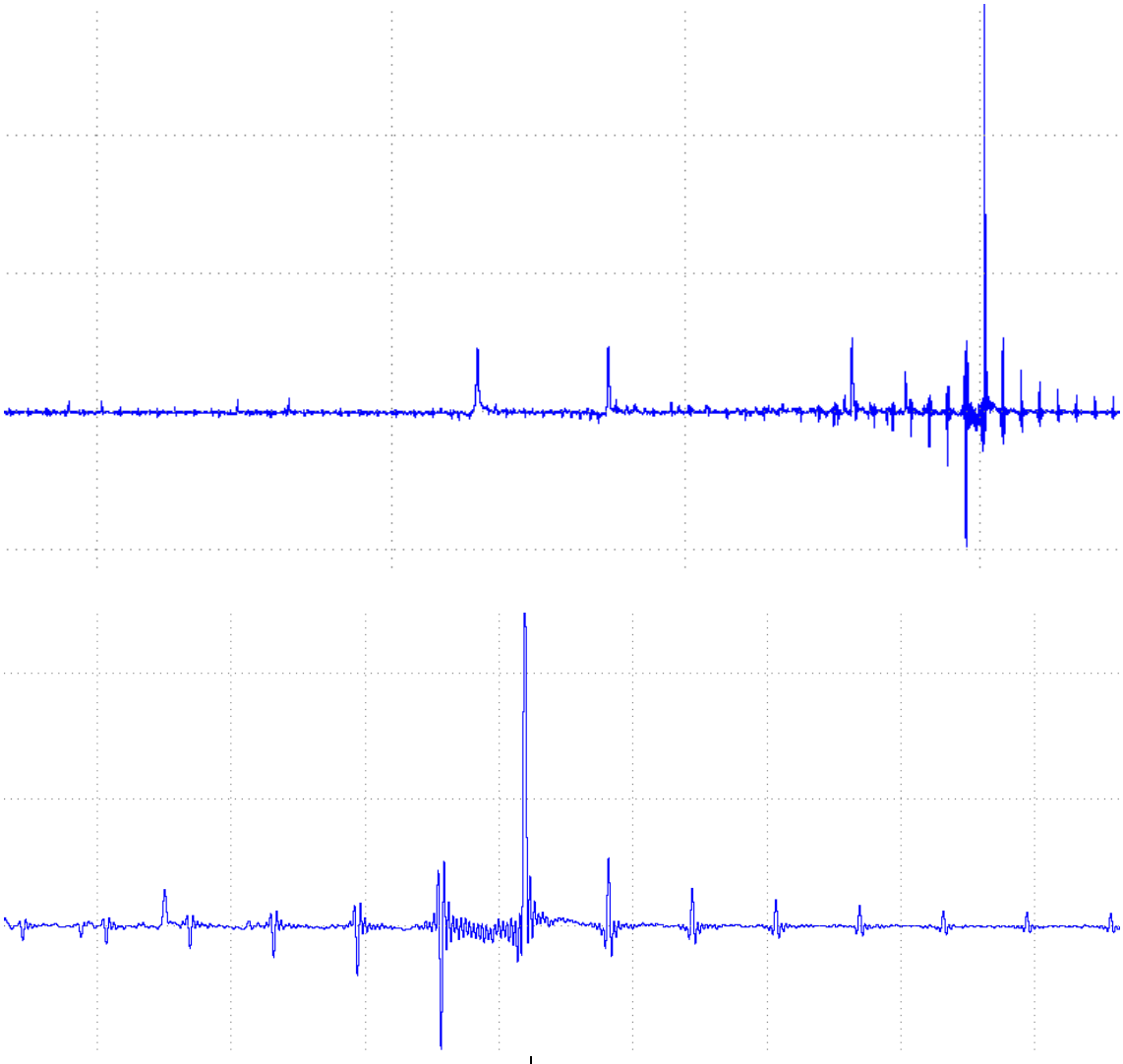

	F1	F2
Sw (ppm)	9.99	0.13
Sw (Hz)	3996.80	50

Figure 29 (Top) PSYCHE-tse (Triple spin echo) Spectra with chunking artefact (Middle) Zoomed in Spectra at 0ppm (Bottom) Sw2 and Sw1 values for experiment.

3996.802/50 = 79.93604, already very close to integer, negligible change in chunking artefact expected. These scans were then repeated with the total sweep width frequency in the direct dimension / total sweep width in the indirect dimension being set to an integer.

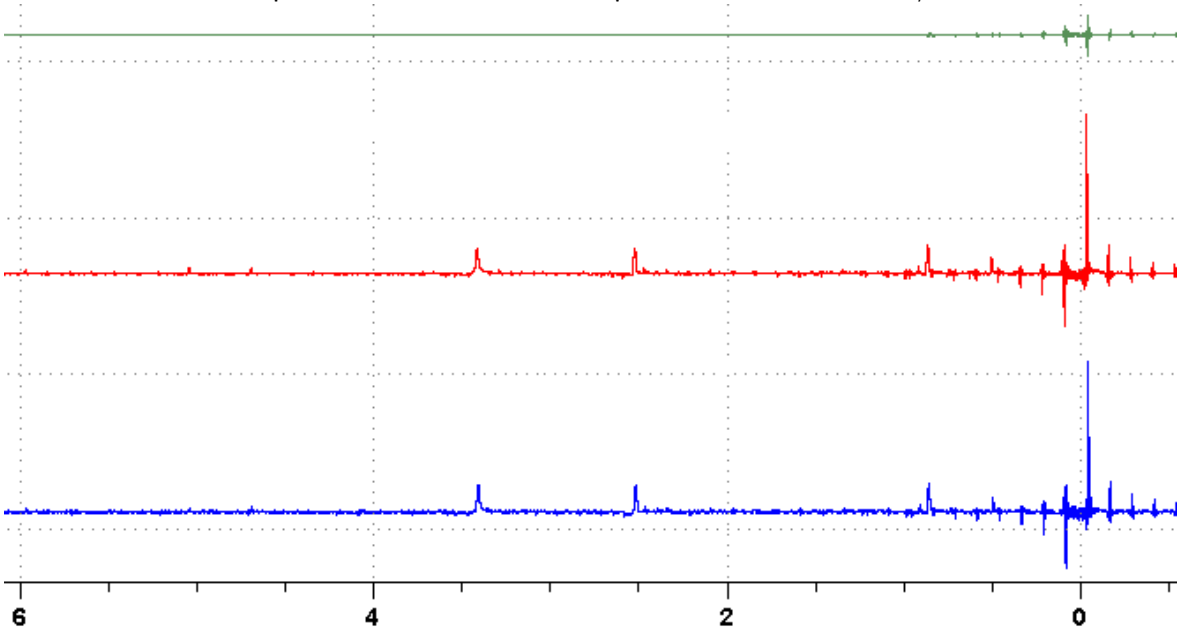

Figure 30 (Blue) Corrected Sw2/Sw1 PSYCHE spectra, (Red) Non-corrected PSYCHE Spectra (Green) Difference Spectra between corrected and non-corrected spectra

Negligible differences are seen for spectra with correction of SWH2/SWH1 compared to non-corrected spectra for PSYCHE-TSE as highlighted by the difference spectra in figure 30. This means that the chunking artefacts observed are being created through a different parameter set issue which needs to be investigated further.

Due to substantial resolution and spectra quality improvements already given by standard PSYCHE acquisitions, it was decided to use standard PSYCHE acquisition rather than employ PSYCHE TSE due the latter's more complicated pulse sequence design not being suitable for use by non-NMR specialists in future applications.

3.2.1.4 Drop point distortion analysis

Inclusion of drop points (deleted data points at start of acquired FID) has been shown to be necessary as modern digital filtering methods distort the first points of a FID. When acquiring multiple FIDs in interferogram acquisitions which are combined to form a complete FID, the artefacts added from distorted data points at the beginning of each fid are much greater as highlighted in figure 31.

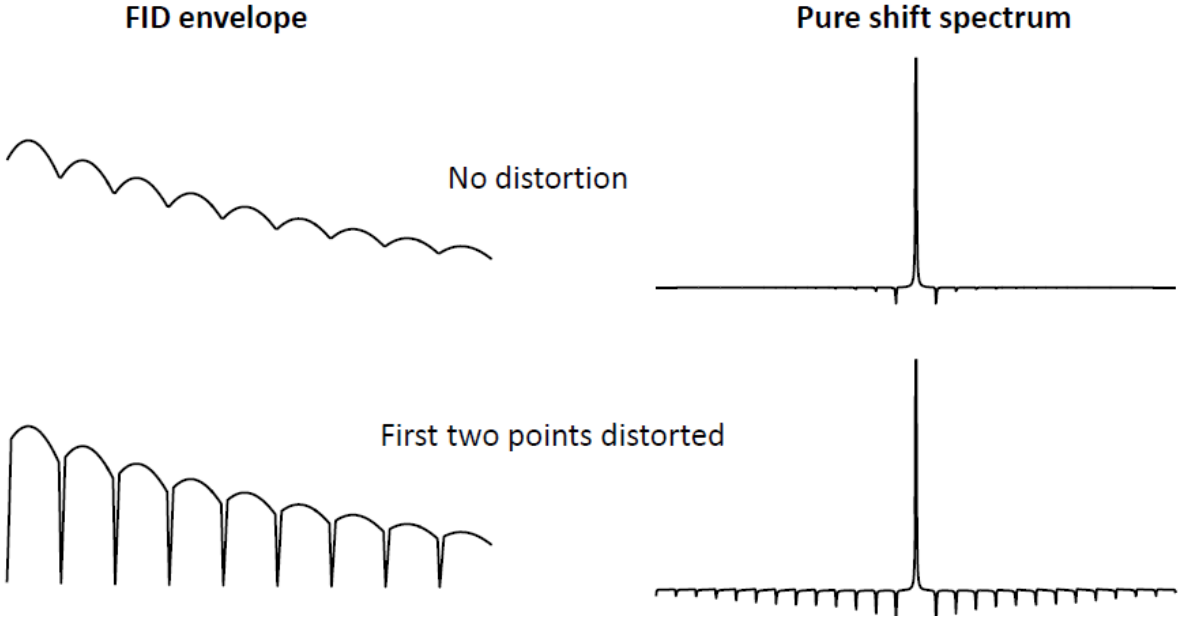

Figure 31 FID envelopes for non distorted and distorted points at the start of the fids in interferogram and respective pure shift spectra

Deletion of the first 4 data points in the individual fids of the interferogram for PSYCHE acquisitions gave the best artefact suppression and the small artefacts that were present after chunking artefacts were removed. With 6 drop points in place the small artefacts begin to increase and S/N is reduced from loss of high amplitude signal points which are present at the start of the acquired FIDs as seen in figure 33.

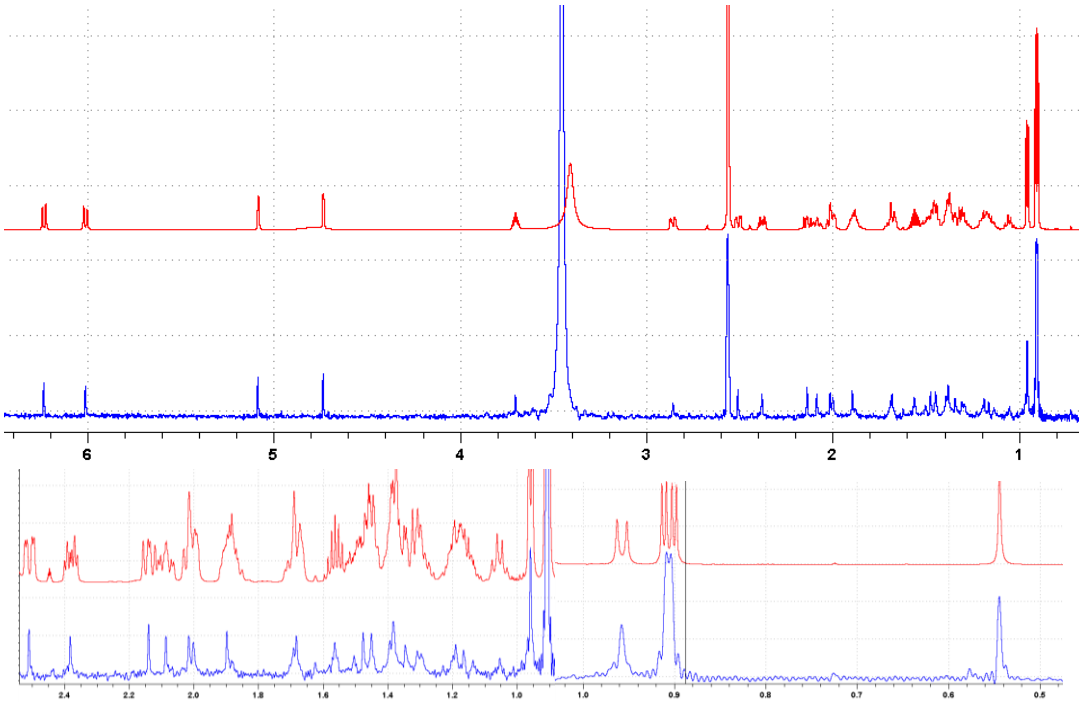

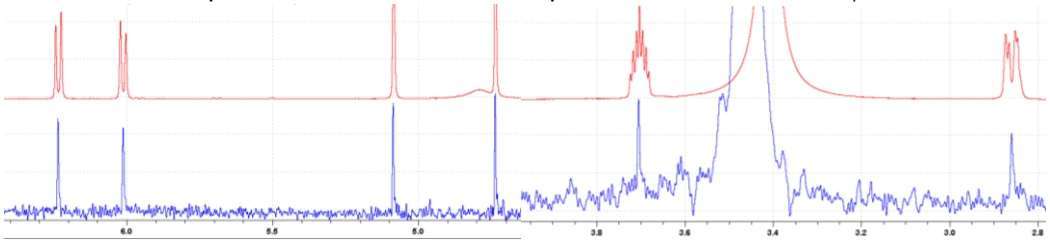

Figure 32 Reference conventionally acquired 1D 1H spectra in red and PSYCHE aacquired 1D 1H spectra with 4 drop points at the start of each chunk of interferogram acquired. (Top) Spectra covering 0.7ppm to 6.4ppm (Middle) Spectra covering range 0.4ppm to 2.5ppm (Bottom) Spectra covering 2.8ppm to 6.4ppm.

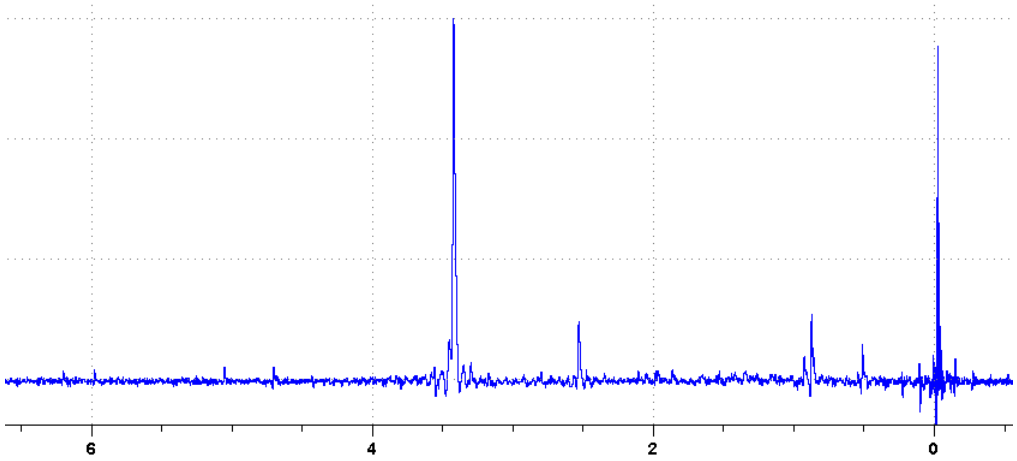

Figure 33 6 Dropped data point PSYCHE acquired 1D 1H spectra

3.2.1.5 PSYCHE Experiments for Greater Resolution

A PSYCHE experiment was then run to further resolve assignment of the crowded aliphatic region of proton environments 6 to 12 as seen in previous 1D ^{1}H acquisition (Figure 22/23) and HSQC acquisition (Figure 24) .

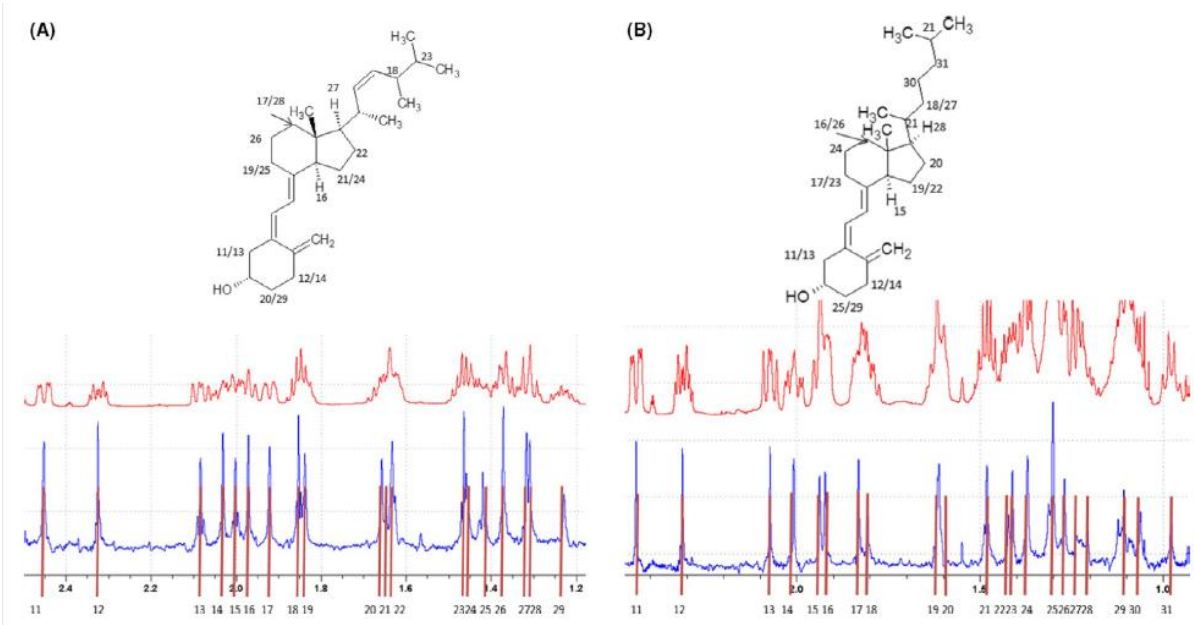

Figure 34 in red, standard proton experiment, in blue, PSYCHE proton experiment with individual proton assignments

3.2.2 Quantitation

To produce spectra for quantitation, the D1 (relaxation delay) in experiments was increased to 10 seconds, this guarantees that D1 > 5*T1 of all nuclei in our reference and the compound is being quantified. The peaks used for quantitation had to have an S/N larger than 50, otherwise they cannot be considered reliable for quantitative analysis. This means that with lower concentration analysis the scan number needs to be increased or change the pulse sequence/parameters to increase the sensitivity of the spectra.

Peaks chosen for integration and subsequent primary ratio method quantitation were selected based upon there multiplicity. Singlets are preferred as they present less variables that determine the integral of peaks, and separation from other peaks within the spectra so to avoid overlapping of integrals. Isolation from other peaks allows us to integrate 99.9% of the peak through integral width selection of 64x the full width at half maximum height.

Primary evaluation of the quantitative reliability of the instrumentation and quantitative parameter set was achieved through analysis of TSP concentration intra samples to measure repeatability and between samples to measure reproducibility.

3.2.2.1 Limits of Detection and Quantitation

Limits of detection and Quantitation (LOD, LOQ) for NMR varies from other techniques. In the traditional definition, LOD is defined as 3:1 ratio S/N and LOQ is defined as 10:1 ratio S/N. For this research and the respective needs of GSK, LOD was defined as a minimum S/N of 3:1 as normal, however due to the different resolution and sensitivity of NMR acquisition compared to traditional techniques, LOQ was defined as a minimum S/N of 50:1 with reference precedence ranging this value from 15-150 but RSD evaluation from preliminary work showed 50:1 S/N ratio gave desired RSD values for industrial applications (107). Selection of vitamin D_2 and D_3 inclusive of formulation

components as the eretic references set at 10mM was done to investigate how the below formulation samples effects TSP concentrations determined through quantitation in TopSpin. This gives a measure of the reliability between samples and whether increasing formulation complexity effects the quantitative ability of qNMR techniques, with the formulation detail table shown in the Full crème formulation section.

Table 2 Eretic Sample details

Sample	Components
B	D_2O only
C	Glycerol 10%
D	Caprylic triglyceride 5%
E	Isostearylisoterate 2%
F	Vegetable Oil 2%
G	Pentylene Glycol 5%
H	Phospholipon 1.5%

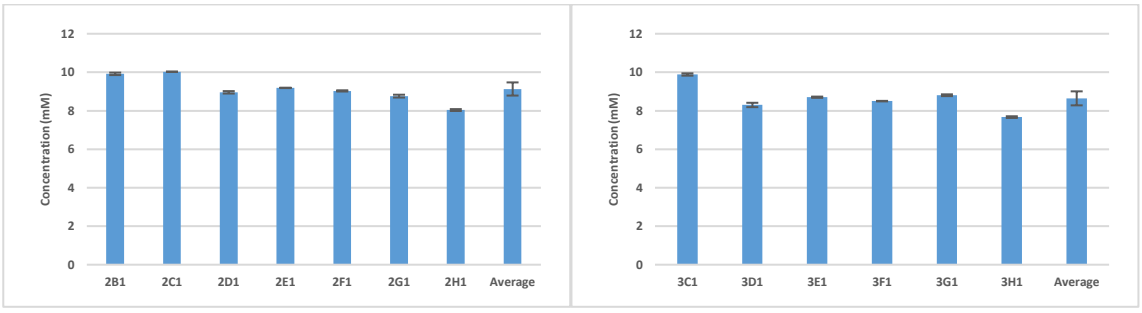

Figure 35 Weighed 10mM of TSP with concentration calculated by TSP peaks generated from a reference eretic value of 10mM of TSP in control samples of 2B1 and 3B1 (D2O) to compare integrals from different solvent systems

With the eretic referencing from the initial set concentration of 10µM, the relative standard deviation between different formulations is <10% and <2% between scans. Samples D to G for both vitamin D_2 and D_3 are not significantly different, with C and H having the same variability from this group for both D_2 and D_3. This suggests that D to G have similar sample properties based upon viscosity in the NMR sample, which is supported by the structural properties of the formulation components both having carboxylic acid groups and aliphatic chains of varying lengths in their

structures. Whereas Glycerol has OH groups but no aliphatic chain. Phospholipon has additional properties through its polar head group formed by the negative phosphate and positive amine groups present.

These differences demonstrate that different formulations would show variations in the acquired signal of reference peaks so eretic quantitation would be inappropriate between different formulation mixtures. However, the low standard deviation observed in similar formulation groups based upon their structural and chemical properties, alongside variation between samples with the same formulation highlights the potential of qNMR between similar formulation samples and demonstrates that data values can be reliably reported as quantitative using an internal reference in these formulations.

3.2.2.2 Preliminary 1D Proton qNMR in idealised samples

For initial quantitative analysis of samples, a standard, non-water suppressed 1D proton experiment of 256 scans was acquired to see what the starting LOD and LOQ was, alongside the reproducibility of these results. This was done with solutions of Vitamin D_2 and D_3 at gravimetric concentrations of 8.3mM then with subsequent samples the concentration was diluted by ten times until the peaks used for quantitation were no longer detectable within the noise.

Table 3 Vitamin D_2 table of concentrations and variability analysis

Gravimetric Conc. (mM)	Experimental Conc. (mM)	RSD	Accuracy	S/N
0.83	0.776	2.265	0.94	755
0.083	0.0778	1.725	0.94	107.2
0.0083	0.00335	13.56	0.4	8.03
0.00083	0.0012	31.99	1.45	4.13
8.3	16.7	0.1547	2.012	4881

Table 4 Vitamin D_3 table of concentration's and variability analysis

Gravimetric Conc. (mM)	Calculated Conc. (mM)	RSD	Accuracy	S/N
0.83	0.4	1.171	0.481	396.5
0.083	0.0364	2.633	0.439	51.7
0.0083	0.00338	90.55	0.408	8.23

8.3	26.14	0.652	3.149	1462

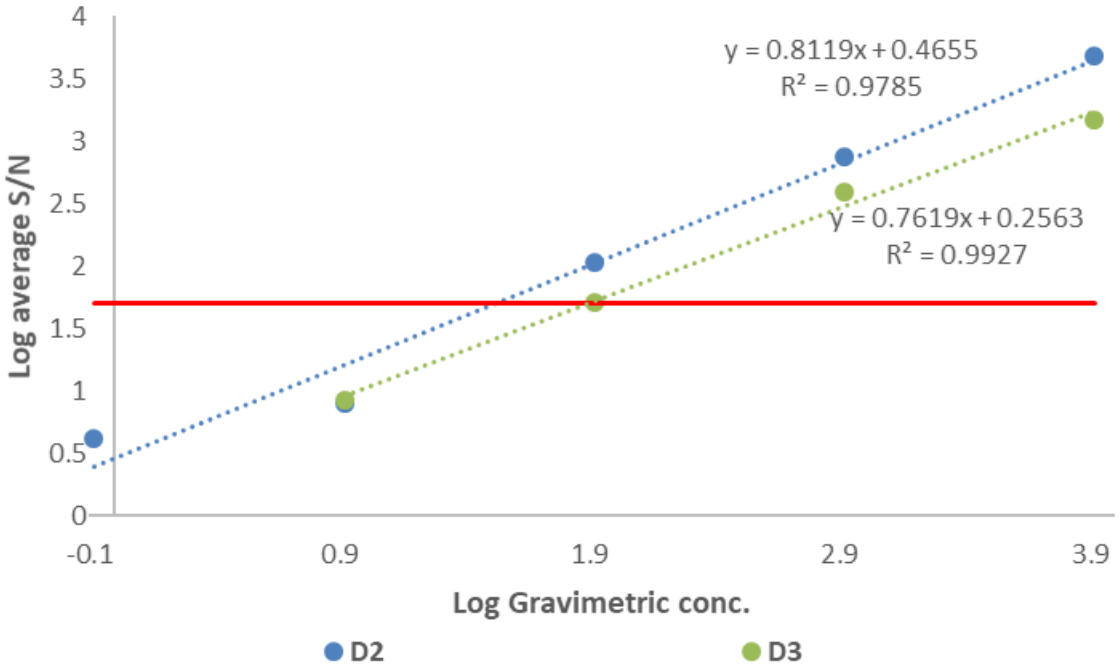

Figure 36 Log (Gravimetric Concentration (µM)) vs Log (Average S/N), Red line shows cut off S/N required for relative quantitation of Integrals (50;1 S/N)

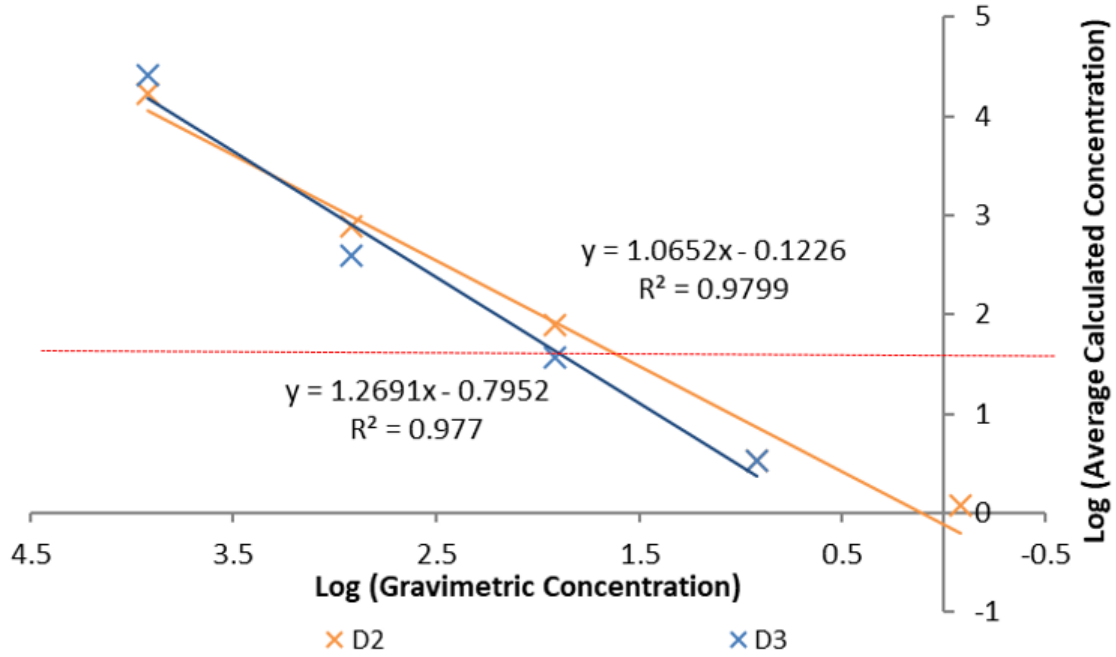

Figure 37 Scatter chart showing the Log of the gravimetric concentration versus the log of the average calculated concentration for each sample of D_2 and D_3 with dashed line highlighting S/N cutoff for LOQ (50:1 S/N)

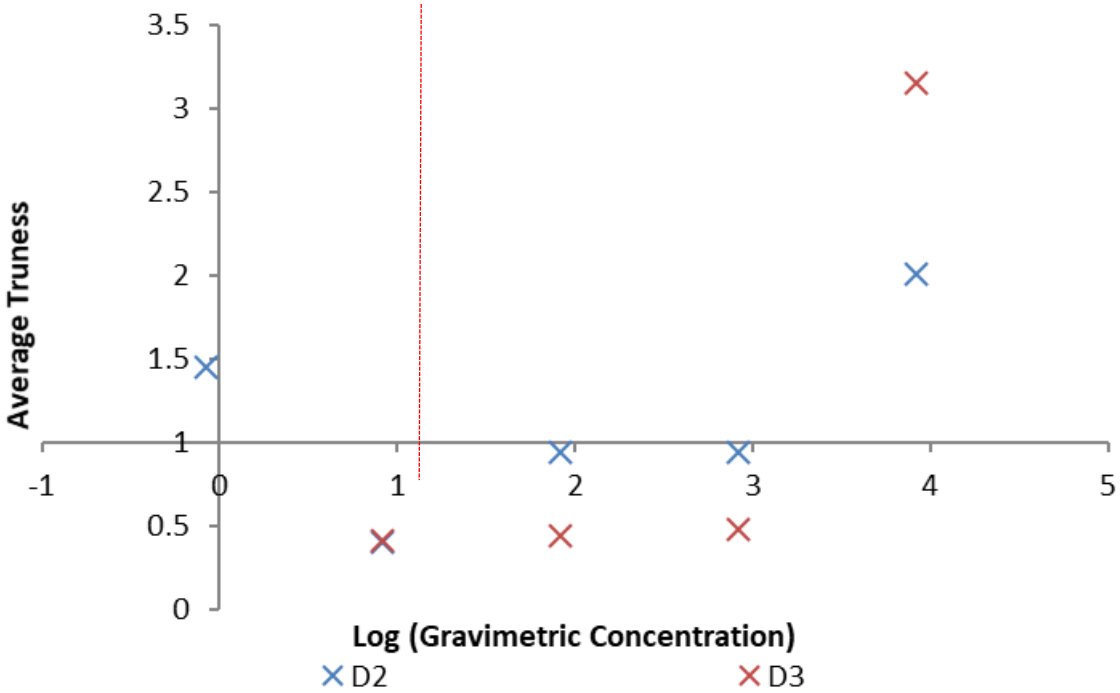

Figure 38 Log (Gravimetric Concentration) versus Average Trueness, shows how the trueness of each sample varies from the ideal of 1, red dashed line shows S/N cutoff (50:1 S/N).

Results from Table 2 and 3 show that with standard 1D ^{1}H NMR spectra a limit of quantification (LOQ) of 100 µmol/L, with RSD's of 1.73 and 2.63 for vitamin D_2 and D_3 respectively can be obtained. However, the trueness values vary between D_2 and D_3, with D_2 having a trueness value of 1.294 (RSD = 0.479) and D_3 trueness of 1.354 (RSD = 1.14294).

From these results, identified limitations using this quantitative technique was primarily the Dynamic range that the NMR spectrometer used could achieve. This is explained by the fact that as gravimetric concentration got closer to the target of 100nM for Vitamin D_2 and D_3 the NMR was still amplifying the free induction decays for the higher abundance peaks in the range of 10mM to 1M concentration. This is meant to not overload the Spectrometer, so RG was automatically set too low to detect Vitamin D peaks of interest at lower concentrations and they have lower S/N than lower LOD.

To reduce signal intensity, concentration of TSP was set relative to the concentration of Vitamin D in the sample instead of set at 10mM consistently, with TSP reference set at 1mM, 0.1mM, 0.01mM and 1µM for respective sample dilutions down to 100nM . Water suppression was also added to do

the same for the broad solvent peak of the water which increases the signal intensity acquired. Multiple suppression techniques could also be used to get rid of the DMSO-d6 peaks, but the small line width of the DMSO peak and relatively low abundance compared to other impurities meant that multiple suppression in acquisitions was not implemented as this would affect the reliability of quantitation through saturation of possible peaks used for integration and concentration determination. Frequency selective experiments were also being pursued to eliminate all peaks except those of interest in TSP and the quantification target but these gave anomalous results for quantitation and setting used for subsequent quantitation were; increasing of the scan number to gain more S/N and increase of the relaxation delay between pulses to guarantee quantitative conditions were met for our target LOQ. A summary of changes to parameter set for optimization is shown in table 4.

Table 5 Optimisation of acquistition parameters

Parameter	Standard qNMR	Optimised qNMR
TSP Conc.	10 mmol/L	[Analyte]
D1	3s	10s
Ns	256	1024
Sw	10ppm	20ppm
Water Suppression	No	Yes
TD	64K	64K

Table 6 Vitamin D_3 table of concentration's and variability analysis

Gravimetric Conc. (mM)	Calculated Conc. (mM)	RSD (%)	Trueness	S/N
5	4.54	0	0.908	56988
0.5	0.46	0.22	0.922	11027
0.05	0.046	0.45	0.924	1594
0.005	0.0046	1.145	0.924	230.5
0.0005	0.000425	18.95	0.85	23.38
0.00005	0.0000421	9.91	0.842	3.52

Table 7 Vitamin D_2 table of concentration's and variability analysis*Peak used for quantitation for 5mM sample was suppressed by water suppression pulse, unable to give consistent quantitation throughout other samples and comparison to D_3 samples so this sample was left out of quantitative analysis.

Gravimetric Conc. (mM)	Calculated Conc. (mM)	RSD (%)	Trueness	S/N
0.5	0.0733	1.9	0.1466	2503
0.05	0.00696	1.07	0.1392	214

0.005	0.00071	7.53	0.142	25
0.0005	0.000112	52.16	0.0224	2.58
0.00005	x	x	x	x

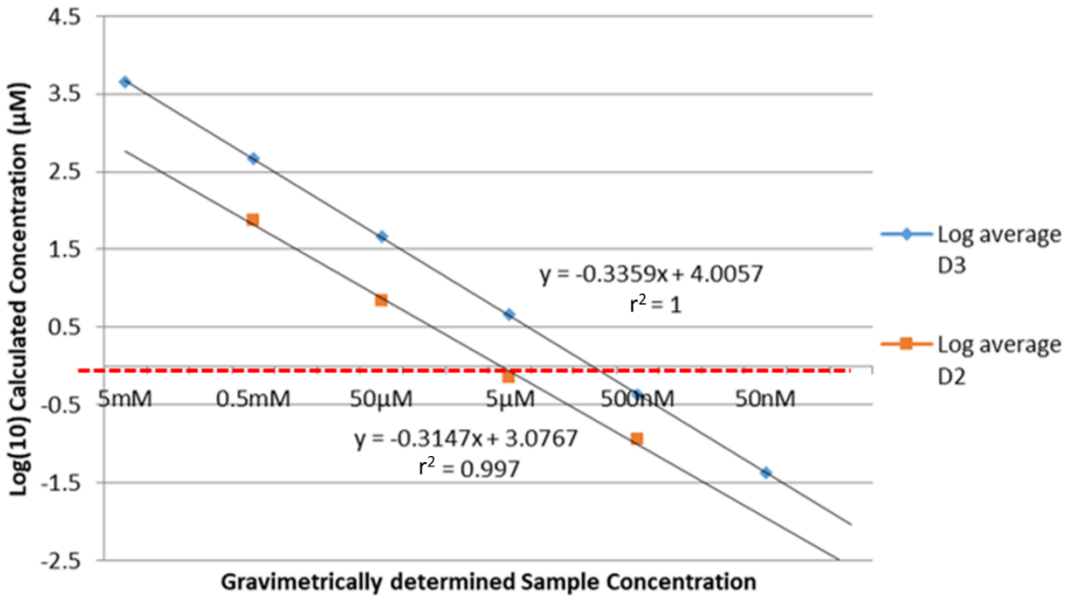

Figure 39 Log graph of determined concentration versus gravimetrically determined concentration, red dashed line shows limit of S/N where quantitation can no longer be achieved

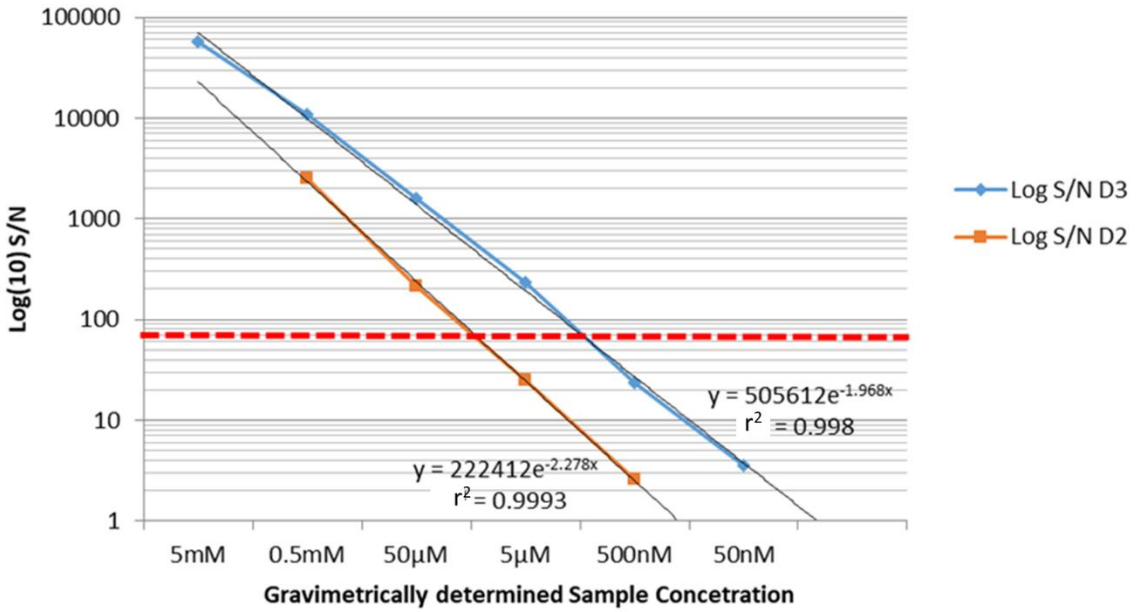

Figure 40 Log S/N chart of D_2 and D_3 showing us how the S/N drops by around the same factor as each dilution and also identify with a dashed red line the cut off point for quantitation

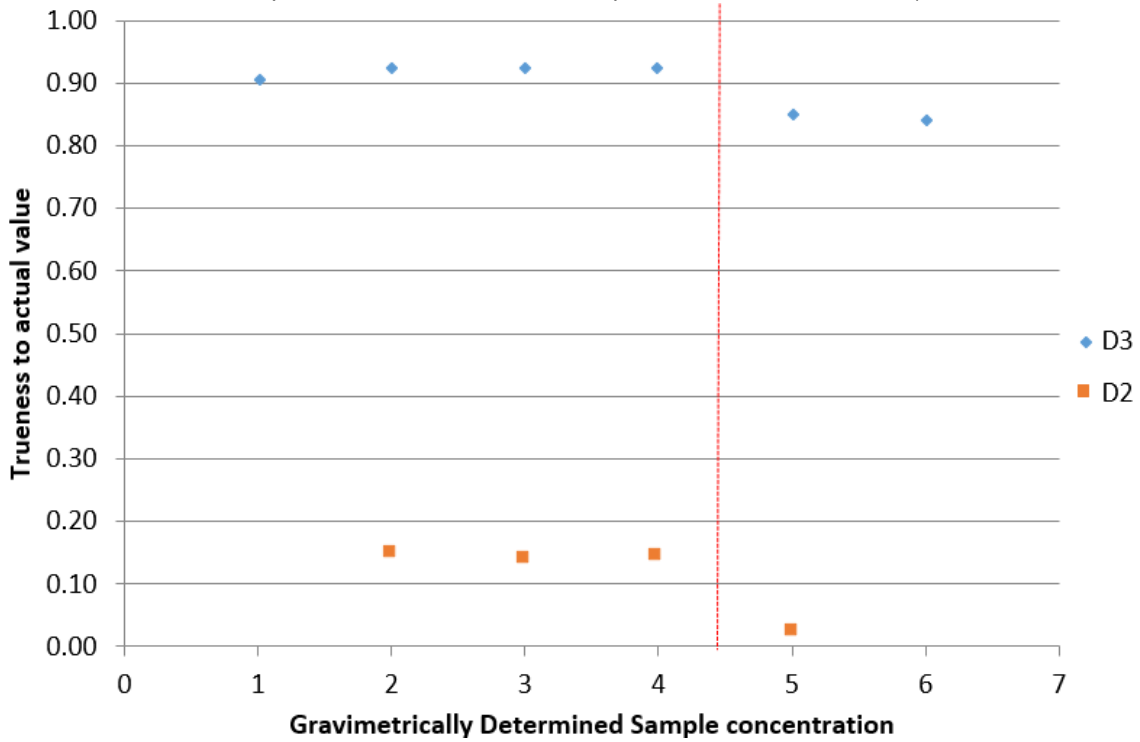

Figure 41 Trueness chart of D_3 and D_2 from calculated concentration and gravimetrically determined concentration, a drop off in trueness when the concentration goes below the threshold of quantitation as shown by the dashed red line.

By optimising certain parameters (Table 4), LOQ was lowered to 10 µmol/L for both vitamin D_2 and D_3 with LOD down to 50 nmol/L for D_3 and 500 nmol/L for D_2. Vitamin D_3 trueness values down to 100 nmol/L from 10mmol/L has an average value of 0.895 ± 0.035 (RMSD = 3.9%) of the gravimetric concentration consistently with RMSD values for each sample's trueness being below 20% with samples within the LOQ having RMSD values <2%. The variances seen between measured LOD between Vitamin D_2 and D3 is suggested to be through the reduced solubility of Vitamin D_2 seen consistently throughout the research.

Whereas with D_2 trueness values, values of 0.09-0.08 down to 10 µmol/L are observed with RSD below 10% however the trueness increases to 0.135 when the concentration drops down to 1 µmol/L with an RSD value of 52.2%, this suggest that Vitamin D_2 precipitates of solution either through solubility issues or subsequent aggregation of vitamin D_2 therefore reducing the calculated concentration by 10 times for every sample consistently. Interestingly, the D_3 spectra is water suppressed however in the vitamin D_2 spectra suppression of the DMSO peaks occurs, this was suggested as an additional possible reason for the differences in the trueness values seen for D_2

and D_3. This effect was not seen in the non-water suppressed samples where the trueness values were consistent between D_2 and D_3, this further supports our suggestion that suppression at different points between samples affects the quantitation, which led to multiple suppression techniques being avoided to reduce further qNMR error.

With targeted results seen for Vitamin D_3 it was decided to progress using D_3 in cream formulation characterisation and concentration determination analysis since the trueness of results in idealised samples was reliable down to the target concentrations for in-vivo analysis.

3.2.3 Separation and isolation of components in a Vitamin D topical cream formulation

Since whole samples are used, which are not chemically or physically separated the samples demonstrate in-situ conditions and how cream components interact with one another and affect not only analysis but delivery of actives.

Initial characterisation of each component for the full cream formulation was achieved through the use of 2D experiments HSQC/COSY and 1D ^{1}H experiments. The 1D ^{1}H assignment of each of the compounds with a table of their relative abundances in the full cream formulation model is shown below. This allows validation of peaks assigned in the complex mixture are the specific compounds of interest and a facilitates acquisition of further DOSY experiments for validation of assignments.

Table 8 Cream component details and gravimetric measurements

Cream Component (w/w)	Volume in 2ml formulation (µL)
Glycerol 10%	158.8
Caprylic triglyceride 5%	105.2
Isostearyl Isostearate 2%	46.8
Vegetable Oil 2%	43
Pentylene Glycol 5%	106.4
Phospholipon 1.5%	30
Panthenol 2%	33.4

Comparing the quantitation of separated compound samples to full formulation samples gives information on whether emulsification of certain compounds occurs through changes in the

detected abundances from the set abundances in formulation. Clear assignments for all components are given but are limited by resolution for specific assignment of all protons, specifically aliphatic chain protons of fatty acids. Resolution of aliphatic chains was thus decided to be studied in a separate research study which is detailed later in this chapter.

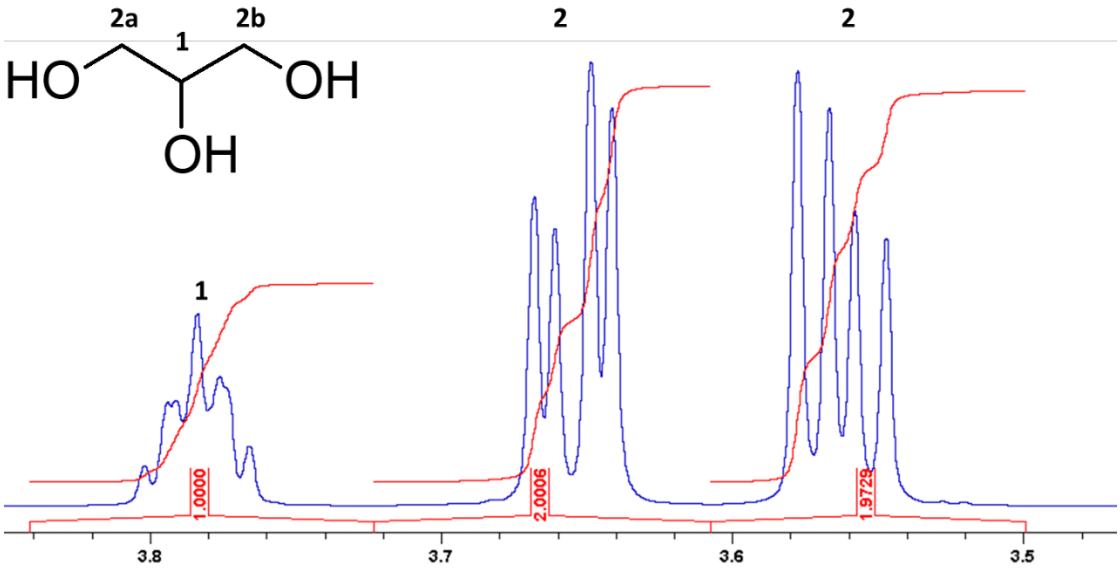

Figure 42 10% Glycerol, with CH_2 peaks assigned at peak number two, and CH peak assigned at peak position 1

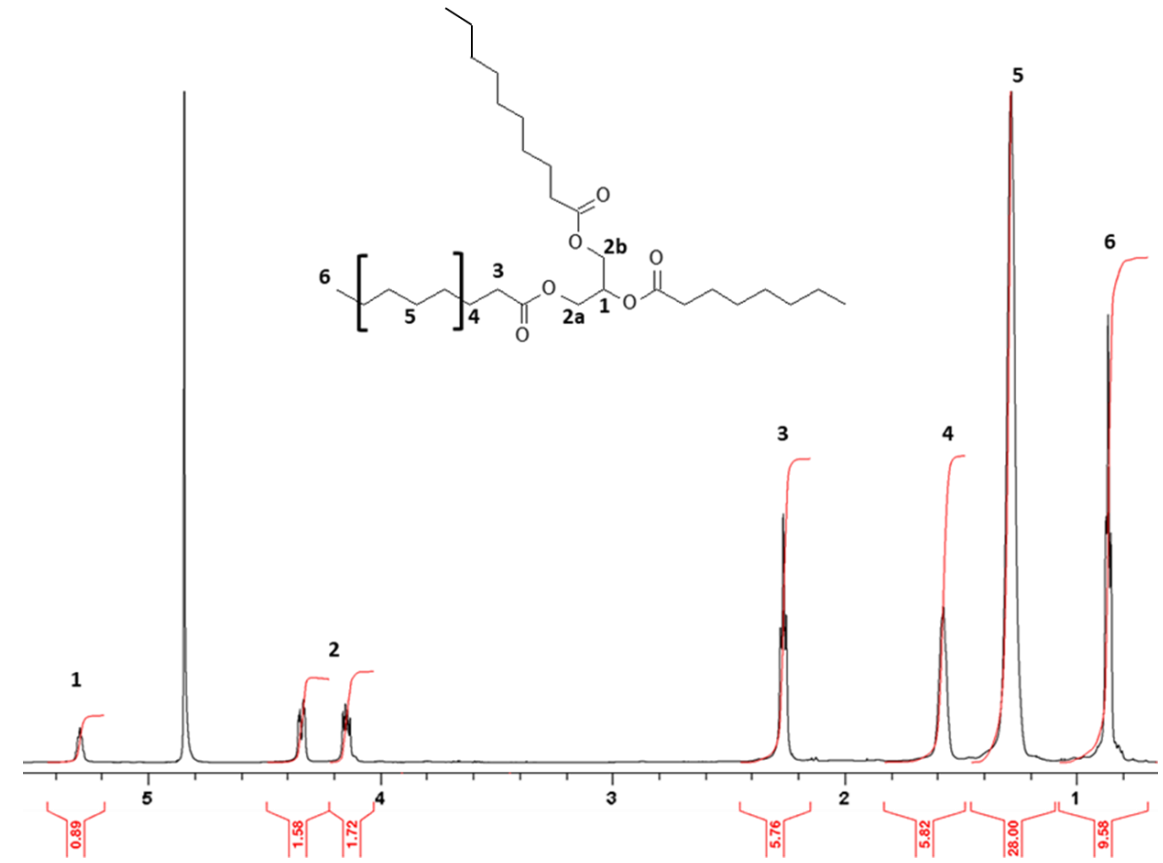

Figure 43 Caprylic triglyceride 5%, Integration shows three times the number of protons as assigned on Caprylic acid because of the Triglyceride nature of this component. Integrals referenced to 5 where brackets identify 14 CH2 groups (C4H8/C4H8/C6H12) present assigned by peak integral 5 with 28 protons giving integral area.

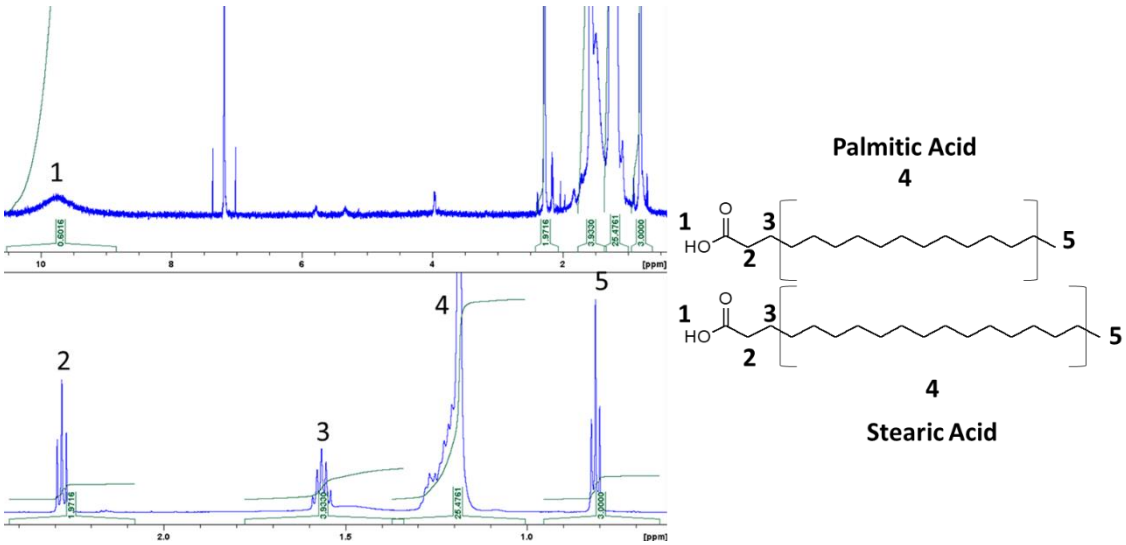

Figure 44 Vegetable oil 2%, broad peaks at assignment 4 because of the mix of fatty acids, structures of the most common fatty acids by composition in the vegetable oil.

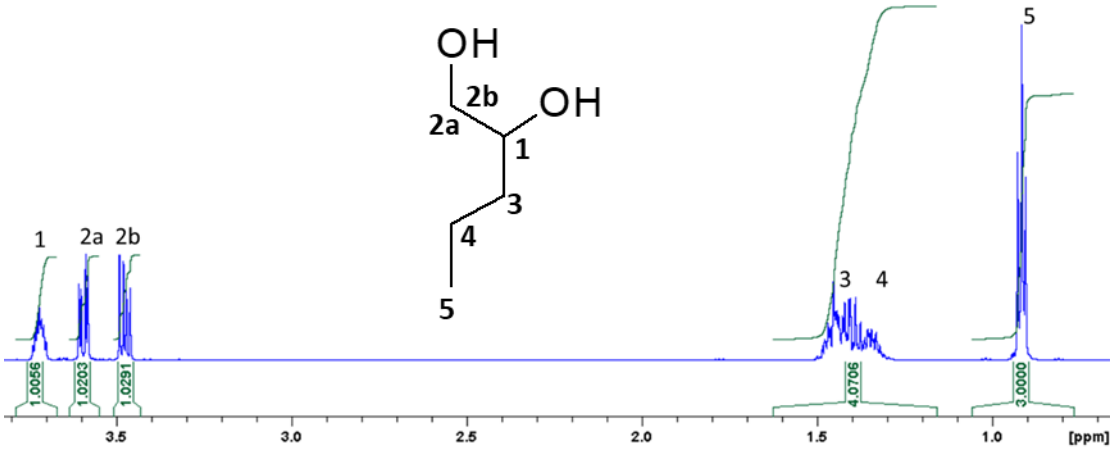

Figure 45 Assigned Pentylene Glycol 5%

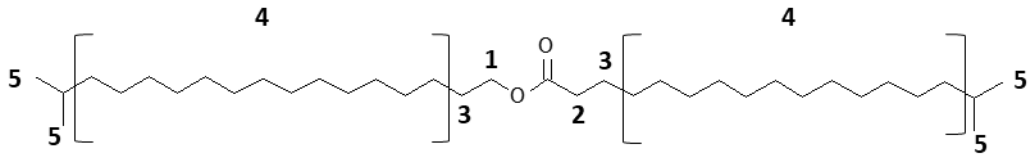

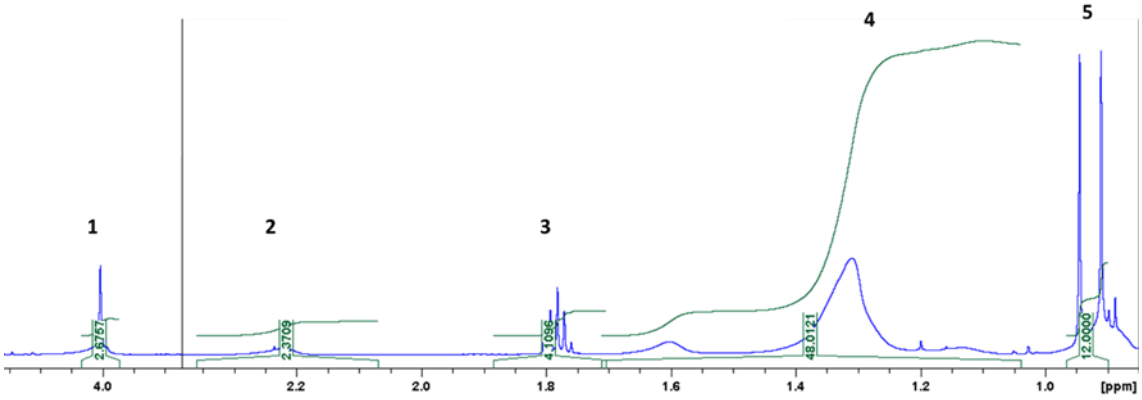

Figure 46 Assigned Isostearyl isostearate 2%

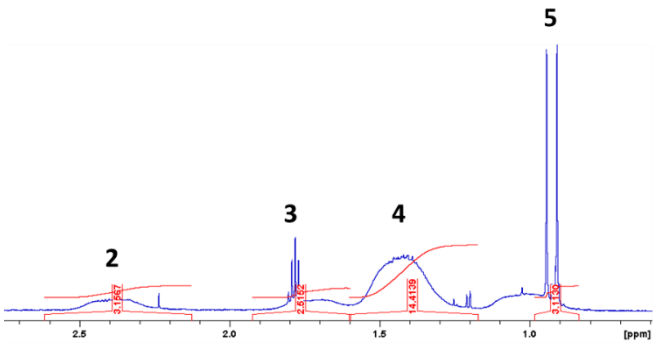

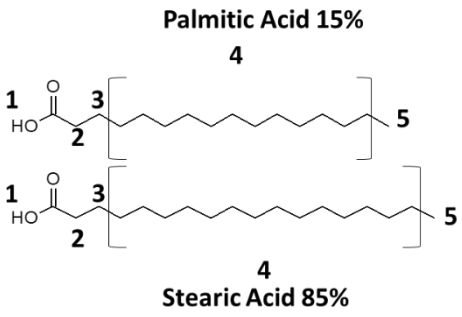

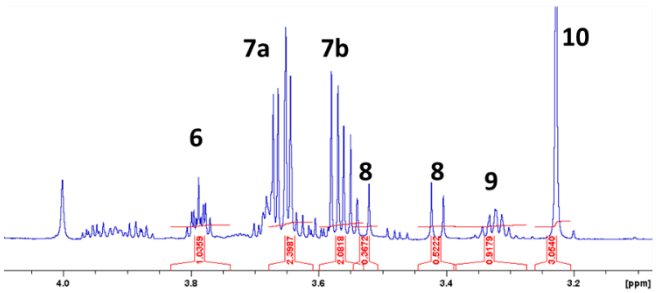

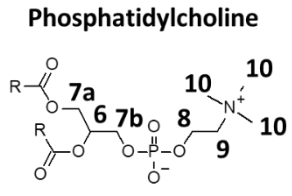

Figure 47 Assigned Phospholipon 1.5%

For phospholipon at the aliphatic chain proton region there is broadening of peaks and extensive overlap between peaks. This effect is seen mainly from two properties associated with phosphlipids, one being that the percentage of each fatty acid is different and secondly through suspected micelle/bicelle formation of phospholipon as the polar head group and non-polar tails interact to form membrane like structures. This presents as broadening of the peaks and prevents appropriate assignment of peaks when not in a solvent that disrupts the formation of micelles/bicelles, which is investigated later in this chapter. For targeted characterisation of phospholipon and its composition of fatty acids, further work could use ^{31}P NMR acquisitions which is demonstrated in the appendix study on dodecylphosphocholine synthetic work (6.2.2).

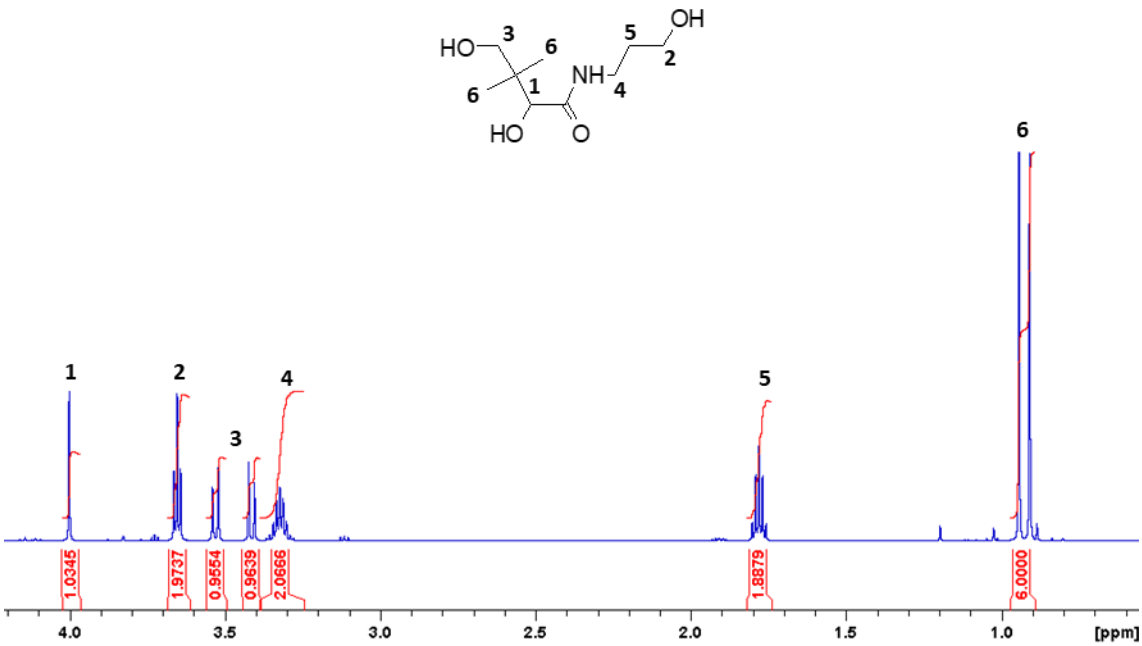

Figure 48 Assigned Panthenol 2%, splitting at 3 is a doublet of doublets that occurs through ambiguity between protons in two different chemical shifts due to OH group causing different J coupling on each proton.

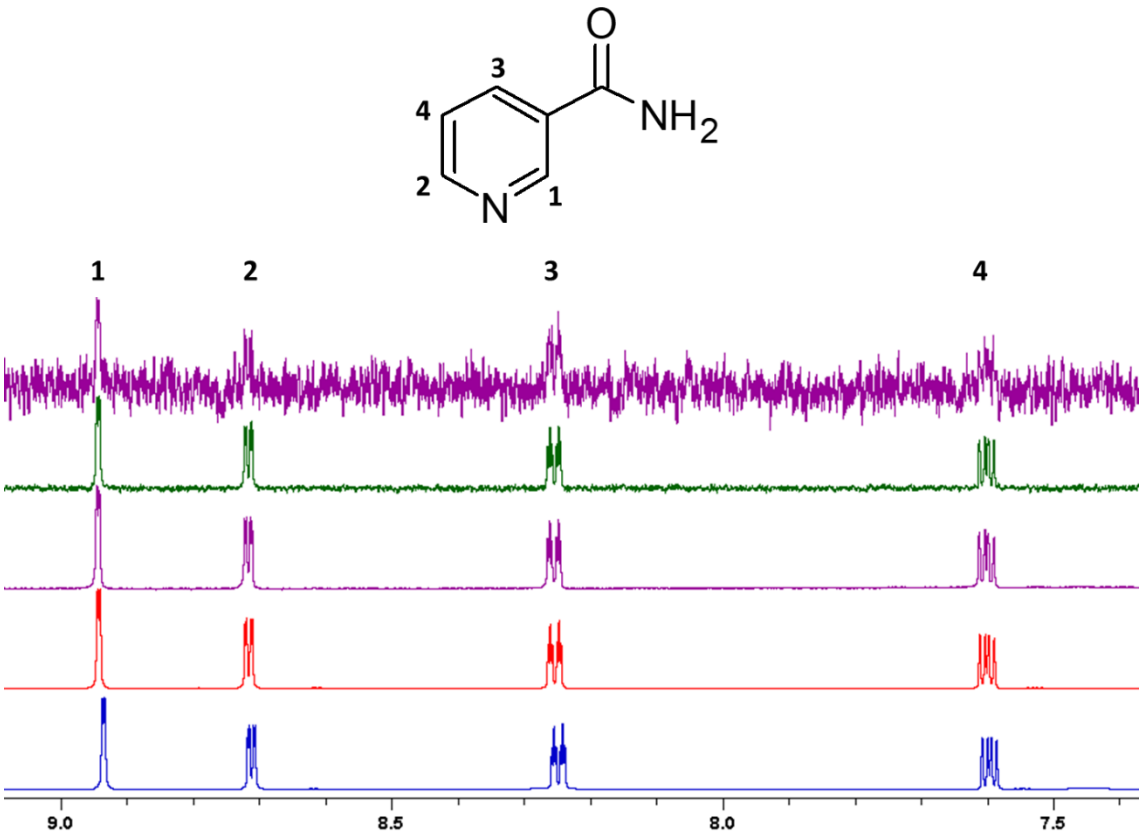

Figure 49 (Blue) Niacinamide 3% w/w, S/N = 10927.65; (Red) 0.3% w/w Niacinamide, S/N = 1742.37; (Purple) 0.003% w/w Niacinamide, S/N = 160.91; (Green) 0.0003%, S/N = 32.15, below threshold for accurate quantitation; (dark purple) 0.00003% w/w Niacinamide, S/N = 4.39, below threshold for accurate quantitation.

Multiple Niacinamide concentrations were prepared to determine LOD and LOQ, as this is an active compound in many topical creams that is important in regards to skin health and is varied depending on consumer needs and accurate determination of abundance is relevant for the formulation chemist in consumer health. A LOD down to 0.00003% is observed, however the LOQ is only down to 0.003% with a standard quantitative experiment as demonstrated by the calculated S/N for integrated peaks.

Table 9 Comparison between gravimetric and calculated concentration of formulation components

Compound	Gravimetric Conc.	Calculated Conc.	Trueness
Glycerol 10%	2860	1680	0.58
Niacinamide 3%	246	261.675	1.06
Panthenol 2%	97.5	139.2	1.42
Pentylene Glycol 5%	480	511.85	1.06
Caprylic triglyceride 5%	90.1	70	0.77
Isostearyl isostearate 2%	37.2	50.7	1.36

Phospholipon 90H 1.5%	25.3	30.54	1.20

3.2.3.1 Cream Formulation Mixtures where Vitamin D_2 and D_3 were detected and quantifiable

After this initial assignment of individual components spectra, preparation of the aforementioned full cream formulation samples with Vitamin D_2 and D_3 added and controls where vitamin D_2 and D_3 was not added was done.

Automatic phase processed HSQC spectra highlight the absence of Vitamin $D_{2/3}$ peaks in the control full cream formulation and presence of corroborating cross peaks in Vitamin $D_{2/3}$ spiked samples.

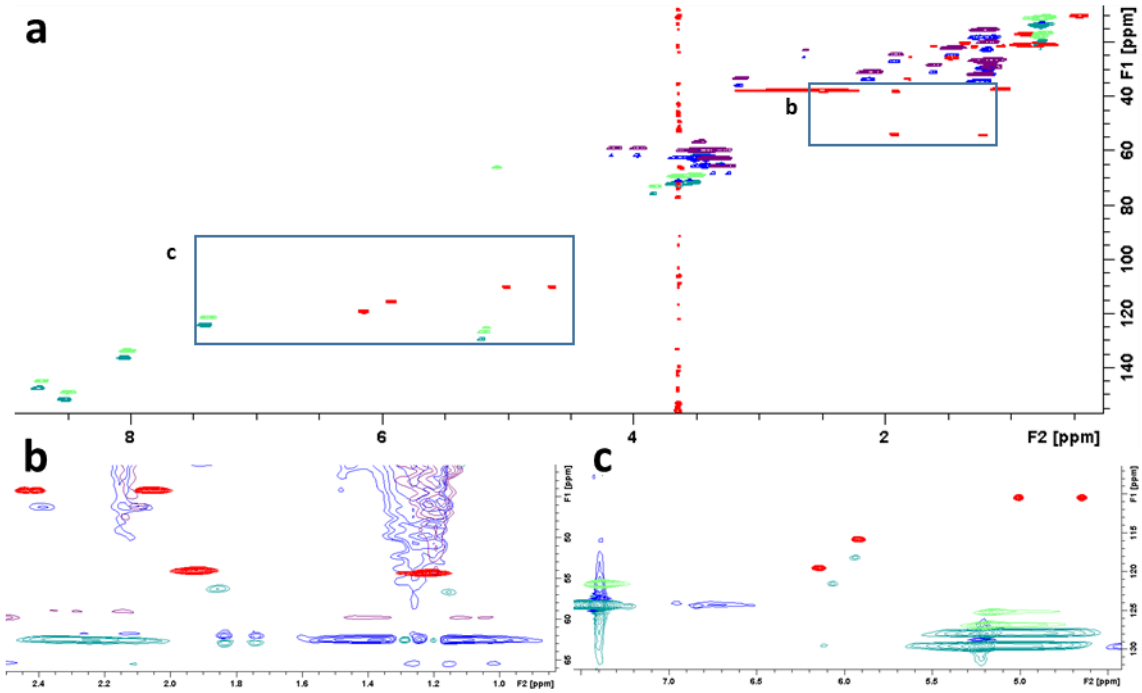

Figure 50 Magnitude phase processed HSQC spectrum highlighting the absence of Vitamin $D_{2/3}$ peaks in the control full cream formulation and presence of cross peaks in Vitamin $D_{2/3}$ spiked samples. Blue and red = $D_{2/3}$ single component sample, Blue and dark green = Full cream Formulation with $D_{2/3}$, Purple and light green = Control full cream formulation. a = Full spectra of all peaks, b = zoomed in peak range from 0.9ppm to 2.5ppm, c = zoomed in peak range from 4.5ppm to 7.5ppm.

With full cream formulation spiked with Vitamin $D_{2/3}$, noise prevents us from being able to observe with HSQC the cross peaks, however peaks are observed at ≈6ppm which match Vitamin $D_{2/3}$.

Elucidation of vitamin D_2 and D_3 peaks in HSQC allows us to assign peaks in the quantitative 1D ^1H acquisition for D_2 and D_3 respectively which allows for us to quantitate previously validated peaks for quantitation from single component D_2 and D_3 samples.

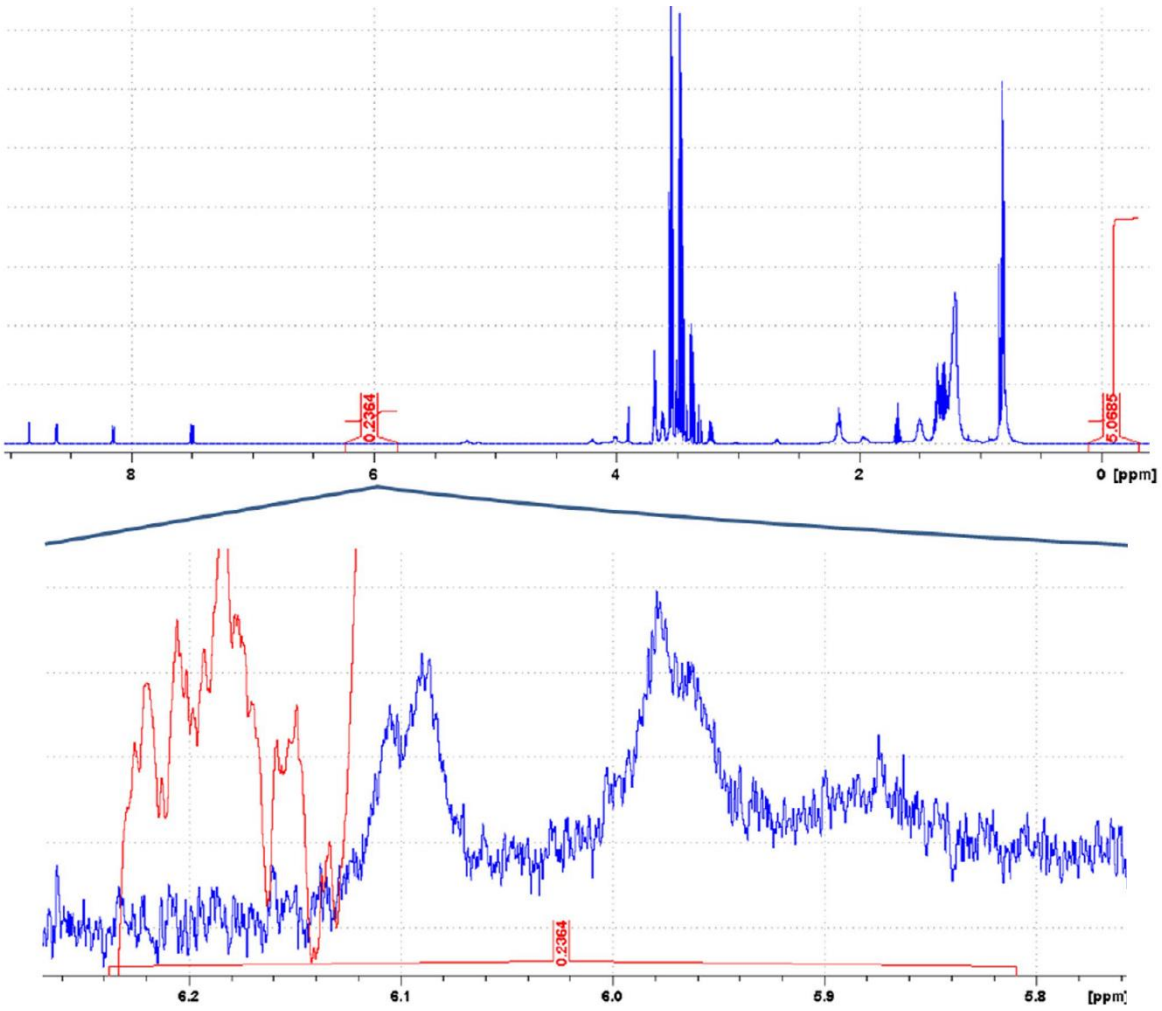

Figure 51 (Top) ^1H NMR spectrum of cream mixture (Glycerol, Caprylic triglyceride, Isostearyl isostearate, Niacinamide, Vitamin D_2, Vegetable Oil, Pentylene Glycol, Panthenol); (Bottom) zoomed in region covering vitamin D_2 alkene peaks

Alongside detection of Vitamin D_2 and D_3 alkene peaks in the full cream formulation they are also observed in caprylic triglyceride and Vegetable oil samples. Formulations containing caprylic triglceride at 5% demonstrate an encapsulation of 1%, with vegetable oil at 2% an encapsulation of around 0.5% of vitamin D_2 and D_3 is observed.

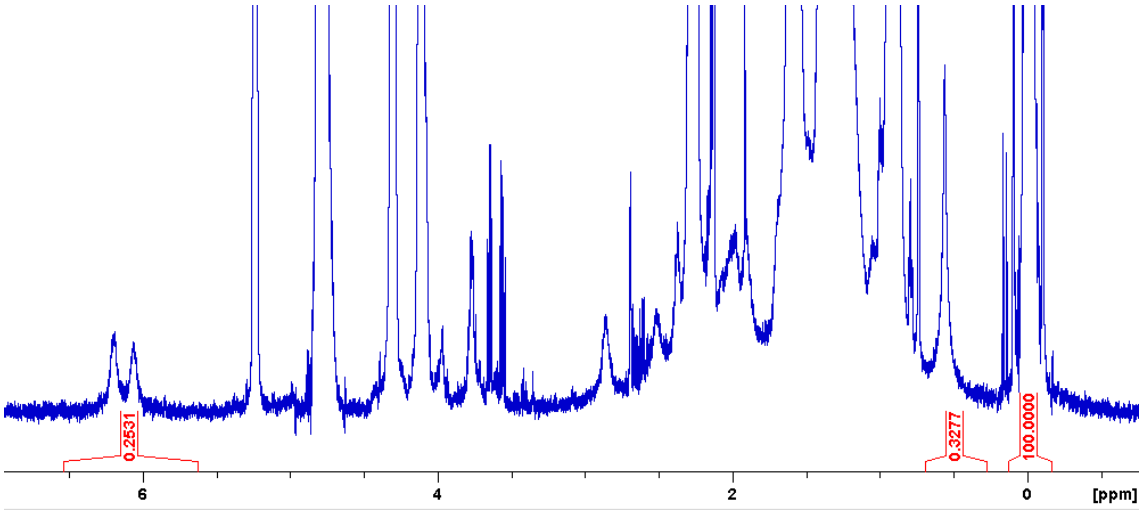

Figure 52 Concentration of Vitamin D_3 in 5% Caprylic triglycerideCaprylic triglyceride, determined to be 113µM and 85µM from integration at 0.5ppm and 6ppm respectively

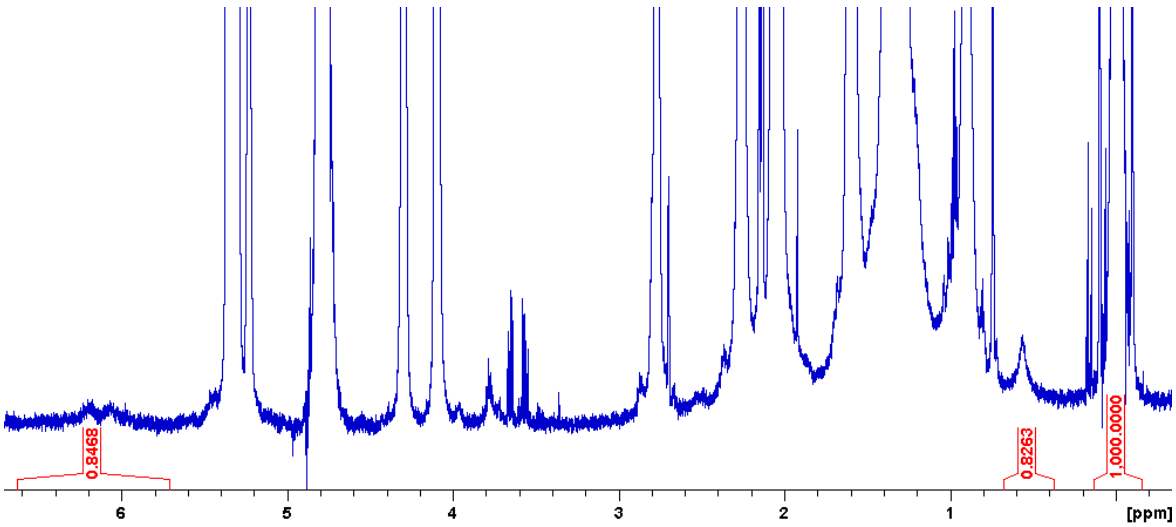

Figure 53 Concentration of Vitamin D_3 in 2% Vegetable Oil, determined to be 56µM and 21µM from integration at 0.5ppm and 6ppm respectively

The two peaks quantified have very different determined concentrations. Overlap of the singlet peak at 0.5ppm, with aliphatic chain peaks for fatty acid formulation components means that values

for 6ppm are taken, as quantitatively these are more reliable to the actual concentration of D_3 present in the formulations.

Table 10 Vitamin D_2 concentrations from single component formulations caprylic triglyceride (CT) and Vegetable Oil (Vo)

	CT 5% (µM)	Vo 2% (µM)
0.5ppm	337	79
6ppm	213	54

Table 9 also demonstrates that vitamin D_2 is detected within the 5% caprylic triglyceride formulation with measured concentrations at 0.5ppm higher than 6ppm to a similar ratio as D_3 due to overlap with higher caprylic triglyceride at 0.5ppm. A similar overlap of peak at 0.5ppm relative to the reduced overlapping at 6ppm is observed so again the value for 6ppm is taken as being more reliable and reported with other formulations.

To prevent the observed separation of more lipophilic compounds from hydrophilic compounds that are included in the formulation a high shear mixer was employed for emulsification of the samples.

3.2.3.2 Quantitation of Vitamin D_2 and D_3 in the full cream formulation

Using the optimised experiment detailed above for quantitation, 1.91mM of D_2 is calculated in the full cream formulation from gravimetrically weighed sample of 10mM D_2.. Homogenisation of the mixtures allowed for greater encapsulation than seen in single component samples (caprylic triglyceride and Vegetable Oil).

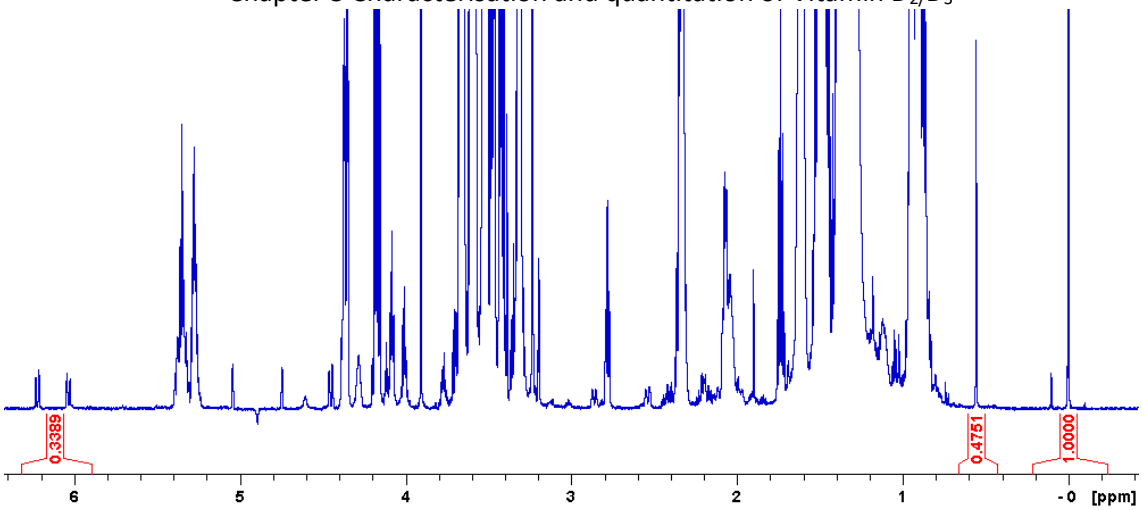

Figure 54 Homogenised full cream emulsion with gravimetrically determined concentration of 10mM. Peaks of TSP (0ppm), and Vitamin D_2 (0.5ppm and 6ppm) assigned

Below 1mM of gravimetrically determined concentration of Vitamin D peaks are not detected above the noise, so for the full cream formulation pure shift and projection display of DOSY spectra was used to produce single self-diffusion coefficient 1D ^1H spectra allowing for resolution and quantitation of identified peaks of interest. Within cream formulations, the peaks used for quantitation in the vitamin D samples are overlapped by the more concentrated cream formulation components. Quantitation is limited to selecting peaks at δ = 6ppm, which are doublets rather than singlets, necessitating the integration of both peaks. Another issue is the homogeneity of the sample, which even after high shear mixing, there is a distinct loss of free vitamin D concentration within the cream, with concentrations of 1.91 mM and 4.47 mmol/L detected from 10 mmol/L D_2 and D_3 samples respectively. It is also possible that in our cream formulation, micellisation of the vitamin D is taking place, thus reducing the amount of free vitamin D in solution which would have a significant impact on the measured Vitamin D with qNMR and can be measured through analysis of peak broadening and reduction in measured to expected concentration. This has implications in terms of skin permeability and vitamin D penetration into the dermis. It is also the case that the large abundance of other analytes to the small detectable vitamin D causes a great loss in S/N for smaller concentration peaks. The micellisation of vitamin D can be investigated through the acquisition of methanol-d4 (MeOD) solvent samples alongside that of the D_2O samples, which causes disruption of any micelles and all vitamin D becoming free in solution. The reason peaks are not visible when micellised is because the Vitamin D is incorporated with much larger structures

and their tumbling rate is slowed, therefore causing broadening of peaks (Shorter T2 relaxation time). This is not seen in MeOD samples as the micelles cannot be formed. Because of this, sharp line shapes are observed for the vitamin D peaks. From the formulation made, it is shown that NMR methodology can be used to measure the capacity of micellisation and with this the optimal amount of drug product or analyte of interest to add into our respective cream formulations. An example is shown below for vitamin D_3 at a concentration of 10 mmol/L.

Using our previously acquired pure shift Vitamin D spectra in DMSO as a reference, 6 peaks that are assigned to vitamin D are observed in our FCF-MeOD samples where micellation is disrupted. The same peaks are present for both Vitamin D_2 and D_3 in MeOD samples at comparable intensities.

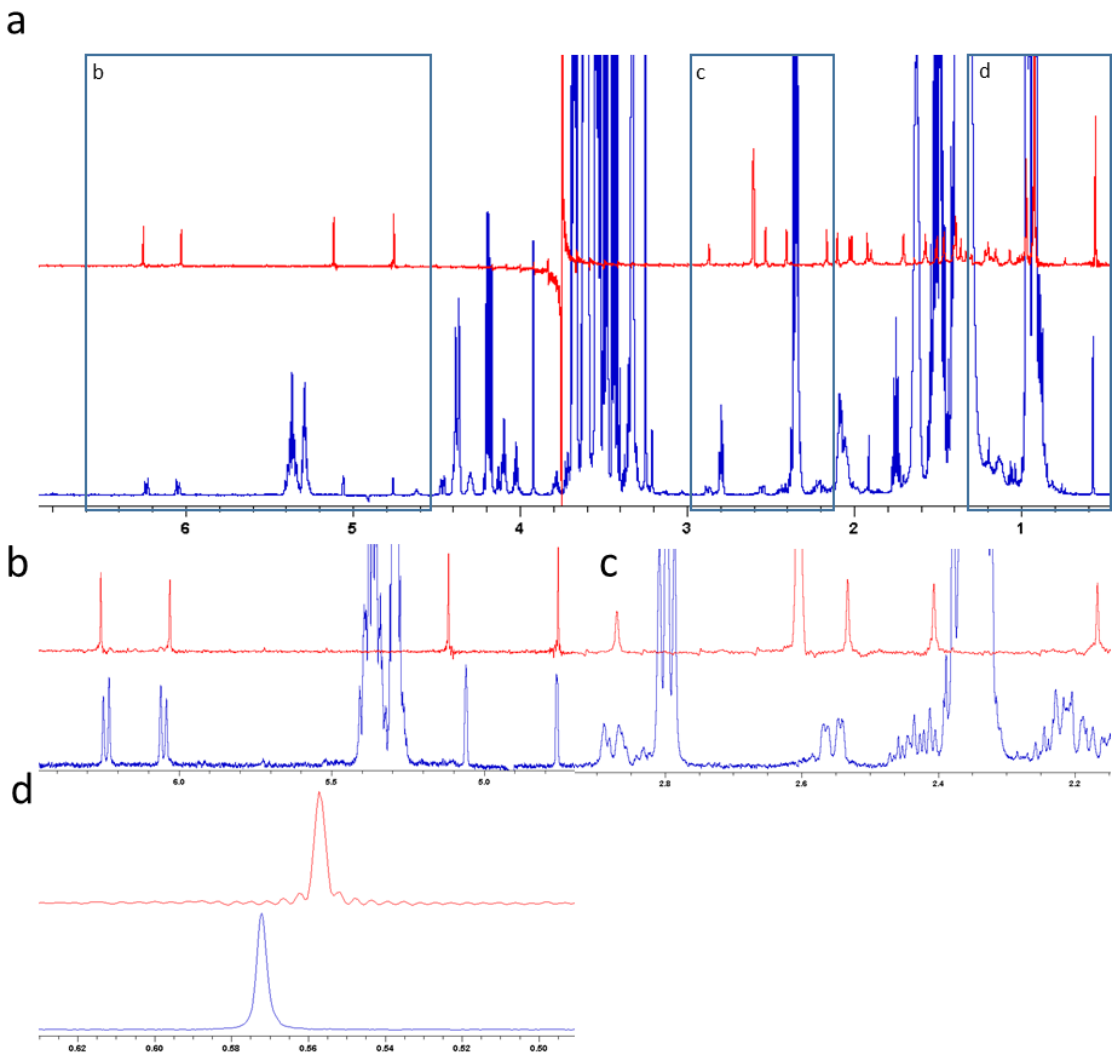

Figure 55 Red = Pure shift of Vitamin D_3 in DMSO-d6, Blue = Full cream formulation in MeOD; a = full spectrum D_3, b-d = selected regions zoomed in to highlight D_3 peaks

The ratio of encapsulated to free Vitamin D3 can then be determined by calculating the difference between measured amounts in FCF in D2O and FCF in MeOD where no encapsulation can occur. This determined ratio is shown in Figure 56.

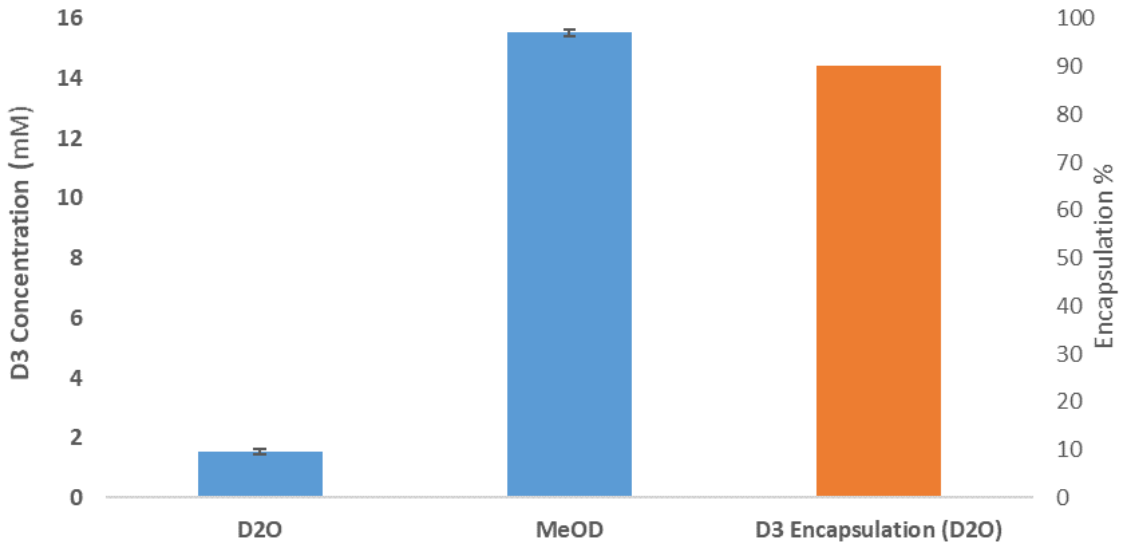

Figure 56 Determined values of free D_3 in FCF through differences seen for non-encapsulated D_3 in D_2O FCF sample and non-encapsulated D_3 in MeOD and percentage encapsulation in D2O shown in orange. This demonstrates the amount of D_3 that has been successfully encapsulated in FCF and whether added Vitamin D3 has exceeded the encapsulation potential of formulation

3.2.3.3 Implementation and Optimisation of PSYCHEiDOSY experiment

For this extension of pure shift into DOSY, the pulse program was taken from the Manchester NMR methodology group and implemented on Kingston UniversitiesNMR Spectrometer. This required editing of the pulse program and setting up of an automation program to allow for suitable running of the pulse sequence to run many samples over a long period of time.

3.2.3.4 Separation of components using PSYCHEiDOSY

For assignment and identification of individual components and peaks within the full cream formulation a diffusion experiment with a pure shift element (PSYCHE) was used. This allows the peaks to be separated by the diffusion characteristics of the respective compounds producing the peaks with suppression of multiplicity. This collapsing of multiplets reduces the overlap between the peaks for the diffusion coefficient calculation therefore giving us a more accurate measurement of the diffusion characteristics.

A sample with exclusively Niacinamide was first acquired with the PSYCHEiDOSY experiment to validate the values produced and whether the results seen corroborated with known values for Niacinamide.

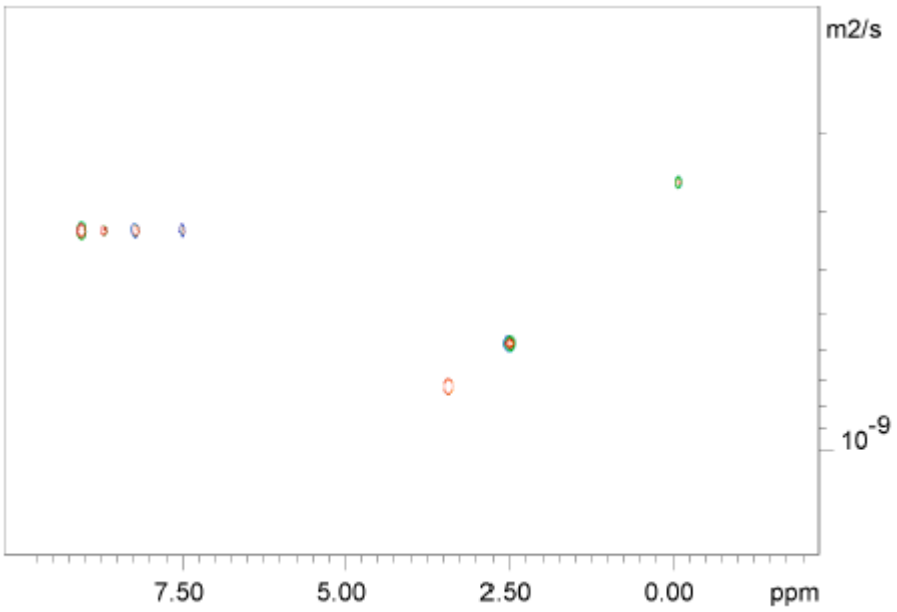

Figure 57 Niacinamide PSYCHEiDOSY spectra displaying diffusion coefficient resolved peaks and separation of clear self-diffusion coefficients for solvents, TSP and Niacinamide.

Table 11 Niacinamide reference sample PSYCHEiDOSY results

Compound	Calculated Log Diff. Coeff.	Actual Log mw
Niacinamide	-9.48 ± 0.035	2.09
Water	-9.14 ± 0.063	1.26
DMSO	-9.24 ± 0.059	1.89
TSP	-9.60 ± 0.048	2.24

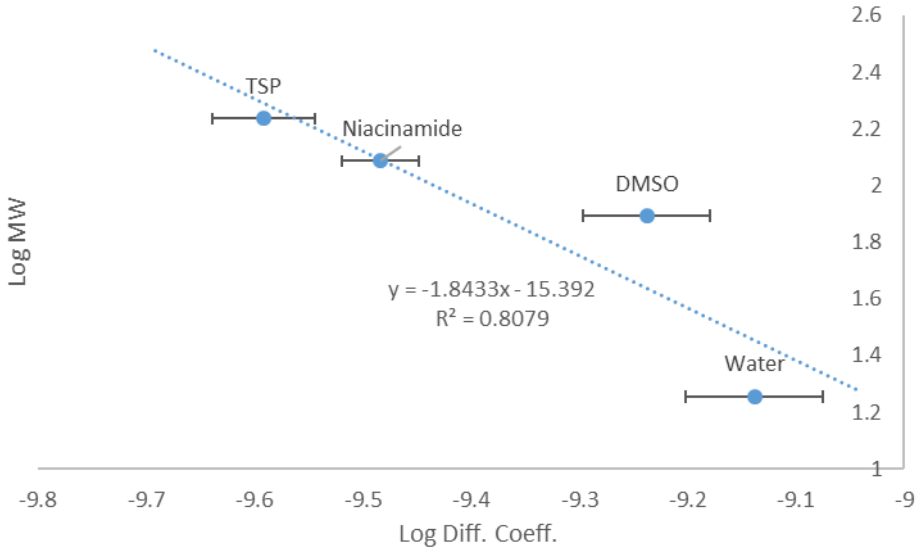

Figure 58 Calibration curve of Log diffusion coefficient values versus Log mw for components of the Niacinamide sample from PSYCHEiDOSY experiments to demonstrate linear relationship between calculated diffusion coefficients and actual molecular weights for subsequent determination of unknown compounds molecular weight.

Acquisition of conventionally acquired DOSY spectra of full cream formulation samples allowed for characterisation of the separate components to different levels of resolution between components. It is observed that lower abundance compounds that have overlapping peaks demonstrate greater error, especially for components Vegetable Oil, Isostearyl Isostearate, Caprylic triglyceride and Phospholipon. The larger abundance components, Glycerol, Pentylene Glycol and Panthenol have another limitation which is due to the extensive overlapping of peaks around 3.4ppm which makes the calculated diffusion coefficients for peaks assigned to one compound variable.

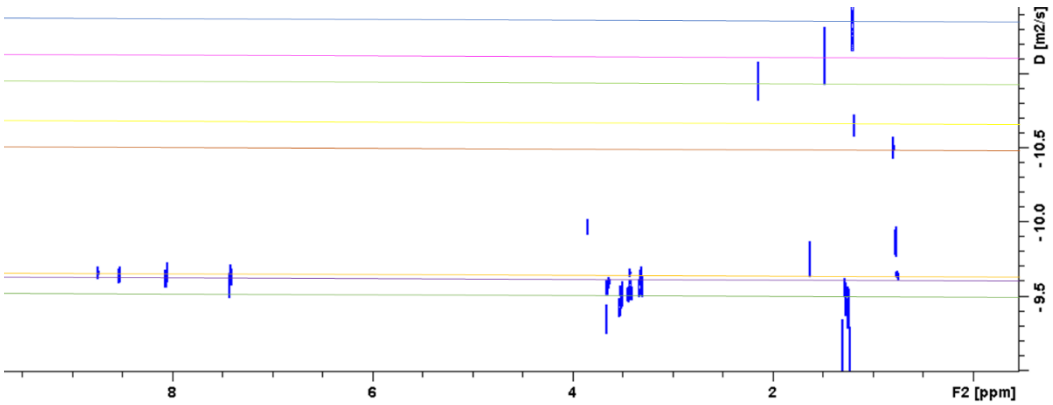

Figure 59 Conventionally acquired LED DOSY spectra of FCF with lines representing centre of highest signal peak for each individual compound (From top; Phospholipon, Isostearyl Isostearate, Caprylic triglyceride, Vegetable Oil, Panthenol, Niacinamide, Pentylene Glycol, Glycerol)

Table 12 Diffusion coefficients for formulation components

Compound	Diff. Coeff. +/- RSM per spectrum		log mw	mw
Glycerol	-9.43	+/- 0.18	1.96	92
Pentylene Glycol	-9.56	+/- 0.35	2.01	104
Niacinamide	-9.66	+/- 0.21	2.08	122
Panthenol	-10.5	+/- 0.62	2.31	205.21
Vegetable Oil	-10.65	+/- 0.5	2.44	280
Caprylic triglyceride	-10.95	+/- 1.28	2.61	408.57
Isostearylisoterate	-11.12	+/- 2.25	2.72	536.97
Phospholipon	-11.39	+/- 2.1	2.89	790.14

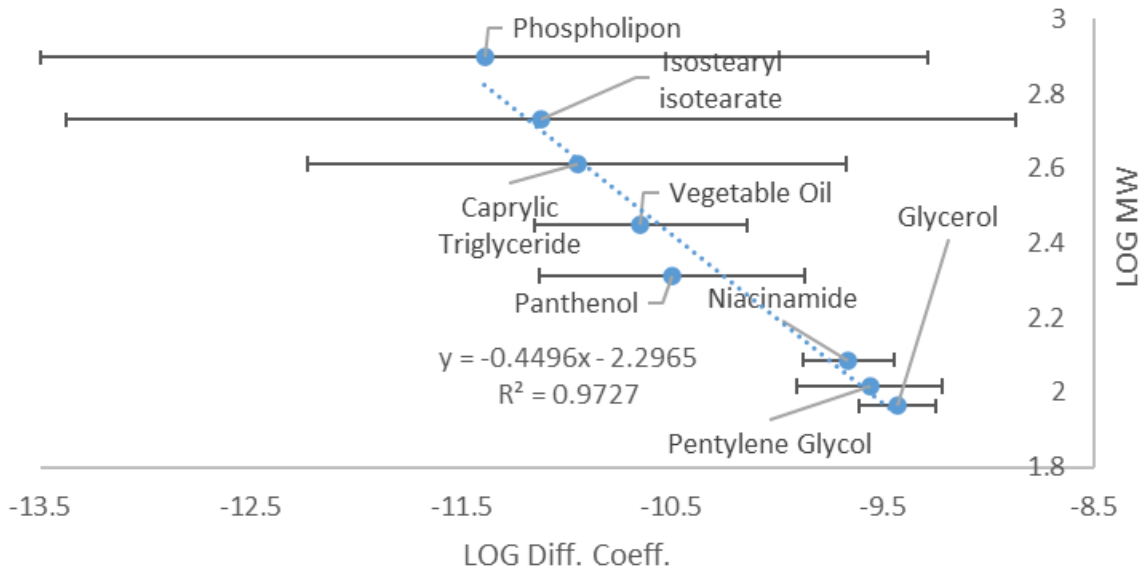

Figure 60 Calibration curve of Log diffusion coefficient values versus Log mw for components of the FCF calculated from conventionally acquired DOSY experiment

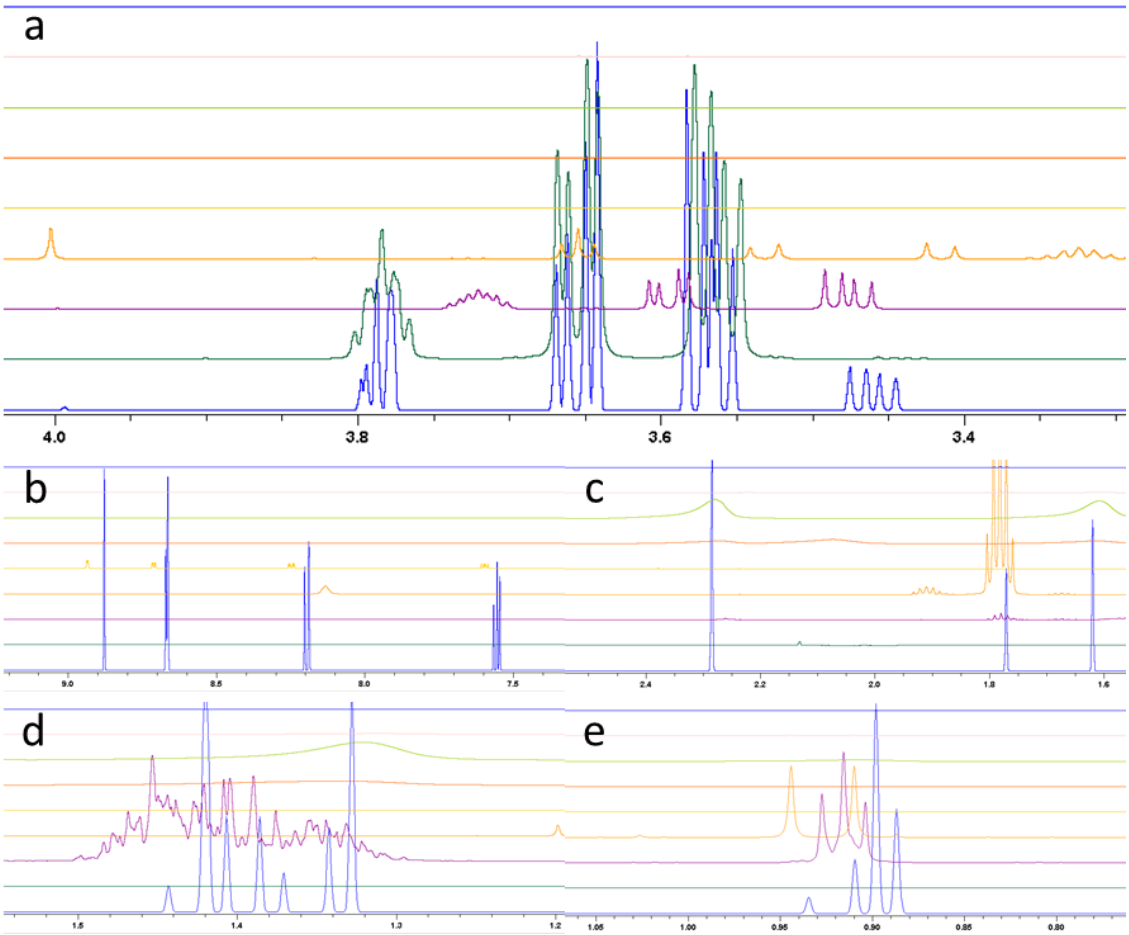

Figure 61 Zoomed in ppm ranges of reference spectra for each individual formulation component (From top; Phospholipon, Isostearyl Isostearate, Caprylic triglyceride, Vegetable Oil, Niacinamide, Panthenol, Pentylene Glycol, Glycerol) and 1D 1H positive projection of conventionally acquired DOSY spectra for full cream formulation sample(Light blue). a = ppm range from 3.3 to 4ppm; b = 7.4ppm to 9.2ppm; c = 1.55ppm to 2.5ppm; d = 1.2ppm to 1.5ppm; e = 0.8ppm to 1.05ppm

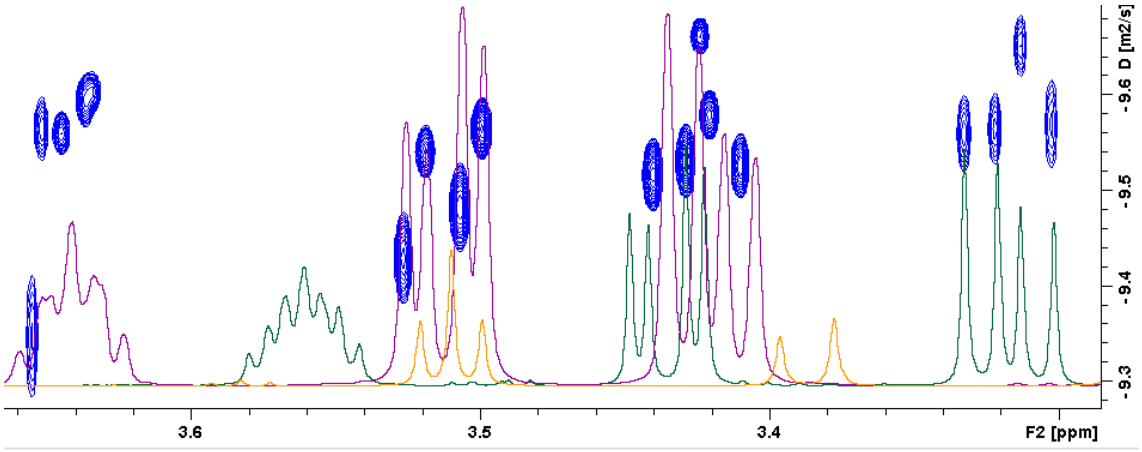

Figure 62 conventionally acquired DOSY spectra overlaid with reference spectra for Panthenol (Orange), Pentylene Glycol (Green) and Glycerol (Purple)

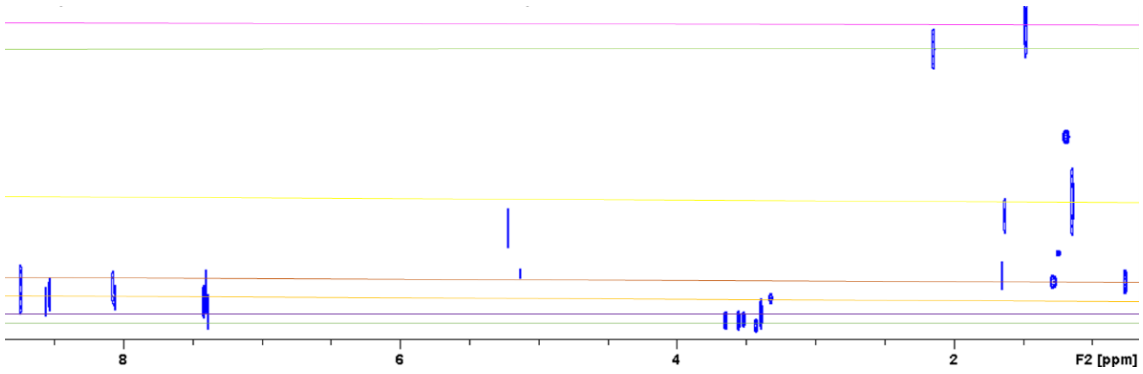

Figure 63 PSYCHEiDOSY spectra of Full Cream formulation with each component identified by lines, from the bottom: Glycerol; Niacinamide; Pentylene Glycol; Vegetable Oil; Caprylic triglyceride; Isostearylisoterate; Phospholipon

Table 13 Calculated Log diffusion coefficients ranked against molecular weights for each formulation compound

Compound	Log Diff. Coeff. +/- RMS/spectrum	log mw	mw
Glycerol	-9.55 +/- 0.081	1.96	92
Pentylene Glycol	-9.62 +/- -0.084	2.01	104
Niacinamide	-9.61 +/- 0.25	2.08	122
Panthenol	-9.87 +/- -0.60	2.31	205.21
Vegetable Oil	-10.02 +/- 0.11	2.44	280
Caprylic triglyceride	-10.25 +/- 0.5	2.61	408.57
Isostearylisoterate	-10.33 +/- 1.09	2.72	536.97
Phospholipon*	X	2.89	790.14

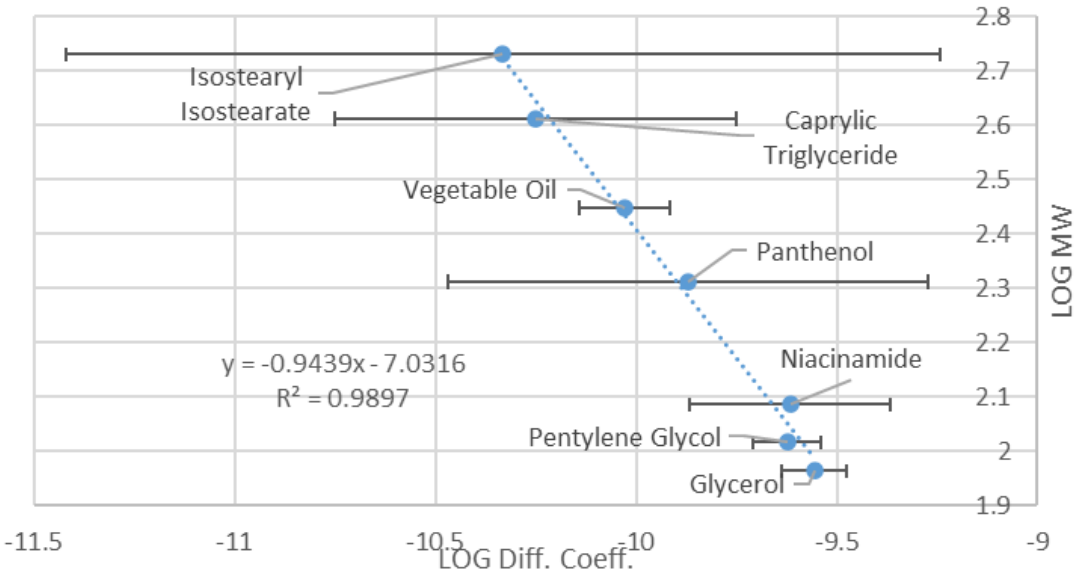

Figure 64 Calibration curve of Log diffusion coefficient values versus Log mw for components of the FCF calculated from PSYCHEiDOSY experiment

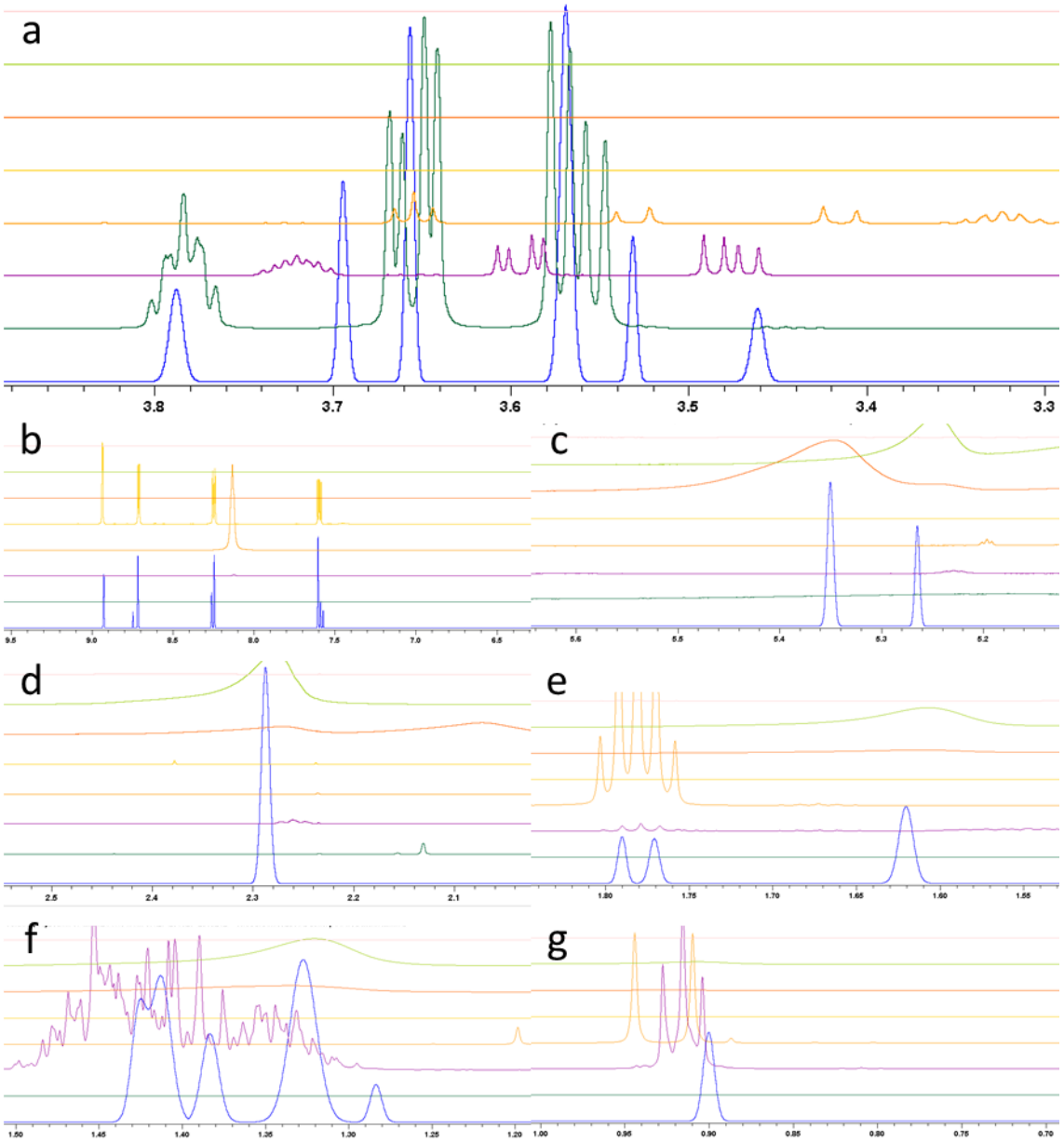

Figure 65 Reference spectra for each individual formulation component (From top; Isostearyl Isostearate, Caprylic triglyceride, Vegetable Oil, Niacinamide, Panthenol, Pentylene Glycol, Glycerol) and 1D 1H positive projection of PSYCHEiDOSY spectra for full cream formulation sample. a = ppm range from 3.3 to 4ppm; b = 6.5ppm to 9.5ppm; c = 5.2ppm to 5.6ppm; d = 2.1ppm to 2.5ppm; e = 1.55ppm to 1.85ppm; f = 1.2ppm to 1.5ppm; 0.7ppm to 0.95ppm

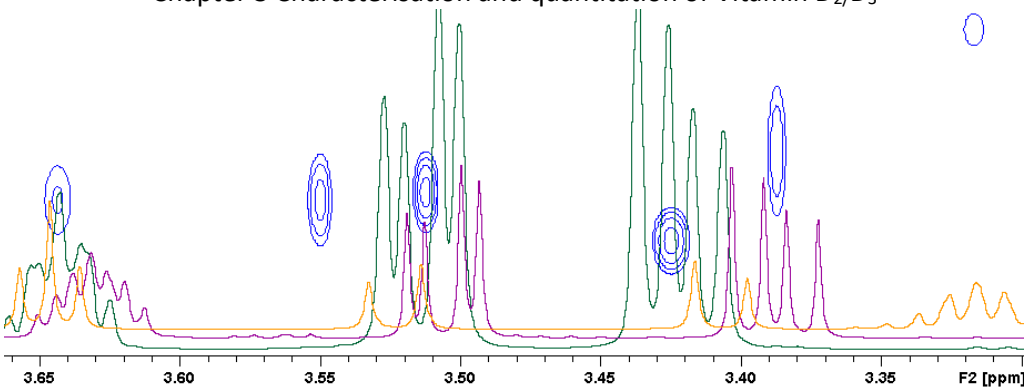

Figure 66 PSYCHEiDOSY spectra overlaid with reference spectras for Panthenol (Orange), Pentylene Glycol (Purple) and Glycerol (Green)

3.2.3.5 Projection displays to demonstrate accuracy of PSYCHEiDOSY

From the full cream formulation encapsulation of at least 1mM of Vitamin D_2 and Vitamin D_3 observed within our emulsion the obstacle to quantitation is assignment of the peaks which can be done through PSYCHEiDOSY, reducing the overlap between the peaks through resolution improvement and having enough S/N for quantitation by optimizing receiver gain for amplification of signal with no requirement for extra scans.

For the last two obstacles frequency selective experiments have been suggested, with pure shift techniques, like that of PSYCHE, also available for these. The group at the University of Manchester have shown a sensitivity increase of 2.5x over that of a traditional 1D spectrum, which when acquired in real time takes the same amount of time. A processing methodology to give similar results to a frequency selective experiment involves calculation of a positive projection using the calculated self-diffusion coefficients of respective formulation components and comparing these to reference spectra. Looking at the projection displays for the conventionally acquired spectra and PSYCHEiDOSY spectra compared to reference spectra of each component, the scope and limitations are highlighted.

Due to sensitivity losses for the 2D and pseudo 3D acquisition there is a loss of lower signal abundance peaks, especially for the lower in abundance peaks. This is highlighted by the lack of any phospholipon peaks seen for the PSYCHEiDOSY spectra and the respective calculated projection. It is also observed from the PSYCHEiDOSY projections and PSYCHEiDOSY spectra overlaid with

reference spectra of Glycerol, Pentylene Glycol and panthenol that there is an increase in the resolution of these peaks and a more consistent measure of the calculated diffusion coefficients for each individual component which as a result gives more accurate projections for each of these compounds relative to conventionally acquired DOSY spectra.

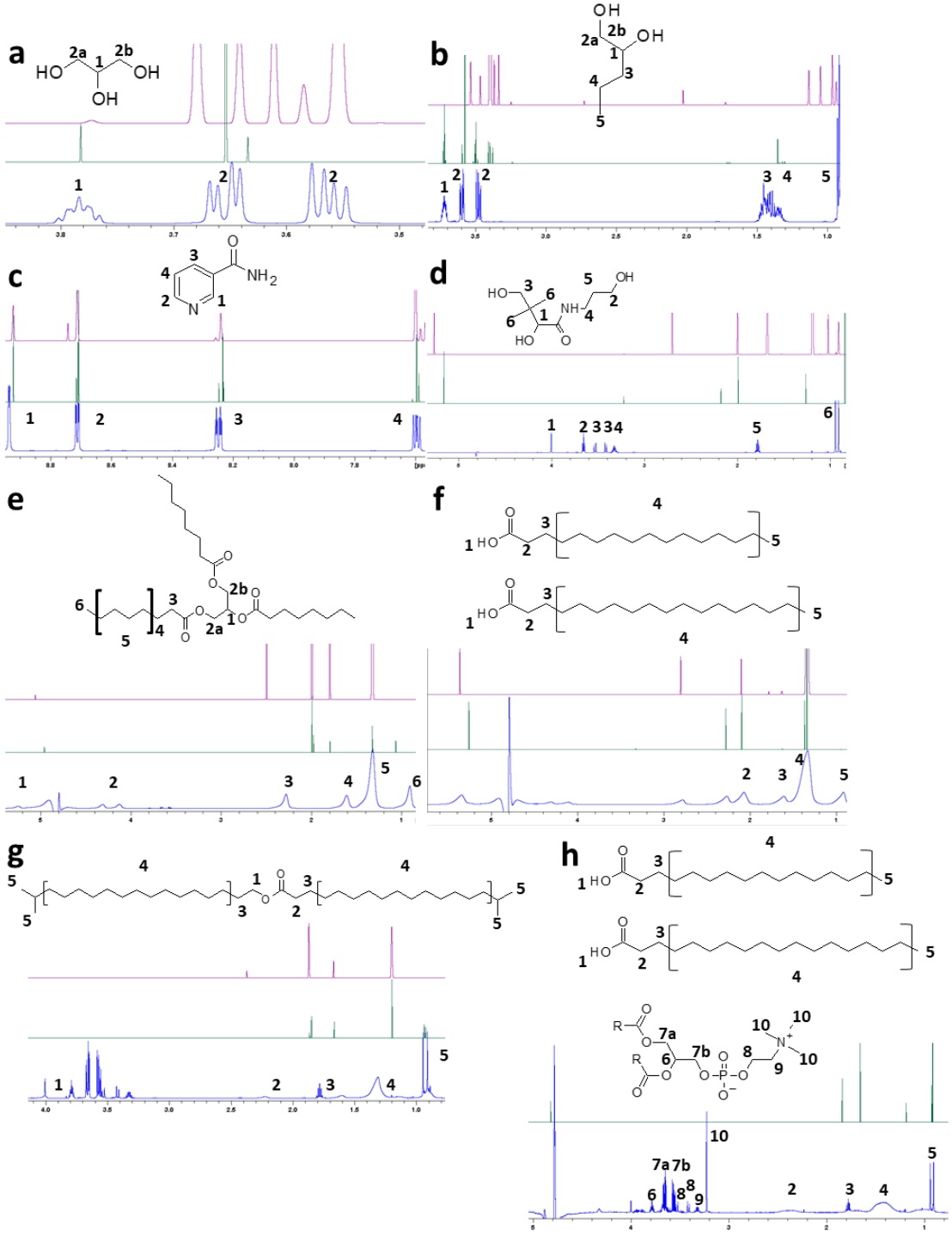

Figure 67 Projection displays from PSYCHEiDOSY (Purple) and conventionally acquired DOSY (Green) calculated from determined diffusion coefficients for each component of full cream formulation compared to reference spectra (Blue). a = Glycerol; b = Pentylene Glycol; c = Niacinamide; d = Panthenol; f = Vegetable Oil; e = Caprylic triglyceride; g = Isostearyl Isostearate; h = Phospholipon 90H.

3.2.4 Fatty acid separation and characterisation studies to elucidate the scope of lipid mixture separation, characterisation and quantitation

Extensive overlap of fatty acid component peaks for full cream formulations meant that these compounds were the largest limiting factor in separation of components based upon their self-diffusion coefficients determined from DOSY acquisition. To investigate ways that the use of pure shift methodology can improve resolution of fatty acid separation and the limitations that still exist for NMR methodology multiple single component and multiple component fatty acid mixtures were prepared to elucidate which peaks could be targeted for separation and determination of mixture components. The below table details the mixtures of fatty acids which were prepared for NMR analysis, alongside these, individual spectra of each fatty acid was created as references for mixtures.

Table 14 Prepared Fatty acid samples

Sample	Fatty acid
1	Lauric
2	Myristic
3	Caprylic
4	Capric
5	Caproic
6	Palmitic
7	Stearic
1&7	
2&7	
3&7	
4&7	
5&7	
6&7	
1-6	
1-7	

Previous studies looking at the composition of fatty acids and separation of compounds has primarily been achieved through the acquisition of 1D ^1H spectra which can differentiate between terminal methyl groups between different fatty acids and also shows comparable quantitation for linoleic acid in vegetable oils compared to GC methods (182). However most methods for the quantitative analysis of fatty acids are for relative abundances of different forms of fatty acid, be

that as triacylglycerides, FFA or phospholipids with separation of fatty acids predominantly achieved through lipid extractions or chromatographical separation methodologies.

In this studyanalysis of fatty acids was initially done with 1D ^1H for preliminary conclusions made on limitations and how far pure shift spectra can increase the scope of fatty acid analysis. Observations of these experiments included the extensive overlap of all fatty acid mixtures made with peak differences between different components reaching a maximum of 0.05ppm. It is however noteworthy to observe that the largest fatty acids peaks aligned and overlapped more to each other than to smaller fatty acids which can be exploited for analysis. Single component sample analysis in reference to mixtures samples did not help in resolving respective peaks from one another. The preparation and acquisition of spectra for two component mixture samples showed how limited conventional 1D ^1H spectra acquisitions are when characterising and quantifying individual components in a complex mixture with all 7 fatty acids showing the same characteristic peaks. Characterisation of single compound samples however is easily achieved through integration of peaks representing CH_2 protons which account for majority of signal abundance in fatty acid spectra and can be used as reference for mixture analysis.

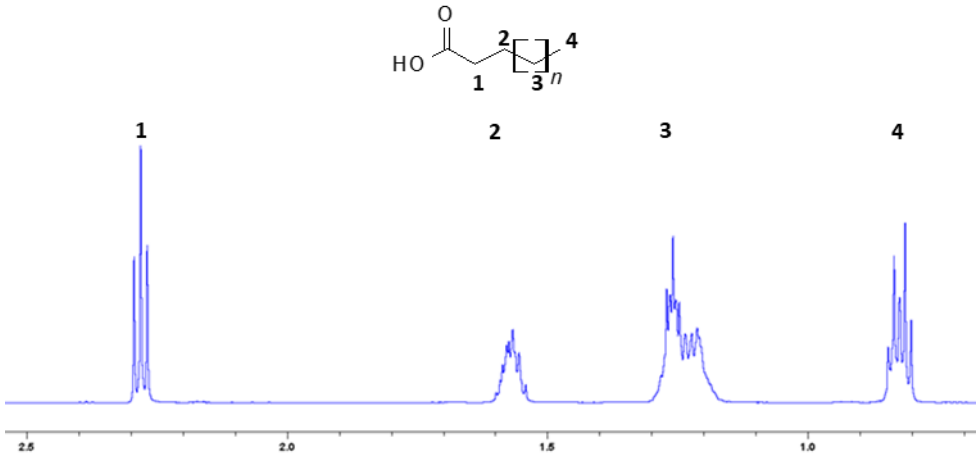

Figure 68 Assigned peaks of fatty acids

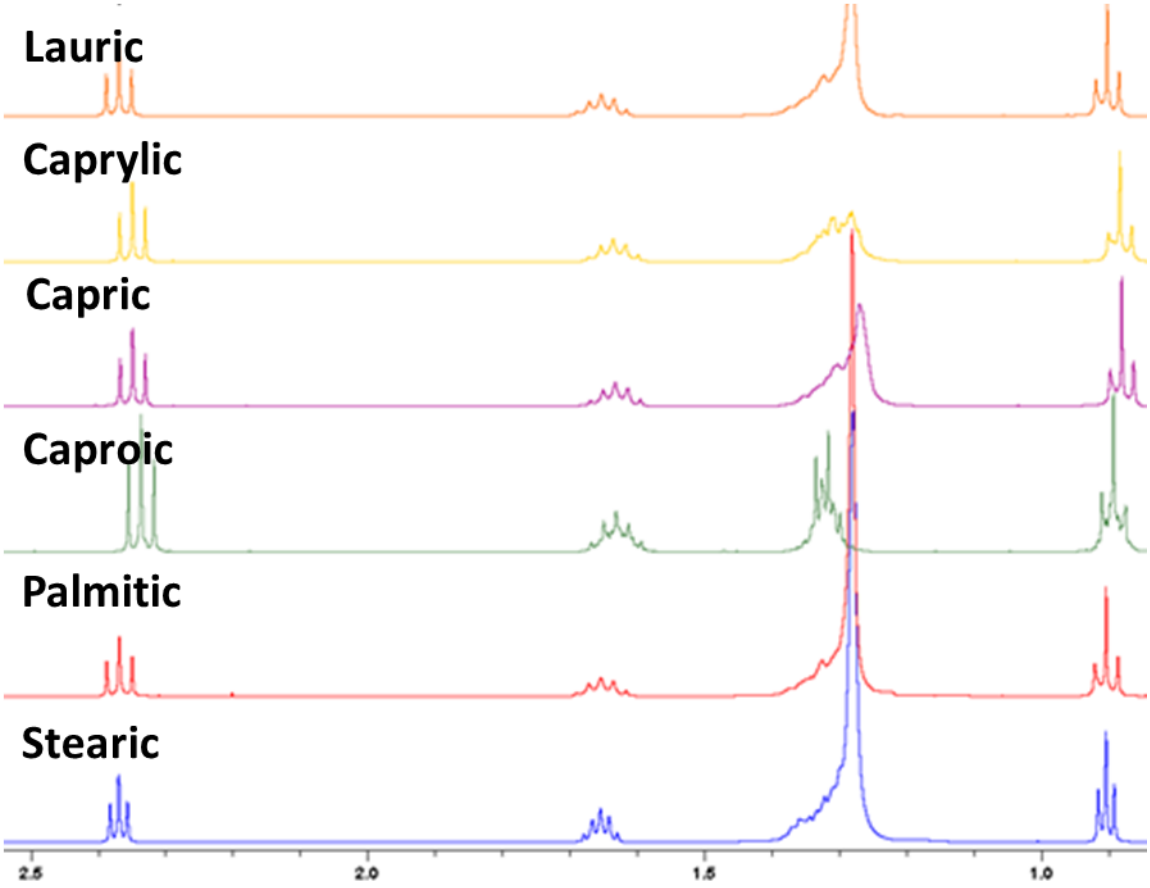

Figure 69 Spectra of 2 compound sample, Caprylic Acid and Caproic Acid

Acquisition of PSYCHE spectra was done to reduce the overlap in several of the peaks. This is shown in the figure below where resolution of peaks at 1ppm can be seen alongside collapsing of peaks at 1.4ppm.

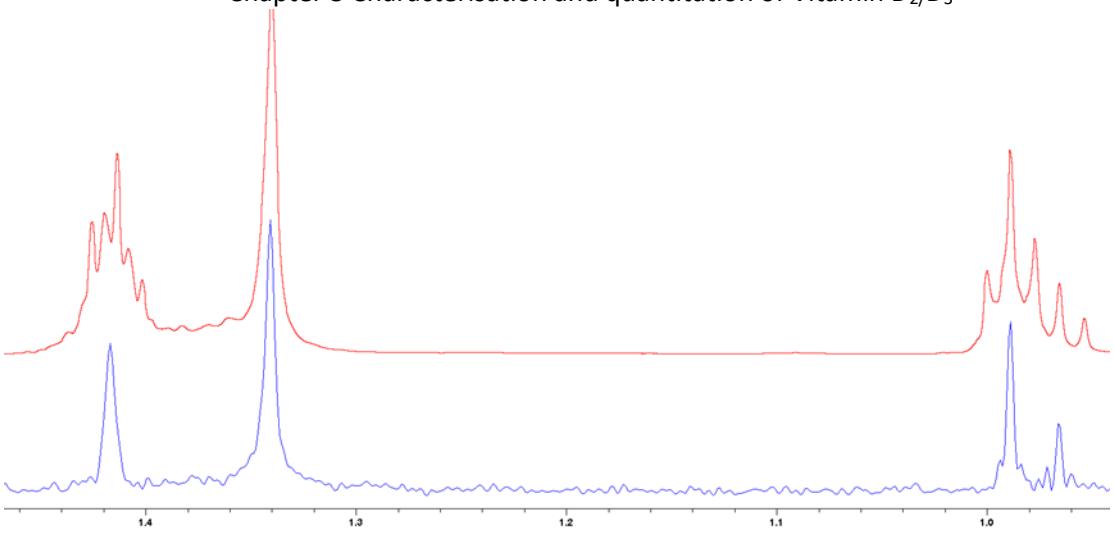

Figure 70 conventionally acquired 1D 1H spectra (Red) and PSYCHE acquired 1D1H (Blue) of 5.6

In 5.6 it is observed that for each peak there is separation between the compounds. This separation has also allowed characterisation of peaks based upon their integration through the use of PSYCHE, despite PSYCHE not using quantitative conditions. This however may not be as big a limitation since characterisation is done through self-integral ratio calculation and shows accurate results compared to expected values. One spectra that stood out from the other 2 component mixtures was that of 5.7 (Caproic and Stearic) which gives the best separation when using PSYCHE acquisition with separation for peaks in the regions of 0.5ppm to 1.5ppm, however again no separation at 1.72 and 2.45ppm is observed which is expected by the subtle proton changes seen near the carboxyl protons over the limited range of proton NMR spectra. This sample is unlike other stearic acid mixtures which predominantly have stearic acid peaks overlapping the other component peaks. This was suggested to be because of the relative bulkiness of stearic acid in the mixtures.

What these findings demonstrated was that comparisons of peaks between fatty acid with relatively large differences between aliphatic chain lengths can be made. The table below illustrates the separation achieved for component mixtures containing the relatively small fatty acid Caproic acid alongside other fatty acids. All samples which contained Caproic acid and other fatty acids with longer aliphatic chains show resolution between peaks assigned 1 and 2 with clear integral ratios determined and number of protons calculated for each peak.

Limitations arise with more than 2 component mixtures, where partial separation is observed but integral ratios between the different peaks are not able to be quantified. Follow up with DOSY was done to see if separation of peaks via size and shape differences could elucidate greater resolution despite the peak overlap seen even for PSYCHE acquisitions. Despite this, distinguishing different mixtures with differences in self-diffusion coefficients seen for overlapped peaks was achievable.

Separation with DOSY mainly occurs at peaks 1, 2 and 3 with distinctively different self-diffusion coefficients calculated within mixtures of components. This shows that DOSY provides a greater scope than only PSYCHE acquisition when considering separation of fatty acid mixtures, however complete mixtures struggle to resolve peaks based upon independent diffusion coefficients.

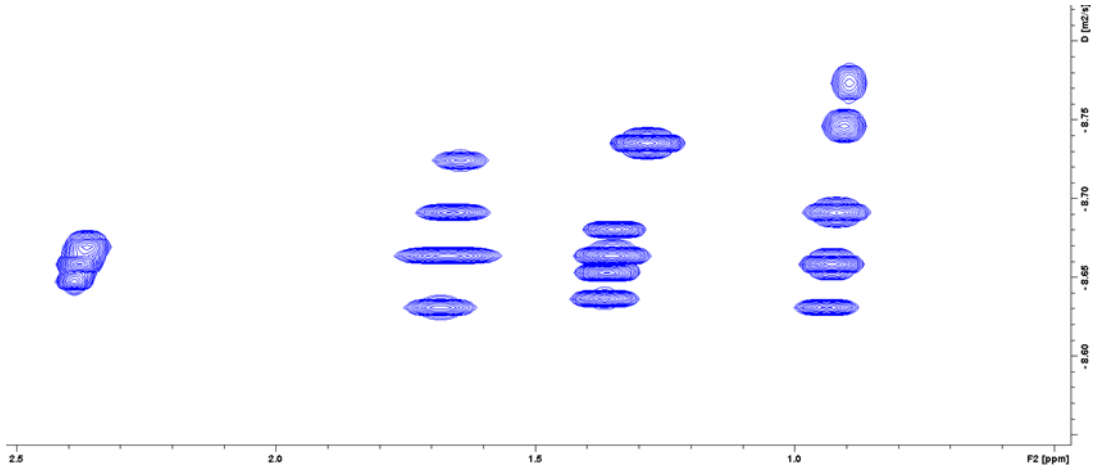

Figure 71 Close up of 2.5 Diffusion Ordered Spectroscopy spectra

The spectra of two component mixture sample 2.5 shows separation for 3 out of 4 peaks, however peaks in between the highest determined self-diffusion coefficient and lowest self-diffusion coefficient present as an error of overlapping peaks. This spectra does however show us that more than one component is present and extrapolation of self-diffusion coefficients for respective components is achieved if peaks at the extremes of low and high self-diffusion coefficient are used to limit the influence of overlap between the peaks. A qualitative comparison of component abundance in the sample mixtures is seen in peaks such as peak 4 which has total overlap and self-diffusion coefficients which are not significantly different, but vary between samples with average

self-diffusion coefficient values for these peaks being lower with a greater abundance of small fatty acids and higher with an abundance of large molecular weight fatty acids. Alongside separation seen for two component mixtures with caproic acid and other relatively larger fatty acid, mixtures containing 3 components that are relatively smaller fatty acids can be distinguished from one another, however larger fatty acids produced large error peaks producing non-significant separation between peaks. To attempt to improve this resolution in larger fatty acid chains PSYCHEiDOSY spectra were acquired to interrogate the effectiveness and possible improvements in separation that can be achieved. Projection calculation of specific self-diffusion coefficient values compared to previously acquired 1D ^{1}H PSYCHE experiments can further validate this technique in separation and characterisation of mixtures. This is demonstrated nicely in the mixture between Lauric and Caproic acid in mixture 1.5 where separation is achieved from diffusion coefficient projection allowing for comparison of integrals relative to each component. This demonstrates clearly in the below figure that the peaks projected for Lauric acids have a larger abundance of CH_2 protons than other proton environments which corroborates with the increased chain length of Lauric acid compared to Caproic acid. To test the reliability and validity of these projections for integral determinations, calculation of these values for all two component mixtures are shown in table 14.

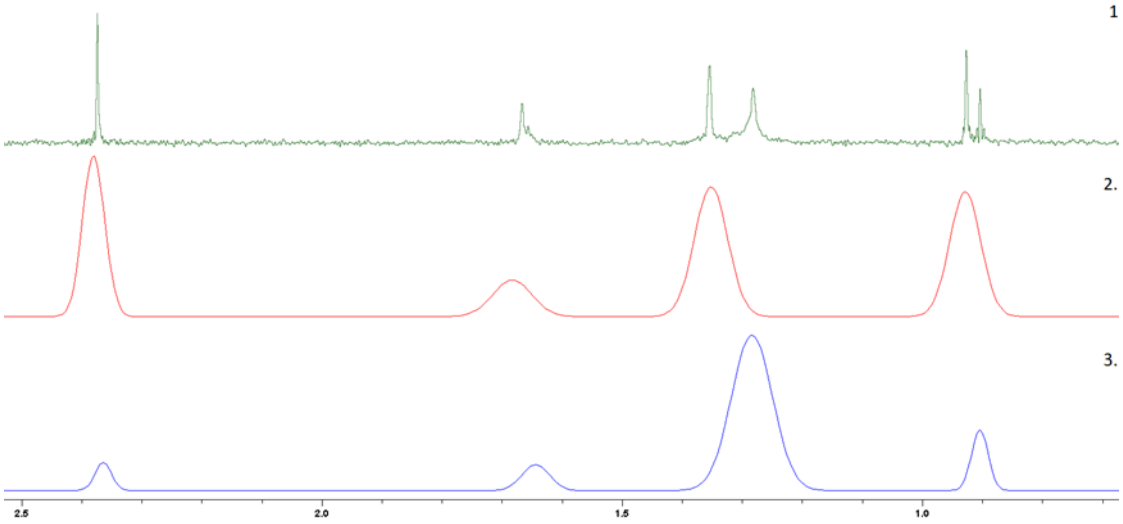

Figure 72 Diffusion Coefficient projections of two mixture sample 1.5 compared against PSYCHE (1) for visual integration comparison of Lauric (3) and Caproic (2) acid.

From table 14, 2 component mixtures have correct integrals for the fatty acid in the sample when compared to Caproic acid, including Stearic acid and Caprylic acid. Whereas for Capric acid and Palmitic acid an error of one CH2 from the expected integral is observed. The worst integral comparisons are for Lauric acid and Mystic acid which have integral differences of two CH2's and three CH_2's respectively. Interestingly it was first thought that this error was due to large difference in abundance as shown in Peak 1 integral ratios, but the largest difference in this value is for 5.6 which has 1 CH_2 change, whereas a low abundance change of 2:1 for 5.4 has the same error associated with it. To evaluate the second assumption that values are affected by the overlap of peak 2 between Caproic and larger fatty acids causing this error as integrals are observed to be lower than expected rather than larger, a plot comparing the self-diffusion coefficients for each components and their fitting standard error per spectrum is shown in figure 72 Alongside this factor the non-quantitative nature of the projection displays must be considered as errors in quantitation of integrals as expected and can be improved upon by implementing experiments such as frequency selective experiments which can be set to give qNMR compatible data.

Table 15 Integrals and integral ratio of 2 sample mixtures (green = expected CH_2 groups; yellow = expected ± 1 CH_2 groups; red = expected ± >1 CH_2 groups)

Component Mixtures	Peak 1 integral ratio	Peak 2 proton ratio	Peak 1 PPM Δ
5.7	3.5:1	(4) : (28 (28))	0.03
5.1	3:1	(4) : (12 (16))	0.03
5.3	2:1	(4) : (8 (16))	0.02
5.4	2:1	(4) : (10 (12))	0.03
5.2	3:1	(4) : (14 (22))	0.03
5.6	5:1	(4) : (22 (24))	0.03

The charting of self-diffusion coefficients further supported the finding that fatty acids become harder to distinguish from one another once they get larger as seen from Caproic acid to Caprylic and Capric acid showing resolution between diffusion coefficients however only significant differences in diffusion coefficients between Caprylic and Capric acid to Palmitic and Myristic acid with no other significant differences observed between the fatty acids. This explains why interpretation of the more complex fatty acid mixtures is hindered in comparison to those prepared with Caproic and larger fatty acids. Error of calculated diffusion coefficient also increases as the length of aliphatic chain increases suggesting that overlap of peaks between Caproic acid peaks and other fatty acid peaks play less of a role than the factor of increased proton environment change adding more error to the attenuation profile constructed by the DOSY pulse sequence.

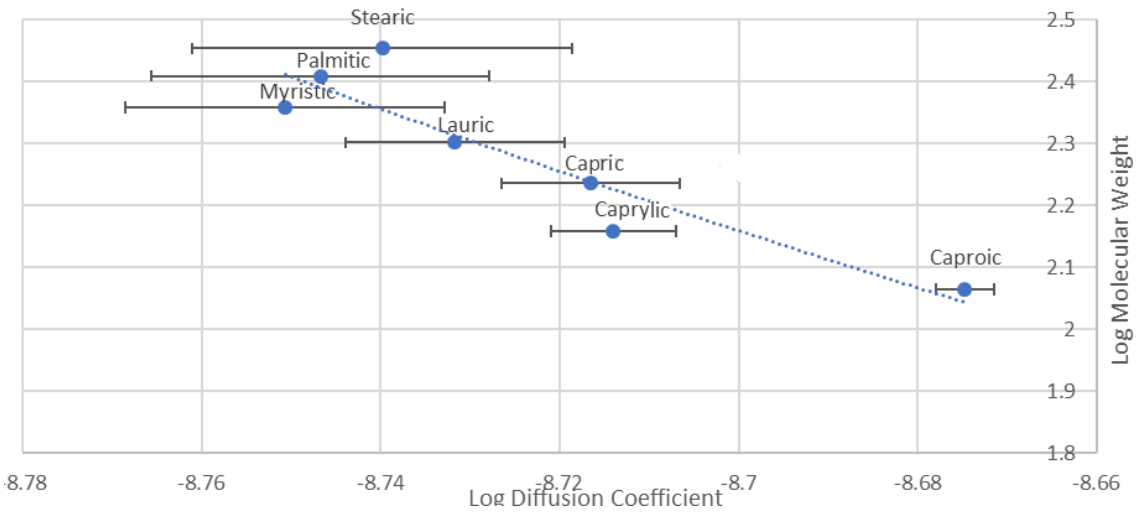

Figure 73 Calibration curve of calculated diffusion coefficients for individual fatty acid samples

Implementation of PSYCHEiDOSY spectra improves the resolution between two component sample mixtures and demonstrates resolution between even the three component mixtures, however the S/N limitation of PSYCHEiDOSY and time required for experiment limits it use for larger component

mixtures which previous PSYCHE and DOSY experiments showed were too extensively overlapped to be appropriate for PSYCHEiDOSY acquisition.

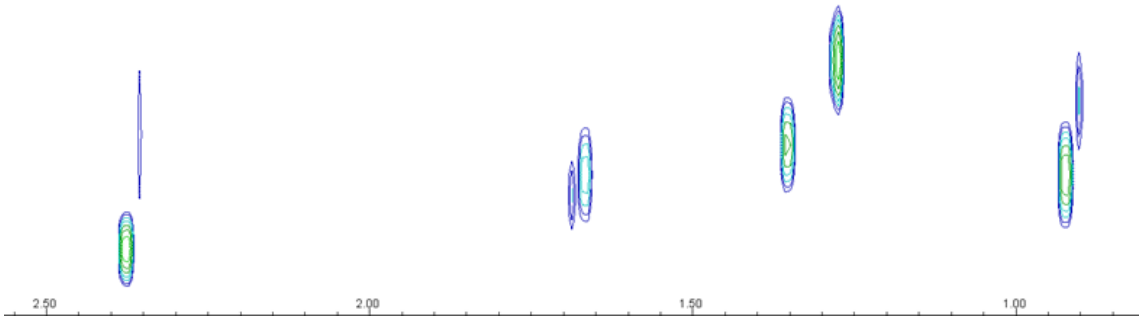

Figure 74 PSYCHEiDOSY of sample 5.7

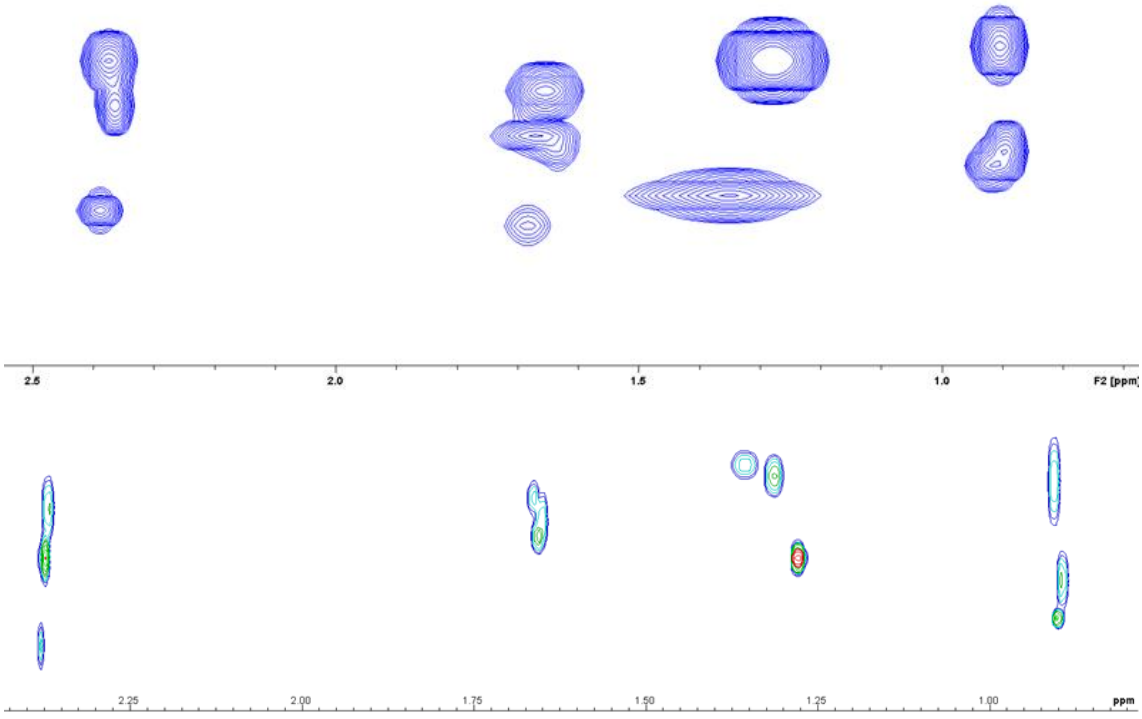

Figure 75 Conventionally acquired DOSY spectra (top) and PSYCHEiDOSY spectra (bottom) of 3 component mixture 2.6.7

Resolution improvements in 3 component mixture samples is observed with the use of PSYCHEiDOSY giving 3 resolved peaks for all 1D ^{1}H PSYCHE peaks apart from peak 3 which gives an average self-diffusion coefficient for mixture as peaks are extensively overlapped. This is very promising for analysis of fatty acids in the future as identified peaks can be targeted for resolution improvement, however the error between self-diffusion coefficient values is still high as seen for

peak 1 and 4 with no significant differences in self-diffusion coefficient values between respective resolved peaks but clear differences in the calculated self-diffusion coefficient values for peak 2 which is affected by the large overlap of much higher signal abundance of one of the components present which shifts all of the peaks to higher self-diffusion coefficients. However the potential for this methodology comparable to previous methods is shown by terminal methyl group separation and characterisation of other peaks which have relatively lower or higher self-diffusion coefficients.

3.3 Discussion

In these studies, the whole structure of vitamin D_2 and D_3 is assigned by ^{1}H NMR and the precise assignment of signals on the steroid ring system through the use of 1D ^{1}H pure shift acquisitions. This will allow for easier analysis of vitamin D metabolism through the qualitative and quantitative tracking of D_2/D_3 in its ergocalciferol, cholecalciferol, calcifedol, calcitriol (Active form) and 24,25-Dihydroxycholecalciferol (inactive form) forms, which all have very similar chemical structures. Appropriate quantitative settings required to be in place for accurate determination of amounts of target compounds are highlighted and how formulation properties can affect the reliability of quantitation of not only actives but also formulation components. NMR can be used to obtain LODs at physiological concentrations of vitamin $D_2/_3$ in simple samples however there is an interesting finding where D_2 was measured over several samples, with different experimental settings was consistently 10x lower in concentration than vitamin D3. This issue was explored and was assumed to be due to solubility differences of vitamin D_2 compared to D3 as different batches were used and different equipment employed to mitigate any user error.

When these techniques were applied to skin cream formulation models, free vitamin D was not observed at the expected concentration in D_2O samples. This suggests that in skin cream, precipitation or micellisation of the vitamin D is occurring, reducing the apparent amount of freely available vitamin D in solution. This result can be demonstrated by the concurrent running of experiments in D_2O with critical micelle concentrations of surfactants, alongside samples run in MeOD, which does not allow the formation of micelles. Whilst it has also been reported that

Vitamin D_3 can be photodegraded at relatively low intensity of UV, no evidence of this was observed in simple solution, and it is unlikely that this is the cause of the lower concentrations observed in the skin cream formulations. Free vitamin D is observed at 15%-40% of the initial concentration through identification of peaks unaffected by encapsulations broadening effects. This means that 15%-40% of vitamin D is unable to permeate skin in the same way as micellised Vitamin D within the cream formulations with the differences in measured values seen from MeOD and D2O solvent variable samples. Further validation of free versus encapsulated Vitamin D can be achieved through further diffusography analysis to see interactions between Vitamin and surfactant as we will see the diffusion characteristics of Vitamin D will vary depending on state, be it micellised or free in solution. There is also an issue with overlapping of target peaks by emulsion peaks. Despite observation of considerable signal overlap, olefin peaks of vitamin $D_2/_3$ at 6 ppm and 0.55 pm are resolved well enough to be detected within the mixtures with peaks at 6ppm showing clear resolution and minimal effects from baseline distortion by high signal intensities of other compounds. The separation of formulation components through pure shift diffusion ordered spectroscopy experiments (PSYCHEiDOSY) demonstrated a non-destructive and automated method for complex mixture analysis for formulations and allowed for individual spectra of each compound to be constructed. However, there was large error seen for compounds that had fatty acid parts, especially with long aliphatic chains present. Investigation of why this was seen and any methodologies that could be employed to improve the results was achieved through fatty acid mixture analysis. It was initially observed that conventionally acquired 1D ^{1}H NMR spectra provided characterisation for single compounds, however it lacked characterisation potential for any more than one fatty acid mixtures through overlapping of peaks. Acquisition of PSYCHE 1D ^{1}H NMR spectra showed that fatty acid mixture peaks could be resolved from one another, but this was limited to comparisons between small and large fatty acids rather than comparisons between larger fatty acids which are more common in our formulations and in biological mixtures. Interestingly PSYCHE allowed for a degree of quantitative characterisation for resolved peaks where CH_2 peaks could be integrated to differentiate between the fatty acids within the mixture. When this

methodology was partnered with projection displays in DOSY further validation of the characterisation of peaks as integral values and self-diffusion coefficient values corroborated the identities and abundances of fatty acids within the mixtures for 2 to 3 component mixture samples.

Despite this potential it was observed that a major limitation existed for DOSY based separation of peaks that the self-diffusion coefficients calculated for larger fatty acids become significantly less variable as aliphatic chain length increase, this meant that DOSY could not distinguish between Palmitic, Myristic and Stearic acid even if there was no overlap between peaks. PSYCHEiDOSY acquisition allowed for a decrease in error caused by peak overlap which allowed for greater resolution seen in 2 and 3 component sample mixtures, unfortunately it was unable to provide separation for mixtures with more components than 3. These findings showed that PSYCHEiDOSY can be extremely useful for separation of complex mixtures, however for larger, structurally similar compounds, fatty acids for example, the limitation is caused by the inherent properties of these compounds in solution being very similar and further investigation using techniques such as matrix assisted or 3D DOSY (HSQC-DOSY) could elucidate greater resolution and potential for this methodology.

The potential of HSQC-DOSY is also demonstrated for this application in a short study on the separation potential of two common formulation components, the permeation enhancer butanediol and moisturiser panthenol. Alongside these new methodologies an aside an appropriate way to compare these results would be through the use of frequency selective pure shift experiments (183). This again would be limited to already resolved peak for fatty acids peaks and other compounds shown by previous PSYCHE experiments but would be an interesting add on to display individual spectra, which in theory would be unaffected by other component effects apart from universal effects of the sample's overall properties which alongside single component spectra could demonstrate how formulation effect different parts of a compound. An added benefit of frequency selective PSYCHE experiments is the finding that S/N ratio per time unit is more than an

order of magnitude more sensitive than a conventionally acquired pure shift experiment, which means that acquisition of several frequency selective experiments on peaks of interest could actually be faster than a broadband experiment if compounds targeted are previously known and resolution of one peak can be shown for a conventional 1D ^{1}H spectra to target frequency to. These experiments can then be implemented into a total correlation spectroscopy pulse sequence for smaller molecules where magnetization can transfer throughout the whole molecule to give all the peaks for a lower abundance compound which would have previously been overlapped or completely hidden from the investigator. A graphical abstract in figure 78 details the potential of these future methodologies for not only separation, but characterisation and quantitation of complex mixtures. If time however does not allow for a 2D selective acquisition, a recent selective 1D ^{1}H NOESY acquisition named GEMSTONE (Gradient-Enhanced Multiplet-Selective Targeted-Observation NMR Experiment) has been demonstrated to show selection of peaks which overlap with multiplets of itself and other compound peaks to give selective spectra for individual multiplets. It has also been highlighted that this pulse sequence is compatible with selective 1D TOCSY, COSY, ROESY and relaxation experiments which demonstrates its great potential for mixture analysis going forward (184).

3.4 Conclusion

Appropriate and novel pulse sequences with calibrated parameters can detect down to the in vivo baseline level of Vitamin D_2 and D_3 in an idealised sample environment. However, for full cream formulations, novel techniques, such as PSYCHEiDOSY and projection display analysis need to be used for accurate separation, characterisation and quantitation of individual components. This is because the dynamic range and complexity of our mixtures is a limiting factor for the NMR hardware, as amplification of our low concentration peaks of interest is prevented by high abundance glycerol peaks, which would overload the receiver and the overlapping of peaks which prevents accurate determination of peak integrals. Therefore, the further implementation of PSYCHEiDOSY and addition of frequency selective experiments will allow for greater reliability and

further validation for quantitation of in-vivo levels of biomarkers which are present in highly concentrated and complex samples in situ, through an automated and non-destructive acquisition methodology.

Looking forward, the implementation of real-time pure shift acquisition instead of interferogram through shortening of the pulse sequence time to fit within the dwell time would reduce the time required for pure shift experiments. Alternatively post-processing methods, such as covariance analysis, can make experiments possible in a suitably short time period. The application of NMR for detecting physiologically relevant concentrations of vitamin D and highlighting the effects of the traditional skin cream matrix on the amount of free vitamin D available has been validated and addressed. In Chapter 5 adaption of this approach is done to consider ex-vivo models for the dermis and assess active permeation using the optimised techniques reported here for both separation, characterisation and quantification.

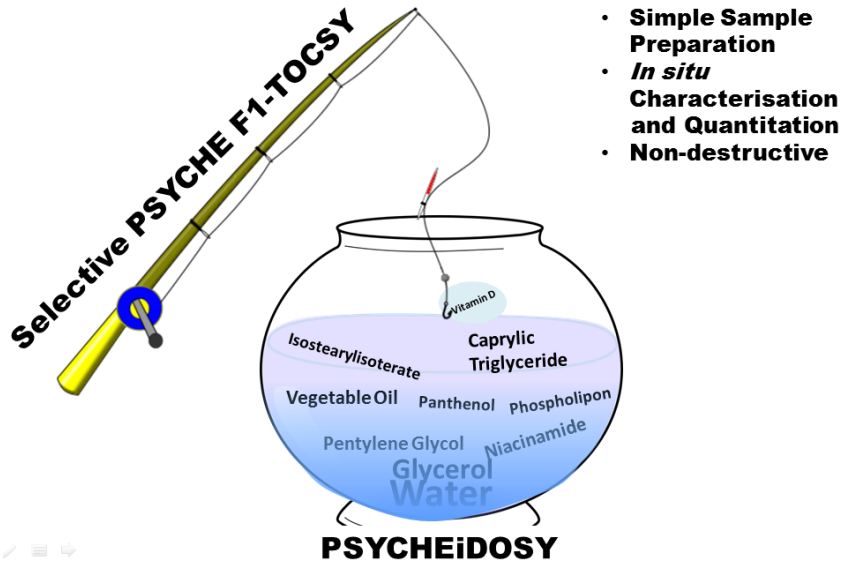

Figure 76 Future Methodology identified as best way to get the resolution and sensitivity required in full cream emulsions

Chapter 4 Utilising validated NMR techniques for the in-situ characterisation and quantitation of key biomarkers and actives in tape stripped ex-vivo skin

The development of a semi-automated and rapid analytical technique for dermatological analysis has become a key aim of many academic and commercial entities through greater awareness of people to skin health and its importance in the 21st century. A proof of concept methodology demonstrating the use of validated non-destructive, in situ NMR techniques for characterisation and quantitation of NMF compounds and actives from topical formulations is presented. This study is the first to combine diffusion NMR, semi-automated quantitation and ex-vivo skin samples to measure NMF and permeation of actives. This work shows that diffusion NMR allows for resolution between formulation components through determination of self-diffusion coefficients. The metabolomics software Chenomx^{tm} is used to identify and quantitate individual NMF components. Comparable results to previous literature on NMF layers in the skin is demonstrated, alongside reinforcing findings on permeation enhancers and heat effects on transdermal delivery of actives and formulation components. The presented methodology has shown great potential as an effective, non-destructive, fast and versatile technique for dermatological analysis of physiology and actives, with future hardware and software developments in NMR making the future of dermatological analysis via NMR very promising.

The separation of complex mixtures in skin analysis by HPLC methods is extensively used in the characterisation and quantitation of NMF components in the skin. The extraction process requires tape strip washing in ammonia solution, evaporation and reconstitution in pure water. Solvent systems and columns must be carefully chosen for specific systems and calibrated with reference standards (195). Tape strip extraction has also been achieved through centrifugation and shaking in KOH solution for at least 2hrs, with alkaline extracts neutralized with acid and shaken again for 2hrs followed by filtration (196). This requires column, flow rate, mobile phase and retention time to be carefully set for each extraction. However with the set out extraction procedure NMR can extract and acquire the data for a sample within an hour for a 600MHz NMR spectrometer with no cryo-probe (Chapter 2.3.2, 2.3.3 and 2.3.4).

Separation of complex mixtures prior to NMR analysis is one of the reasons why it is not more commonly used, however the use of pulsed field gradients and spin echoes can be exploited to achieve virtual separation. These techniques can calculate differences in translational diffusion through fitting of attenuation profiles of compounds to the Stejskal-Tanner equation alongside removal of large molecules through relaxation time filtering (197). Differences in diffusion coefficients gives resolution between single molecule peaks in NMR spectra and can be optimised through the use of pseudo 2D and 3D acquisition techniques. NMR analysis through separation, characterisation and quantitation allows the elucidation of multiple concentrations for identified compounds of interest within a single sample that has not been chemically or physically treated beforehand.

The use of NMR metabolomics software package Chenomx^{tm} has demonstrated the potential of NMR as a non-destructive metabolite quantifier (198), exploiting its capacity for use as a primary method for quantification through an integral ratio method (107). The scope for quantitation is also increased as a tolerance for hydrophilic and hydrophobic elements within biological mixtures is intrinsic to NMR. In addition, NMR demonstrates high sample throughput by automation, with potential of remote desktop applications for simplification of use.

For this study analysis is limited to the surface, keratinized, anuclear cells extracted from the top 12 layers of the stratum corneum removed via tape stripping . This limitation however does not obstruct the analysis of water retention potential and the most important aspect of the skin as a barrier to physiological, chemical and microbe attack at the surface *Stratum corneum* level.

4.1 Initial findings

Standard 1D ^{1}H spectra from the two control groups and five treatment groups were initially visually compared to identify common elements of all spectra, namely PBS buffer, solvent peaks and tape strip peaks. These were assigned to remove confusion with treatment compounds and Chenomx^{tm}

assignments of NMF compounds. One limitation immediately observed during this initial assignment was the overlap of fatty acid peaks from the skin's intercellular lipid matrix and those added in treatment groups.

4.1.1 Assignment and removal of PBS control without tape strip data from samples

Tape strips were prepared as described in section 2.3.2, 2.3.3 and 2.3.4 with initial analysis done to normalize all spectra to the internal reference peak which is constant at 100µM for all samples. This allowed for visual inspection of spectra and qualitative observations made about each treatment type and tape strip layer comparisons.

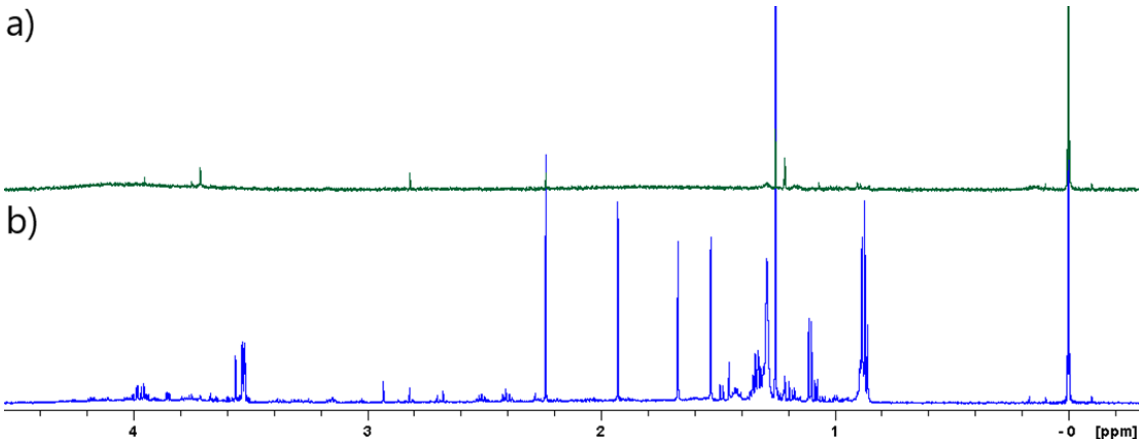

Figure 77 Comparison between PBS buffer control (a) and Tape Strip control (b)

Secondly the observation of the two set control groups: no tape strip, deuterated PBS buffer and internal reference TSP; tape strip of skin with no treatment applied, deuterated PBS buffer and internal reference TSP. This observation allows for the assignment of peaks that are part of the PBS buffer, non-treated skin, acetate strip and the treatments added to the skin. Using the control containing only PBS, calculation of the difference spectra with all other reference normalized sample spectra removes peak interference by solvent peaks that would be consistent throughout all sample spectra. One limitation found during this assignment was the overlap of fatty acid peaks from the skin surface and those added through the topical treatments applied.

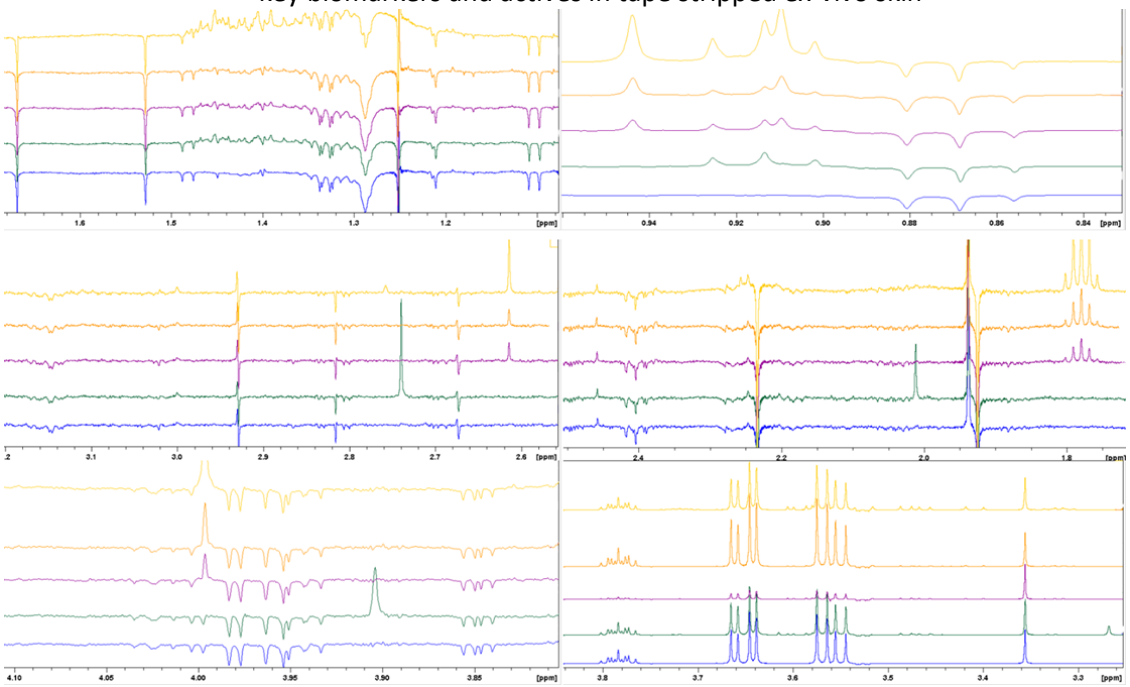

Figure 78 Difference spectra between treatments and control sample, positive peaks show increased abundance in treatment samples compared to negative peaks with increased abundance in control samples. Yellow = BW70; Orange = BW; Purple = V; Green = AI; Blue = P.

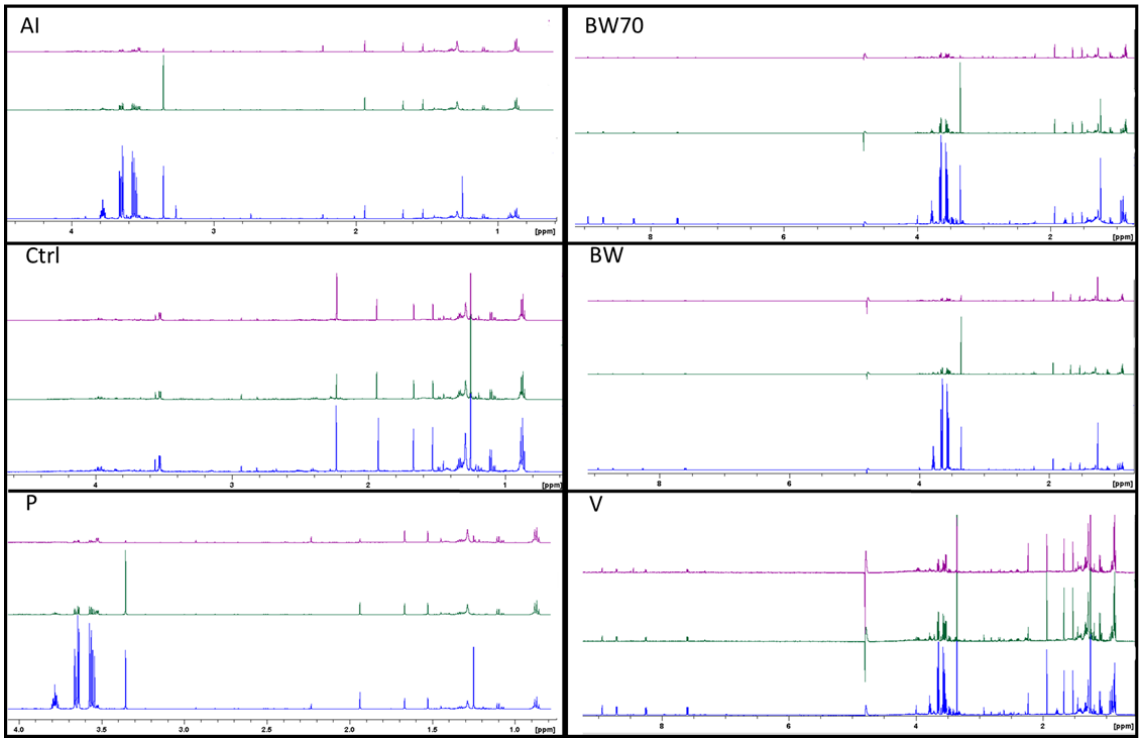

Figure 79 Spectral comparison between layer groups 1/2/3 (Blue, Green, and Purple respectively)

Component signals throughout the layers are observed, especially in the treatment samples where peaks, surmised to be topical formulation components, drop in intensity at a much greater rate than peaks representative of skin and tape strip elements seen in the control groups. Detection and

quantification of formulation peaks is achieved throughout the twelve layers of each treatment, alongside peaks corresponding to skin compounds in the tape strip control.

4.1.2 Regional Analysis

Since NMR spectra are dependent on resolution through chemical environment of targeted nuclei, analysts can compare sample spectra to each other through signal abundance in different areas of the spectra when quantitative conditions are met, and abundance of signal is normalized to an internal or external reference set at a constant value between samples being compared.

4.1.2.1 Functional Group analysis

The first method of analysis was regional comparison of spectra. Initial quantitative comparison of layers was done by regional percentage abundance of the total signal with the sum of integrals normalized to 100, with integrals covering the Aliphatic (0.50 – 2.50ppm), Alcoholic (2.50 – 4.40ppm), Methoxy/Vinylic (4.9 – 6ppm), conjugated and non-conjugated alkenes (6 – 8.4) and carboxylic, aldehydes and amide functional groups (8.40 – 10.30) ranges. Large changes between adjacent layers is observed, which can be explained by skin furrows and the inherent heterogeneity of skin layers. This led us to group the acquired layers (see more in materials and methods), as seen in previous literature (49) to compensate for these discrepancies between individual layers. From the regional percentage abundance analysis, clear differences are seen between the Aliphatic and Alcoholic regions of treatments when compared to the control tape strips with the abundance of alcohol being higher in treatments. This is primarily explained by the addition of glycerol and glycols which are common ingredients in formulations designed for skin. In treatments V, BW and BW70, an increased abundance in carboxylic peaks is observed. This is explained by the presence of Niacinamide in these treatments, which adds signal to the conjugated/non-conjugated alkenes region, the carboxylic, aldehyde and amide region.

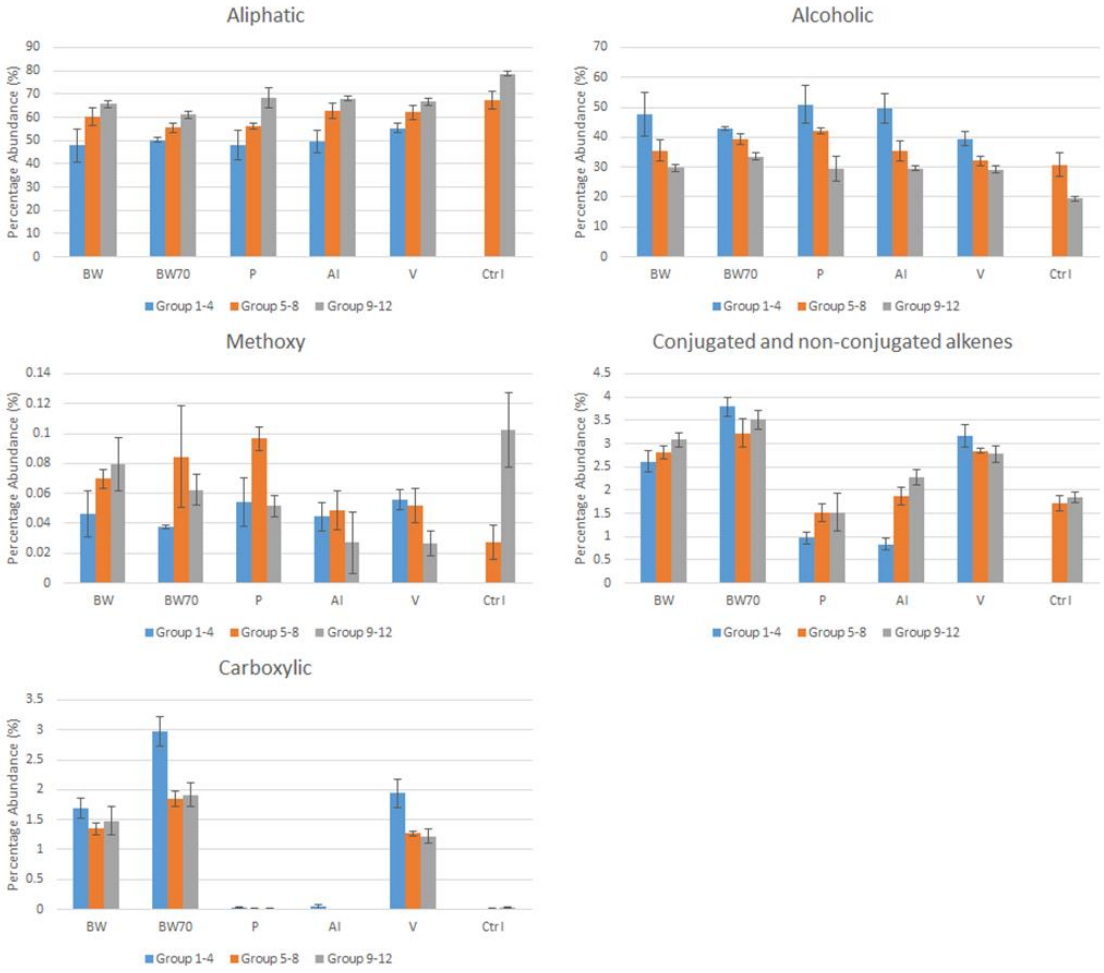

Figure 80 Relative percentage abundances of functional groups for the different treatments, mean ± standard deviation.

Interestingly in figure 80 the most significant changes are observed between groups which are shared for all treatments, apart from the carboxylic abundances where only BW, BW70 and V have peaks in this part of the spectra.

4.1.2.2 Free fatty acid study using abundance analysis

It has been previously demonstrated that the lipid composition of the *Stratum corneum* varies between layers. The compounds of interest in the stratum corneum lipid matrix are phospholipids, cholesterol-3-sulphate, ceramide, cholesterol, sterol esters and free fatty acids. However for this study through the extraction process used and limitations of NMR acquisition, meant that larger molecules such as phospholipids and ceramides are unlikely to be observed through removal in the centrifugation step of extraction as they will be separated from supernatant. This means that observations and interpretation on the levels of cholesterol, cholesterol-3-sulphate, sterol esters

and free fatty acids can be achieved in this study if peaks can be elucidated from the acquired data. After observing the limitations of the complex spectra associated with cholesterol, cholesterol-3-sulphate, and sterol esters, it was decided to evaluate lipid composition in this study primarily on free fatty acid levels as a whole mixture rather than individual separated fatty acids.

Qualitative observations can be made on relative abundance and saturation level of free fatty acids, however separation of fatty acids as shown in Chapter 3 highlights the limitations encountered in single molecule characterisation and quantitation. For free fatty acids it was expected from the aforementioned previous studies (207) to see an initial decrease in free fatty acids after level 1, with smaller fatty acids decreasing in abundance at deeper layers in comparison to the larger fatty acids e.g., C24:0. This also correlated to the observation of reduced unsaturated fatty acids relative to saturated fatty acids as layer number increased. These findings however were only done down to 5 layers where in this study samples go down to 12 layers, allowing for an increased scope in the observation of fatty acid abundance (207).

Here targeting of the methyl, olefin adjacent and carboxyl group adjacent protons of the fatty acids present within samples was done. Since significant overlap of these peaks from the complex mixture of fatty acids exists the findings from these results are limited. This limitation is highlighted in the large abundance discrepancy seen between the methyl peak at 0.8ppm integrated for three protons per single molecule to the olefin and carboxyl adjacent protons integrated as 2 per single molecule. The discrepancy between these groups is a factor of 10x, where normalization of the reference peak to 10 for the methyl peak abundance measurement and to 100 for the olefin and carboxyl peaks. However there is a similar trend for the olefin and carboxyl peaks which is absent for the methyl peaks where no significant change is seen so this suggests that the methyl peak is made from a much larger sample of molecules than the olefin and carboxyl peaks, possibly suggesting that ceramides abundance are added here whereas free fatty acids are seen at 2.4ppm and 2.5ppm. Multiplet peaks appear at 1.9ppm and 2.2ppm with similar abundances to peaks

shown here throughout samples. However, these peaks are overlapped extensively and were not suitable for integral comparison.

The methyl peaks highlighted in figure 80 show that there is a large triplet peak with several peaks to the left of the peaks that are overlapped. These overlapped peaks are at a relatively similar abundance to the other peaks highlighted here but they are completely overlapped by the larger triplet peak that quantitation or integral calculation for this peak is inappropriate.

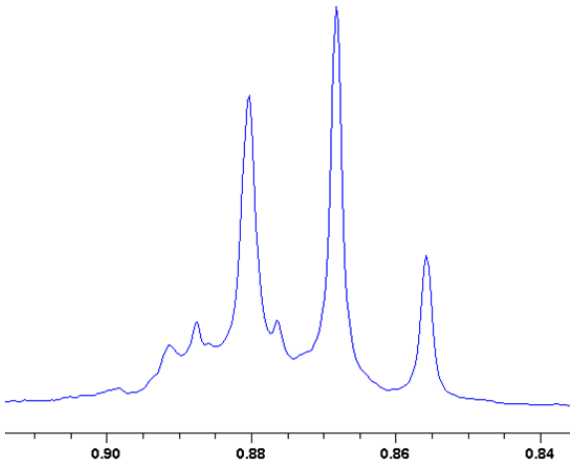

Figure 81 Suspected lipid methyl group peak, triplet, Jhh = 7.54Hz

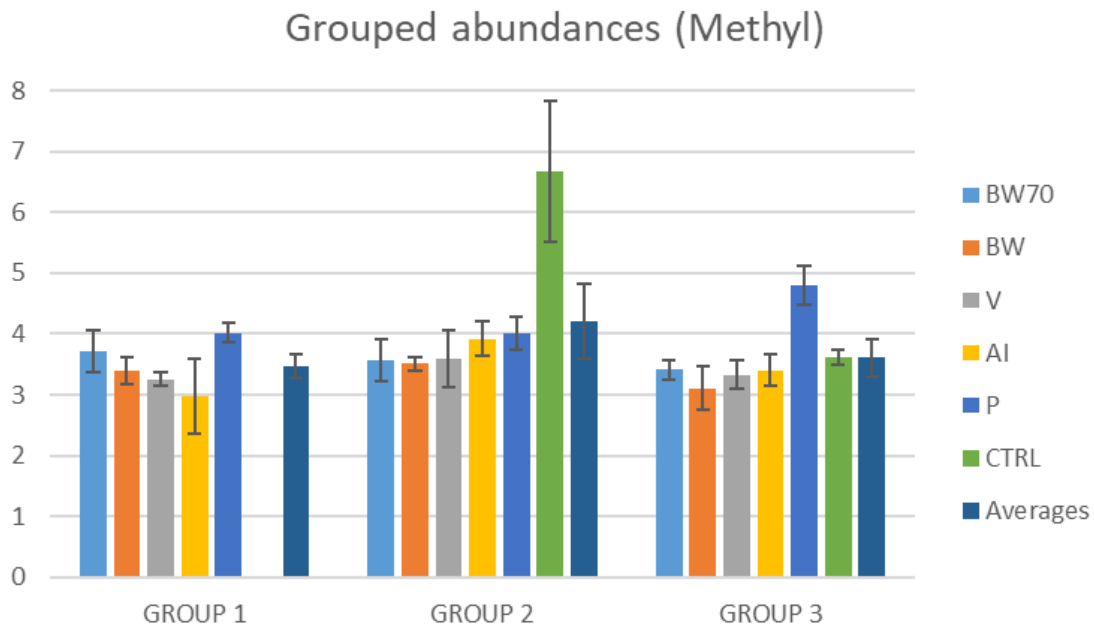

Figure 82 Grouped average methyl abundances for treatments, normalised to TSP integral set at 10, mean ± standard deviation

Unlike the previous findings which showed a decrease in lipids as layers went from 1 to 3 to 5, no significant difference is observed in treatment samples apart from a significant increase from group

1 to group 2 in the AI formulation treatment. The large abundance of this peak seen in the control sample also makes a significant increase in the average of samples from group 1 (Tape Strips 1-4) to 2 (Tape Strips 5-8), however the large contribution by the control sample which is absent from group 1 means the findings from this are limited. A significant drop in several of the treatments from Group 2 to Group 3 which matches previous findings on a decrease in the lipid composition of the skin. One treatment that is the reverse of this trend with the Physiogel treatment demonstrating a significant increase in methyl peak intensity in group 3 samples compared to group 1 and 2 which are relatively high compared to other treatments. This suggests an alternative method of action of Physiogel to other treatments in relation to lipid composition in the *Stratum corneum*.

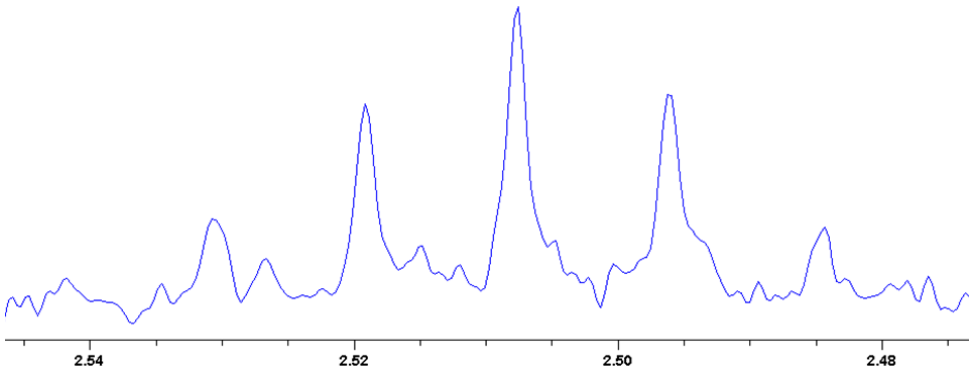

Figure 83 Proposed Olefin peak of skin lipids, quintet, 6.98Hz, which suggests 2 alkene groups present

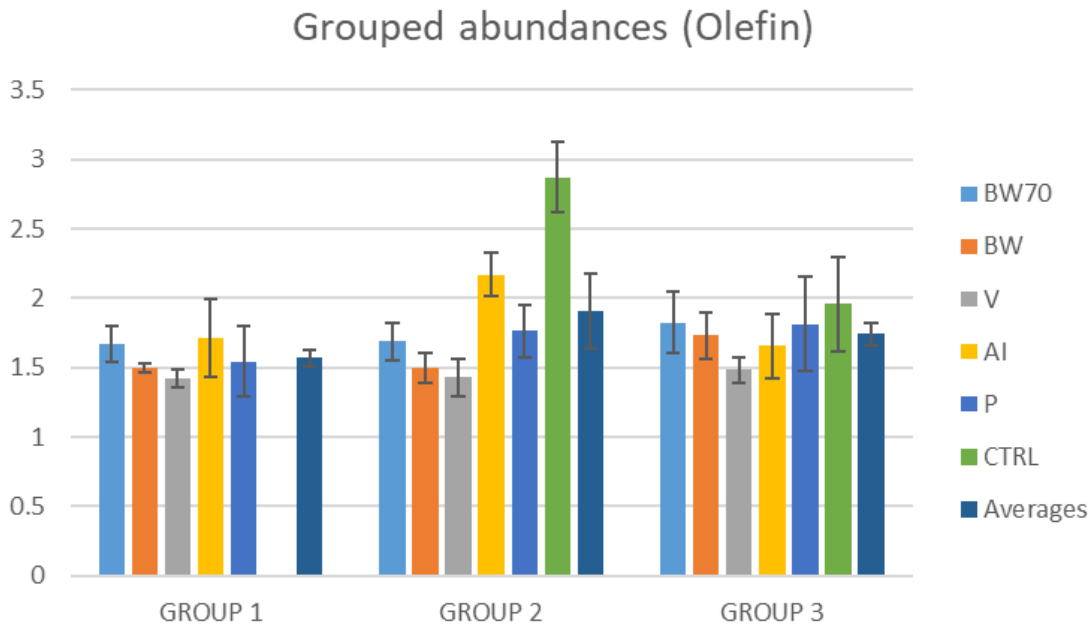

Figure 84 Grouped average olefin abundances for treatments, normalised to TSP integral set at 100, mean ± standard deviation

From the olefin peak abundances a similar trend in the abundances is seen with methyl groups, with increases from group 1 to 2, and no significant change to group 3 in the average results. There are only significant changes seen between groups for treatment AI and controls. The significant changes seen between physiogel treatment groups for the methyl abundances are no longer seen, which means that saturated fatty acids are more likely introduced by physiogel than unsaturated fatty acids into the deeper layers.

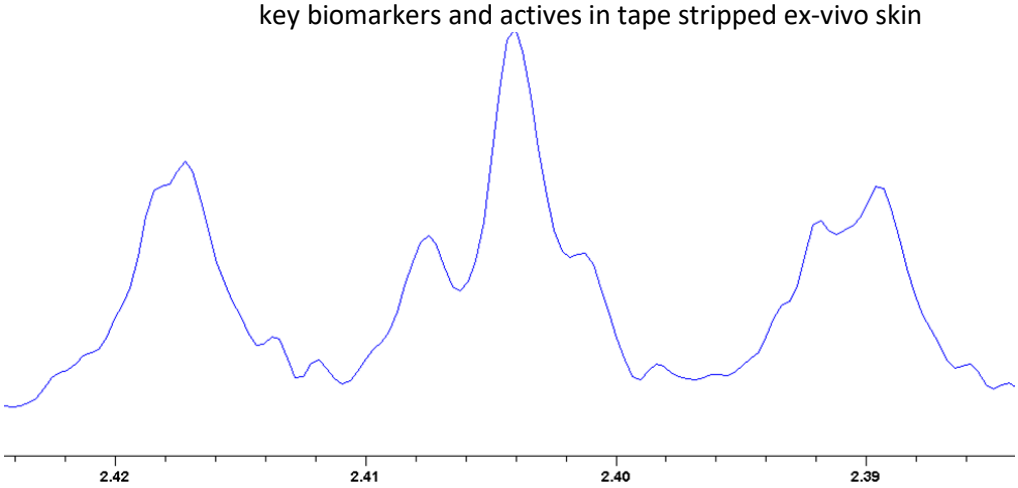

Figure 85 Proposed carboxyl peak of skin lipids, triplet, Jhh = 7.86Hz

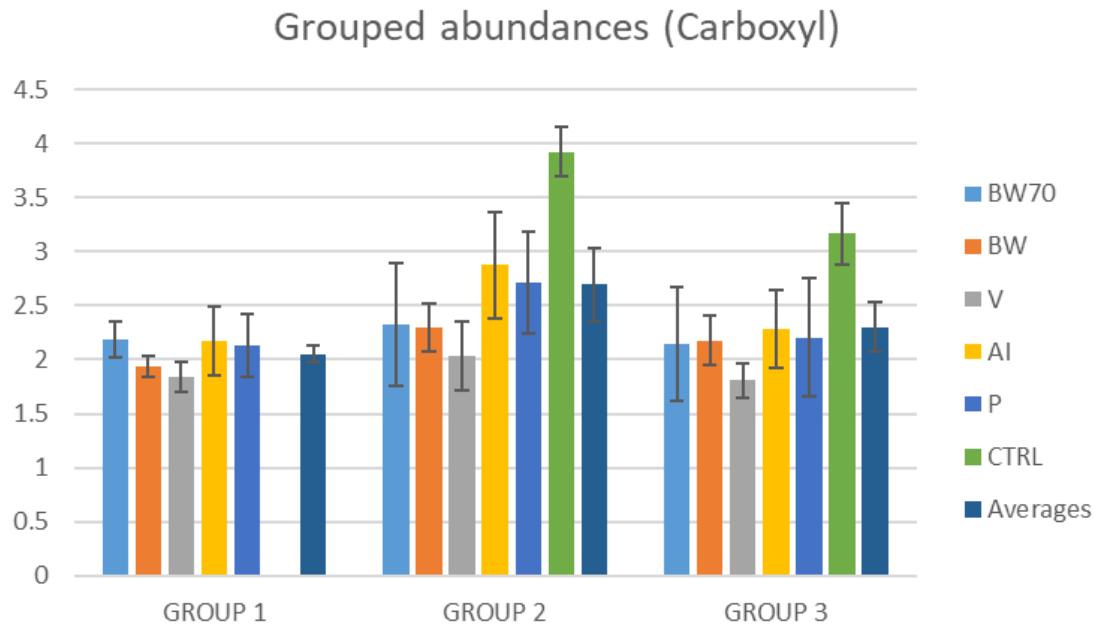

Figure 86 Grouped average carboxyl abundances for treatments, normalised to TSP integral set at 100, mean ± standard deviation

From the average results for the proposed carboxyl peak intensities, a significant increase in the average grouped results from group 1 to group 2 with no significant change between group 2 and 3 is observed. This matches the trends seen for the proposed methyl and olefin peaks. This study shows an initial increase in proposed fatty acid peaks for proposed olefin and carboxyl adjacent protons from group 1 to group 2 samples, with subsequent reduction in intensity of peaks from samples 6 to 11 with a spike at sample 12 seen. These changes are not seen for the methyl peak intensities throughout layers, with an initial drop in intensity at layer 4 which corroborates previous findings but quickly goes back to levels seen at tape strip 1. These findings are limited by the nature

of the analysis as validation of assignment is incomplete as only chemical shift, j-coupling, and presence in the skin are confirmed with couplings characterisation of molecules limited by overlap and poor S/N for CH_2 peaks specifically that would give more detail on identity of fatty acids.

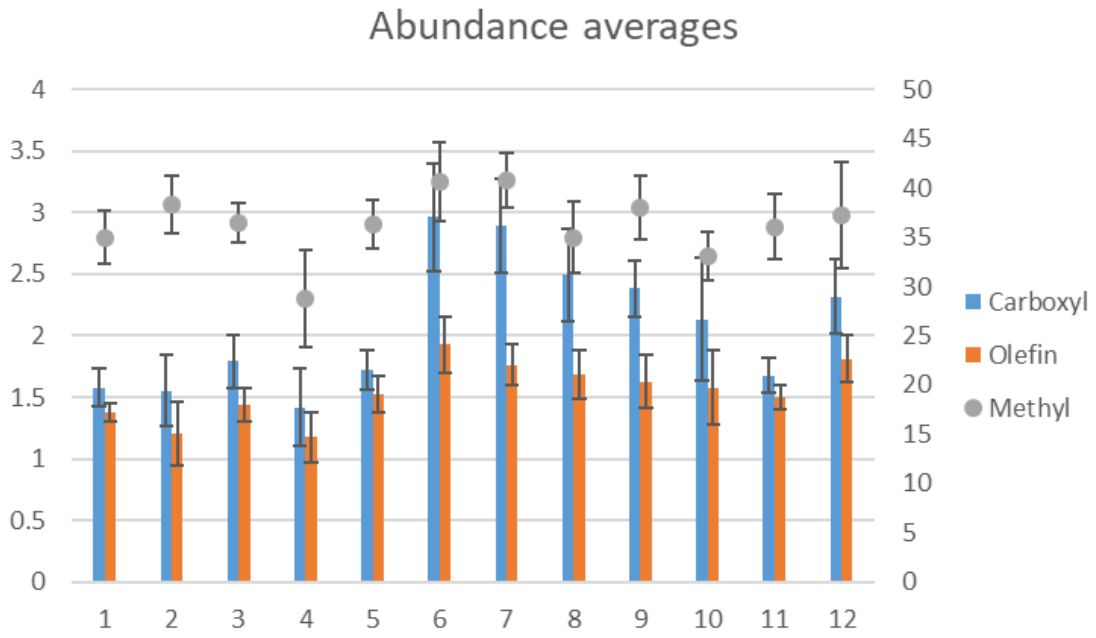

Figure 87 Combined chart of Methyl, Olefin and Carboxyl abundances with integral of TSP set to 100 mean ± standard deviation (n = 3)

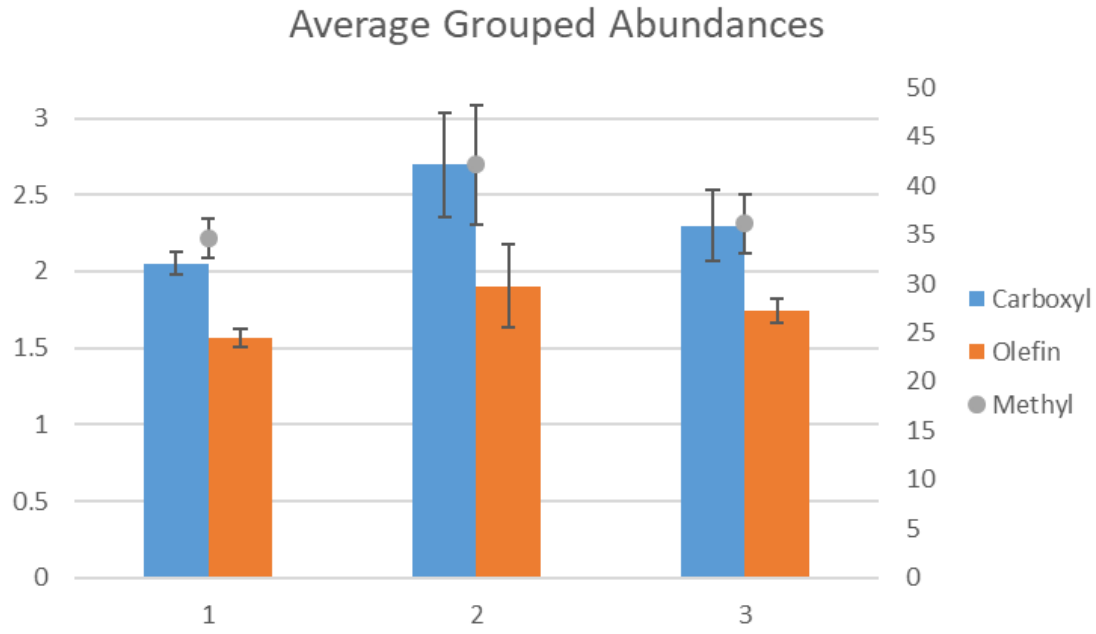

Figure 88 Combined chart of grouped Methyl, Olefin and Carboxyl abundances with integral of TSP set to 100 with mean ± standard deviation (n = 3)

The other finding that was interesting seen in previous studies was that as you increased the layer number the ratio of unsaturated to saturated lipids was decreased. Comparable results to this from the abundance data demonstrated an increase in the proposed carboxyl adjacent peaks to olefin

adjacent peaks which suggests that the overall FFA composition is made up of more saturated fatty acids at these layers from 6 onwards where no significant difference between carboxyl abundance and olefin abundance was seen up to tape strip 5. But it is seen that this decrease in the ratio of abundance of unsaturated to saturated is only significant to tape strip layer 9 as it is suspected that all FFA levels drop at this layer so that the relative abundances of saturated and unsaturated become statistically non significantly different as they are within the 95% statistical significance threshold determined by the standard deviation calculated from triplicate values. P values were set at 0.05 to define statistically significant change etc.

4.2 NMF

4.2.1 Introduction to treatments, separation, characterization of topical components

Larger compounds; cell fragments, proteins and large peptides will be removed in the extraction process, this analysis focuses on the assignment and quantitation of small active compounds that permeate through layers of the skin. Niacinamide is found in several topical treatments and is easily characterized and can be observed through all the tape strips extracted for the treatments that contain Niacinamide. For this stage of the study the semi-automated nature of the metabolite software Chenomx^{tm} is exploited which allows for the fitting of the mixture spectra to reference databases of metabolites. This allows for accurate characterisation and uniform quantitation of NMF compounds which are metabolites of *Stratum corneum* differentiation and the process of desquamation. Identification of NMF compounds and other metabolites related to proper skin functioning and hydration was done to give weight to findings. These included hygroscopic amino acids and metabolic markers. These were then fitted using Chenomx^{tm} with respective fittings of each compound described below and included in appendix.

4.2.2 NMF Chenomx^{tm} fitting

Hygroscopic compounds, such as glycine and threonine, are excluded from this analysis due to extensive overlap with topical components in the treatment samples which makes the fitted

concentration of these compounds disproportionate to expected values and other values seen in the skin. The values for glycine and threonine are calculated by Chenomx therefore not interfering with other fittings through linear deconvolution nature of fitting but values are not realistic for these compounds so it is appropriate for them not to be included considering the effects their values would have on statistical analysis and conclusions. Below the fitting for each of the compounds quantified is described and fitting of assigned ppm values is included in the appendix for each individual compound.

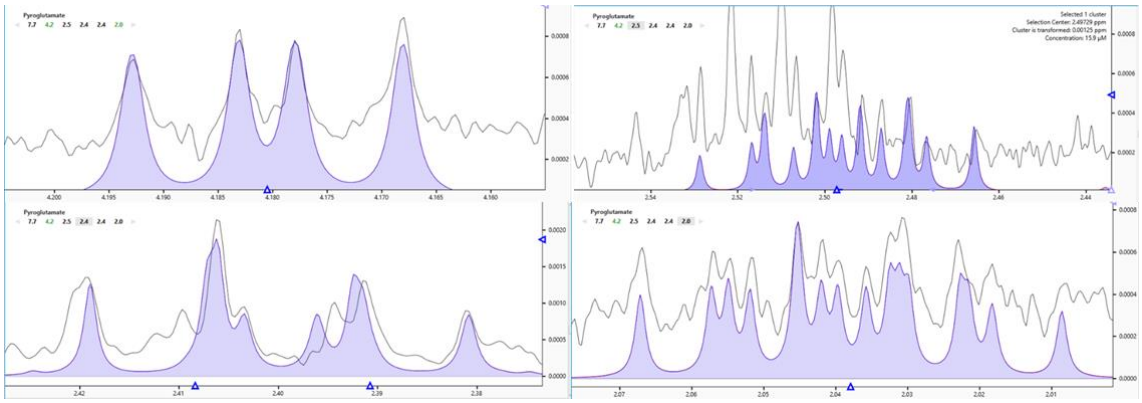

Figure 89 Chenomx fittings for Pyroglutamate

The most common NMF analysed in dermatology is Pyroglutamate (PCA) so successful fitting of this in samples from Chenomx showed great potential for quantitative NMR in the field of dermatology. Chenomx^{tm} shows reliable fitting for peaks at 4.2ppm, 2.4ppm and 2.04ppm, however a limitation was seen where peaks could not be automatically fit at 2.5ppm due to overlap of peaks with peaks previously proposed to be olefin peaks related to more abundant fatty acids.

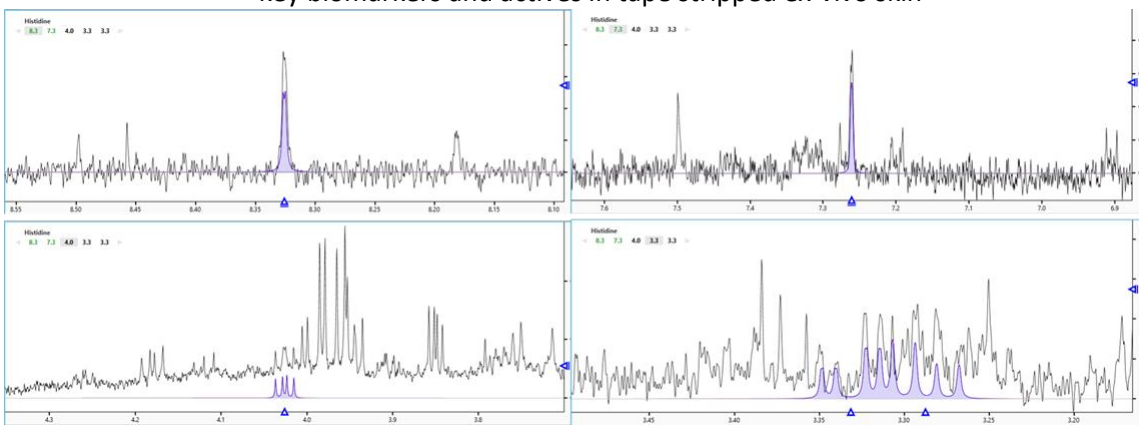

Figure 90 Chenomx fittings for Histidine

Histidine fitting in Chenomx[tm] shows reliable fitting at all peaks but automatic fitting only occurs at 8.33ppm and 7.25ppm whereas peaks at 4ppm and 3.3ppm are overlapped by other peaks present in close proximity. Urocanate fitting in Chenomx demonstrated automatic fitting for all peaks, this is because of the lack of peaks present after 5ppm allowing for peaks to have good resolution and subsequent good fitting in Chenomx. Alanine fitting in Chenomx is done automatically at 1.45ppm however due to extensive overlap at 3.8ppm fitting is not successful at this location. This is due to the abundance of Methoxy/Vinylic groups present in the skin and formulations. Serine showed automatic fitting of all peaks, with resolution between peaks seen at 3.85ppm to 4ppm, as the large overlap of peaks by glycols and glycerol is avoided at 3.4-3.8ppm. Automatic fitting for aspartate is seen at 2.8 and 2.7 with fitting failing at 3.9 due to the multiplicity of the peak making the peak below the S/N threshold, it can be manually fitted but quantitation is achieved through the automatic fitting. Lactate required manual fitting due to the low abundance and low S/N of peak at 4.1 and the overlap of peak at 1.3ppm with fatty acid peaks that dominate the aliphatic region of the spectra. Creatine is successfully fitted at both its peak sites. Creatine is benefitted by the singlet nature of its proton peaks which gives a larger S/N which makes fitting easier. Manual fitting is required for citrate due to low S/N and the reliability of quantitation is questionable for this metabolism marker. Formate is automatically fitted by Chenomx[tm] as its one non-labile proton is resolved clearly at 8.46ppm. Due to the low S/N of peaks for glutamate and the overlap of these peaks by larger peaks and broad peaks means that manual fitting is used for quantitation. This poor

fitting shows how the glutamate results are limited when analysing the skin with this extraction process and acquisition methodology.

Table 16 Summary of reference deconvolution fitting of Chenomx for target NMFs in tape strip samples

NMF	Automatic fitting	Manual fitting	Failed fitting
Pyroglutamate	x		
Histidine	x		
Glutamate		x	
Formate	x		
Citrate		x	
Creatine	x		
Lactate		x	
Aspartate	x		
Serine	x		
Alanine	x		
Urocanate	x		
Glycine			x
Threonine			x

4.2.3 Inter-sample analysis of NMF concentration in different layers

Initial comparison of the total composition of all our tape strips to literature values gave a measure of the reliability of our technique compared to validated techniques for NMF quantitation. These results gave us confidence that Chenomx^{tm} was reliably picking the correct peaks for each respective compound.

Acceptably true results for free amino acids (FAA), PCA, Lactate, Creatinine are seen whereas Citrate and Formate levels are a lot higher in calculated composition compared to literature values. This discrepancy can be explained by the way that citrate and formate usually exist in biological mixtures, with ionic bonding to ions in the skin, which literature values show makes up 12% of NMF composition. Since quantitation of sodium, potassium and magnesium is not possible using this technique there are a number of assumptions made about the molecular form of formate and citrate which are normally maintained in salt forms so the NMF composition of sodium, magnesium and potassium would begin to make up the discrepancy seen in our measured values and literature values for the chemical composition of NMF (208).

Table 17 Percentage composition of NMF compounds in all samples versus individual treatment samples and literature values (208)

Total	Calc. (%)	Liter. (%)
FAA	57.56	40
PCA	15.78	12
Lactate	10.74	12
Creatinine	1.73	1.5
Citrate	3.31	0.5
Formate	10.85	0.5

AI	Calc.(%)
FAA	58.33
PCA	15.01
Lactate	12.82
Creatinine	2.13
Citrate	2.60
Formate	9.08

P	Calc. (%)
FAA	59.17
PCA	17.09
Lactate	10.55
Creatinine	1.40
Citrate	3.13
Formate	8.63

V	Calc. (%)
FAA	52.74
PCA	14.82
Lactate	12.86
Creatinine	1.48
Citrate	3.75
Formate	14.32

BW	Calc. (%)
FAA	58.95
PCA	15.84
Lactate	7.97
Creatinine	1.74
Citrate	3.35
Formate	12.12

BW70	Calc. (%)
FAA	58.36
PCA	16.22
Lactate	9.26
Creatinine	1.83
Citrate	3.81
Formate	10.49

Summing of the NMF values also allows for evaluation of the differences seen between treatments and compares the values to the control samples for group 2 and 3 samples. Calculation of the average sums of treatments without the contribution of the control samples is done as they do not have the results for group 1 where extractions showed anomalous results while extraction was being optimised. This allows for a more accurate comparison and trendline to be derived for the

summed grouped data. From the trendline, a positive correlation between group and concentration with a high R^2 value and low standard deviation is seen for averages in group 1 and 3. A large standard deviation for group 2 is present but this is clearly through large deviation from other treatments by the AI formulation. Despite this large standard deviation, a clear significant increase from group 1 to 2 and group 2 to 3 is still observed. With the control samples a different relationship between group 2 and group 3 is observed with a decrease in the sum of group NMF, however group 3 matches the sums for other treatments to a greater degree than the Ctrl sample in group 2 that only shows a sum of NMF that is comparable to the AI treatment.

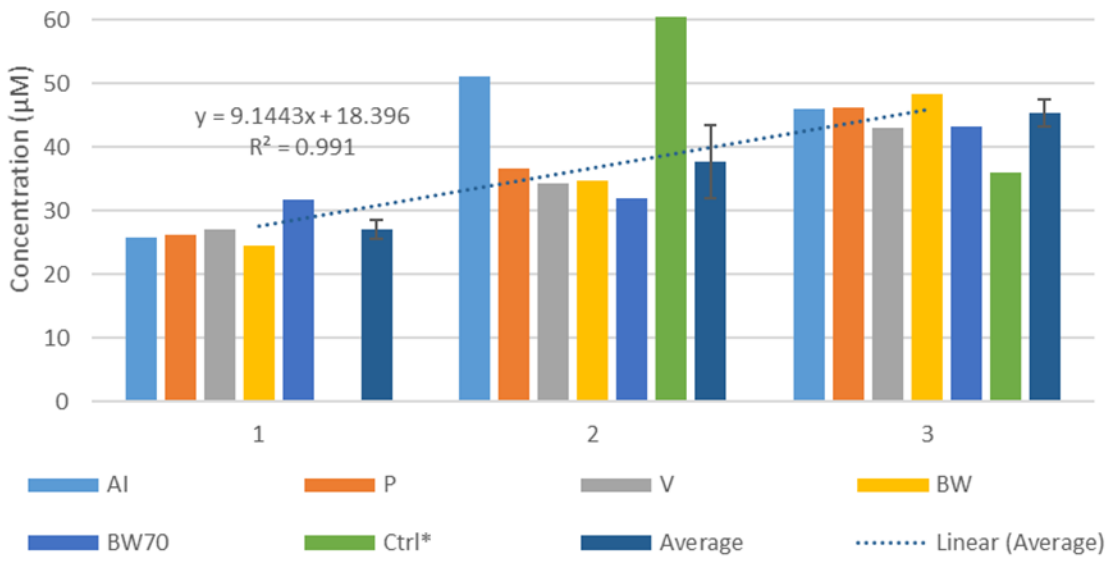

Figure 91 Comparisons of Summed grouped NMF data with trendline illustrating the changes between groups of samples using average data points for construction

Comparisons made on the sum of total NMF in groups for each treatment allows comparisons on whether large deviations are present from averages in any of the treatments. All treatments are within the standard deviation of the average apart from the control that only accounts for group 2 and 3 so this sum will be expected to be a third lower and AI which has a distinct increase seen for group 2 compared with all other treatments which explains this difference.

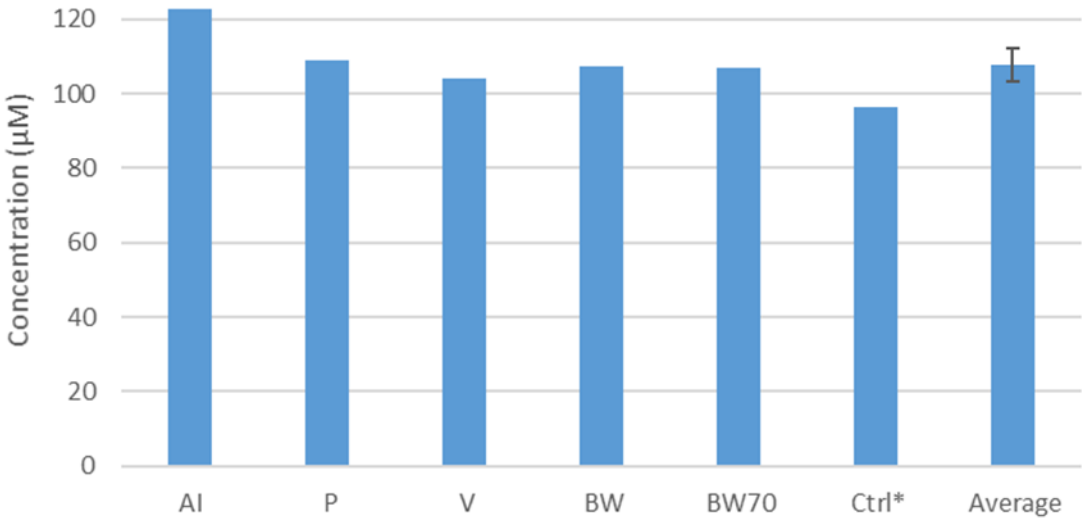

Figure 92 Comparison of full grouped NMF Sums for each treatment type and average values with mean ± standard deviation, * only summed over group 2 and 3

After showing corroborating total NMF composition results to previous literature, individual NMF comparisons between treatments and groups of tape strips was investigated. The 4 main NMFs: PCA, Glutamate, Histidine and Urocanate were compared independently of other compounds then previously reported correlations were evaluated with the results acquired.

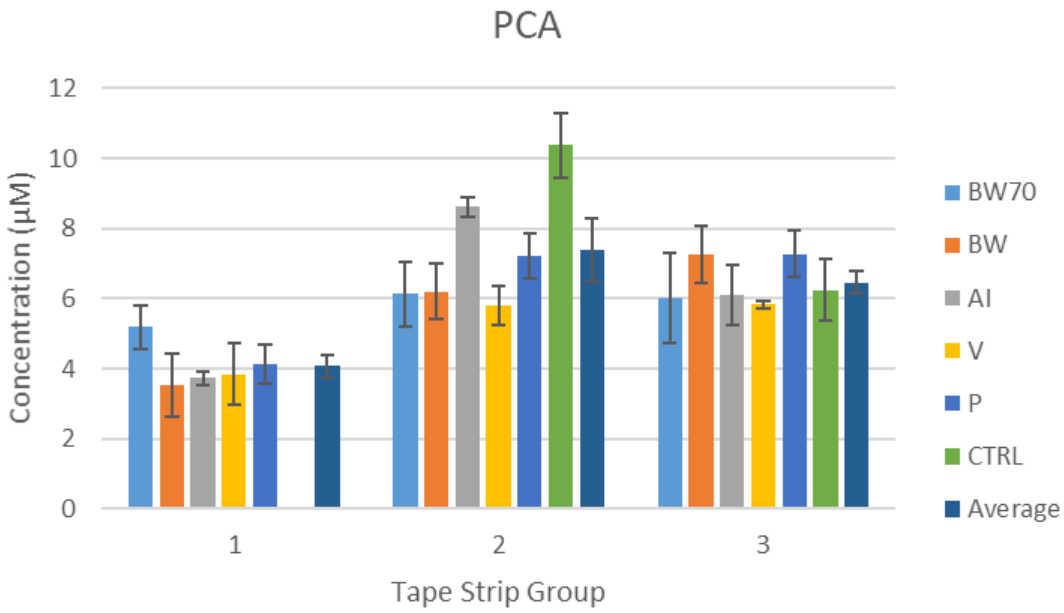

Figure 93 PCA NMF values for all treatments mean ± experimental standard deviation (n = 3)

For PCA a significant increase between 1 and 2 for all treatments apart from BW70 treatments observed. On average a significant decrease after group 2 for group 3 samples is seen, but this

decrease is considerably affected by the significant changes seen for treatment AI and control samples.

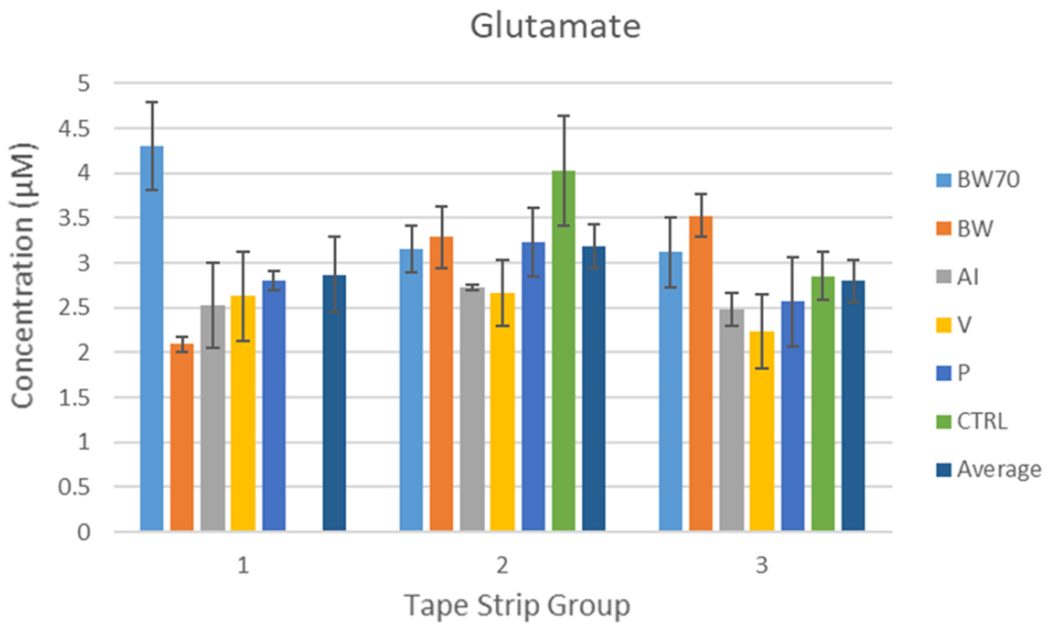

Figure 94 Glutamate NMF values for all treatments mean ± experimental standard deviation (n = 3)

No significant changes for glutamate are seen on average, but significant increases are observed in group 1 to 2 for treatment BW and a significant decrease from group 1 to 2 for treatment BW70. The significant increase from group 1 to 2 for treatment BW demonstrates a correlation to PCA however the significant decrease from group 1 to 2 for treatment BW70 highlights the limitations of Glutamate through overlap of peaks with broader underlying peaks highlighted previously for the BW70 samples, leading to a lack of automatic fitting of glutamate in Chenomx^{tm}.

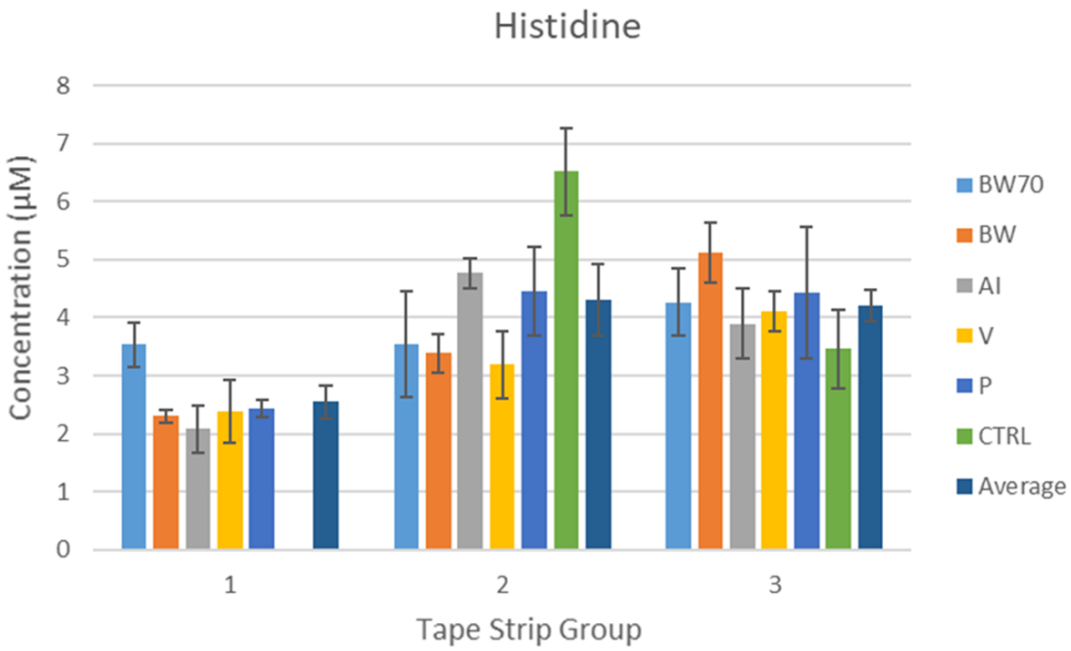

Figure 95 Histidine NMF values for all treatments mean ± experimental standard deviation (n=3)

A similar trend for Histidine to that of PCA is demonstrated with an average significant increase from group 1 to group 2, with significant increases seen for treatments BW, AI and P.

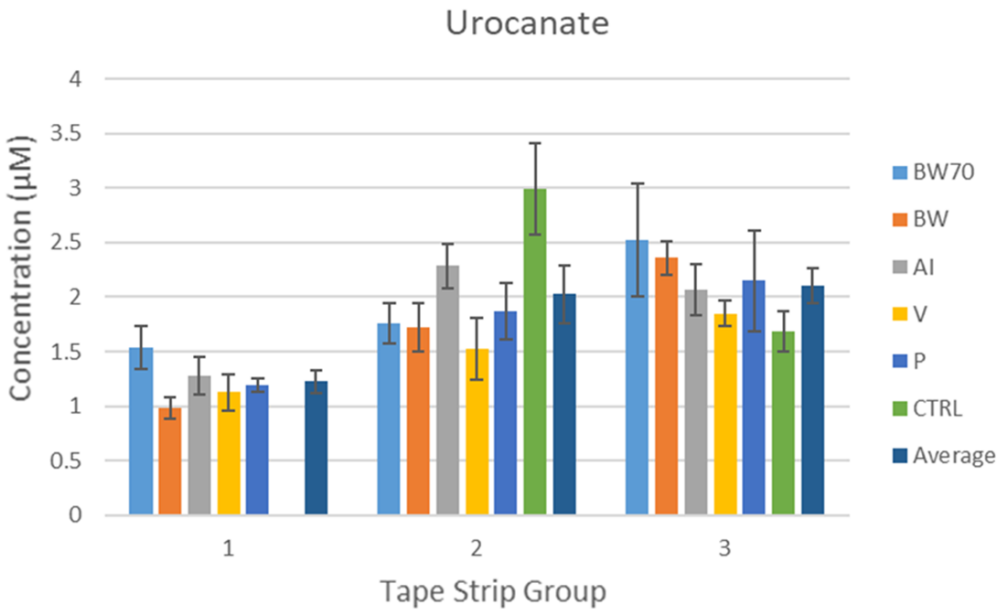

Figure 96 Urocanate NMF values for all treatments mean ± experimental standard deviation (n=3)

Urocanate again shows interesting results with significant average increases from group 1 to group 2 with significant increase in treatments BW, AI and P matching the increases seen in histidine which corroborate previous findings that the levels of Histidine and Urocanate are correlated. There is

also a matching significant increase in treatment BW from group 2 to 3, however there is an extra significant increase from group 2 to group 3 seen in BW70 which is absent for histidine concentrations.

Comparing the significant changes seen between groups of tape strip layers in different treatments can give comparisons on how the methodologies quantitative potential varies and give a measure of how differently treated skin varies in NMF values. For PCA and Glutamate it is expected to see a correlation between these two compounds, being that PCA is the cyclic derivative of glutamate, however a significant increase which correlates between the two compounds is only seen in treatment BW, with all other treatments presenting a significant increase for PCA and no change seen for glutamate. An exception is seen in BW70 treatments where PCA shows no change and a decrease is seen in glutamate. This lack of correlation for most of the treatments between PCA and Glutamate can be explained by the inherent error seen between tape strip layers for glutamate, especially in samples where no significant change is observed with a non-significant increase in the average values but consideration must be made on the overlap of peaks in the Chenomx^{tm} fitting limiting the reliability for findings on glutamate.

The consistent significant increases for PCA across all groups apart from BW70 can be explained by high concentrations of PCA in group 1 as concentrations of PCA for group 2 samples in the BW70 treatments are consistent with those seen for other treatments. This difference of BW70 is seen for all 4 of the main NMF compounds where group 1 samples have greater concentrations consistently, this illustrates the changes in NMF levels after thermal treatment of the skin which may be a response to retain moisture at surface layers to mitigate drying from a warmer external environment.

Significant changes vary between different NMF compounds, with expected correlation of changes seen for Histidine and Urocanate for group 1 to 2 for all samples, with treatments AI, P and BW

showing a significant increase in both Histidine and urocanate. However, treatment V and BW70 show no change, this can be explained for BW70 as its peaks are seen to be higher for layers 1 – 4 when compared to all the other treatments, alongside effects from heat treatment. The treatment V shows no significant change between group 1 and 2 but does demonstrate a non-significant increase but the error between individual tape strip samples prevents a statistically significant increase to be observed.

Table 18 Group 1 to 2 significant changes

Compound	AI	P	V	BW	BW70	Average
PCA	Increase	Increase	Increase	Increase	No Change	Increase
Glutamate	No Change	No Change	No Change	Increase	Decrease	No Change
Histidine	Increase	Increase	No Change	Increase	No Change	Increase
Urocanate	Increase	Increase	No Change	Increase	No Change	Increase

For group 2 to 3 there are consistently no significant changes seen for all treatments which correlates the NMF compounds nicely together. Apart for the AI treatment where a consistent decrease is observed across PCA, Glutamate and Histidine, with no change in Urocanate concentrations. For all the other treatments, they match the no change seen for the average, however increases in Histidine and Urocanate for V, BW and BW70 is seen which shows that the formulation that these treatments share may have an effect on the levels of histidine and Urocanate that AI and P do not have.

Table 19 Group 2 to 3 significant changes

Compound	AI	P	V	BW	BW70	Average
PCA	Decrease	No Change	No Change	No Change	No Change	No Change
Glutamate	Decrease	No Change	No Change	No Change	No Change	No Change
Histidine	Decrease	No Change	Increase	Increase	No Change	No Change
Urocanate	No Change	No Change	No Change	Increase	Increase	No Change

After the interpretation of these significant change tables it was postulated that it may be prudent to start classifying P and AI together as their base formulations are both Physiogel. Alongside this grouping V, BW and BW70 were compared more as a group since their base formulation was that of the Bluewater formulation.

These main NMF compounds have been extensively quantified and their correlations to each investigated widely but significant differences between groups for other compounds relevant to skin health and hydration is seen, specifically hygroscopic amino acids and metabolic markers.

The first hygroscopic amino acid analysed was Serine, as it is one of the most hygroscopic amino acids, therefore it is appropriate to monitor its abundance throughout samples (209) alongside serine, glycine and alanine are hygroscopic amino acids which play a role in water retention in the skin (210). This means that if these can be quantified in the skin, conclusions on the water retention potential and relative dryness or health of the skin can be made. Characterisation and quantification of the acidic amino acid Aspartate, which is shown as a biomarker in the skin for disease conditions and also as an immunoreactive agent in inflammatory responses is also a key biomarker to analyse for skin health (211) (212).

Observation of the measured concentrations of amino acids and metabolic markers (Creatinine, Citrate and Formate) show similar abundances to the NMF compounds, despite creatinine and citrate being distinctly the lowest concentrated compounds seen. Interestingly for the amino acids and metabolomics markers when compared to the NMF values the large concentrations in group 1 for BW70 are not seen suggesting that heat has no effect on these compounds' abundance within the skin. This suggests that the NMF compounds (PCA, Glutamate, Histidine and Urocanate) have a role in temperature dependent mechanisms whereas amino acids and metabolic markers do not. Apart from possibly formate in BW70, but this increase in group 1 samples is also observed in treatment P, which could also be explained by addition of sodium formate in the formulations as a stabilizer in the treatments which permeate to group 1 layers through high abundance in P formulations and increased permeation through temperature treatment in BW70 which does not then permeate to group 2 and 3 layers of the skin.

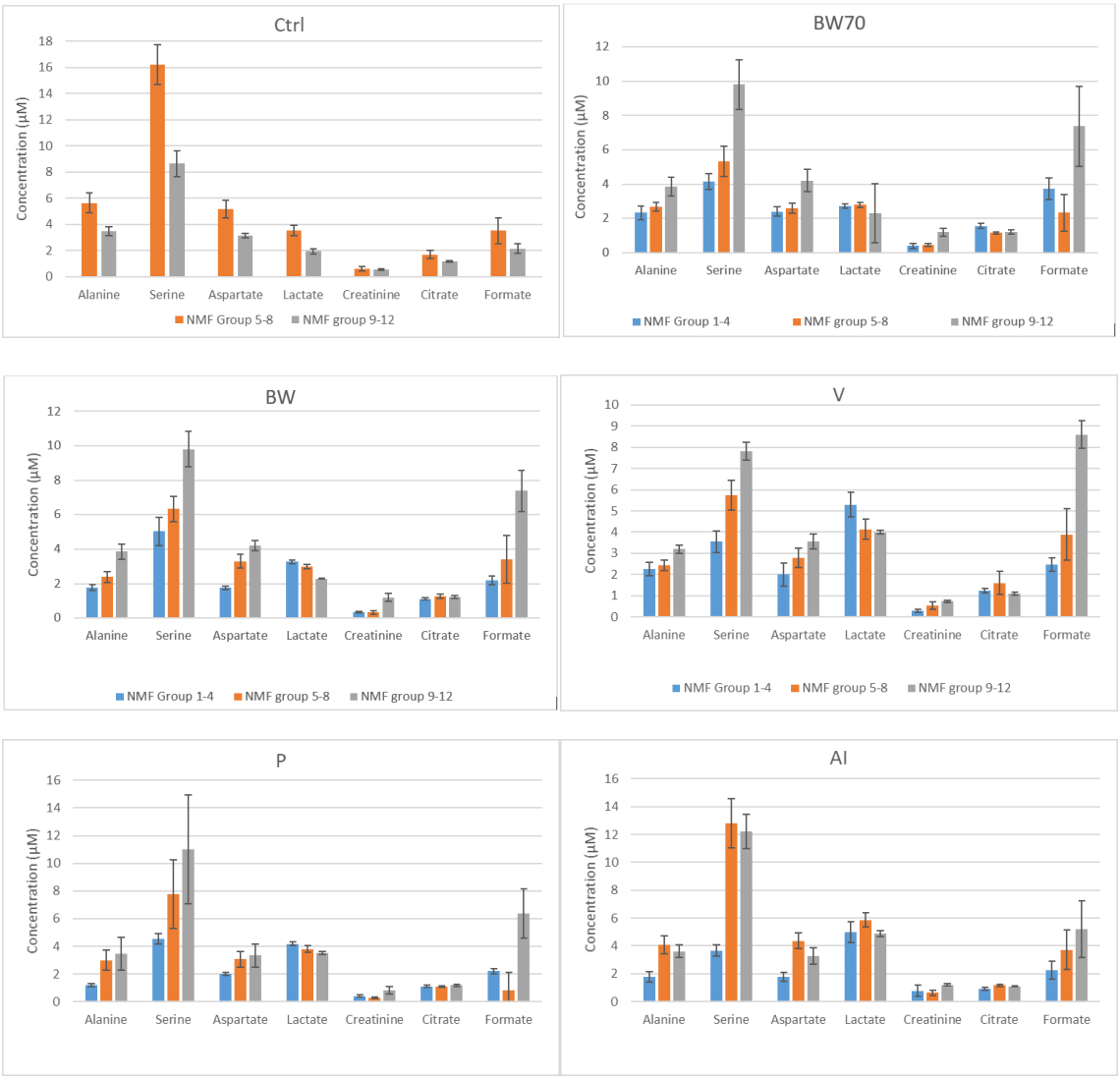

Figure 97 Ctrl, BW70, BW, V, P and AI treatment hygroscopic amino acid and metabolomics marker grouped concentrations mean ± standard deviation

For the amino acids a consistent increase for group 1 to 2 for AI and P formulations is seen and the differences seen with V, BW and BW70 suggest different effects upon the concentration of amino acids by these different groups of formulations. However inconsistency for V and BW is observed between amino acids with Serine being increased for V and Alanine and Aspartate being increased for BW however there are non-significant increases from group 1 to 2 seen throughout treatments V, BW and BW70 with varying degrees of increases which could be explained by a later onset of the increase in amino acids. This is demonstrated by the significant increase seen between group 2 and 3 for amino acids.

Table 20 Significant increases between Group 1 and 2 for amino acids

Compound	AI	P	V	BW	BW70
Alanine	Increase	Increase	No Change	Increase	No Change
Serine	Increase	Increase	Increase	No Change	No Change
Aspartate	Increase	Increase	No Change	Increase	No Change

Significant increases for group 2 to group 3 amino acids shows consistent correlations between the two Physiogel formulations, AI and P, where no change is seen between groups. Whereas consistent increases for formulations of the Bluewater formulations, in V, BW and BW70 are seen. These results combined with the increases demonstrated for group 1 to 2 show that amino acids in all treatments increase from group 1 to 3 but the large increase for AI and P is in the earlier layers whereas deeper layer increases occur for the Bluewater formulations. This suggests that the actions of the Physiogel formulations is pulling the hygroscopic amino acids to the surface, therefore drawing water to the surface of the skin, rather than the Bluewater formulations which are keeping the water retention in the deeper layers and not having this drawing effect to the surface. Even with temperature application that was previously stated to have less of an effect may even minimise drawing of hygroscopic amino acids to the surface by preventing an increase from group 1 to group 2, but this conclusion is limited by the scope of this study.

Table 21 Significant increases between Group 2 and 3 for amino acids

Compound	AI	P	V	BW	BW70
Alanine	No Change	No Change	Increase	Increase	Increase
Serine	No Change	No Change	Increase	Increase	Increase
Aspartate	No Change	No Change	Increase	Increase	Increase

The metabolomics marker showed very little correlation between the two different formulation types, but did show correlations between creatinine and formate concentrations changes from group 1 to 2 and group 2 to 3 with only treatment V and AI having slightly inconsistent significant changes in group 1 to 2 changes and group 2 to 3 changes respectively. The correlations between creatinine and formate was formed though a universal increase across the 5 treatments, with only Formate in the AI treatment not increasing, but the errors between layers for AI in group 2 and 3 are quite large and a non-significant increase is observed. Interestingly for lactate there is a decrease for all treatments from group 1 to 3 apart from BW70, this

suggests a role for lactate in the acid mantle of the surface of the skin more than formate. There is predominantly no change for citrate between groups apart from negatively correlating changes between AI and BW70 treatments, with an increase for AI and a decrease for BW70 which suggests that AI may increase the pH mediating effects of Citrate whereas the decrease seen for BW70 may be explained by thermal effects which also effects the levels of lactate as previously stated. It is seen that all other Bluewater formulations demonstrate decreases. This shows that the thermal effects seem to affect the composition of the acid mantle of the skin.

Table 22 Metabolomic markers Group 1 to 2 significant changes

Compound	AI	P	V	BW	BW70
Lactate	No Change	Decrease	Decrease	Decrease	No Change
Creatinine	No Change	No Change	Increase	No Change	No Change
Citrate	Increase	No Change	No Change	No Change	Decrease
Formate	No Change	No Change	No Change	No Change	No Change

Table 23 Metabolomic markers Group 2 to 3 significant changes

Compound	AI	P	V	BW	BW70
Lactate	Decrease	Decrease	No Change	Decrease	No Change
Creatinine	Increase	Increase	Increase	Increase	Increase
Citrate	No Change	No Change	No Change	No Change	No Change
Formate	No Change	Increase	Increase	Increase	Increase

4.2.4 Statistical analysis (Principal Component Analysis) of NMF variability between layers and treatments

Observations on the statistically significant differences between NMF values of different treatment sample groups can be made, however this is limited when quantifying the variability seen and how variability correlates quantifiably between different compounds within our samples. Principal component analysis (PCA) can be exploited to calculate principal components of data points within a data matrix that are considered as points in p-space. These direction vectors, with vector line direction that best fits the data while still remaining orthogonal to the first vector selected are then used to perform a change of basis on the data, with minimal number of principal components. The PCA plots are made up the principal components that determine the majority of the variation seen. Thus all plots are PC1 vs PC2 which explains more than 70% of the variability seen for all plots, the addition of extra principal components e.g. PC3, would be superfluous therefore it is ignored.

The first analysis done was all the tape strips groups together which demonstrated that the groups separate predominantly due to their group number predominantly based upon their principal component 1 (linearly uncorrelated variable that explains most of the variance in the data,PC1) values, with group 1 values at a range of 0.02 to 0.1, group 2 ranging from -0.3 to 0.2 and group 3 ranging from -0.6 to -0.2. PC2 does separate groups and explains 28% of variability but shows large variability for BW70, AI, P, and V, however the BW treatments have a negative linear trend from group 1 to group 3 along the PC2 axis. An outlier is observed for BW1 as it overlaps in the region of group 2 samples, with BW70's group 1 being on the boundary between the two groups, this suggests that the formulation of the vehicle does not have the same effects on variability seen and is more like that seen for P1 and AI1. The variability between group 3 samples is predominantly seen through PC2 with PC1 values for group 3 sample, BW70 aside, being very similar.

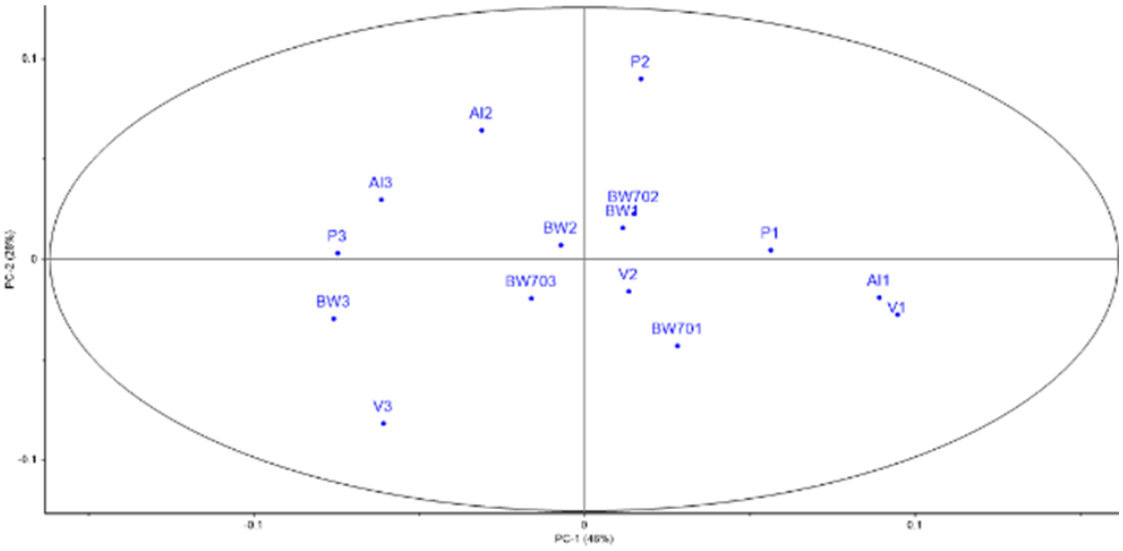

Figure 98 All treatments tape strip extractions Scores plot for Grouped NMF data, PC1 (46%) against PC2 (28%)

The correlation loadings seen for all the compounds shows the previously reported close correlation between Histidine and Urocanate, with low correlation observed between PCA and Glutamate, despite them both being positively loading. Interestingly Glutamate is closer to correlating to Lactate and Citrate but again this finding is limited by the reliability of Chenomx^{tm} fitting for glutamate. Serine variability demonstrates a very strong influence on PC1 and is not

correlated strongly to other amino acids Alanine and Aspartate which are closely correlated. Interestingly the metabolism markers Citrate and lactate are very closely correlated but creatine is not, this again supports the previous observations of data. Formate is distinct in contribution to variability through closer correlations to amino acids than metabolism markers. This is surprising as formate and citrate are usually grouped together when calculating NMF's in the skin.

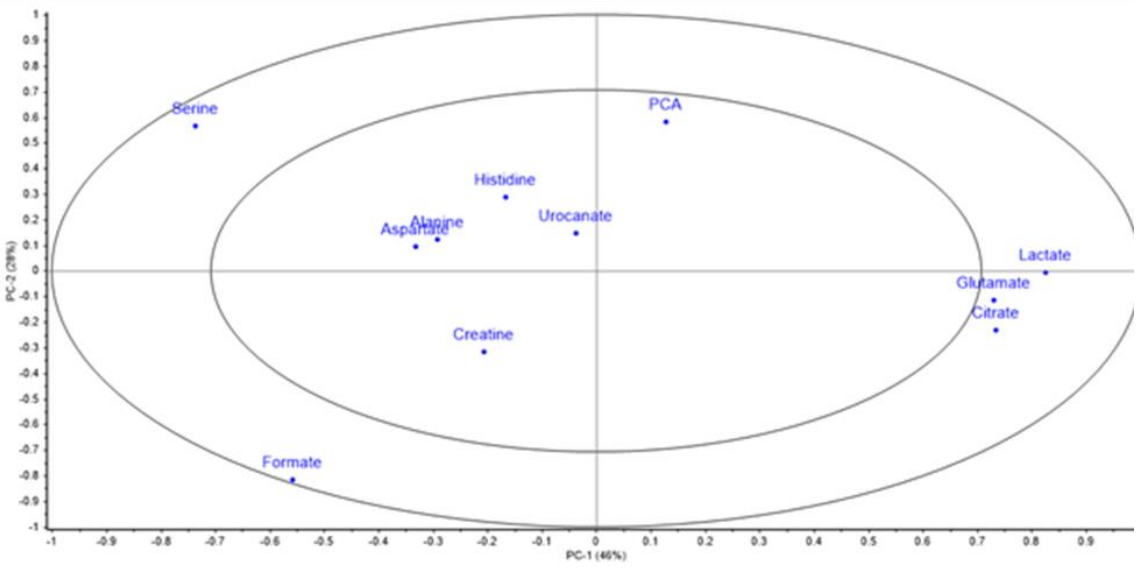

Figure 99 All treatments tape strip extractions correlation loading plot for Grouped NMF data, PC1 (46%) against PC2 (28%)

As previously noted in the previous section it is appropriate when comparing the variability seen between the treatments to break up the treatments into Physiogel group P and AI and Bluewater treatments; V, BW and BW70. This is especially significant when bringing together the NMF and topical components for correlation analysis. For this no real changes are seen in the scores plot when analysing the data separately but what is interesting is how the correlation loadings of different compounds changes. In the Bluewater formulations serine and creatine now have a strong correlation whereas this was not seen before. Glutamate is also more strongly correlated to PCA rather than Citrate and lactate which matches more with previous literature findings where PCA is a breakdown product of Glutamate. Alanine also becomes distinct in its contribution to variability, being closer to the NMF's PCA and glutamate than the other hygroscopic amino acids Serine and aspartate.

The scores plot for the Physiogel treatments shows a more group dependent configuration where with clear grouping of groups together particularly for group 1 and 3 tape strips with group 2 samples being separated by PC2 which can be explained by the uniquely large rise in concentrations for AI2 samples.

It is demonstrated through the correlation loading plot that the NMFs PCA and histidine are closely correlated alongside the hygroscopic amino acid aspartate. Whereas Urocanate and Glutamate especially are closer correlated to Citrate and lactate. Contradictorily it is also observed that citrate and lactate have negative correlation loadings whereas in the Bluewater formulation they have positive correlation loadings with serine, histidine and aspartate showing the same inversion of correlation loading.

4.3 Permeation profiling of topical components

Abundance analysis and semi-automated quantitative analysis of NMF components has been extensively studied in previous work but the use of NMR in the study of active compounds and drug permeation in the skin is a fruitful area for research considering the current methodologies which are time consuming, destructive and require chemical or physical treatment for separation of individual compounds.

Demonstration of the previous methodologies that have been validated for use in complex mixture characterisation, separation and quantitation use in *ex-vivo* skin samples is highlighted. Developing from the work done on whole formulations from bottle, transitioning to changes in concentration once applied to the skin.

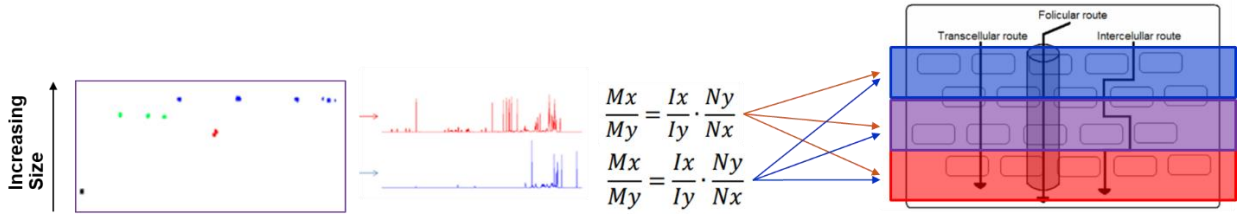

Figure 100 Illustrative representation of methodology

4.3.1 Characterisation of proposed topical peaks by 2D NMR

The first step required for this work was the characterisation of peaks that were present in treatment samples in the difference spectra. 1D ^{1}H regional analysis highlighted what type of compounds were being added into the treatment samples. This analysis was however limited to understanding what functional groups exist, but compounds that are added to formulations for permeation enhancement, alongside skin health enhancement actives can be understood, suspected compounds can be identified and characterised.

For full characterisation of most abundant actives and permeation enhancers 2D spectra, COSY, HSQC and DOSY were acquired. COSY spectra showed that all the peaks at 7.6ppm to 9ppm were coupled to each other, this further confirmed the suspicion that these peaks were assigned to Niacinamide as these peaks and couplings matched the previous chapter's assignments for Niacinamide added into formulations.

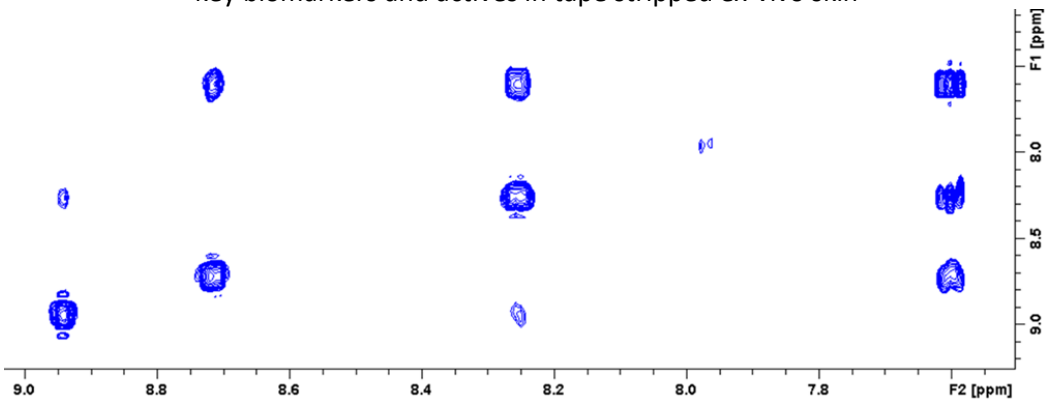

Figure 101 COSY cross peaks for proposed Niacinamide in bluewater formulations

Glycerol peaks are also assigned from the previous chapter which have strong couplings to each other at 3.5ppm, alongside suspected panthenol and Pentylene glycol which have couplings seen at 2ppm-3.2ppm/3.6pmm and 3.4-3.45ppm respectively.

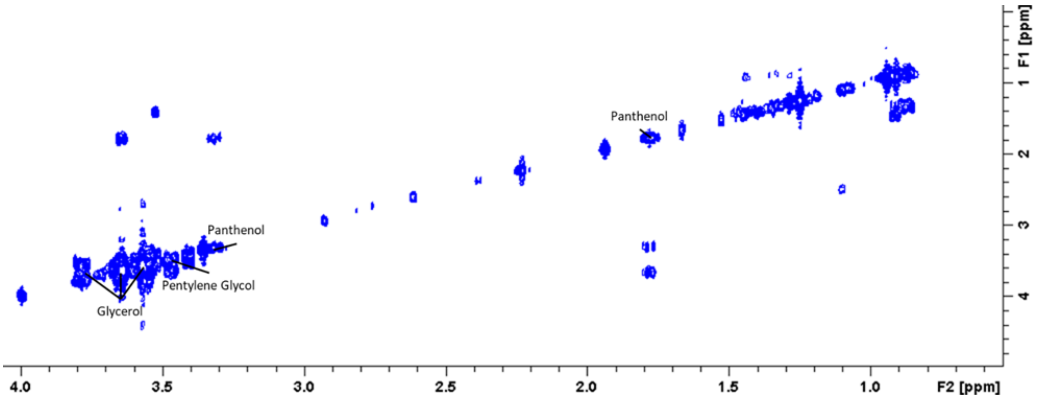

Figure 102 COSY cross peaks for proposed Glycerol, Pentylene Glycol and Panthenol in bluewater formulations

4.3.2 **DOSY** validation of peak correlations

To confirm the peak correlations seen in the 2D COSY and HSQC spectra are for the proposed molecules, Glycerol, Niacinamide, Panthenol and Pentylene Glycol DOSY spectra were acquired. This allows for assignment of peaks to specific diffusion coefficients and subsequent characterisation of a respective peaks molecules shape and size.

DOSY spectra with peaks selected for the proposed molecules, Glycerol, Niacinamide, Pentylene Glycol and Panthenol are acquired. Initial survey experiments were run to optimise the P30 and D20 values required for full attenuation profiling of 2% gradient power to 98% gradient power with these scans highlighted in figure 102.

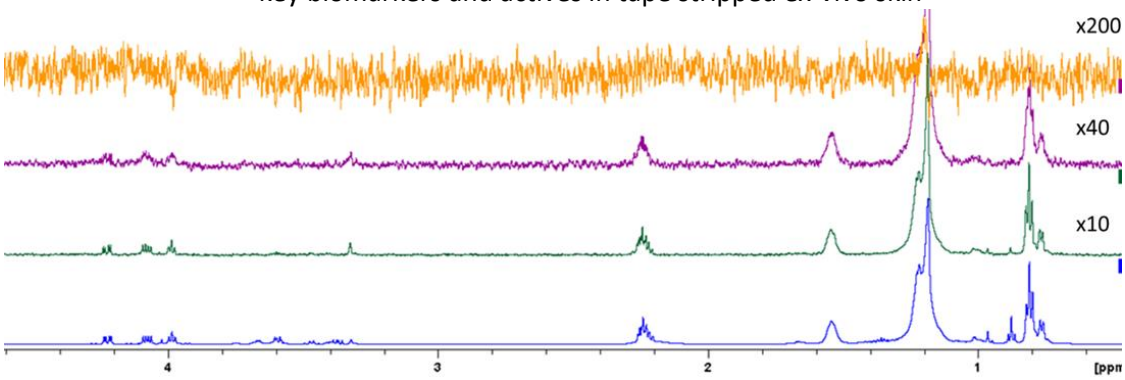

Figure 103 1D DOSY Survey scan with varying D20 and P30 times: Blue = 2% GPZ6; Green = 98% GPZ6, P30 = 750µs, D20 = 0.1s; Purple = 98% GPZ6, P30 = 850µs, D20 = 0.1s; Orange = 98% GPZ6, P30 = 1050µs, D20 = 0.1s.

With P30 set at 850µs the attenuation profile of higher abundance compounds is best described through reduction of signal down to 2.5%, whereas when P30 is set at 750µs the attenuation is only described down to 10% signal intensity. It is also shown that once the P30 values are raised to 1050µs that signal needs to be amplified over 200x to observe any signal seen for the largest peak height, this shows the limitations past 850µs P30 value, as detail of attenuation profile will be explained over a limited power range.

With the P30 values and D20 values optimised for the attenuation profile a 2D DOSY spectra is acquired. Self-diffusion coefficients were then assigned for each component peak and the value for highest intensity for individual compounds taken for calibration curve formulation and construction of projection display.

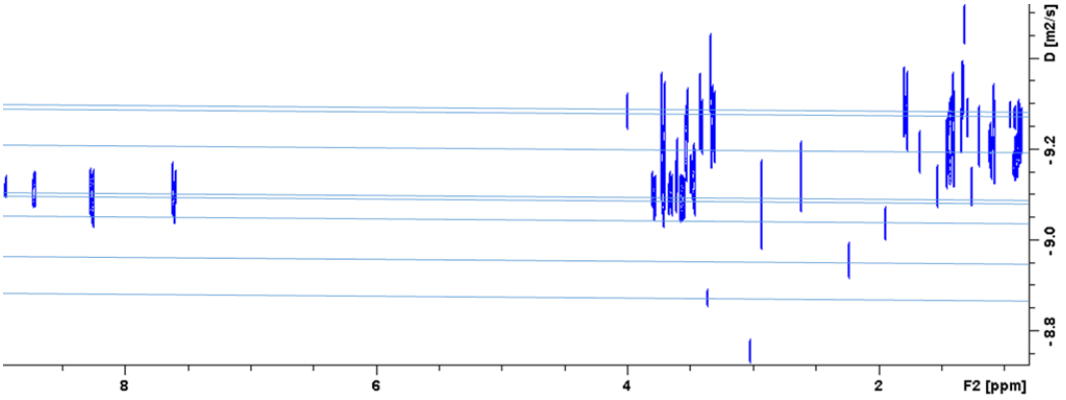

Figure 104 Annotated 2D DOSY spectra to show independent self-diffusion coefficient values identified

Once these values are determined the mean square error per spectrum for each peak gives us the contour size in the exported DOSY spectra in topspin and the error reported here for calibration

curve determination. This gives reference for how much contours when at max intensity overlap with each other but when intensity is modulated in TopSpin software it clearly distinguishes these peaks and no overlap is seen between them.

Table 24 Calibration curve table with assigned compounds for BW70 tape strip layer 1, log diff coeff. values mean +/- root mean square error per spectrum

Compouds	log diff coeff. (m2/s)	log FW	FW (kg/mol)
Methanol	-8.87 +/- 0.034	1.51	32
Acetone	-8.95+/- 0.074	1.76	58
Acetate	-9.04 +/- 0.08	1.78	60
Glycerol	-9.11 +/- 0.048	1.96	92.1
Pentylene Glycol	-9.17 +/- 0.11	2.02	105
Niacinamide	-9.12 +/- 0.040	2.09	122
Proposed fatty acid	-9.27 +/- 0.10	2.41	256
Panthenol	-9.28 +/- 0.055	2.31	205

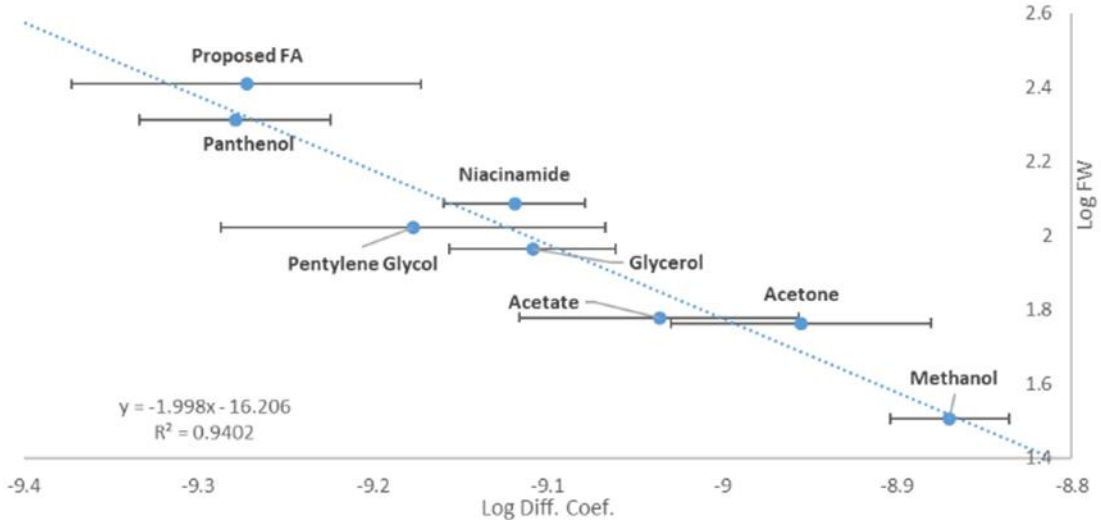

Figure 105 Calibration curve for formulation components with linear trendline calculated from Log diffusion coefficients vs Log Fw values.

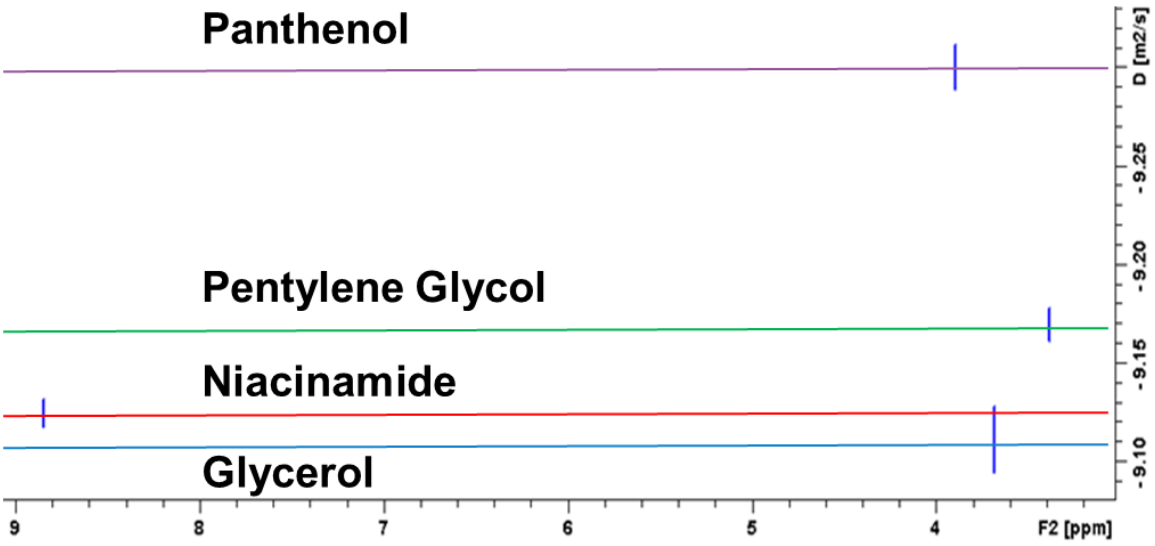

Figure 106 Assigned DOSY fit spectra peaks representing highest abundance peaks of each compound

From the calculated calibration curve constructed there is a linear correlation of y = -1.998x – 16.206, with a R^2 value of 0.9402 highlighting the strong correlation between log diffusion coefficients and log FW for the identified formulation compounds. With higher abundance compounds the error is lower, such as Niacinamide and Glycerol, but low error is also observed for compounds that have minimal overlap with other peaks like methanol. Unfortunately for Panthenol and Pentylene glycol their peaks have greater error which is due to partial overlap of peaks chosen for diffusion coefficient calculation. This effect of peak overlap on the error of diffusion coefficient calculation is exemplified by the peak for the free fatty acid composition of the samples. The error for the calculated diffusion coefficient alongside the calibration curve suggests a range of molecular

weight for the free fatty acid of 105 to 305 Daltons. This shows the limitations of this technique for the accurate determination of molecular weight determination, but scope of the technique for separation and promising recent work done by Evans et al at Aston (213) and Gareth Morris's group at Manchester (214) is making this tool powerful for the analytical chemist.

Constructing projection displays at middle points of the contours for each compounds specified by their formula weight and calibration curve allows us to acquire individual spectra for each compound and identify peaks that may have been omitted from analysis or not observed previously.

In the glycerol projection the glycerol peaks are clearly observed in the projection and are well resolved. This is because of the large S/N of the original spectra glycerol peaks and through the low overlap with other abundant peaks. However, some peaks have different intensities to other peaks in the projection display and this is due to partial overlap with peaks adjacent to it. This is observed by an increase in the size of peak relative to other peaks at 3.54ppm which has peaks present for other compounds present at ppm range 3.48ppm to 3.53ppm.

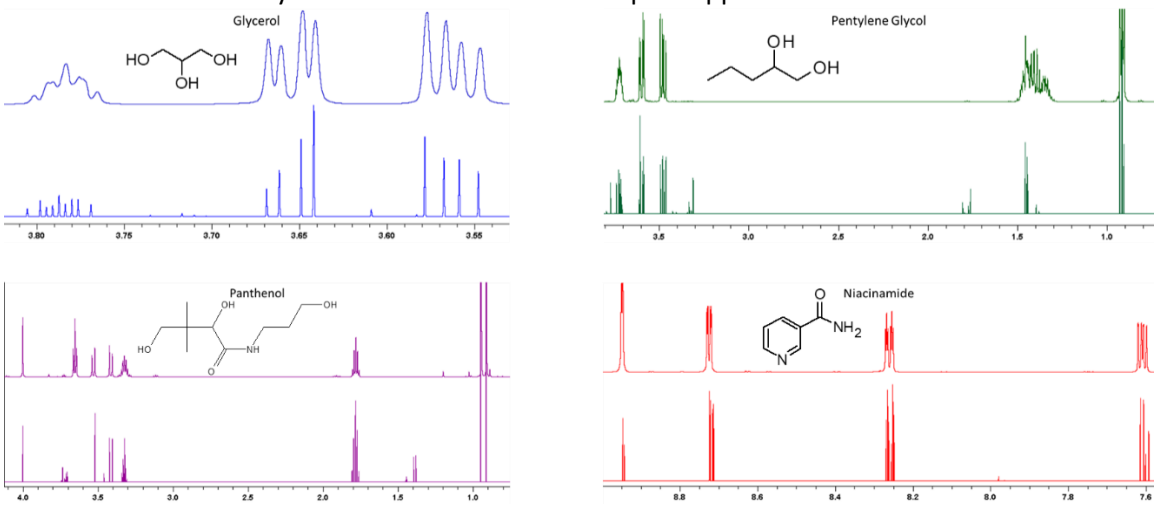

Figure 107 1D Diffusion coefficient projections of 2D DOSY spectra correlating to individual compounds 1D

These peaks are then seen in the Pentylene glycol projection which has peaks at 3.48 to 3.51, where the peak at 3.5ppm is higher than the adjacent peak at 3.51ppm due to the peak at 3.51ppm peaks partial overlap with glycerol peaks.

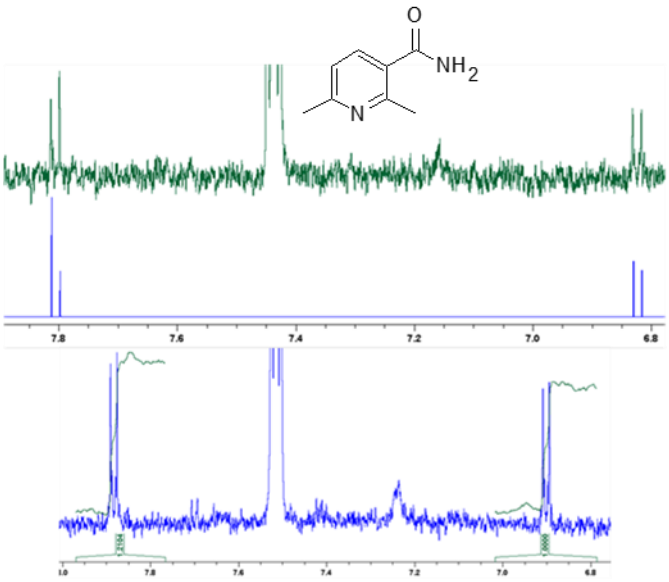

Figure 108 Niacinamide derivative identified through ODSY projection

The peaks for panthenol are illustrated clearly at 0.8, 1.2, 1.4, 3.2 and 3.85ppm, with its peaks at 3.5ppm to 3.6ppm being resolved but also greatly affected by extensive overlap with Glycerol in the spectra. This produces large errors in the diffusion coefficient calculation. Despite this overlap however these peaks are observable and can be assigned to the panthenol molecule.

Niacinamide projection displays show very low error due to the clear resolution of the peaks from other peaks present in the spectra. The coupling constants, appropriate relative integrals and also the number of peaks matches those expected for Niacinamide as shown in previous chapter.

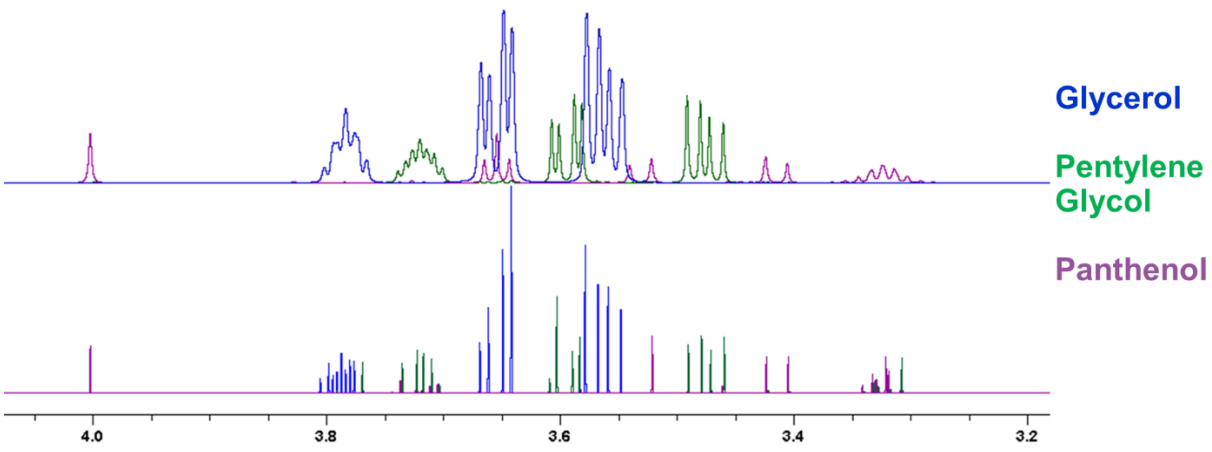

Figure 109 Zoomed in region of 3.2ppm to 4ppm highlighting resolution of previously overlapping peaks in PSYCHEiDOSY projections of Glycerol, Pentylene Glycol and Panthenol (bottom) compared to reference spectra (Top)

Peaks are seen in the Niacinamide projection at 7.85ppm and 6.9ppm shown in figure 108, when looking at the j-couplings in the proton spectra it can be characterised as a Niacinamide derivative. The 8.8-8.9Hz J coupling observed for each peak doublet suggests the formation of an Niacinamide derivative that is formed from substitution of an alky group to the aromatic ring from small fatty acids through radical substitution. Assumed structure of these peaks from previous literature investigation implies that Niacinamide reacts with alkyl radicals, specifically Ethanoic acid, and forms 3 compounds preferentially. It is assumed to be formed through a reduction pathway to produce piperidine-3-carboxamide, 1,4,5,6-tetrahydropyridine-3-carboxamide and 1,4-dihydropyridine-3-carboxamide (215). The 2,6-dimethylpyridine-3-carboxamide matches the coupling constants 8.8-8.9Hz when compared to much lower coupling constants for the other two preferential compounds (216). Identification of breakdown products like this is important when determining changes in composition from bottle to skin, alongside giving an opportunity to evaluate time from excision of sample to acquisition of data.

4.3.3 Quantitative permeation profiling of topical components identified

Once all peaks have been identified for each compound, quantification can be done. Selection of peaks for quantitation takes into account peaks that have; low to no overlap, highest relative signal to noise and either singlet peaks or the lowest multiplicity peaks for each compound respectively . This allows for the greatest reliability of quantitation and scope of quantitation down to the concentrations seen for limit of detection and quantitation in previous chapters (100nM - 10µM).

4.3.4 Niacinamide and derivative permeation profiling

Levels of Niacinamide were quantified as the main active in the Bluewater formulations and how the different formulations and application of them affected the permeation of Niacinamide in the skin was analysed. There are clear increases in permeation from tape strip layer 1 to 9 for the BW70 formulation. Significant permeation increases for Niacinamide are observed in formulation BW compared to V for tape strip layers 1 and 2, alongside this the trend line shows relatively higher permeation down to layer 7. These changes show that thermal treatment increases the permeation of Niacinamide in these formulations extensively, considering this is the only variable between BW and BW70. The uncharacterized actives that are present in BW compared to V also explain the increased permeation in relation to these two treatments. It is also shown that these trends are shared with the Niacinamide derivative, which can be quantified down to layer 7 in BW70 however in BW and V it can only be quantified to layer 3 with the trendlines for V and BW crossing over one another. This demonstrates that conclusions can be made on BW70 compared to V and BW but it is not appropriate to make conclusions on concentrations in BW and V for this compound. There is also a correlation between the levels of Niacinamide and derivative, through observation of increased permeation of Niacinamide for BW70 to layer 7 and detection of derivative to the same layer.

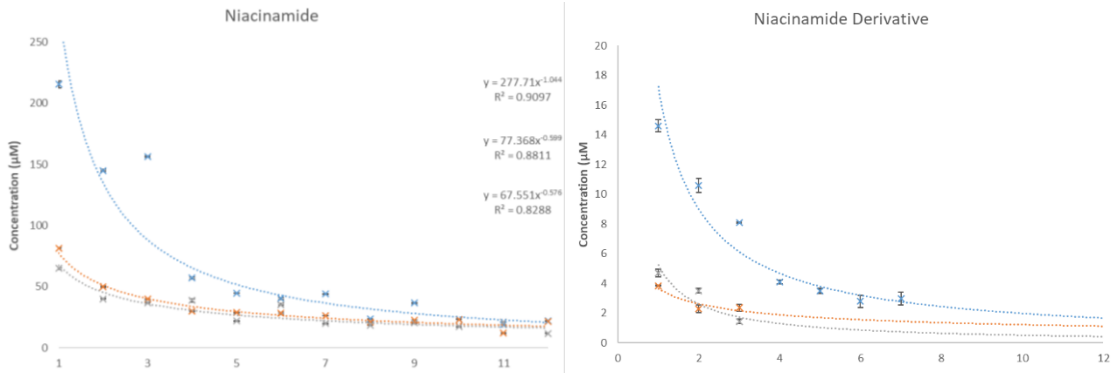

Figure 110 Permeation profiles of Niacinamide (top) and Niacinamide derivative (Bottom), in treatment tape strips (BW70 = Blue; BW = Orange; Vehicle = Grey;), mean +/- SD. With equations and R^2 values for each treatment power trendline.

4.3.5 Glycerol permeation profile

Glycerol, which was present in all the formulations was selected next for quantitation and profiling of permeation. The findings were comparable to Niacinamide where the trendline for BW70 permeation is higher than all other treatments. Conversely though, permeation of glycerol in the first layers of the samples is not the highest in the BW70 samples with BW, P and AI formulations having higher initial glycerol permeation into the skin. After this initial difference, BW70 has consistently higher permeation than all other treatments up to and including layer 3. The order of permeation for glycerol is BW70, P, BW, AI then V, with Physiogel classified mainly as a moisturiser, where Glycerol induces drawing of moisture to the surface is key, has a lower permeation than BW70 on average for the first 3 layers. Also its tape strip layer 1 permeation abundance in comparison to BW is contrary to this design where the BW formulation permeates glycerol at layer 1 to the highest levels. Glycerol permeation is lowest for the vehicle formulation with distinctly low permeation at tape strip 1 in comparison to other treatments at around 10-15% the permeation of other treatments. This finding is interesting to see that Pentylene glycol which is present in all formulations apart from Physiogel which does not have much effect on the permeation of glycerol and other elements, which is contrary to its purpose as a permeation enhancer to mediate permeation. The other main permeation enhancement property would be how soluble glycerol is in the formulations and able to be delivered into skin layers.

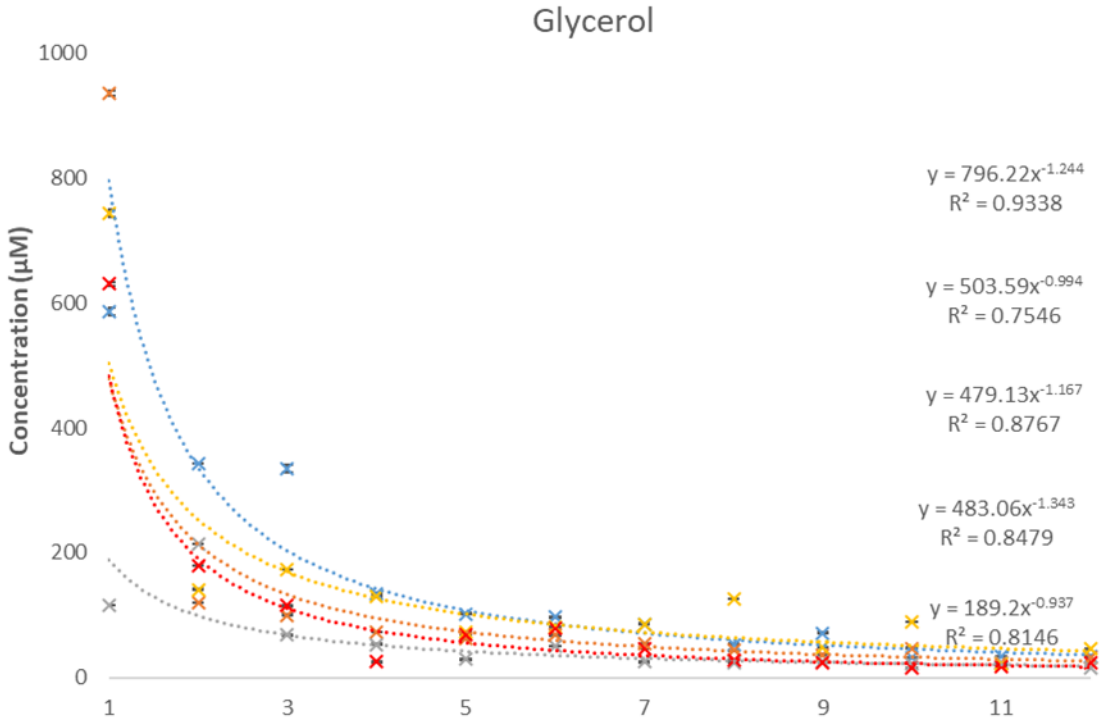

Figure 111 Permeation profiles of Glycerol in treatment tape strips (BW70 = Blue; BW = Orange; Vehicle = Grey; Physiogel = Orange; AI = Red), mean +/- SD. With equations and R^2 values for each treatment power trendline demonstrating a correspondence to Fickian diffusion described previously.

4.3.6 Pentylene Glycol permeation profile

Since Pentylene glycol is a permeation enhancer for actives and drug compounds in formulations it is important to measure where this permeates too so that understanding of where delivered actives will end up in the skin. Again BW70 has the highest permeation and is consistently highest permeating throughout all tape strips to a significant amount. The permeation profiles for Pentylene glycol show an interesting trend where the drops in concentration are less than those seen for other compounds. Despite this observation however all other treatments are relatively consistent in the concentrations of Pentylene glycol in layers and differences between layers are not significant after layer 2, apart from permeation seen in BW70 samples. The power value for the negative correlation for Pentylene glycol are also similar to Niacinamide so this suggests a correlation between Pentylene Glycol level and Niacinamide levels as they permeate through the skin at similar rates.

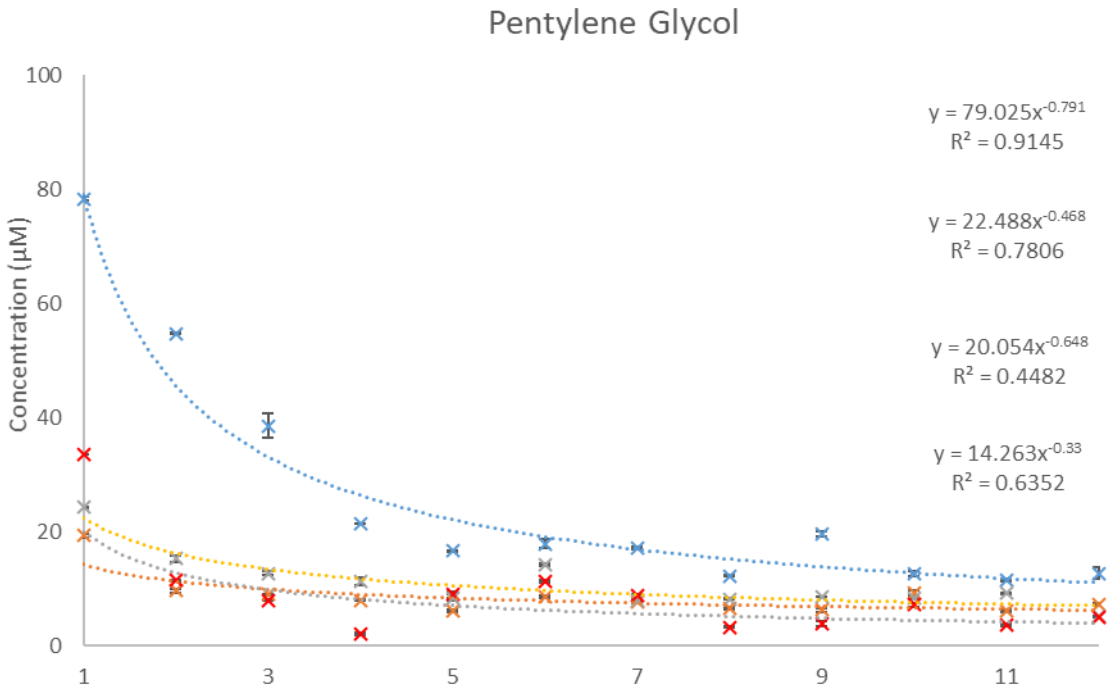

Figure 112 Permeation profiles of Pentylene Glycol (BW70 = Blue; BW = Orange; Vehicle = Grey; AI = Red), mean +/- SD. With equations and R2 values for each treatment power trendline.

4.3.7 Panthenol permeation profile

Panthenol is an active found in the Bluewater group of formulations and is predominantly used for moisturisation alongside a reported antimicrobial activity. It can be compared to glycerol permeation, despite being applied at much lower concentrations initially as seen by tape strip layer 1 concentration. Again, like the other compounds in the Blue water formulations, BW70 has significant increases in permeation from BW and V for layers up to 10. It is also observed that BW has significantly higher permeation than V for the first 4 layers of the skin. The closest power value of negative correlation for panthenol is to glycerol which suggests a similar mechanism of permeation for both these moisturisers as there is a large drop in permeation from tape strip layer 1 to 12.

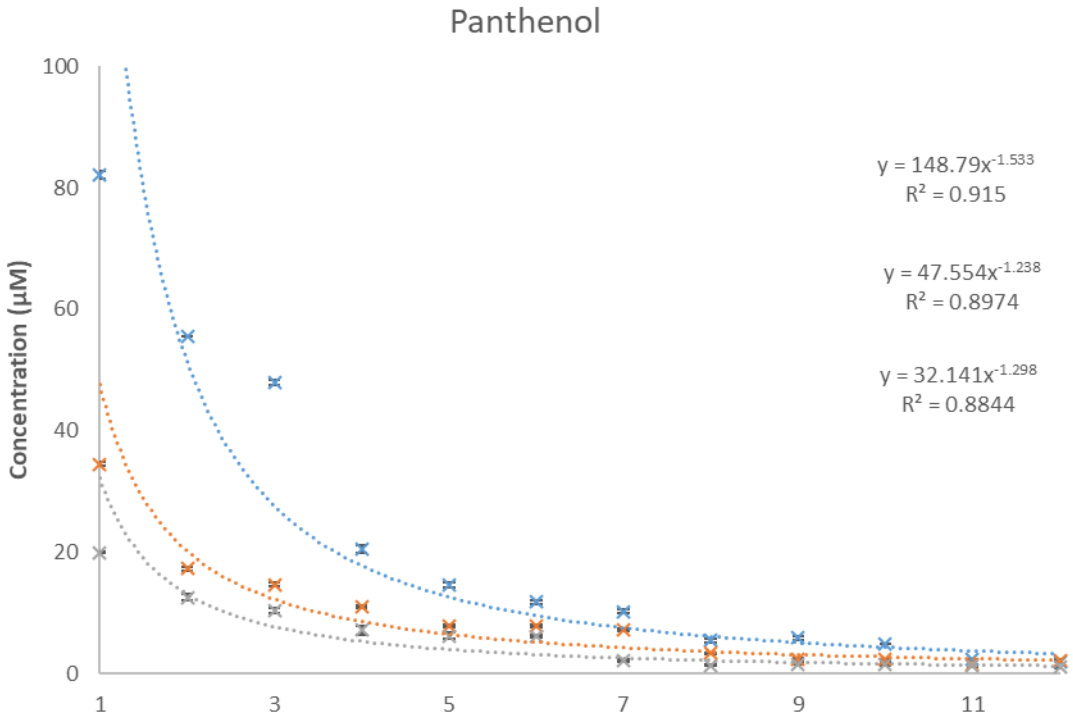

Figure 113 Permeation profiles of Panthenol (BW70 = Blue; BW = Orange; Vehicle = Grey), mean +/- SD. With equations and R^2 values for each treatment power trendline

For reference, the values and standard deviation for each of the compound permeation profiles, and highlighted outliers, are included in the appendix.

4.3.8 Statistical analysis of topical treatment data (PCA)

Quantification of the correlations and variability seen between the permeation for different compounds by principal component analysis is done.

For this analysis data was grouped for ease of observation and interpretation of the data, specifically to investigate the proposed correlation between the different formulation compounds. Preliminary analysis of the data sets for Bluewater formulations was done as these samples contained all the compounds quantified. The scores plot is useful to see how variability differs between groups of the samples. As for the BW1, its variability is distinct to that seen for all the other groups of samples. This demonstrates that group 1 samples for BW1 have high levels of permeation but group 2 and 3 have very low relative permeation demonstrating a large drop in permeation from group 1. BW70_1 and BW70_2 are very close to each other on the scores plot

which highlights the increased permeation seen throughout group 1 and 2 for all compounds and that variability seen in these groups are very similar. V1 is close to BW70_1 and BW70_2 however V2 is much closer to V3 which highlights the low starting permeation for V1 which is comparable to variation in permeation for both BW70_1 and BW70_2. There is a large change which means that the scores point for V1 is distinctly different in variability to V2 and V3. The main finding is that BW1 relative to BW2 and BW3 is very similar to V1 relative to V2 and V3, whereas BW70_3 shows an inverse relationship to BW70_1 and BW70_2. This demonstrates nicely how BW70 treatment increases permeation across both group 1 and 2 rather than only group as demonstrated for BW and V.

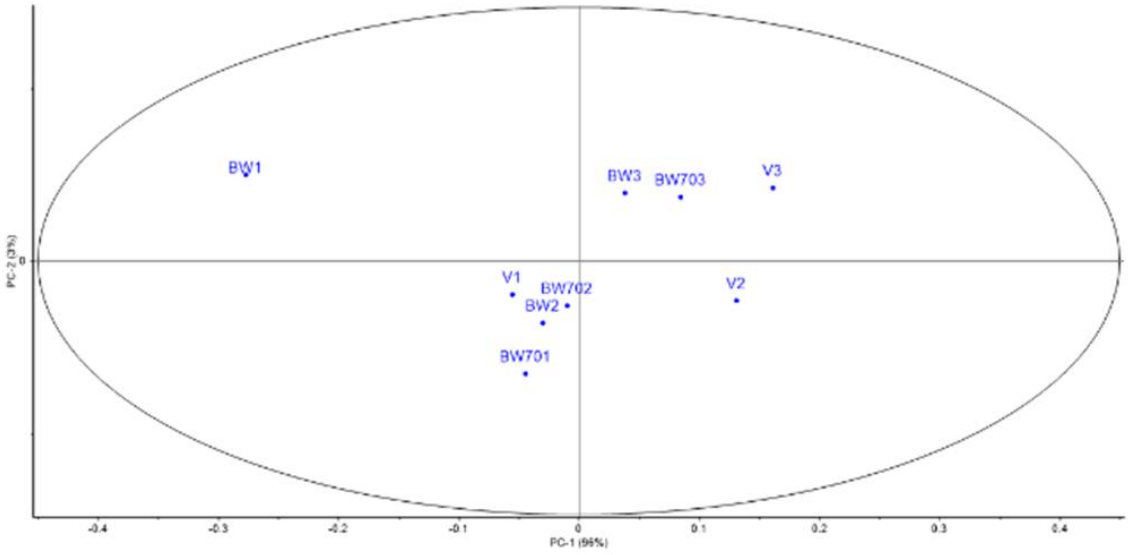

Figure 114 Grouped Bluewater formulations (BW, BW70 and V) permeation profile data of Pentylene glycol, panthenol, glycerol and niacinamide PCA scores plot with PC1 (96%) against PC2 (3%)

The correlation loading plots also confirms the previously proposed correlations between Pentylene glycol and Niacinamide variability. However the proposed correlation between Glycerol and Panthenol, all be it is present but it is much weaker than the correlation between Pentylene Glycol and Niacinamide.

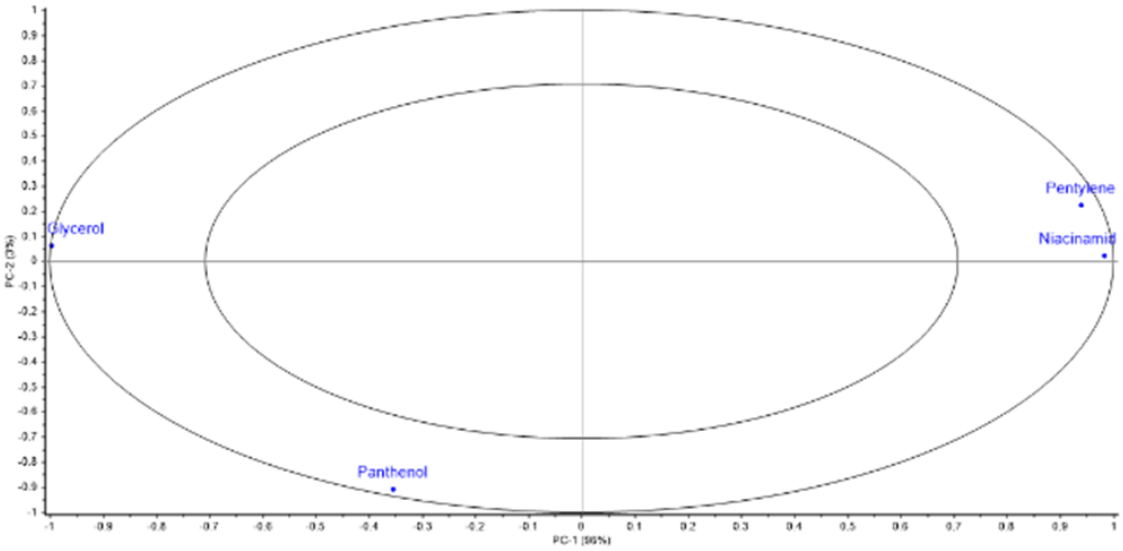

Figure 115 Grouped Bluewater formulation permeation profile data PCA correlation loadings with PC1 (96%) against PC2 (3%) for scores plot in figure 114

4.3.8.1 BW sample formulation component variation analysis

For further clarification of the above findings and to evaluate the individual compound groupings individual treatment datasets were analysed. From the scores plot it is seen that BW1 contributes most to the variability seen for group 1 when compared to group 2 and 3 with all samples from 2 to 12 showing a gradual change in variation but no distinct difference.

Previous findings on correlations corroborate with these findings, but correlations are reduced for Niacinamide and Pentylene Glycol in the samples. This is suggested from previous discussions to be due to Pentylene glycol not permeating through the skin as much as BW70 which means that the permeating influence on Niacinamide concentrations is reduced.

4.3.8.2 BW70 sample formulation variation analysis

For the BW70 scores plot an almost inverse relationship is seen where deeper layers, 9 to 12 are distinctly separated from the rest of the samples, with samples 2 to 6 especially showing very close relationships between their variabilities.

The correlation loadings for the compounds match those seen before a much closer correlation between Pentylene glycol and Niacinamide, with a higher correlation seen between Panthenol and glycerol. This shows that the effects of each of the compounds when permeating at higher levels may have a much greater effect on other formulation components.

4.3.8.3 V sample formulation variation analysis

With the analysis of the V treatments similar scores plot to BW is seen, except that the PC2 is inversed for the samples. This is explained by the negative correlation for panthenol seen in this treatment. With all other correlation loadings not being significantly different to BW correlation loadings. This finding is interesting as it shows that variability for panthenol is positively correlation loaded for BW and BW70 but with V, which only lacks actives its variation becomes inversed.

4.3.8.4 Formulations containing Pentylene glycol and glycerol (AI, BW70, BW and V) variation analysis

The AI formulation is added to the data sets to interpret how its variability in Pentylene glycol and Glycerol compares with the Bluewater formulations. Panthenol and Niacinamide data are not included in this analysis as this would skew the results as AI does not have any detectable levels of either. Initial inspection of the AI treatments show a close scores plot to BW for group 1, however the relationship between group 2 and 3 variability is not the same where these are distinct from one another unlike BW and V.

With the AI added the same correlations for Glycerol and Pentylene Glycol as previously noted are seen with only slight changes in PC2 correlation loading.

4.3.8.5 Combination of topical compounds with NMF data for statistical variance analysis

It was decided to see whether topical components being added to the analysis would resolve groups or the treatments to a greater degree and also elucidate any relationships between permeation of actives to NMF concentrations. The results showed that the addition of NMF datasets to the analysis gave greater resolution between the groups, specifically groups 2 and 3 for BW and V and groups 1 and 2 for BW70. There was no improvement in resolution for treatments as variability was predominantly explained by PC1 with only 6% of variability explained by PC2.

The correlation loadings plot shows the most likely compounds to affect the NMF levels would be Pentylene glycol and Niacinamide relatively, with Panthenol and Glycerol having an inverse

correlation loading to all NMF values. The correlation loading plot however does demonstrate the limitation of comparing these two groups of variables from topical application and skin NMF levels. With the Physiogel results the same results are seen with groups resolved to a greater degree, but treatment resolution is lacking. The same correlation loading plot where all NMFs correlation loadings are distinctly different to that of Glycerol is seen. Scores plots and correlation loading plots for these findings are included in the appendix as they did not show significantly different findings than previous scores and correlation loadings plots.

4.3.9 Oneshot-HSQC of Butanediol and panthenol

Implementation of suggested experiment from Chapter 3, HSQC-DOSY was done on a permeation enhancer, Butanediol and the previously described moisturizer panthenol to demonstrate potential for resolution improvement when determining diffusion coefficients and producing single component HSQC spectra.

The 3D acquisition of HSQC-DOSY uses the One-shot DOSY pulse sequence with $^{1}H^{13}C$ correlation achieved via double inept transfer elements added to the pulse sequence. This pulse sequence design allows for the acquisition of DOSY spectra in one scan which is important when considering the time required for a 3D acquisition.

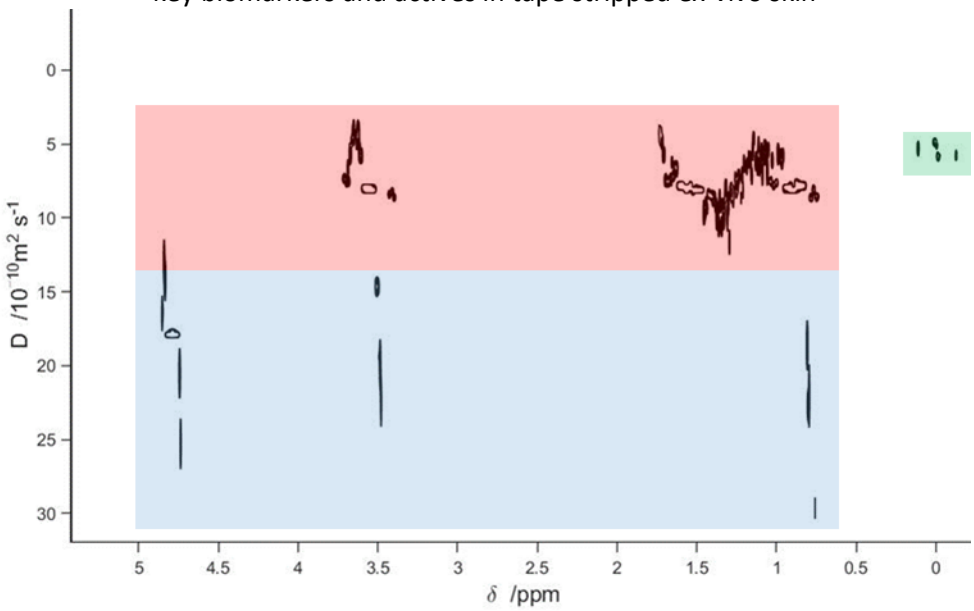

Figure 116 Butanediol and panthenol Oneshot DOSY

The One-shot DOSY spectra demonstrates the large overlap of peaks for butanediol and panthenol which introduces the large error seen for the calculated diffusion coefficients of respective compound peaks. It is seen that for peaks at 3.5ppm show 3 distinct diffusion coefficients rather than the two expected and these have large errors especially for peaks suspected to be for Butanediol. Panthenol peaks show a smaller range of diffusion coefficients for respective peaks but still show clear differences between peak diffusion coefficients which causes larger error when determining average molecule self-diffusion coefficients from individual peaks.

The acquisition of HSQC-DOSY spectra demonstrates clear resolution between respective compound peaks with clearly resolved HSQC projections being constructed from self-diffusion coefficient values for Butanediol and Panthenol respectively. The observation of more than the two expected diffusion coefficient values in the conventionally acquired one-shot DOSY experiment is also resolved and the expected number of diffusion coefficient values are observed. Despite clear resolution between compounds the diffusion coefficient error is quite large for each peak, so for any studies on more complex mixtures the experiment will need to be optimised with changes to D20 and P30 values to interrogate the best settings for each mixture type and complexity. This methodology could also be implemented on studies set up with matrix assisted samples for analysis

of fatty acid containing compounds to determine the degree that resolution can be improved beyond previously discussed methods.

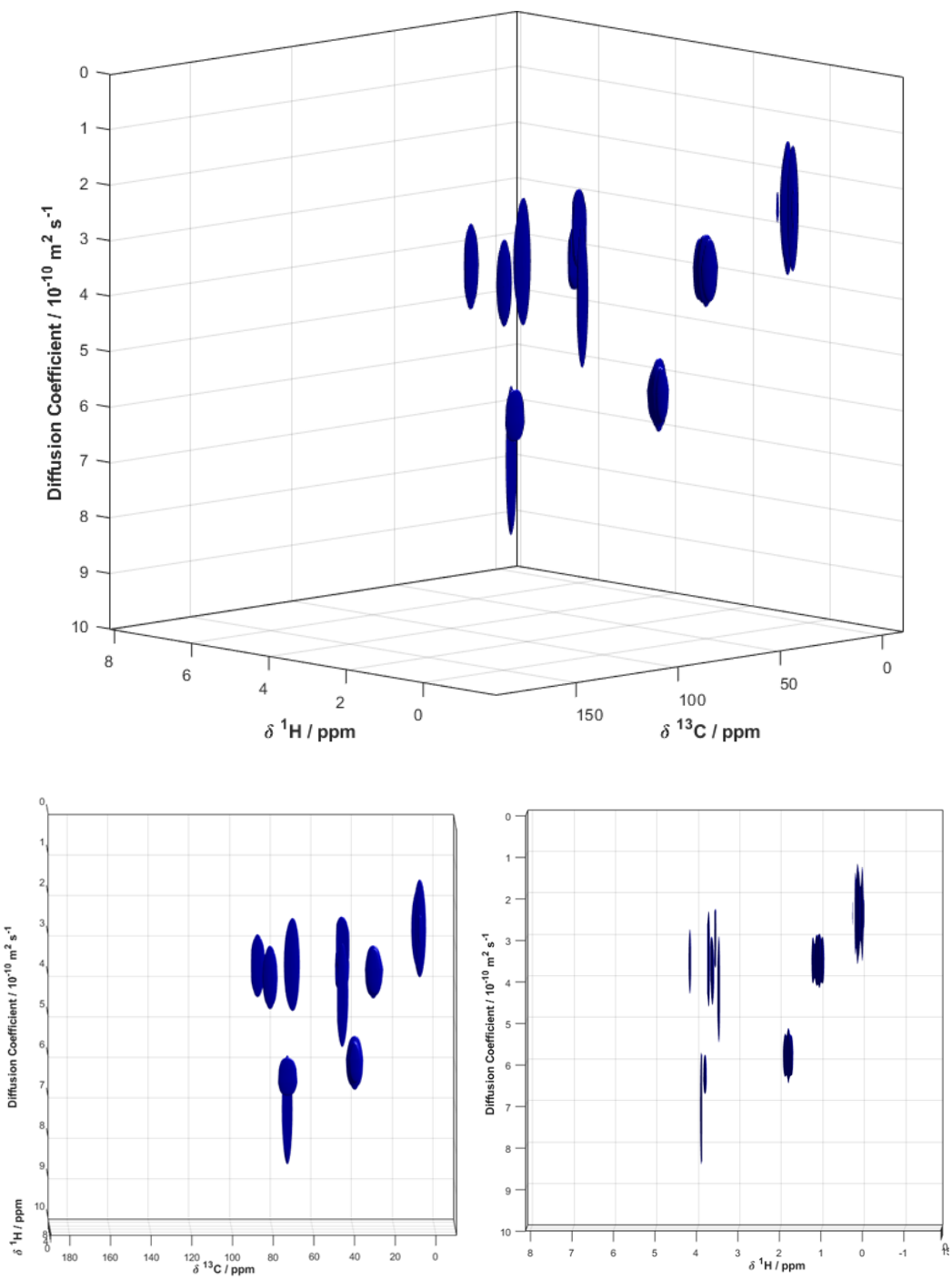

Figure 117 (Top) Pseudo-3D DOSY plot of One-shot–HSQC spectrum of butanediol and panthenol sample, (bottom right) 2D projection along F2 (1H) and (bottom left) 2D projection along F1 (13C)

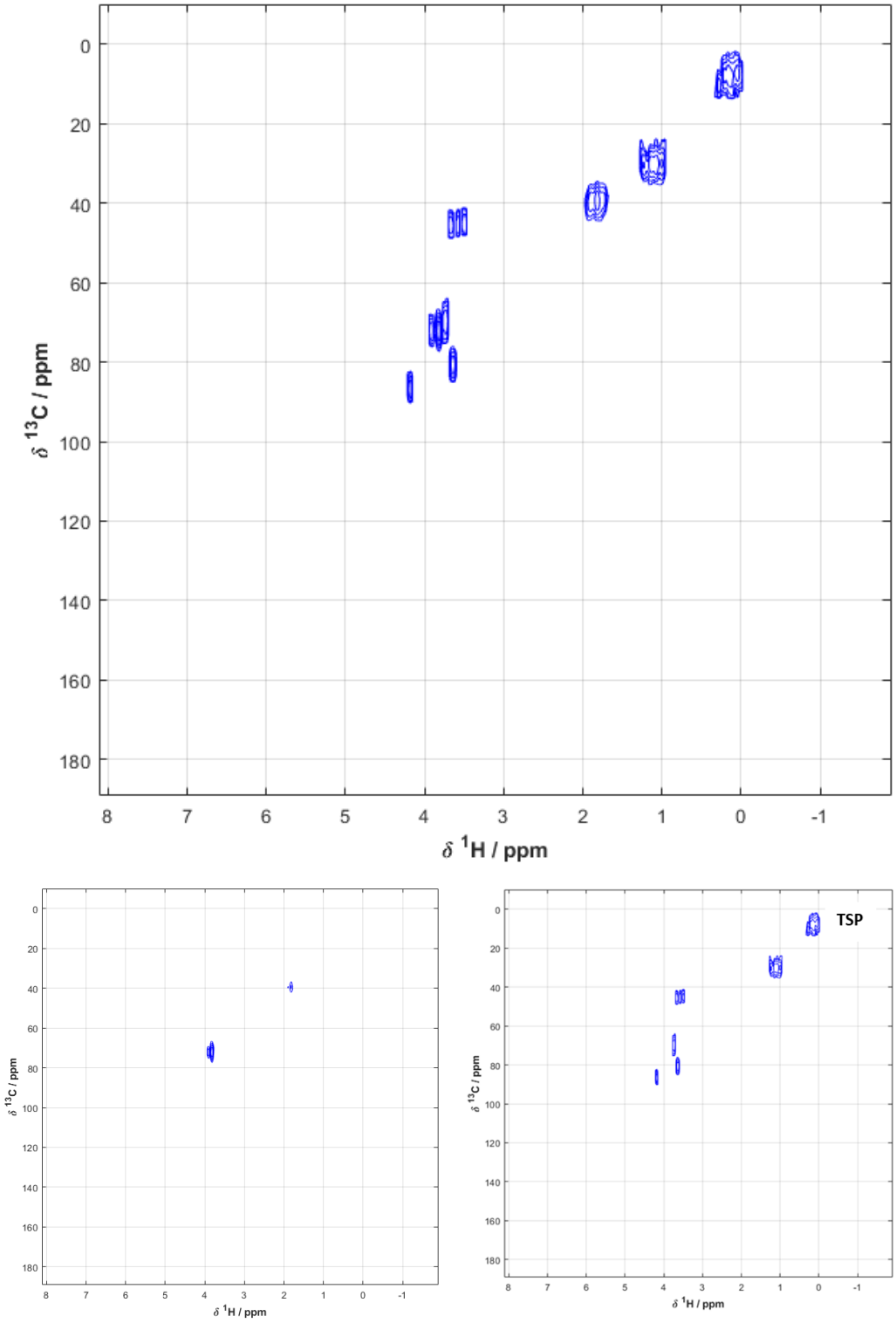

Figure 118 2D slice extracted from the 3D spectrum of the results of Oneshot–HSQC experiment on a mixture of Panthenol and Butanediol in DMSO-d6 and TSP. a)2D spectrum obtained by integrating the region between 0 × 10^{-10} and 9.03 × 10^{-10} m2 s–1 in the diffusion dimension, where all peaks are observed, (bottom left) 2D spectrum obtained by integrating the region between 6.44 × 10^{-10} and 6.46 × 10^{-10} m^2 s^{-1} in the diffusion dimension, where butanediol peaks are observed, (bottom right) 2D spectrum obtained by integrating the region between 0 × 10^{-10} and 4.84 × 10^{-10} m2 s–1 in the diffusion dimension, where panthenol and TSP peaks are observed

4.4 Discussion

For dermatological analysis applications these results highlight the scope and limitations of NMR techniques from characterisation of tape strip extractions to conclusions on how varying concentrations of formulation components affect active delivery in the skin and how these effects correlate to NMF variation in skin layers.

The method of qualitative abundance analysis allowed for rough fingerprinting of the different topical treatments applied to our skin samples and compared their overall formulation permeation which would allow at a glance differentiation between a topically treated skin sample and controls. This however is greatly limited in that it does not give information on specific compounds within the formulations or how the treatment affects the overall effectiveness of permeation. Concentration analysis of proposed fatty acids from FW determination via diffusion coefficient determination however cannot be done as FW determination could not be validated. So this led to free fatty acid (FFA) relative abundance measurements being done, with the assumption that the free fatty acids are a mix of palmitic acid and linoleic acid predominantly in the skin. This abundance analysis does however make assumptions that all the lipophilic elements of the extracellular elements of the skin are collected and the membranes of corneocytes on the surface of the skin.

4.4.1 NMF

Sum of NMF composition in treatments, and averaged values being in accordance with previous literature values demonstrates the reliability of this analysis and allows for confidence in further analysis of the skin layers.

In the treatments the trends for each NMF component are very similar, as seen in figure 3, such that as the tape strips go from group 1 to group 3 layers trends match for each NMF. The significant changes detected for NMF levels match that of previous findings that levels of NMF increase as layers go deeper into the *Stratum corneum*, however at the number of tape strips that was done during this study, this conclusion may be premature, and deeper layer analysis would be useful to

increase the scope of these findings. Highlighting the significant changes for group to group NMF concentration changes allowed us to see that changes vary depending on formulation grouping, with correlations seen in Physiogel treatments (P and AI) and Blue water formulations (BW, AI and V).

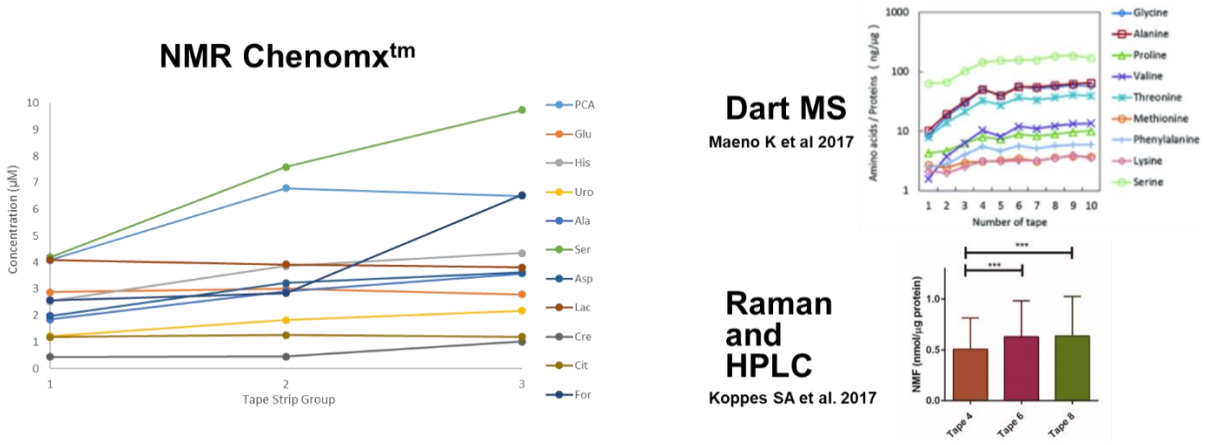

Figure 119 Comparison of NMF concentration determination between NMR Chenomx[tm] and other commonly used techniques (67)(217)

Through the use of principal component analysis grouping of tape strip groups based upon their respective components variability can be achieved however it was unable to determine grouping of different treatment types from this statistical analysis. It was able to distinguish between groupings of treatments and differences with clear resolution between all groups apart from BW70 groups 1 and BW group 1 where the differences for BW70 may be explained by the heat effects of the skin which make the surface have greater energy kinetics and higher diffusion of NMF's between layers or suggested effects of the increased permeation of topical compounds. The variability seen for P could be explained by the drawing effect of treatment P to the surface where formulation has been applied and crystallised. The effects seen for BW70 group 3 may be because of the heat treatment affecting the heterogeneity of NMF compounds. The correlation loading plots also allows us to validate previously reported positive correlations between correlated NMF compounds, specifically PCA and glutamate, Histidine and Urocanate. It is however surprising to see no specific correlations between metabolic markers, with a few specific correlations seen between hygroscopic amino acids.

4.4.2 Permeation profiling of topical components

2D NMR acquisitions (DOSY, HSQC and COSY) were used successfully to identify individual topical molecules within the tape strip extractions. Using DOSY, eight compounds with distinguishable self-diffusion coefficients are determined. These identified compounds are then used to build a calibration curve which further validates assignments from COSY and HSQC experiments. The 4 selected topical compounds were detected for all the Bluewater formulation treatment tape strips. Alongside these known formulation components, characterisation and quantitation of a Niacinamide derivative from DOSY projection analysis was possible. Identification of breakdown products like this is important when thinking of the changes in composition from bottle to skin.

NMR also allows determination of the structure of new derivatives formed and with increases in resolution and sensitivity of NMR spectroscopy being seen at exponential rates through hardware and software innovations. This provides real scope for the measurement and correlation of derivatives to environment, formulation type and skin condition.

NMR was also able to show permeation enhancement through chemical enhancers, specifically here with the example of Pentylene glycol which does not demonstrate increased permeation for all compounds, with only Niacinamide showing correlations to Pentylene Glycol.

4.4.3 Conclusion

This study corroborated previously reported findings about NMF values and how permeation of formulation compounds can be varied by formulation composition and thermal treatment. As an analytical method it demonstrated a non-destructive method unlike most commonly used analytical techniques, while allowing for sample retention and in-situ analysis. The relatively simple extraction procedure, quick sample preparation using a semi-automated approach to NMR quantitation and comparison provides further benefits of NMR over other analytical methodologies.

The benefits of this method is the time required for extraction to acquisition of NMR spectra which can minimise the effects of degradation and derivatisation of target analytes while allowing for monitoring of derivatives as demonstrated by Niacinamide derivative permeation profile. It also presents analyte concentrations which are non-chemically treated and illustrates in-situ relative concentration.

In future work this methodology can be supplemented with *Stratum corneum*/vehicle partition coefficients (Km), maximum flux (J), enhancement factor (EF), and 24-h receptor concentration (Q24h) determination for formulation evaluation and permeation enhancement candidates. It can also be employed in the analysis of NMFs in different skin types, areas and models to validate previous findings and provide additional information that other methods cannot provide in a set time scale with in-situ conditions.

Chapter 5 References

1. Gould J. Superpowered skin. **Nature**. 2018 Nov 1;563(7732):S84-.

2. Candi E, Schmidt R, Melino G. The cornified envelope: a model of cell death in the skin. **Nature reviews Molecular cell biology**. 2005 Apr;6(4):328-40.

3. Hoste E, Kemperman P, Devos M, Denecker G, Kezic S, Yau N, Gilbert B, Lippens S, De Groote P, Roelandt R, Van Damme P. Caspase-14 is required for filaggrin degradation to natural moisturizing factors in the skin. **Journal of investigative dermatology**. 2011 Nov 1;131(11):2233-41.

4. Sandilands A, Sutherland C, Irvine AD, McLean WI. Filaggrin in the frontline: role in skin barrier function and disease. **Journal of cell science**. 2009 May 1;122(9):1285-94.

5. Scott IR, Harding CR. Filaggrin breakdown to water binding compounds during development of the rat stratum corneum is controlled by the water activity of the environment. **Developmental biology**. 1986 May 1;115(1):84-92.

6. Alfery DD, Rauscher LA. Tetanus: a review. **Critical care medicine**. 1979 Apr;7(4):176-81.

7. Nusse R, Brown A, Papkoff J, Scambler P, Shackleford G, McMahon A, Moon R, Varmus H. A new nomenclature for int-1 and related genes: the Wnt gene family. **Cell**. 1991 Jan 25;64(2):231.

8. Makrantonaki E, Brink TC, Zampeli V, Elewa RM, Mlody B, Hossini AM, Hermes B, Krause U, Knolle J, Abdallah M, Adjaye J. Identification of biomarkers of human skin ageing in both genders. Wnt signalling-a label of skin ageing?. **PloS one**. 2012 Nov 30;7(11):e50393.

9. Curto EV, Lambert GW, Davis RL, Wilborn TW, Dooley TP. Biomarkers of human skin cells identified using DermArray DNA arrays and new bioinformatics methods. **Biochemical and biophysical research communications**. 2002 Mar 8;291(4):1052-64.

10. Wang AS, Dreesen O. Biomarkers of cellular senescence and skin aging. **Frontiers in genetics**. 2018 Aug 23;9:247.

11. Visscher MO, Carr AN, Winget J, Huggins T, Bascom CC, Isfort R, Lammers K, Narendran V. Biomarkers of neonatal skin barrier adaptation reveal substantial differences compared to adult skin. **Pediatric Research**. 2020 Jun 29:1-0.

12. Kishibe M. Physiological and pathological roles of kallikrein-related peptidases in the epidermis. **Journal of dermatological science**. 2019 Aug 1;95(2):50-5.

13. Tian XQ, Chen TC, Lu ZH, Shao QI, Holick MF. Characterization of the translocation process of vitamin D3 from the skin into the circulation. **Endocrinology**. 1994 Aug 1;135(2):655-61.

14. Hawker NP, Pennypacker SD, Chang SM, Bikle DD. Regulation of human epidermal keratinocyte differentiation by the vitamin D receptor and its coactivators DRIP205, SRC2, and SRC3. **Journal of Investigative Dermatology**. 2007 Apr 1;127(4):874-80.

15. Liu PT, Stenger S, Li H, Wenzel L, Tan BH, Krutzik SR, Ochoa MT, Schauber J, Wu K, Meinken C, Kamen DL. Toll-like receptor triggering of a vitamin D-mediated human antimicrobial response. **Science**. 2006 Mar 24;311(5768):1770-3.

16. Adams JS, Ren S, Liu PT, Chun RF, Lagishetty V, Gombart AF, Borregaard N, Modlin RL, Hewison M. Vitamin d-directed rheostatic regulation of monocyte antibacterial responses. **The Journal of Immunology**. 2009 Apr 1;182(7):4289-95.

17. Gombart AF, Borregaard N, Koeffler HP. Human cathelicidin antimicrobial peptide (CAMP) gene is a direct target of the vitamin D receptor and is strongly up-regulated in myeloid cells by 1, 25-dihydroxyvitamin D3. **The FASEB journal**. 2005 Jul;19(9):1067-77.

18. Frohm M, Agerberth B, Ahangari G, Ståhle-Bäckdahl M, Lidén S, Wigzell H, Gudmundsson GH. The expression of the gene coding for the antibacterial peptide LL-37 is induced in human keratinocytes during inflammatory disorders. **Journal of Biological Chemistry**. 1997 Jun 13;272(24):15258-63.

19. Koczulla R, Von Degenfeld G, Kupatt C, Krötz F, Zahler S, Gloe T, Issbrücker K, Unterberger P, Zaiou M, Lebherz C, Karl A. An angiogenic role for the human peptide antibiotic LL-37/hCAP-18. **The Journal of clinical investigation**. 2003 Jun 1;111(11):1665-72.

20. Rawlings AV, Harding CR. Moisturization and skin barrier function. **Dermatologic therapy**. 2004 Feb;17:43-8.

21. Nakagawa N, Sakai S, Matsumoto M, Yamada K, Nagano M, Yuki T, Sumida Y, Uchiwa H. Relationship between NMF (lactate and potassium) content and the physical properties of

the stratum corneum in healthy subjects. **Journal of investigative dermatology**. 2004 Mar 1;122(3):755-63.

22. Kezic S, Kammeyer A, Calkoen F, Fluhr JW, Bos JD. Natural moisturizing factor components in the stratum corneum as biomarkers of filaggrin genotype: evaluation of minimally invasive methods. **British journal of dermatology**. 2009 Nov;161(5):1098-104.

23. McAleer, M. A., Jakasa, I., Raj, N., O'Donnell, C. P., Lane, M. E., Rawlings, A. V., ... & Irvine, A. D. (2018). Early-life regional and temporal variation in filaggrin-derived natural moisturizing factor, filaggrin-processing enzyme activity, corneocyte phenotypes and plasmin activity: implications for atopic dermatitis. **British Journal of Dermatology**,179(2), 431-441.

24. https://www.uniprot.org/uniprot/P20930

25. Voegeli R, Rawlings AV, Breternitz M, Doppler S, Schreier T, Fluhr JW. Increased stratum corneum serine protease activity in acute eczematous atopic skin. **British Journal of Dermatology**. 2009 Jul;161(1):70-7.

26. M. Takahashi and T. Tezuka, The content of free amino acids in the stratum corneum is increased in senile xerosis**. Arch. Dermatol. Res.** 2004 295(10), 448–452 .

27. E. Girbal-Neuhauser, J. J. Durieux, M. Arnaud, P. Dalbon, M. Sebbag, C. Vincent, et al., The epitopes targeted by the rheumatoid arthritis-associated anti filaggrin autoantibodies are posttranslationally generated on various sites of (pro)filaggrin by deimination of arginine residues. **J. Immunol.** 1999 162(1), 585–594.

28. Pietzke M, Meiser J, Vazquez A. Formate metabolism in health and disease. **Molecular metabolism**. 2020 Mar 1;33:23-37.

29. Akram M. Citric acid cycle and role of its intermediates in metabolism. **Cell biochemistry and biophysics**. 2014 Apr 1;68(3):475-8.

30. Lenz H, Schmidt M, Welge V, Schlattner U, Wallimann T, Elsässer HP, Wittern KP, Wenck H, Stäb F, Blatt T. The creatine kinase system in human skin: protective effects of creatine

[against oxidative and UV damage in vitro and in vivo. **Journal of Investigative Dermatology**. 2005 Feb 1;124(2):443-52.

31. https://books.google.co.uk/books?hl=en&lr=&id=JpfgVgb62nsC&oi=fnd&pg=PA213&dq=Glycerol+formulations+stratum+corneum&ots=fmAgv0BpAs&sig=4gDwnpPg1V7JarS4EwaNf8m-qYg&redir_esc=y#v=onepage&q&f=false

32. Camargo Jr, F. B., Gaspar, L. R., & Maia Campos, P. M. Skin moisturizing effects of panthenol-based formulations. **Journal of cosmetic science**, 2011 62(4), 361.

33. Heuschkel, S., Wohlrab, J., Schmaus, G., & Neubert, R. H. Modulation of dihydroavenanthramide D release and skin penetration by 1, 2-alkanediols. **European journal of pharmaceutics and biopharmaceutics**. 2008 70(1), 239-247.

34. Duracher, L., Blasco, L., Hubaud, J. C., Vian, L., & Marti-Mestres, G. The influence of alcohol, propylene glycol and 1, 2-pentanediol on the permeability of hydrophilic model drug through excised pig skin. **International journal of pharmaceutics**. 2009 374(1-2), 39-45.

35. Farah, H. A., Brown, M. B., & McAuley, W. J. Enhanced Follicular Delivery of Finasteride to Human Scalp Skin Using Heat and Chemical Penetration Enhancers. **Pharmaceutical Research**, 2020 37, 1-12.

36. Farah, H. A., Brown, M. B., & McAuley, W. J. Heat enhanced follicular delivery of isotretinoin to the skin. **Pharmaceutical research**, 2019 36(8), 124.

37. Caserta, F., Brown, M. B., & McAuley, W. J. The use of heat and chemical penetration enhancers to increase the follicular delivery of erythromycin to the skin. **European Journal of Pharmaceutical Sciences**, 2019 132, 55-62.

38. Zhang Y, Kung CP, Sil BC, Lane ME, Hadgraft J, Heinrich M, Sinko B. Topical Delivery of Niacinamide: **Influence of Binary and Ternary Solvent Systems. Pharmaceutics**. 2019 Dec;11(12):668.

39. Godin B, Touitou E. Transdermal skin delivery: predictions for humans from in vivo, ex vivo and animal models. **Advanced drug delivery reviews**. 2007 Sep 30;59(11):1152-61.

40. Poumay Y, Coquette A. Modelling the human epidermis in vitro: tools for basic and applied research. **Archives of dermatological research**. 2007 Jan 1;298(8):361-9.

41. Friend DR. In vitro skin permeation techniques**. Journal of controlled release**. 1992 Jan 1;18(3):235-48.

42. Wester RC, Maibach HI. In vivo methods for percutaneous absorption measurements. **Drugs and the pharmaceutical sciences**. 1999;97:215-27.

43. Netzlaff F, Schaefer UF, Lehr CM, Meiers P, Stahl J, Kietzmann M, Niedorf F. Comparison of bovine udder skin with human and porcine skin in percutaneous permeation experiments. **Alternatives to laboratory animals: ATLA**. 2006 Oct 1;34(5):499-513.

44. Anissimov YG, Roberts MS. Diffusion modeling of percutaneous absorption kinetics. 1. Effects of flow rate, receptor sampling rate, and viable epidermal resistance for a constant donor concentration. **Journal of pharmaceutical sciences**. 1999 Nov;88(11):1201-9.

45. Flynn G. Physiochemical determinants of skin absorption. **Principles of route-to-route extrapolation for risk assessment**. 1990:93-127.

46. Raj, N., Parisi, N., Rawlings, A. V., Voegeli, R., Lane, M. E., Munday, M., & Gibbons, S. Biomarkers of skin health and barrier efficiency. **Journal of Investigative Dermatology.** 2015 May Vol. 135, pp. S64-S64.

47. Raj, N., Voegeli, R., Rawlings, A. V., Doppler, S., Imfeld, D., Munday, M. R., & Lane, M. E. A fundamental investigation into aspects of the physiology and biochemistry of the stratum corneum in subjects with sensitive skin. **International Journal of cosmetic science.** 2017 39(1), 2-10.

48. McAleer, M. A., Jakasa, I., Raj, N., O'Donnell, C. P., Lane, M. E., Rawlings, A. V., ... & Irvine, A. D. Early-life regional and temporal variation in filaggrin-derived natural moisturizing factor, filaggrin-processing enzyme activity, corneocyte phenotypes and plasmin activity: implications for atopic dermatitis. **British Journal of Dermatology**, 2018 179(2), 431-441.

49. Raj N, Voegeli R, Rawlings AV, Gibbons S, Munday MR, Summers B, Lane ME. Variation in stratum corneum protein content as a function of anatomical site and ethnic group. **International Journal of Cosmetic Science**. 2016 Jun;38(3):224-31.

50. Lademann J, Jacobi U, Surber C, Weigmann HJ, Fluhr JW. The tape stripping procedure–evaluation of some critical parameters. **European Journal of Pharmaceutics and Biopharmaceutics**. 2009 Jun 1;72(2):317-23.

51. Pleitez MA, Lieblein T, Bauer A, Hertzberg O, von Lilienfeld-Toal H, Mäntele W. In vivo noninvasive monitoring of glucose concentration in human epidermis by mid-infrared pulsed photoacoustic spectroscopy. **Analytical chemistry**. 2013 Jan 15;85(2):1013-20.

52. Gorcea M, Hadgraft J, Moore DJ, Lane ME. In vivo barrier challenge and initial recovery in human facial skin. **Skin Research and Technology**. 2013 Feb;19(1):e375-82.

53. Knutson K, Krill SL, Zhang J. Solvent-mediated alterations of the stratum corneum**. Journal of controlled release**. 1990 Jan 1;11(1-3):93-103.

54. Mak VH, Potts RO, Guy RH. Oleic acid concentration and effect in human stratum corneum: non-invasive determination by attenuated total reflectance infrared spectroscopy in vivo. **Journal of controlled release.** 1990 Mar 1;12(1):67-75.

55. Ongpipattanakul B, Burnette RR, Potts RO, Francoeur ML. Evidence that oleic acid exists in a separate phase within stratum corneum lipids. **Pharmaceutical research**. 1991 Mar 1;8(3):350-4.

56. Potts RO, Francoeur ML. Lipid biophysics of water loss through the skin. **Proceedings of the National Academy of Sciences.** 1990 May 1;87(10):3871-3.

57. Alberti I, Kalia YN, Naik A, Bonny JD, Guy RH. Effect of ethanol and isopropyl myristate on the availability of topical terbinafine in human stratum corneum, in vivo. **International journal of pharmaceutics**. 2001 May 21;219(1-2):11-9.

58. Kim KH, Jheon S, Kim JK. In vivo skin absorption dynamics of topically applied pharmaceuticals monitored by fiber-optic diffuse reflectance spectroscopy. Spectrochimica Acta Part A: **Molecular and Biomolecular Spectroscopy**. 2007 Mar 1;66(3):768-72.

59. Kim J, Salvatore GA, Araki H, Chiarelli AM, Xie Z, Banks A, Sheng X, Liu Y, Lee JW, Jang KI, Heo SY. Battery-free, stretchable optoelectronic systems for wireless optical characterization of the skin. **Science advances**. 2016 Aug 1;2(8):e1600418.

60. Garrison MD, Doh LM, Potts RO, Abraham W. Effect of oleic acid on human epidermis: Fluorescence spectroscopic investigation. **Journal of controlled release**. 1994 Oct 1;31(3):263-9.

61. Wang S, Zhao J, Lui H, He Q, Zeng H. In vivo near-infrared autofluorescence imaging of pigmented skin lesions: methods, technical improvements and preliminary clinical results. **Skin Research and Technology**. 2013 Feb;19(1):20-6.

62. Seidenari S, Arginelli F, Dunsby C, French PM, König K, Magnoni C, Talbot C, Ponti G. Multiphoton laser tomography and fluorescence lifetime imaging of melanoma: morphologic features and quantitative data for sensitive and specific non-invasive diagnostics. **PLoS One**. 2013 Jul 26;8(7):e70682.

63. Caprioli RM, Farmer TB, Gile J. Molecular imaging of biological samples: localization of peptides and proteins using MALDI-TOF MS. **Analytical chemistry**. 1997 Dec 1;69(23):4751-60.

64. Bunch J, Clench MR, Richards DS. Determination of pharmaceutical compounds in skin by imaging matrix-assisted laser desorption/ionisation mass spectrometry. **Rapid communications in mass spectrometry**. 2004 Dec 30;18(24):3051-60.

65. Avery JL, McEwen A, Flinders B, Francese S, Clench MR. Matrix-assisted laser desorption mass spectrometry imaging for the examination of imipramine absorption by Straticell-RHE-EPI/001 an artificial model of the human epidermis. **Xenobiotica.** 2011 Aug 1;41(8):735-42.

66. Hart PJ, Francese S, Claude E, Woodroofe MN, Clench MR. MALDI-MS imaging of lipids in ex vivo human skin. **Analytical and bioanalytical chemistry.** 2011 Jul 1;401(1):115-25.

67. Maeno K, Shida Y, Shimada H. Direct quantitative analysis of the natural moisturizing factor (NMF) in the stratum corneum by direct analysis in real time mass spectrometry (DART-MS). **Analytical Methods**. 2017;9(33):4851-7.

68. Imhof RE, Zhang B, Birch DJ, Mandelis A. Progress in photothermal and photoacoustic science and technology. **PTR Prentice Hall, Englewood Cliffs (USA)**. 1994;2:185-236.

69. Kalia YN, Guy RH. The electrical characteristics of human skin in vivo. **Pharmaceutical research.** 1995 Nov 1;12(11):1605-13.

70. Sun Q, Tran M, Smith BW, Winefordner JD. Zinc analysis in human skin by laser induced-breakdown spectroscopy. **Talanta.** 2000 Jun 21;52(2):293-300.

71. Sun Q, Tran M, Smith B, Winefordner JD. In-situ evaluation of barrier-cream performance on human skin using laser-induced breakdown spectroscopy. **Contact dermatitis.** 2000 Nov;43(5):259-63.

72. Lahjomri F, Benamar N, Chatri E, Leblanc RM. Study of the diffusion of some emulsions in the human skin by pulsed photoacoustic spectroscopy. **Physics in Medicine & Biology.** 2003 Jul 30;48(16):2729.

73. Bindra RM, Imhof RE, Mochan A, Eccleston GM. Opto-thermal technique for in-vivo stratum corneum hydration measurement**. Le Journal de Physique IV.** 1994 Jul 1;4(C7):C7-465.

74. Xiao P, Imhof RE. Optothermal skin-water concentration gradient measurement. InLaser-Tissue Interaction VII. **International Society for Optics and Photonics.**1996 May 7 (Vol. 2681, pp. 31-41).

75. White EA, Orazem ME, Bunge AL. Characterization of damaged skin by impedance spectroscopy: mechanical damage. **Pharmaceutical research**. 2013 Aug 1;30(8):2036-49.

76. White EA, Orazem ME, Bunge AL. Characterization of damaged skin by impedance spectroscopy: Chemical damage by dimethyl sulfoxide. **Pharmaceutical research**. 2013 Oct 1;30(10):2607-24.

77. Hatcher ME, Plachy WZ. Dioxygen diffusion in the stratum corneum: an EPR spin label study. **Biochimica et Biophysica Acta (BBA)-Biomembranes**. 1993 Jun 18;1149(1):73-8.

78. Gay CL, Murphy TM, Hadgraft J, Kellaway IW, Evans JC, Rowlands CC. An electron spin resonance study of skin penetration enhancers. **International journal of pharmaceutics.** 1989 Jan 1;49(1):39-45.

79. Haag SF, Fleige E, Chen M, Fahr A, Teutloff C, Bittl R, Lademann J, Schäfer-Korting M, Haag R, Meinke MC. Skin penetration enhancement of core–multishell nanotransporters and invasomes measured by electron paramagnetic resonance spectroscopy. **International journal of pharmaceutics**. 2011 Sep 15;416(1):223-8.

80. Carrola J, Bastos V, de Oliveira JM, Oliveira H, Santos C, Gil AM, Duarte IF. Insights into the impact of silver nanoparticles on human keratinocytes metabolism through NMR metabolomics. **Archives of Biochemistry and Biophysics**. 2016 Jan 1;589:53-61.

81. Bezema FR, Marttin E, Roemele PE, Brussee J, Bodde HE, De Groot HJ. 2H NMR evidence for dynamic disorder in human skin induced by the penetration enhancer azone. **Spectrochimica Acta Part A: Molecular and Biomolecular Spectroscopy**. 1996 Jul 15;52(7):785-91.

82. Kreilgaard M, Pedersen EJ, Jaroszewski JW. NMR characterisation and transdermal drug delivery potential of microemulsion systems. **Journal of controlled release**. 2000 Dec 3;69(3):421-33.

83. Hua L, Weisan P, Jiayu L, Ying Z. Preparation, evaluation, and NMR characterization of vinpocetine microemulsion for transdermal delivery. **Drug development and industrial pharmacy**. 2004 Jan 1;30(6):657-66.

84. Musazzi UM, Santini B, Selmin F, Marini V, Corsi F, Allevi R, Ferretti AM, Prosperi D, Cilurzo F, Colombo M, Minghetti P. Impact of semi-solid formulations on skin penetration of iron oxide nanoparticles. **Journal of nanobiotechnology**. 2017 Dec;15(1):1-0.

85. Van Landeghem M, Danieli E, Perlo J, Blümich B, Casanova F. Low-gradient single-sided NMR sensor for one-shot profiling of human skin**. Journal of Magnetic Resonance.** 2012 Feb 1;215:74-84.

86. Bergman E, Sarda Y, Ritz N, Sabo E, Navon G, Bergman R, Nevo U. In vivo assessment of aged human skin with a unilateral NMR scanner. **NMR in Biomedicine**. 2015 Jun;28(6):656-66.

87. Dias M, Hadgraft J, Glover PM, McDonald PJ. Stray field magnetic resonance imaging: a preliminary study of skin hydration. **Journal of Physics D: Applied Physics.** 2003 Jan 29;36(4):364.

88. Backhouse LJ. GARField NMR profiling of skin hydration and care product application. **University of Surrey (United Kingdom)**; 2005.

89. Ciampi E, van Ginkel M, McDonald PJ, Pitts S, Bonnist EY, Singleton S, Williamson AM. Dynamic in vivo mapping of model moisturiser ingress into human skin by GARfield MRI. **NMR in Biomedicine**. 2011 Feb;24(2):135-44.

90. McDonald PJ, Akhmerov A, Backhouse LJ, Pitts S. Magnetic resonance profiling of human skin in vivo using GARField magnets. **Journal of pharmaceutical sciences**. 2005 Aug;94(8):1850-60.

91. Koch RL, Micali G, Burt CT, Lee DJ, West DP, Solomon LM. Measurement of flurbiprofen absorption in vivo through human skin using 19Fluorine nuclear magnetic resonance. **Journal of investigative dermatology**. 1993 Apr 1 (Vol. 100, No. 4, pp. 594-594)

92. Schwarz JC, Hoppel M, Kählig H, Valenta C. Application of quantitative 19F nuclear magnetic resonance spectroscopy in tape-stripping experiments with natural microemulsions. **Journal of Pharmaceutical Sciences.** 2013 Aug 1;102(8):2699-706.

93. Zemtsov A, Dixon L, Cameron G. Human in vivo phosphorus 31 magnetic resonance spectroscopy of psoriasis: A noninvasive tool to monitor response to treatment and to study pathophysiology of the disease**. Journal of the American Academy of Dermatology**. 1994 Jun 1;30(6):959-65.

94. Packer KJ, Sellwood TC. Proton magnetic resonance studies of hydrated stratum corneum. Part 2.—Self-diffusion. **Journal of the Chemical Society, Faraday Transactions 2: Molecular and Chemical Physics.** 1978;74:1592-606.

95. Packer KJ, Sellwood TC. Proton magnetic resonance studies of hydrated stratum corneum. Part 1.—Spin–lattice and transverse relaxation. **Journal of the Chemical Society, Faraday Transactions 2: Molecular and Chemical Physics.** 1978;74:1579-91.

96. Foreman MI. A proton magnetic resonance study of water in human stratum corneum. **Biochimica et Biophysica Acta (BBA)-General Subjects.** 1976 Jul 21;437(2):599-603.

97. Abraham W, Downing DT. Deuterium NMR investigation of polymorphism in stratum corneum lipids. **Biochimica et Biophysica Acta (BBA)-Biomembranes**. 1991 Sep 30;1068(2):189-94.

98. Abraham W, Downing DT. Lamellar structures formed by stratum corneum lipids in vitro: a deuterium nuclear magnetic resonance (NMR) study. **Pharmaceutical research.** 1992 Nov 1;9(11):1415-21.

99. Kitson N, Thewalt J, Lafleur M, Bloom M. A model membrane approach to the epidermal permeability barrier. **Biochemistry.** 1994 May 1;33(21):6707-15.

100. Maeno K. Direct Quantification of Natural Moisturizing Factors in Stratum Corneum using Direct Analysis in Real Time Mass Spectrometry with Inkjet-Printing Technique. **Scientific reports.** 2019 Nov 28;9(1):1-0.

101. Raj N, Voegeli R, Rawlings AV, Doppler S, Imfeld D, Munday MR, Lane ME. A fundamental investigation into aspects of the physiology and biochemistry of the stratum corneum in subjects with sensitive skin. **International journal of cosmetic science.** 2017 Feb;39(1):2-10.

102. Dapic I, Jakasa I, Yau NL, Kezic S, Kammeyer A. Evaluation of an HPLC method for the determination of natural moisturizing factors in the human stratum corneum. **Analytical letters.** 2013 Sep 22;46(14):2133-44

103. Sauce R, de Oliveira Pinto CA, Velasco MV, Rosado C, Baby AR. Ex vivo penetration analysis and anti-inflammatory efficacy of the association of ferulic acid and UV filters. **European Journal of Pharmaceutical Sciences.** 2020 Sep 28:105578.

104. Le Gresley, Adam, Simpson, Emma, Sinclair, Alex, Williams, Neil, Burnett, Gary, Bradshaw, David and Lucas, Robert (2015). The application of high-resolution diffusion NMR for the characterisation and quantification of small molecules in saliva/dentifrice slurries. **Analytical Methods**, 7(6), p. 2323.

105. Holick, M. F. (2016). Biological effects of sunlight, ultraviolet radiation, visible light, infrared radiation and vitamin D for health. **Anticancer research**, 36(3), 1345-1356.

106. Fardus-Reid F, Warren J and Le Gresley A. Validating heteronuclear 2D quantitative NMR. **Analytical Methods**, 2016 8(9), pp. 2013-2019.ISSN (print) 1759-9660.

107. Le Gresley A, Fardus F and Warren J, Bias and uncertainty in non-ideal qNMR Analysis. **Critical reviews in analytical chemistry / CRC**, 2015 45(4), pp. 300-10. ISSN (print) 1547-6510.

108. Giraudeau P, Frydman L. Ultrafast 2D NMR: an emerging tool in analytical spectroscopy. **Annual review of analytical chemistry**. 2014 Jun 12;7:129-61.

109. Purcell EM, Torrey HC, Pound RV. Resonance absorption by nuclear magnetic moments in a solid. **Physical review**. 1946 Jan 1;69(1-2):37.

110. Bloch F, Graves AC, Packard M, Spence RW. Spin and magnetic moment of tritium. **Physical Review**. 1947 Mar 15;71(6):373.

111. Ernst RR, Anderson WA. Application of Fourier transform spectroscopy to magnetic resonance**. Review of Scientific Instruments**. 1966 Jan;37(1):93-102.

112. Li, J. S., Ruths, J., Yu, T. Y., Arthanari, H., & Wagner, G. Optimal pulse design in quantum control: A unified computational method. **Proceedings of the National Academy of Sciences**, 2011 108(5), 1879-1884

113. Maeda H, Yamazaki T, Nishiyama Y, Hamada M, Hashi K, Shimizu T, Suematsu H, Yanagisawa Y. Development of Super-High-Field NMR Operated Beyond 1 GHz Using High-Temperature Superconducting Coils. **eMagRes**. 2007 Mar 15:1109-20.

114. Bornet A, Maucourt M, Deborde C, Jacob D, Milani J, Vuichoud B, Ji X, Dumez JN, Moing A, Bodenhausen G, Jannin S. Highly repeatable dissolution dynamic nuclear polarization for heteronuclear NMR metabolomics. **Analytical chemistry**. 2016 Jun 21;88(12):6179-83.

115. Castañar L. Pure shift 1H NMR: what is next?. **Magnetic Resonance in Chemistry**. 2017 Jan;55(1):47-53.

116. Pauli GF, Godecke T, Jaki BU, Lankin DC. Quantitative 1H NMR. Development and potential of an analytical method: an update. **Journal of natural products**. 2012 Apr 27;75(4):834-51.

117. Hu K, Wyche TP, Bugni TS, Markley JL. Selective quantification by 2D HSQC0 spectroscopy of thiocoraline in an extract from a sponge-derived Verrucosispora sp. **Journal of natural products**. 2011 Oct 28;74(10):2295-8.

118. Schulze-Sünninghausen D, Becker J, Koos MR, Luy B. Improvements, extensions, and practical aspects of rapid ASAP-HSQC and ALSOFAST-HSQC pulse sequences for studying small molecules at natural abundance. **Journal of Magnetic Resonance**. 2017 Aug 1;281:151-61.

119. Porcelli F, Verardi R, Shi L, Henzler-Wildman KA, Ramamoorthy A, Veglia G. NMR structure of the cathelicidin-derived human antimicrobial peptide LL-37 in dodecylphosphocholine micelles. **Biochemistry**. 2008 May 20;47(20):5565-72.

120. Le Gresley A, Simpson E, Sinclair AJ, Williams N, Burnett GR, Bradshaw DJ, Lucas RA. The application of high resolution diffusion NMR for the characterisation and quantification of small molecules in saliva/dentifrice slurries. **Analytical Methods**. 2015;7(6):2323-32.

121. Lepre CA, Moore JM, Peng JW. Theory and applications of NMR-based screening in pharmaceutical research. **Chemical reviews**. 2004 Aug 11;104(8):3641-76.

122. Mayer M, Meyer B. Characterization of ligand binding by saturation transfer difference NMR spectroscopy. **Angewandte Chemie International Edition**. 1999 Jun 14;38(12):1784-8.

123. Mayer K, Meyer S, Reinholz-Muhly M, Maus U, Merfels M, Lohmeyer J, Grimminger F, Seeger W. Short-time infusion of fish oil-based lipid emulsions, approved for parenteral nutrition, reduces monocyte proinflammatory cytokine generation and adhesive interaction with endothelium in humans. **The Journal of Immunology**. 2003 Nov 1;171(9):4837-43.

124. Pellecchia M, Bertini I, Cowburn D, Dalvit C, Giralt E, Jahnke W, James TL, Homans SW, Kessler H, Luchinat C, Meyer B. Perspectives on NMR in drug discovery: a technique comes of age. **Nature reviews Drug discovery**. 2008 Sep;7(9):738-45.

125. Jayalakshmi V, Krishna NR. Complete relaxation and conformational exchange matrix (CORCEMA) analysis of intermolecular saturation transfer effects in reversibly forming ligand–receptor complexes. **Journal of Magnetic Resonance**. 2002 Mar 1;155(1):106-18.

126. Moseley HN, Curto EV, Krishna NR. Complete relaxation and conformational exchange matrix (CORCEMA) analysis of NOESY spectra of interacting systems; two-dimensional transferred NOESY. **Journal of Magnetic Resonance, Series B**. 1995 Sep 1;108(3):243-61.

127. Wishart DS, Greiner R, Rosborough TA, Lefebvre BA, Epstein NA, Newton JB, Wong WR, inventors; Chenomx Inc, assignee. Automatic identification of compounds in a sample mixture by means of NMR spectroscopy. **United States patent US 7,191,069.** 2007 Mar 13.

128. Claridge TD. High-resolution NMR techniques in organic chemistry. Elsevier; 2016 Apr 22.

129. Levitt MH, Freeman R, Frenkiel T. Broadband heteronuclear decoupling. **Journal of Magnetic Resonance**. 1982 Apr 1;47(2):328-30.

130. Shaka AJ, Keeler J, Frenkiel T, Freeman RA. An improved sequence for broadband decoupling: WALTZ-16. **Journal of Magnetic Resonance**. 1983 Apr 1;52(2):335-8.

131. Kupce E, Freeman R. Adiabatic pulses for wideband inversion and broadband decoupling. **Journal of magnetic resonance**. 1995;115(2):273-6.

132. Fu R, Bodenhausen G. Broadband decoupling in NMR with frequency-modulated ‘chirp’pulses. **Chemical physics letters**. 1995 Nov 3;245(4-5):415-20.

133. Anderson WA, Freeman R. Influence of a second radiofrequency field on high-resolution nuclear magnetic resonance spectra. **The Journal of Chemical Physics**. 1962 Jul 1;37(1):85-103.

134. Meyer NH, Zangger K. Simplifying proton NMR spectra by instant homonuclear broadband decoupling. **Angewandte Chemie International Edition**. 2013 Jul 8;52(28):7143-6.

135. Garbow JR, Weitekamp DP, Pines A. Bilinear rotation decoupling of homonuclear scalar interactions. **Chemical Physics Letters**. 1982 Dec 17;93(5):504-9.

136. Zangger K. Pure shift NMR. **Progress in nuclear magnetic resonance spectroscopy**. 2015 Apr 1;86:1-20.

137. Castañar L, Nolis P, Virgili A, Parella T. Full sensitivity and enhanced resolution in homodecoupled band-selective NMR experiments. **Chem. Eur. J.** 2013 Dec 16;19(51):17283-6.

138. Griesinger C, Sørensen OW, Ernst RR. Two-dimensional correlation of connected NMR transitions. **Journal of the American Chemical Society**. 1985 Oct;107(22):6394-6.

139. Sørensen OW, Griesinger C, Ernst RR. Time reversal of the evolution under scalar spin-spin interactions in NMR. Application for. omega. 1 decoupling in two-dimensional NOE spectroscopy. **Journal of the American Chemical Society**. 1985 Dec;107(25):7778-9.

140. Zangger K, Sterk H. Homonuclear broadband-decoupled NMR spectra. **JMagR**. 1997 Feb;124(2):486-9.

141. Pell AJ, Keeler J. Two-dimensional J-spectra with absorption-mode lineshapes. **Journal of Magnetic Resonance**. 2007 Dec 1;189(2):293-9.

142. Oschkinat H, Pastore A, Pfändler P, Bodenhausen G. Two-dimensional correlation of directly and remotely connected transitions by z-filtered COSY. **Journal of magnetic resonance**. 1986;69:559-66.

143. Kakita VM, Shukla VK, Bopardikar M, Bhattacharya T, Hosur RV. Measurement of 1 H NMR relaxation times in complex organic chemical systems: Application of PSYCHE. **RSC advances**. 2016;6(102):100098-102.

144. Santacruz L, Hurtado DX, Doohan R, Thomas OP, Puyana M, Tello E. Metabolomic study of soft corals from the Colombian Caribbean: PSYCHE and 1 H-NMR comparative analysis. **Scientific reports**. 2020 Mar 25;10(1):1-1.

145. Zhao Q, Liu Y, Ma H, Qiao Y, Chao J, Hou X, Wang Y, Wang Y. Combination of pure shift NMR and chemical shift selective filters for analysis of Fischer-Tropsch waste-water. **Analytica Chimica Acta**. 2020 Mar 17.

146. Bo Y, Feng J, Xu J, Huang Y, Cai H, Cui X, Dong J, Ding S, Chen Z. High-resolution pure shift NMR spectroscopy offers better metabolite discrimination in food quality analysis. **Food Research International**. 2019 Nov 1;125:108574.

147. Lopez JM, Cabrera R, Maruenda H. Ultra-Clean Pure Shift 1 H-NMR applied to metabolomics profiling. **Scientific reports**. 2019 May 3;9(1):1-8.

148. Kakita VM, Rachineni K, Hosur RV. Ultraclean Pure Shift NMR Spectroscopy with Adiabatic Composite Refocusing Pulses: Application to Metabolite Samples. **ChemistrySelect**. 2019 Sep 13;4(34):9893-6.

149. Foroozandeh M, Castañar L, Martins LG, Sinnaeve D, Poggetto GD, Tormena CF, Adams RW, Morris GA, Nilsson M. Ultrahigh-resolution diffusion-ordered spectroscopy. **Angewandte Chemie**. 2016 Dec 12;128(50):15808-11

150. Stilbs P. Molecular self-diffusion coefficients in Fourier transform nuclear magnetic resonance spectrometric analysis of complex mixtures. **Analytical Chemistry**. 1981 Nov 1;53(13):2135-7.)

151. Howe PW. Selective diffusion spectroscopy using excitation sculpting. **Magnetic Resonance in Chemistry**. 2017 May;55(5):433-7.

152. Zubkov M, Dennis GR, Stait-Gardner T, Torres AM, Willis SA, Zheng G, Price WS. Physical characterization using diffusion NMR spectroscopy. **Magnetic Resonance in Chemistry.** 2017 May;55(5):414-24.

153. Liebau J, Ye W, Mäler L. Characterization of fast-tumbling isotropic bicelles by PFG diffusion NMR. **Magnetic Resonance in Chemistry**. 2017 May;55(5):395-404.

154. Fredi A, Nolis P, Cobas C, Parella T. Access to experimentally infeasible spectra by pure-shift NMR covariance. **Journal of Magnetic Resonance**. 2016 Sep 1;270:161-8.

155. Billeter, M. Non-uniform sampling in biomolecular NMR. J Biomol NMR 68, 65–66 (2017).

156. Zhang B, Powers R, O'Day EM. Evaluation of Non-Uniform Sampling 2D 1H–13C HSQC Spectra for Semi-Quantitative Metabolomics. **Metabolites**. 2020 May;10(5):203.

157. Beyer T, Diehl B, Holzgrabe U. Quantitative NMR spectroscopy of biologically active substances and excipients. **Bioanalytical Reviews**. 2010 Dec 1;2(1-4):1-22.

158. Pauli GF. qNMR—a versatile concept for the validation of natural product reference compounds. **Phytochemical Analysis: An International Journal of Plant Chemical and Biochemical Techniques**. 2001 Jan;12(1):28-42.

162. Holick MF. Resurrection of vitamin D deficiency and rickets. **The Journal of clinical investigation**. 2006 Aug 1;116(8):2062-72.

163. Tian XQ, Chen TC, Lu ZH, Shao QI, Holick MF. Characterization of the translocation process of vitamin D3 from the skin into the circulation. **Endocrinology**. 1994 Aug 1;135(2):655-61.

164. Haddad JG, Matsuoka LY, Hollis BW, Hu YZ, Wortsman J. Human plasma transport of vitamin D after its endogenous synthesis. **The Journal of clinical investigation**. 1993 Jun 1;91(6):2552-5.

165. Matsuoka LY, Ide L, Wortsman J, Maclaughlin JA, Holick MF. Sunscreens suppress cutaneous vitamin D3 synthesis. **The journal of clinical endocrinology & metabolism**. 1987 Jun 1;64(6):1165-8.

166. Aloia JF, Talwar SA, Pollack S, Yeh J. A randomized controlled trial of vitamin D3 supplementation in African American women. **Archives of Internal Medicine**. 2005 Jul 25;165(14):1618-23.

167. Clemens TL, Henderson SL, Adams JS, Holick MF. Increased skin pigment reduces the capacity of skin to synthesise vitamin D3. **The Lancet**. 1982 Jan 9;319(8263):74-6.

168. Holick M, Matsuoka L, Wortsman J. Age, vitamin D, and solar ultraviolet. **Lancet (British edition)**. 1989;2(8671):1104-5.

169. Hawker NP, Pennypacker SD, Chang SM, Bikle DD. Regulation of human epidermal keratinocyte differentiation by the vitamin D receptor and its coactivators DRIP205, SRC2, and SRC3. **Journal of Investigative Dermatology**. 2007 Apr 1;127(4):874-80.

170. Bikle DD, Pillai S. Vitamin D, calcium, and epidermal differentiation. **Endocrine Reviews**. 1993 Feb 1;14(1):3-19.

171. Liu PT, Stenger S, Li H, Wenzel L, Tan BH, Krutzik SR, Ochoa MT, Schauber J, Wu K, Meinken C, Kamen DL. Toll-like receptor triggering of a vitamin D-mediated human antimicrobial response. **Science**. 2006 Mar 24;311(5768):1770-3.

172. Adams JS, Ren S, Liu PT, Chun RF, Lagishetty V, Gombart AF, Borregaard N, Modlin RL, Hewison M. Vitamin d-directed rheostatic regulation of monocyte antibacterial responses. **The Journal of Immunology**. 2009 Apr 1;182(7):4289-95.

173. Holick MF. Vitamin D: a D-Lightful health perspective. **Nutrition reviews**. 2008 Oct 1;66(suppl_2):S182-94.

174. Raulio S, Erlund I, Männistö S, Sarlio-Lähteenkorva S, Sundvall J, Tapanainen H, Vartiainen E, Virtanen SM. Successful nutrition policy: improvement of vitamin D intake and status in Finnish adults over the last decade. **The European Journal of Public Health**. 2017 Apr 1;27(2):268-73.

175. Norman AW, Bouillon R. Vitamin D nutritional policy needs a vision for the future. **Experimental Biology and Medicine**. 2010 Sep;235(9):1034-45.

176. Ogan D, Pritchett K. Vitamin D and the athlete: risks, recommendations, and benefits. **Nutrients**. 2013 Jun;5(6):1856-68.

177. Annweiler C, Karras SN, Anagnostis P, Beauchet O. Vitamin D supplements: a novel therapeutic approach for Alzheimer patients. **Frontiers in pharmacology**. 2014 Jan 28;5:6.

178. Emwas AH, Roy R, McKay RT, Tenori L, Saccenti E, Gowda G, Raftery D, Alahmari F, Jaremko L, Jaremko M, Wishart DS. NMR Spectroscopy for Metabolomics Research. **Metabolites**. 9 (7), 123.

179. Tian XQ, Chen TC, Lu ZH, Shao QI, Holick MF. Characterization of the translocation process of vitamin D3 from the skin into the circulation. **Endocrinology**. 1994 Aug 1;135(2):655-61.

180. Haddad JG, Matsuoka LY, Hollis BW, Hu YZ, Wortsman J. Human plasma transport of vitamin D after its endogenous synthesis. **The Journal of clinical investigation**. 1993 Jun 1;91(6):2552-5.

181. Wishart DS, Knox C, Guo AC, Eisner R, Young N, Gautam B, Hau DD, Psychogios N, Dong E, Bouatra S, Mandal R, Sinelnikov I, Xia J, Jia L, Cruz JA, Lim E, Sobsey CA, Shrivastava S, Huang P, Liu P, Fang L, Peng J, Fradette R, Cheng D, Tzur D, Clements M, Lewis A, De Souza A, Zuniga A, Dawe M, Xiong Y, Clive D, Greiner R, Nazyrova A, Shaykhutdinov R, Li L, Vogel HJ, Forsythe I: HMDB: a knowledgebase for the human metabolome. **Nucleic Acids Res**. 2009 Jan;37(Database issue):D603-10. doi: 10.1093/nar/gkn810. Epub 2008 Oct 25.

182. Knothe G, Kenar JA. Determination of the fatty acid profile by 1H-NMR spectroscopy. **European Journal of Lipid Science and Technology**. 2004 Feb;106(2):88-96.

183. Castañar L, Pérez-Trujillo M, Nolis P, Monteagudo E, Virgili A, Parella T. Enantiodifferentiation through frequency-selective pure-shift 1H Nuclear magnetic resonance spectroscopy. **ChemPhysChem**. 2014 Apr 4;15(5):854-7.

184. Kiraly, P., Kern, N., Plesniak, M..P., Nilsson, M., Procter, D..J., Morris, G..A. and Adams, R..W. Needles from haystacks: single-scan selective excitation of individual NMR signals in overlapping multiplets. **Angew**. **Chem. Int. Ed.** 2020

195. McAleer MA, Jakasa I, Raj N, O'Donnell CP, Lane ME, Rawlings AV, Voegeli R, McLean WH, Kezic S, Irvine AD. Early-life regional and temporal variation in filaggrin-derived natural moisturizing factor, filaggrin-processing enzyme activity, corneocyte phenotypes and plasmin activity: implications for atopic dermatitis. **British Journal of Dermatology**. 2018 Aug;179(2):431-41.

196. Raj N, Voegeli R, Rawlings AV, Doppler S, Imfeld D, Munday MR, Lane ME. A fundamental investigation into aspects of the physiology and biochemistry of the stratum corneum in

subjects with sensitive skin. **International journal of cosmetic science**. 2017 Feb;39(1):2-10.

197. Stejskal EO, Tanner JE. Spin diffusion measurements: spin echoes in the presence of a time-dependent field gradient. **The journal of chemical physics.** 1965 Jan 1;42(1):288-92.

198. Zhang T, Huang F, Li B, Huang C, Xu C, Lin K, Lin D. NMR-based metabolomic analysis for the effects of Huiyang Shengji extract on rat diabetic skin ulcers. **Journal of Ethnopharmacology**. 2020 May 19:112978.

199. Raj N, Voegeli R, Rawlings AV, Gibbons S, Munday MR, Summers B, Lane ME. Variation in stratum corneum protein content as a function of anatomical site and ethnic group. **International Journal of Cosmetic Science**. 2016 Jun;38(3):224-31.

200. Bonte F, Saunois A, Pinguet P, Meybeck A. Existence of a lipid gradient in the upper stratum corneum and its possible biological significance. **Archives of dermatological research**. 1997 Jan 1;289(2):78-82.

201. Verdier-Sévrain S, Bonté F. Skin hydration: a review on its molecular mechanisms. **Journal of cosmetic dermatology**. 2007 Jun;6(2):75-82.

202. Luo Q, Hong J, Xu H, Han S, Tan H, Wang Q, Tao J, Ma N, Cheng Y, Su H. Hygroscopicity of amino acids and their effect on the water uptake of ammonium sulfate in the mixed aerosol particles. **Science of The Total Environment**. 2020 May 11:139318.

203. Chan MN, Choi MY, Ng NL, Chan CK. Hygroscopicity of water-soluble organic compounds in atmospheric aerosols: Amino acids and biomass burning derived organic species. **Environmental science & technology.** 2005 Mar 15;39(6):1555-62.

204. Ono S, Yamauchi M. Glutamate and aspartate are decreased in the skin in amyotrophic lateral sclerosis. **Acta neurologica scandinavica**. 1992 Nov;86(5):481-4.

205. Nordlind K, Johansson O, Lidén S, Hökfelt T. Glutamate-and aspartate-like immunoreactivities in human normal and inflamed skin. **Virchows Archiv B**. 1993 Dec 1;64(1):75-82.

206. Wishart DS, Greiner R, Rosborough TA, Lefebvre BA, Epstein NA, Newton JB, Wong WR, inventors; Chenomx Inc, assignee. Automatic identification of compounds in a sample mixture by means of NMR spectroscopy. **United States patent US 7,191,069.** 2007 Mar 13.

207. Bonte F, Saunois A, Pinguet P, Meybeck A. Existence of a lipid gradient in the upper stratum corneum and its possible biological significance. **Archives of dermatological research**. 1997 Jan 1;289(2):78-82.

208. Verdier-Sévrain S, Bonté F. Skin hydration: a review on its molecular mechanisms. **Journal of cosmetic dermatology**. 2007 Jun;6(2):75-82.

209. Luo Q, Hong J, Xu H, Han S, Tan H, Wang Q, Tao J, Ma N, Cheng Y, Su H. Hygroscopicity of amino acids and their effect on the water uptake of ammonium sulfate in the mixed aerosol particles. **Science of The Total Environment**. 2020 May 11:139318.

210. Chan MN, Choi MY, Ng NL, Chan CK. Hygroscopicity of water-soluble organic compounds in atmospheric aerosols: Amino acids and biomass burning derived organic species. **Environmental science & technology**. 2005 Mar 15;39(6):1555-62.

211. Ono S, Yamauchi M. Glutamate and aspartate are decreased in the skin in amyotrophic lateral sclerosis. **Acta neurologica scandinavica**. 1992 Nov;86(5):481-4.

212. Nordlind K, Johansson O, Lidén S, Hökfelt T. Glutamate-and aspartate-like immunoreactivities in human normal and inflamed skin. **Virchows Archiv B.** 1993 Dec 1;64(1):75-82.

213. Evans R, Hernandez-Cid A, Dal Poggetto G, Vesty A, Haiber S, Morris GA, Nilsson M. Matrix-assisted diffusion-ordered NMR spectroscopy with an invisible matrix: a vanishing surfactant. **RSC advances**. 2017;7(1):449-52.

214. Dal Poggetto G, Castañar L, Adams RW, Morris GA, Nilsson M. Dissect and divide: putting NMR spectra of mixtures under the knife. **Journal of the American Chemical Society**. 2019 Mar 19;141(14):5766-71.

215. Sil BC, Moore DJ, Lane ME. Use of LC-MS analysis to elucidate by-products of niacinamide transformation following in vitro skin permeation studies. **International journal of cosmetic science.** 2018 Oct;40(5):525-9.

216. Tada M, Yokoi Y. Modification of pyridine-3-carboxamide (nicotinamide) by radical substitution. **Journal of heterocyclic chemistry**. 1989 Jan;26(1):45-8.

217. Koppes SA, Kemperman P, Van Tilburg I, Calkoen-Kwa F, Engebretsen KA, Puppels GJ, Caspers PJ, Kezic S. Determination of natural moisturizing factors in the skin: Raman microspectroscopy versus HPLC. **Biomarkers**. 2017 Aug 18;22(6):502-7.

218. Schoenberger T, Bundeskriminalamt Hibbert D, Le Gresley A, Adams K, Glossary of Methods and Terms used in Analytical Spectroscopy. **Analytics S.** 2019

219. Robertson C, Lucas RA, Le Gresley A. Scope and limitations of nuclear magnetic resonance techniques for characterisation and quantitation of vitamin D in complex mixtures. **Skin Research and Technology**. 2020 Jan;26(1):112-20.

Chapter 6 Appendix

6.1 Project introductions

Several projects were done during this research that were of consumer health research interest but out of the scope of the research story of this thesis. They are detailed here for reference purposes from main text when considering separate project idea and interesting research ideas that arose but were not fully accomplished by the author independently.

6.1.1 Squalene

A compound of interest is Squalene which is a skin surface lipid making up 15% of the sebum produced by the sebaceous gland. It has also been identified as having a key role in protection from oxygen radicals produced through photolysis of porphyrin by UVB and UVC after sun exposure. It has been suggested that oxidation followed by polymerisation of squalene occurs and could be a causative agent for comedone (black head) production through the encapsulation of keratin, when the polymers of squalene fill the sebaceous gland and prevent desquamation of cells on the outer layer of the *Stratum corneum*.

6.1.2 Antimicrobial peptides

Antimicrobial peptides are evolutionary conserved innate immune defensive compounds that were initially only thought to have bactericidal activity from initial discovery of lysozyme by Alexander Fleming. This perception has changed dramatically since this first AMP, with a more fitting name for antimicrobial peptides being defensins, such as the alpha and beta defensins present in mammalian cells.

AMPs have been shown to have several other key active roles apart from bactericidal activity involving several up-field pathways for wound healing, immune system activation e.g. inflammation, and vasculature development. Key indications of these roles are shown in the altered levels of antimicrobial peptides in dermatological pathologies. Specifically psoriasis, which can be used as a model of an inflammation environment and has been utilised to discover multiple AMPs: alpha, beta Defensin's; psoriasin; RNase 7. Research has also shown the importance of AMPs for

skin infection resistance and immune response through the targeted deletion of certain AMPs. One example of this was the use Metallopreotease-7-deficient mice where all alpha-defensins were deleted and showed reduced clearance of bacteria and significantly higher mortality rates upon pathogen challenge.

Antimicrobial peptides (AMP) are present in *Stratum corneum* secretions; their major role is in innate immunity, acting as inhibitors of microbial pathogens. This inhibition occurs because of the ability of the AMP to attach, align with and then insert into the microbial phospholipid bilayer. As this occurs, the peptide will form transmembrane pores that lead to the disruption and destabilization of the bacterial cell membrane, eventually leading to bacterial lysis. AMPs have been observed to preferentially target replicating bacteria at the site of division.

AMPs are well characterised by analytical techniques, including NMR. However, the quantitation of the structural and affinity information of AMPs by Saturation Transfer Difference (STD) has only just started to be explored, with Sivertson et al (1) demonstrating the use of STD NMR on AMPs. This project will look at the interaction of human AMPs with membrane models using quantitative STD NMR.

Alongside the detailed bactericidal activity of AMPs, it also serves several other roles in the innate immune system, wound healing and inflammation. These roles are mediated through the stimulus or inhibition of certain active compounds

6.1.3 Dermal and commercial formulation analysis

Elucidation of how these NMR methodologies can be exploited in studies of dermis based compounds apart from NMF will include investigation of squalene in light of its proposed role in comodonegenesis and the scope of ligand binding studies with non-isotopically enriched AMPs with model membranes at in-vivo concentrations.

6.2 Results

6.2.1 Application of NMR analysis to various compounds and formulation actives

In this chapter the use of NMR methodology for characterisation and quantitation of various dermis compounds, including squalene and the AMP cathelicidin (LL-37) is evaluated. Highlighting of Syn-Up is also done as a promising ingredient in dermatological treatments and evaluation of NMR's potential for its characterisation and quantitation in different real world topical formulations and how respective peaks can be shifted depending on formulation. Optimisation of STD-TOCSY is also achieved through parameter changes and the use of processing methodologies which allow for resolution and S/N gains though reduction of transients without loss of information using a model system of human serum albumin (HSA) and tryptophan.

6.2.1.1 Syn-Up

6.2.1.2 Assignment

The assignment of Syn-Up peaks was achieved with NMR mini-suite experiments 1D1H, 1H-1H COSY and 1H-13C HSQC. Using the multiplicity and J coupling constants of the peaks in relation to database and prediction software values, accurate assignment of each peak to an aromatic proton environment is achieved. This allowed peaks to be identified for quantitation of Syn-Up in different mixtures.

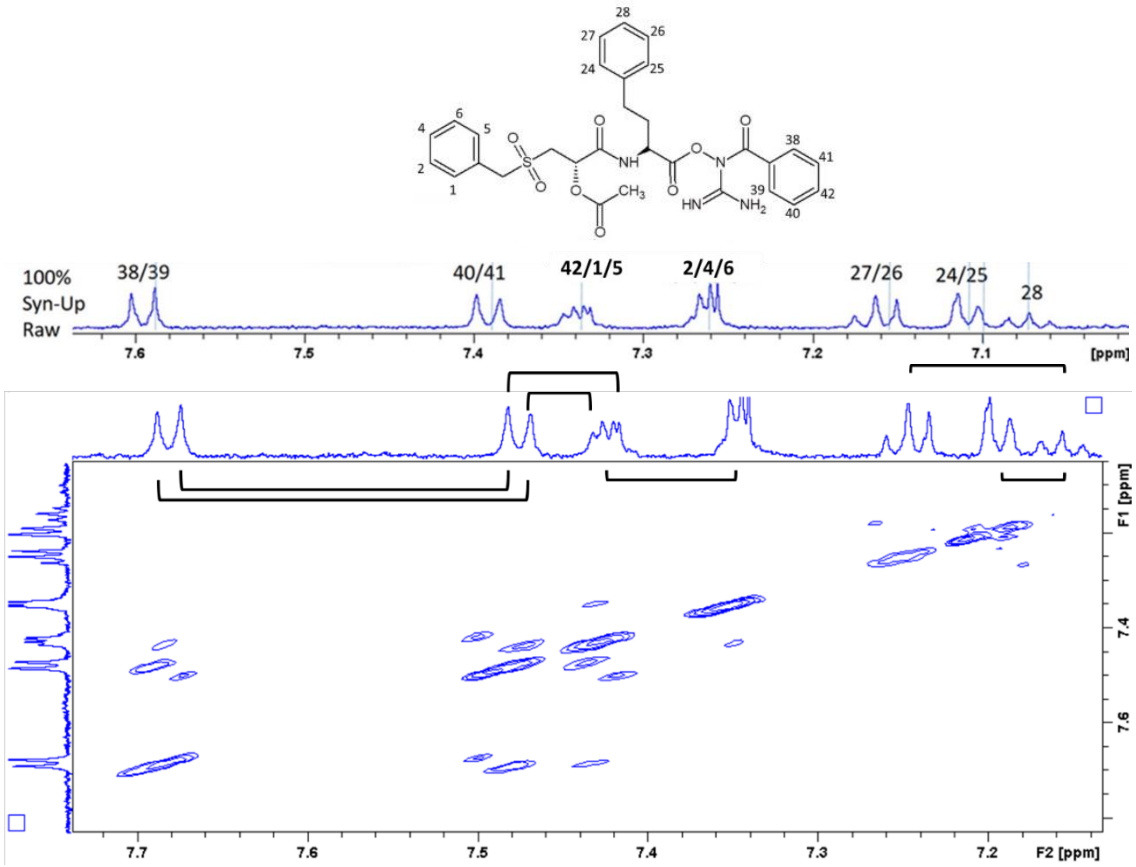

Figure 120 Assigned 1D1H spectra and 1H1H COSY spectra showing couplings for Syn-Up in 50-70% Glycerol

Aromatic peaks are the only peaks visible in the 50-70% glycerol sample as all peaks for the aliphatic protons are close to the peaks for glycerol and are thus overlapped.

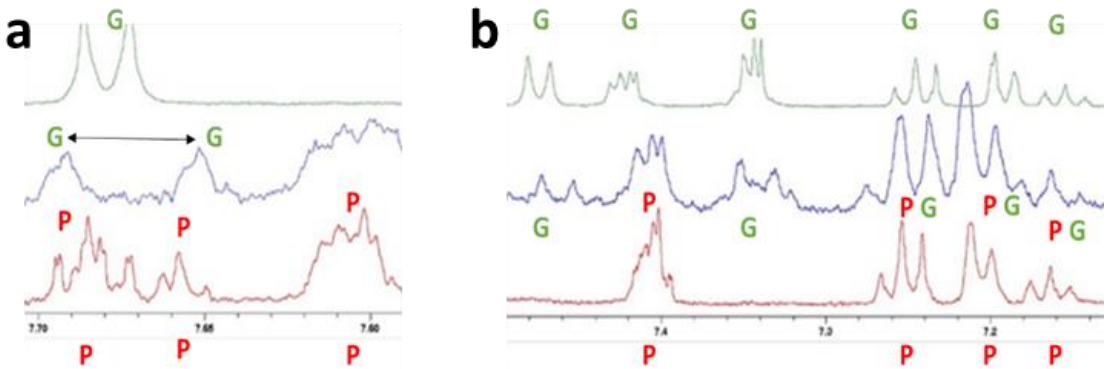

Figure 121 Syn-Up in glycerol(Green), Physiogel with 50% glycerol (blue) and Physiogel Spectra (red), Glycerol and Physiogel Syn-Up peaks labelled (G + P). a = zoomed in region of 7.6ppm to 7.7ppm; b = 7.15ppm to 7.5ppm

One aspect of the work that was interesting was that when the percentage of glycerol was made around 50-70% the peaks of Syn-Up shifted and line shape narrowed. However when glycerol is added to Physiogel to a percentage around 50-70% the peaks split into the peaks similar to those seen in glycerol at 50-70% in Syn-Up raw and Physiogel.

When identified in Physiogel (Fig 83) through sample mixing, peaks for 24-28 are the best for quantitation as they can be reliably identified from the reference spectra of Syn-Up, as peaks do not move or overlap with other peaks. A much greater S/N for these specific Syn-up peaks in most of the mixtures tested is observed which gives greater reliability of quantitation.

6.2.1.3 Quantitation

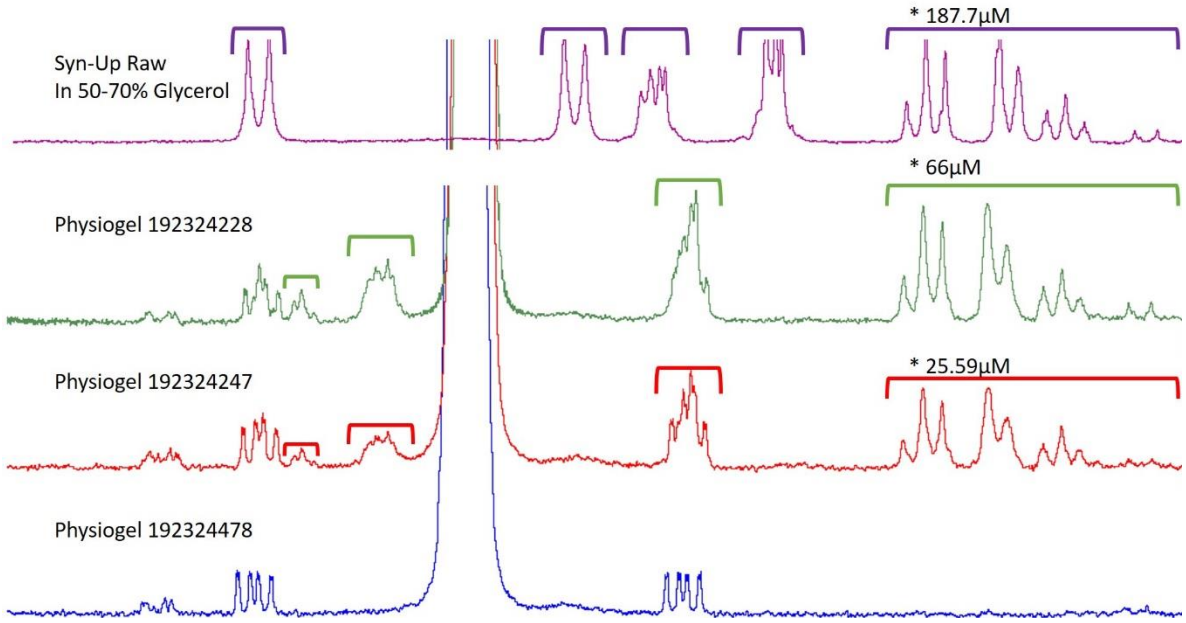

Figure 122 qNMR of Syn-Up in Glycerol, and different Physiogel batches 1-3, *Peaks used for quantitation as other peaks have overlap with Niacinamide peaks

From the qNMR of the different batches received it was determine that the 3 Physiogel samples have varying concentrations of Syn-Up present within the formulations. With Physiogel 192324228 having a concentration of 66µM, Physiogel 192324247 having 25.59µM and Physiogel 192324478 having no Syn-Up detected in the sample. A consistent difference is observed in the concentration of Syn-Up within the Syn-Up raw through the Physiogel samples, where the next dilute sample has [Syn-Up] = n-1[Syn-Up] / 3 as shown in figure 84.

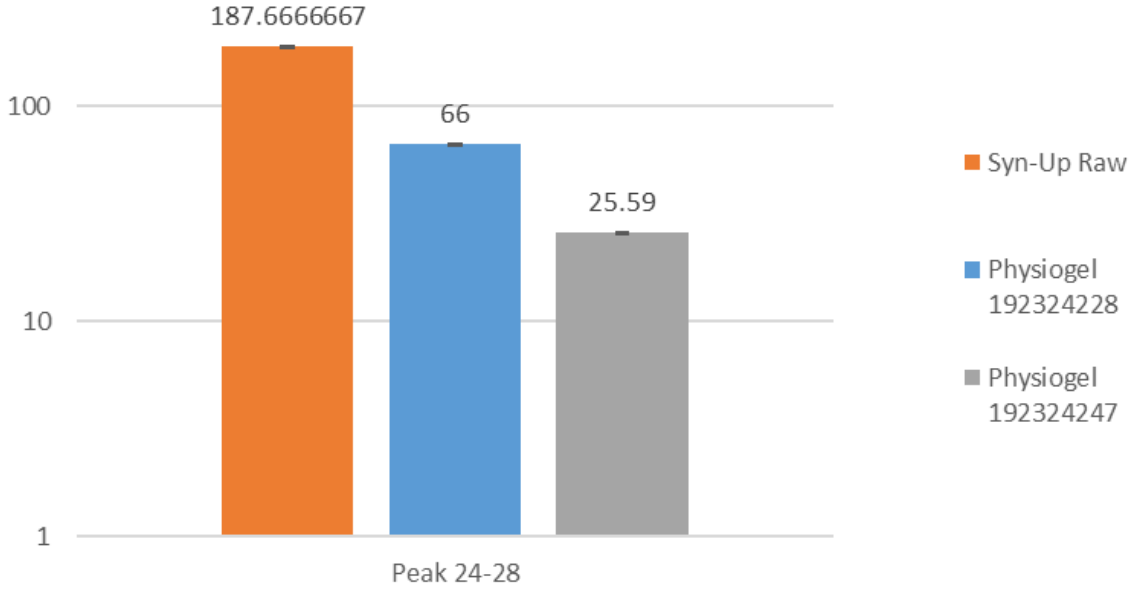

***Figure 123** Syn-Up Log concentration values for the samples*

6.2.2 AMP characterisation, deuterated DPC synthesis and STD TOCSY implementation and optimisation

NMR fragment-based drug discovery has been recognised as a widely applicable screening method (185). Lepre has reviewed the construction of a fragment library through development of NMR screening and what to do following a screen to improve drug discovery based upon the findings of the screens (186). Saturation based methodologies are a crucial element of screening with NMR through the effect of equalising the spin-state populations of nuclei under the influence of a static magnetic field (B_0). As the molecular weight of a protein increases, its correlation time t_c will become larger and spin diffusion becomes more efficient, this means that larger proteins and peptides sizes can be exploited to transfer magnetic saturation through efficient spin diffusion. The observed operational limit for studying protein-ligand interactions by STD-NMR is in the millimolar-to-nanomolar dissociation constant (kD) ranges. Additional experiments such as the Carr–Purcell Meiboom–Gill (CPMG) pulse sequence, provide a useful supplement to both STD NMR and WATERLOGSY approaches for drug discovery screening and interaction analysis. In STD pulse sequences, a spin lock is implemented which dramatically reduces the broad background protein signal to provide a relatively flat baseline which reduces effects on target drug peaks and also increases SNR. In standard proteins a spin lock of 30ms works well, however in protein studies where the molecular weight is over 100kDa a more suitable time is 10-20ms. Smaller molecular weight proteins inversely require longer spin lock times, with times up to 50ms being reported.

The calculation of STDamp which gives quantitative values for protein – ligand interaction depends on the below equation and also the stoichiometry and kinetics of binding between ligand and protein to determine ligand excess.

Equation 5

$$STDamp = \left(\frac{I - Io}{Io}\right) x\ Ligand\ Excess$$

Group Epitope Mapping (GEM) provides definitive information regarding ligand binding orientation. GEM was first applied in 2001 with the 120-kDa protein lectin Ricinus Communis Agglutinin I (RCA/20) and its binding relationship with saccharide ligands (187). 90 and 180 degree Hard pulses, cover essentially broadband width of chemical shifts; whereas the use of soft pulses, covers a small range of chemical shifts for targeted saturation of protein resonances which can prevent improper saturation of ligand peaks. Non-square wave pulses are designed for "soft" pulse applications to limit this unwanted excitation. Soft square pulses create irradiation sidebands in addition to the central excitation band which must be considered when placing the saturation pulses for STD. If the Gaussian pulse length is reduced from 50ms to 10ms, but the STD off/STDon position is maintained 7.7 times improvement in S/N is observed. Eburp2 with 50ms was selected as the S/N increase is useful but greater STDdiff data was observed with 50ms as its excitation profile prevented inappropriate excitation of ligand peaks which were otherwise excited with shorter Gaussian pulse lengths. A NOE difference experiment would ideally use a 50ms Gaussian pulse because the tip of the excitation profile is very narrow, the STD methodology was used for this project as it showed higher spectra quality. Saturation points were swept for detection of the safest on-resonance setting that did not distort relative intensities, but provides the most efficient saturation transfer, hence greatest S/N, and this point is shown in the 1D ^{1}H STD spectra for tryptophan. As the STDamp is saturation time dependent, data was acquired over a range of times and created the STD build-up curve for each resonance peak of tryptophan which demonstrated with our instrument and experimental set up that 4s gave the best spectral quality and a plateau SNR and STDamp.

Further analysis of data can allow for calculation of STD_{FIT} which gives a realistic measure of proximity for each ligand proton to respective protein and an improved measure on STD_{AMP} for GEM analysis. Calculation of these for the 1D ^{1}H STD experiments of tryptophan and HSA however for the acquisition of STD TOCSY experiments this was not done as acquisition of 5 different time experiments was very time consuming and also showed breakdown changes for compounds investigated in the >6 hours required for all experiments acquired on our instrumentation. Calculation of STD_{FIT} is illustrated in the below equations.

Equation 6

$$STD_{amp} = STD_{ampmax}(1 - e^{-kSTDt})$$

$$STD_{FIT} = k_{STD} * STD_{max}$$

STD_{max} and K_{STD} define the plateau of STD_{amp} and the STD rate constant, these can be used to obtain the slope for each curve when saturation is zero (STD_{zero})The relative STD_{FIT} is therefore, a realistic measure of the proximity of each ligand proton to the protein and an improved measure of STD_{data} for GEM analysis. Limitations of STD experiments however is that when directly correlating dissociation constants, there is no discrimination observed between specific and non-specific ligand binding. For this study 1.5mM of ligand is needed astransfer to STD-TOCSY requires the largest S/N possible in regards to experiment time and number of transients.

The use of a 2D ^{1}H STD experiment, STD-TOCSY is introduced which is an additional route into determining the bound conformation of ligands through increased resolution of more complex ligands and their interaction to respective proteins. Data from STD-TOCSY experiments highlights changes in the relative TOCSY cross peak resonances which demonstrate how coupling changes between protons which is in proximity to saturated ligand and can be used to detect proximity of amino acids of respective larger peptides and proteins to saturated target through differences seen for the fingerprint region of NH cross peaks seen in the TOCSY spectra of our selected peptides.

When acquiring the STD-TOCSY spectra a lower F1 resolution and 32 points of linear prediction to circumvent this lower F1 resolution was used. It is also demonstrated how covariance processing can be done to not only increase resolution greatly but allows for even lower F1 transients to be acquired. These processing methodologies are implemented to reduce the experiment time which

is substantially longer with the addition of the STD steps to the 2D acquisition as two 2D spectra are acquired and calculation of small differences seen between them where increasing the S/N is so important to avoid low abundance peaks being below the LOD. STD-TOCSY data analysis also requires the standard TOCSY spectrum to be acquired for calculation of STD_{amp} as the current STD-TOCSY experiment is a difference only acquisition as the STDon and STDoff are subtracted via phase cycling with the data processed and only STDdiff spectrum being produced. A 1D ^{1}H STDdiff spectrum is acquired first and then optimised settings are evaluated and transferred to the 2D STD experiments for the STD components of the STD-TOCSY pulse sequence. The 2D components of the pulse sequence are the same as that of a conventional Mlev TOCSY acquisition; however the experiment is acquired increased scan number and fewer f1 points due to exploitation of linear prediction and covariance processing methods. Additional experiments that should be run in the future would be 2D NOESY, STD-NOESY and STD-HSQC alongside already acquired NOESY, HSQC, TOCSY and STD-TOCSY. However with the non-isotopically enriched peptide being investigated as a ligand rather than a saturation target during this study ways to speed up 2D STD experiments were evaluated with how reliable these methods are compared to each other. Methods for this speeding up of acquisition include NUS, covariance processing, and parameter optimization.

6.2.2.1 Saturation transfer difference results

6.2.2.1.1 STDamp factor enhancement

Calibration of the on resonance pulses for protein saturation and transferred magnetisation to ligand increases is achieved by the placement of saturation shown below but enhancement of STDamp can be achieved through increasing saturation time until a STDmax is reached which prevents experimental time loss but also have the best spectral quality.

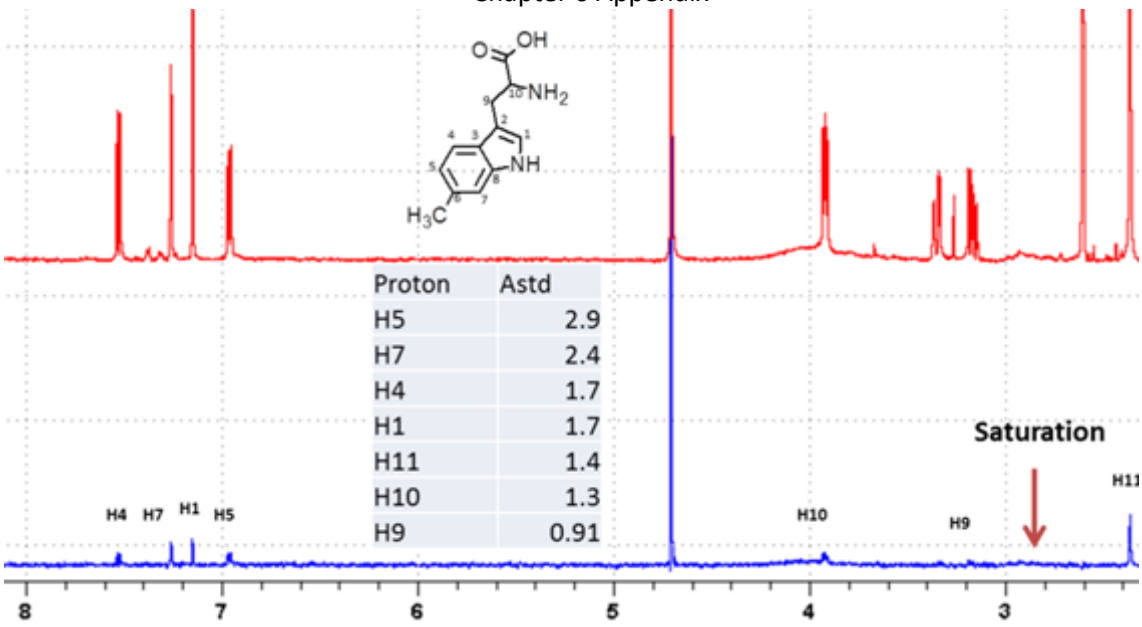

Figure 124 HSA, 7-methyl Tryptophan STD reference spectra (red) and STD spectra (Blue) with calculated Astd values for each respective proton which demonstrates saturation transfer

Before acquiring STD-TOCSY spectra, acquisition of a TOCSY spectra for reference and also investigating how much resolution is effected through implementation of covariance processing which can afford with only 16 transients set in the indirect dimension compared to the 128 transients set in the non-covariance processed spectra.

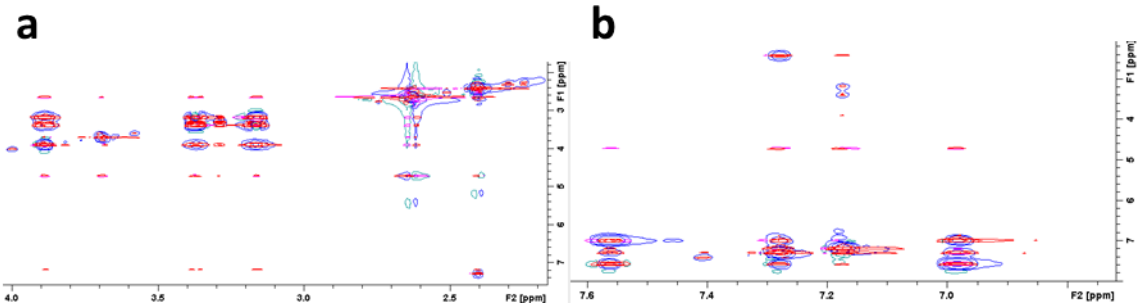

Figure 125 Red = Covariance processed TOCSY (16 F1 TD) (red) and the non-covariance processed TOCSY (128 TD in F1 with zero filling to 1024 SI) (blue). a = zoomed in region from 2.2ppm to 4ppm; b = zoomed in region from 6.8ppm to 7.6ppm

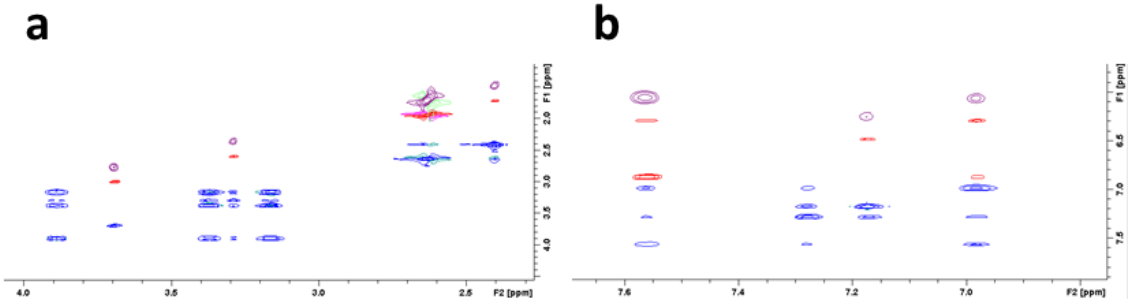

Figure 126 Purple = non-covariance processed STD-TOCSY, Red = Covariance processed STD-TOCSY with added scans at same time scale with reduced transients in F1, Blue = TOCSY with covariance processed spectra with reduced F1 transients. a = zoomed in region from 2.3ppm to 4ppm; b = zoomed in region from6.8ppm to 7.6ppm

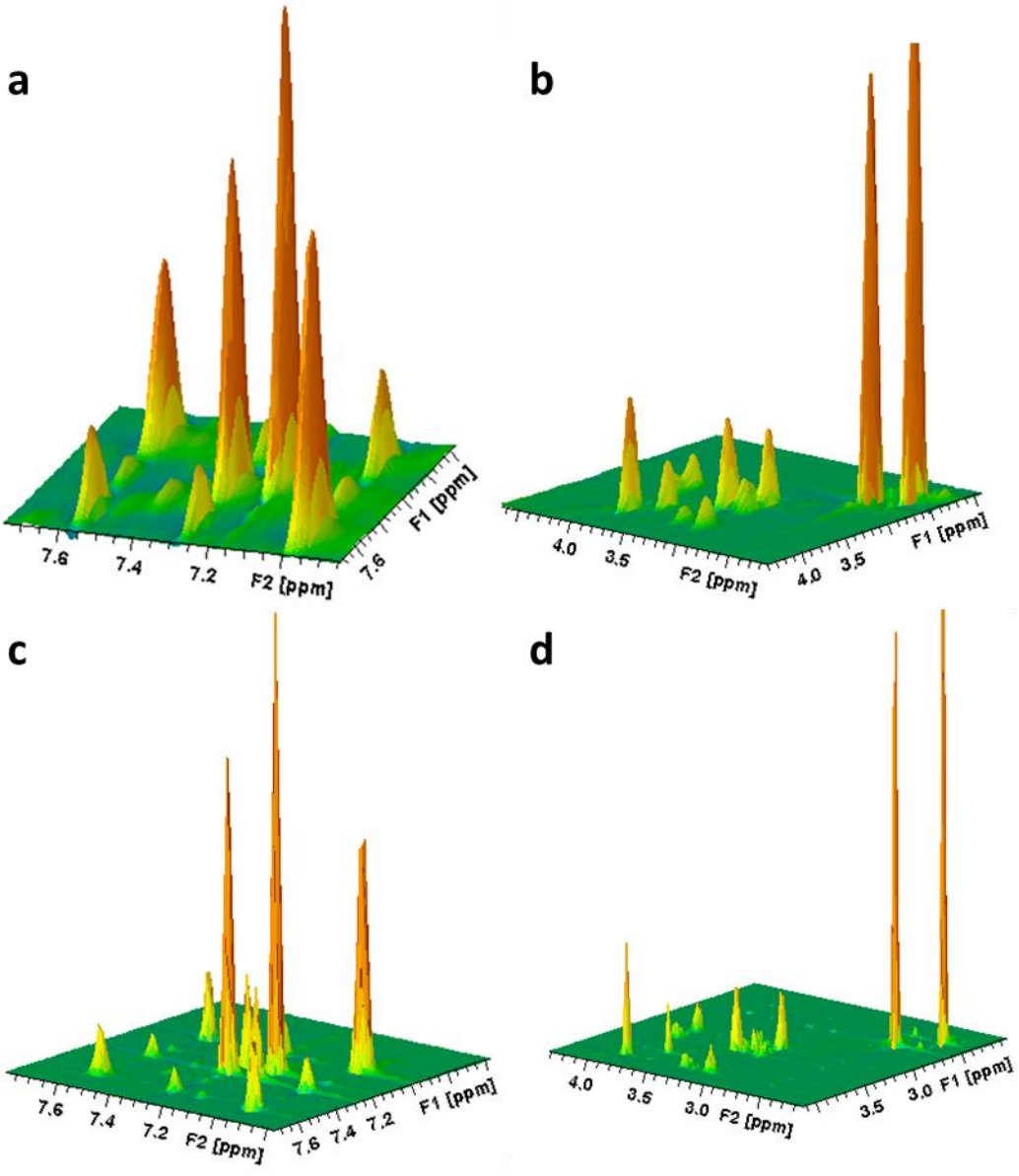

Figure 127 Comparison of covariance processed TOCSY spectra (a+ b) versus non covariance processed TOCSY spectra (c + d)

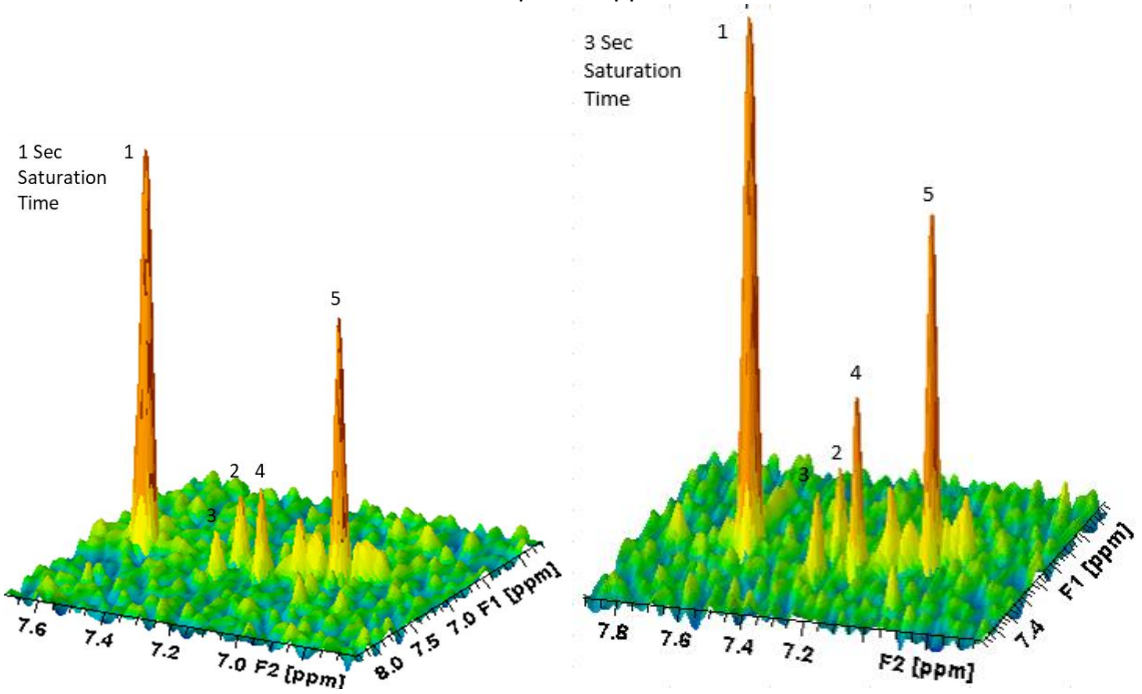

Figure 128 Comparison of TOCSY spectra with varying saturation pulse time

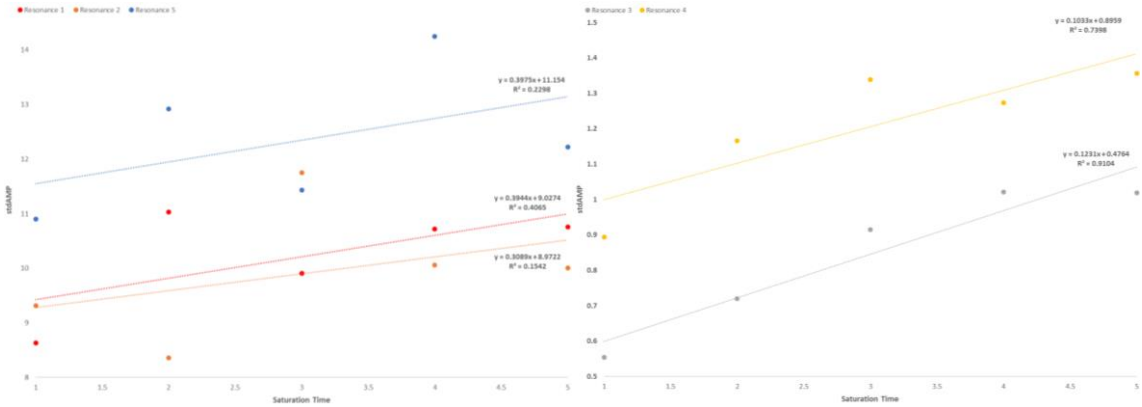

Figure 129 Saturation time vs stdAMP values

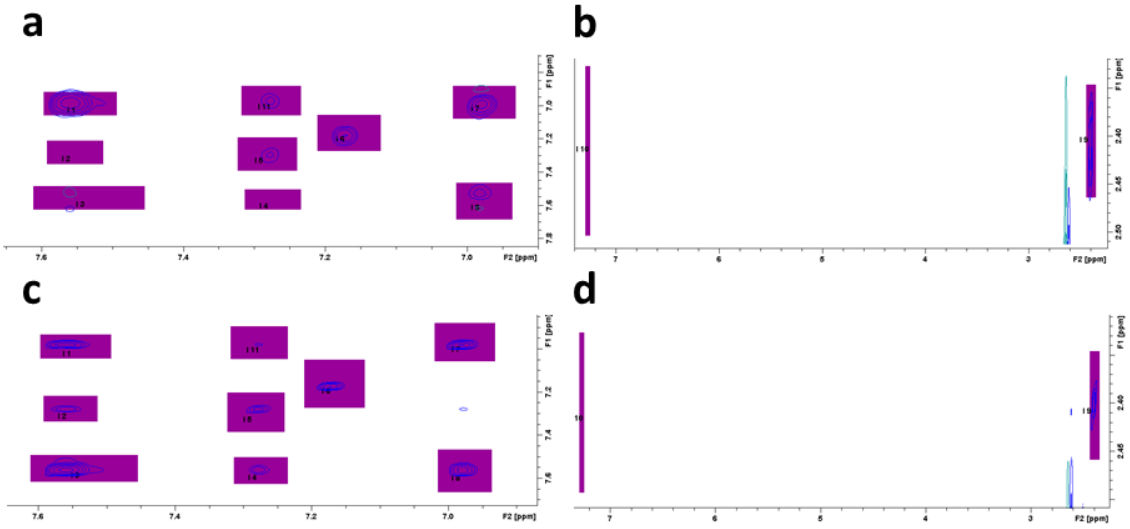

Figure 130 Non covariance processed STD-TOCSY (a + b) and Covariance Processed STD TOCSY (c + d) spectra with numbered peaks

Table 25 Integrals for STD TOCSY and STD TOCSY Covariance processed peaks and rankings

Cross Peak	STD TOCSY	STD TOCSY Cov
1	21.03	43.65
2	9.97	35.03
3	5.16	108.76
4	0.24	38.70
5	0.88	3.35
6	1.91	5.16
7	15.51	5.44
8	0.81	48.02
9	0.53	0.83
10	0.76	2.48
11	12.16	1.39

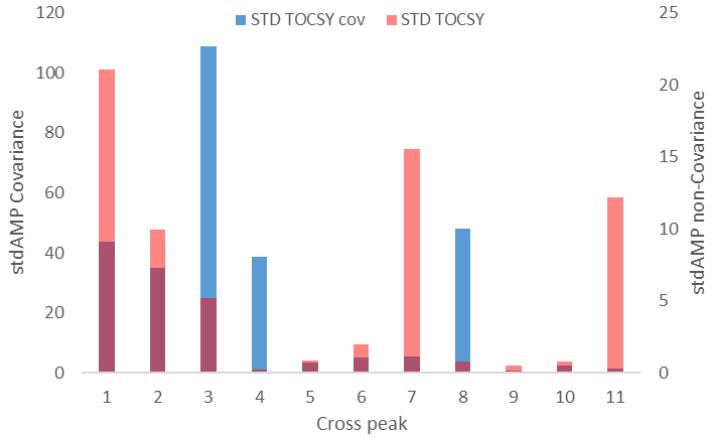

Figure 131 Comparative calculated stdAMP for STD TOCSY and covariance processed STD TOCSY

Non-Cov ranking	Cov ranking
1	3
7	*8
11	1
2	*4
3	2
6	7
5	6
8	5
10	10
9	11
4	9

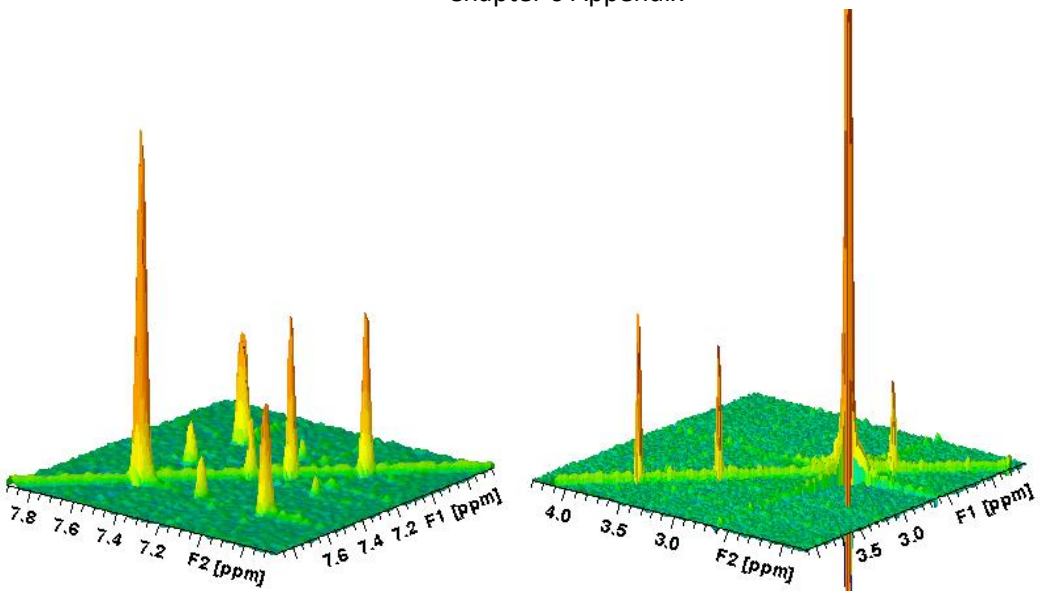

Figure 132 3D Contour representation of covariance processed STD tocsy spectra shwing the relative intensitry of cross peaks

After implementation of STD-TOCSY and demonstration of how optimisation gives results for qualitative analysis of GEM, the synthetic routes for deuterated dodecylphosphocholine (DPC) was evaluated through initial synthesis of DPC followed by deuterium/hydrogen exchange. This synthetic work would then lead to subsequent micellation and STD-TOCSY analysis for LL-37 binding studies to micellised deuterated DPC.

6.2.2.1.2 Synthesis of DPC

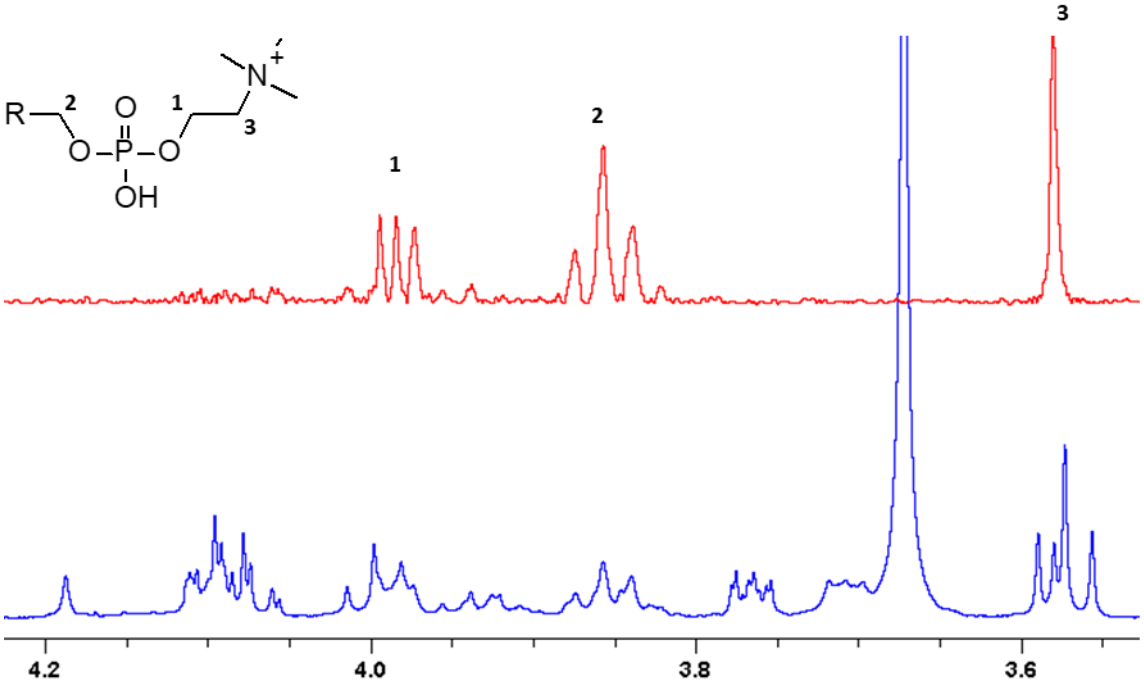

Figure 133 Dodecyl Phosphocholine ^{31}P HMQC projection (Red) and total positive projection of all ^{31}P HMQC ^{1}H peaks

Peak 3 has a splitting error, believe this is from the intensity of overlapping peaks in this area.

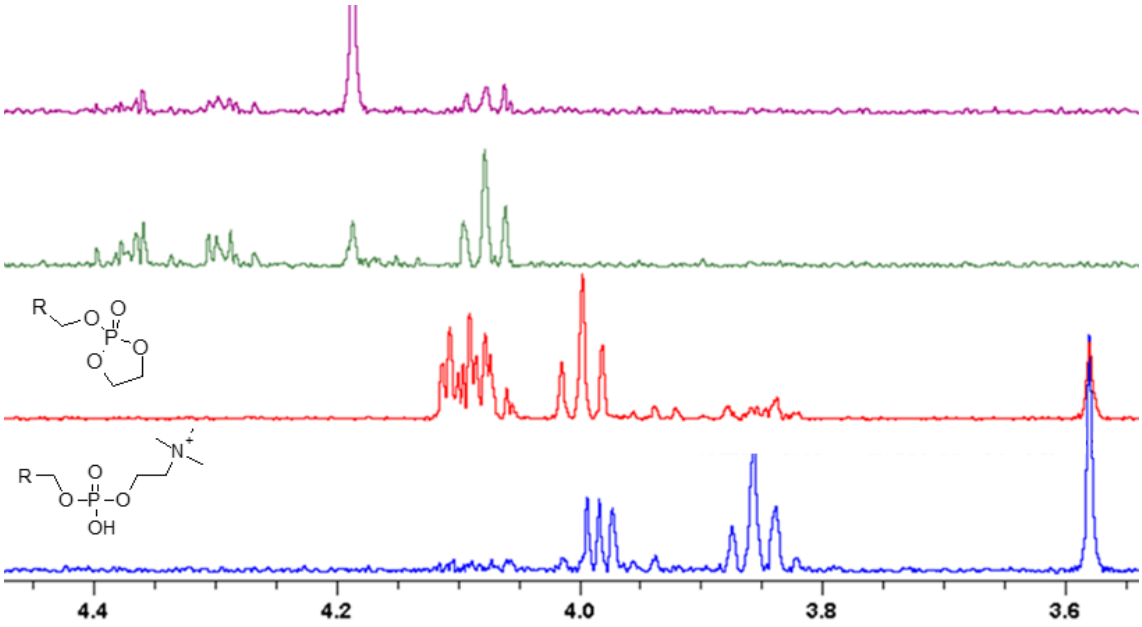

Figure 134 Comparison of 1H projections from 31P-1H HMQC spectra

The spectra of the starting material for the trimethylamine addition step is around two times the concentration of the final DPC product as shown by the scaling of peaks, this is not quantifiably reliable but gives an indication that the reaction did not go to completion.

This could be because of the reaction temperature being too low during parts of the experiments. This would require a longer experiment time for completion of the reaction. There is also a limiting factor in the trimethylamine diluted in ethanol, which means less trimethylamine is available for the ring breaking and substitution on the phosphine synthon.

6.2.2.1.3 Lauric Acid deuteration

After successful synthesis of DPC from lauric acid, phosphoryl chloride and trimethylamine as starting materials, evaluation of deuteration protocols for lauric acid deuteration was done as previous studies have demonstrated H/D exchange in fatty acids of varying aliphatic chain lengths to differing degrees with varying reaction conditions.

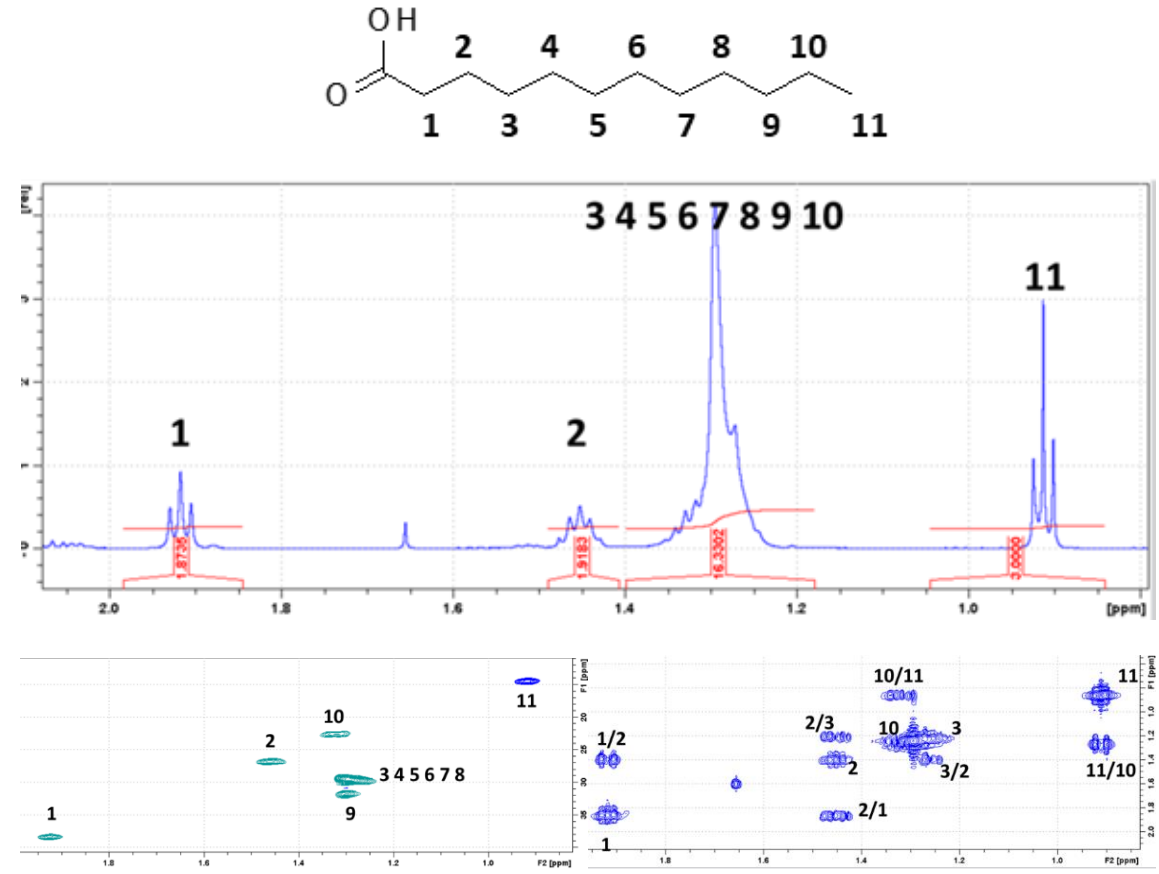

Figure 135 Assignment of Lauric acid

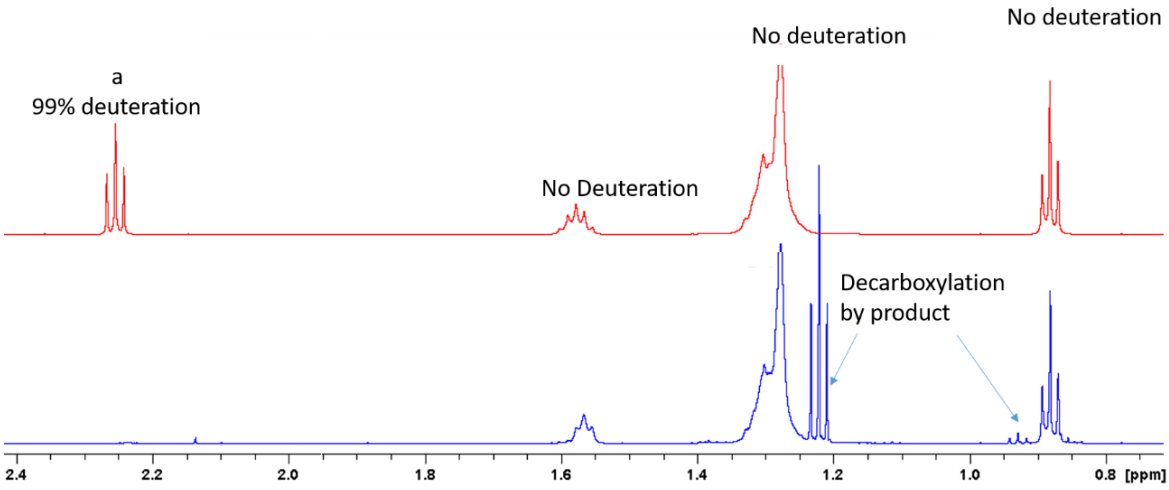

Figure 136 Spectra of non-deuterated lauric acid (red) and experiment 1 (blue)

Table 26 Deuteration %'s for experiments 1, 2 and 3

Chemical shift	LA_D1 (%D)	LA_D2 (%D)	LA_D3 (%D)
0.8ppm	0	84	70
1.25ppm	0	82	50

1.55ppm	0	82	50
2.24ppm	99	83	70

6.2.2.2 LL-37 assignment

Since our cathelicidin (LL-37) was not isotopically enriched in N15 and C13 which would increase S/N for 2D spectra automatic assignment and structure characterisation software predominantly used in drug discovery fragment analysis was not possible as this would require 2D NOESY, 2D COSY, 2D TOCSY, 2D HSQC and 2D HMBC experiments to be acquired for proper amino acid numbering assignment and dihedral angle determination between amino acid. These acquisitions would require experiment times beyond the scope of our instrumentation and sample concentrations due to solubility of materials. However investigation of the scope of our instrumentation and determination of methods which can be used to improve spectral quality can be done. Spectral quality for peptides can then be reviewed by looking at the fingerprint region, where the number of backbone NH's should roughly match the number of non-proline residues. Spin-system-identification is found at the spectral region: NH-αH-βH (TOCSY: F2 = 6.5-12ppm; F1 = 0-5ppm). Alongside the sequence specific assignment using the fingerprint region of COSY/TOCSY and NOESY in multiple display.

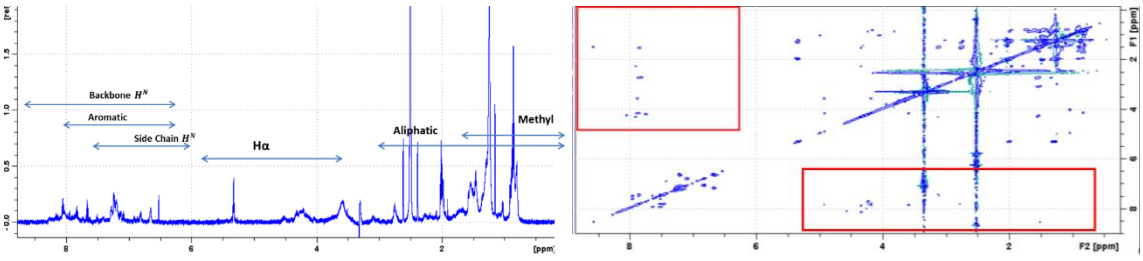

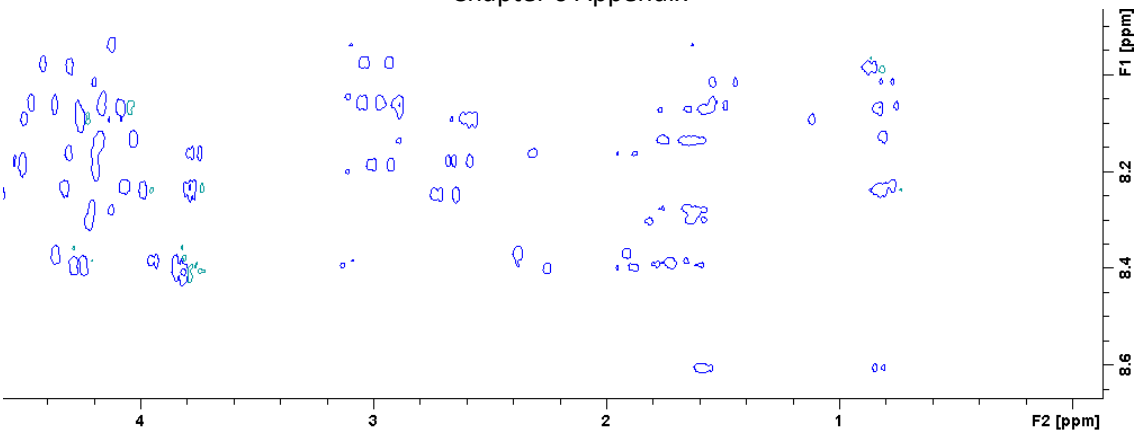

Figure 137 Region assigned 1D 1H Spectra, TOCSY with fingerprint regions highlighted and zoomed in fingerprint region of covariance processed LL-37 TOCSY highlighting cross peaks associated with amino acids.

Table 27 Amino Acid Reference table for LL-37 AA assignment

AA	NH	α	β	Others
Gly	8.39	3.97		
Val	8.44	4.18	2.13	γCH3 0.97, 0.94
Ile	8.19	4.23	1.9	γCH2 1.48, 1.19
				γCH3 0.95
				δCH3 0.89
Leu	8.42	4.38	1.65,1.65	γH 1.64
				δCH3 0.94, 0.90
Pro		4.44	2.28,2.02	γCH2 2.03, 2.03
				δCH2 3.68, 3.65
Ser	8.38	4.5	3.88,3.88	
Thr	8.24	4.35	4.22	γCH3 1.23
Glu	8.37	4.29	2.09,1.97	γCH2 2.31, 2.28
Lys	8.41	4.36	1.85,1.76	γCH2 1.45, 1.45
				δCH2 1.70, 1.70
				εCH2 3.02, 3.02
				εNH3 7.52
Arg`	8.27	4.38	1.89, 1.79	γCH2 1.70, 1.70
				δCH2 3.32, 3.32
				NH 7.17, 6.62
Asn	8.75	4.75	2.83, 2.75	γNH2 7.59, 6.91
Gln	8.41	4.37	2.13, 2.01	γCH2 2.38, 2.38
				δNH2 6.87, 7.59
Phe	8.23	4.66	3.22, 2.99	2,6H 7.30
				3,5H 7.39
				4H 7.34

Table 28 27 out of 37 assigned amino acids for LL-37

AA	F2 (ppm)	F1 (ppm)
Lys	4.097	7.9253

Leu	4.278	8.599
Leu	3.972	8.225
Leu	4.021	8.12
Leu	4.067	8.6601
Ser	4.0521	8.22
Ser	4.29	8.15
Phe	4.408	7.965
Phe	4.494	8.176
Lys	4.146	8.035
Lys	4.179	8.12
Lys	3.837	8.3731
Lys	3.801	8.3862
Arg	4.11	7.929
Arg	4.148	8.0426
Arg	4.177	8.193
Arg	4.273	8.3894
Val	4.288	7.975
Val	4.3	8.2239
Thr	4.242	8.082
Glu	4.2571	8.0611
Iso	4.109	8.2715
Iso	4.156	8.1288
Iso	4.2421	8.0625
Asn	4.575	8.241
Phe	4.458	8.0521
Pro	3.9161	8.3741

The following sequence is shown with proposed amino acids that are not detectable in spectra due to overlap and low SNR; *LLGDFFRKSKEKIGKEFKRIVQRIKDFLRNLVPRTES.* Assignment of 27 out of 37 amino acids was possible and highlighted in red the amino acids that were unable to be assigned in this research. Further assignment would require enriched peptide or a higher magnetic power instrumentation but this shows the scope of characterisation of small peptide fragments with the instrumentation and a non-enriched peptide. Therefore it was decided to test with these assignments whether transfer of saturation could be seen to the amino acids that were assigned. Interestingly all amino acids that could not be identified were part of the alpha helix structure so this may limit this research however it also may give reasons as to why assignment failed through overlap of peaks rather than low sensitivity.

6.2.2.2.1 Ligand Binding limitations encountered

Despite experimental optimization of STD-TOCSY done previously saturation transfer from deuterated DPC to LL-37 was not observed. This was interpreted to be because of no active spins allowing for spin diffusion throughout the DPC micelle, therefore preventing NOEs from taking place between LL-37 and deuterated DPC. Partially deuterated DPC could be an alternative however again it would need to be tested to see if saturation transfer was large enough to transfer through NOEs from DPC micelles to LL-37. Non-deuterated DPC is inappropriate as it does not form large enough micelles to reduce T2 time enough to broaden its respective peaks so this ends up with overlap of lower abundance LL-37 peaks. Further investigation of the use of STD-TOCSY for LL-37 and other AMP interaction analysis would require different models of bacterial membranes or viable membranes prepared in PBS buffer to give LL-37 interaction analysis and GEM, rather than structural analysis previously shown with LL-37 and DPC micelles.

6.2.3 Squalene project

6.2.3.1 Background

Comedonegenesis and premature skin ageing are two of the most common dermatological conditions that are diagnosed on non-dermatologically pathogenic individuals. Both of these conditions have been linked to compositional changes and production rate of the sebum(188)(189). For this study investigation of how one of the components of sebum; Squalene, is affected by temperature induced free radical reactions and photochemical induced reactions; which allows to model the effects of sun damage on the skin.

Squalene was chosen as it has been identified as an oxygen radical quencher by conversion to squalene epoxide. Squalene epoxides have been shown to induce comedogenesis (190).

Comedones result from abnormalities in the proliferation and differentiation of ductal keratinocytes[4]. Abnormalities in sebaceous gland lipid composition have been implicated in the induction of ductal keratinocyte hyperproliferation leading to comeodogenesis (191).

An increase in fatty free acids and squalene has been blamed for inducing comedones. It has been shown that squalene peroxides are highly comeodogenic whereas squalene itself is not[3]. Squalene peroxides are seen to be formed from UVA irradiation and identified as highly UVA sensitive SSL breakdown products (192).

Suggestions of Squalene epoxides role in the accumulation of keratin in comedone affected pilosebaceous units (193). Squalene is a skin surface lipid which makes up 15% of the sebum produced by the sebaceous gland. It has also been identified as having a key role in protection from oxygen radicals produced through photolysis of porphyrin by UVB and UVC from sun exposure (194).

The proposed mechanism for comeodonegenesis is polymerization of squalene, alongside the demonstrated peroxidation that occurs when this event takes place. This process can be a causative agent for comedone (black head) production through the encapsulation of keratin when the polymers of squalene fill the sebaceous gland.

For this work a model system of sebum shall be produced with squalene, free radical initiators and a stable solvent system. This model system shall be exposed to varying amounts of UVC radiation to determine the amount of irradiation required to produce polymerization; alongside or in the absence of oxygenation. These experiments will contribute to the knowledge of comedone prevention, through analysis of the degree of polymerization, polydispersity of squalene polymers, alongside understanding the limits of polymerization in our model.

Preliminary experiments were done with a known mechanism for free radical initiation with temperature set to the breakdown temperatures of Initiators AIBN and BP (Reflux condensation reaction in Toluene done). Photochemical experiments with UVC irradiation of free radicals were then implemented to commence initiation of free radical polymerization between initiator and monomer. This was done in the presence of oxygen and also in an oxygen free environment with nitrogen flowing over it. The Solvent toluene was removed for the oxygen excluded experiments

because of its known absorbance of UVC which would could prevent break down and initiation of free radicals. Photochemical experiments are a better model for skin surface lipid interactions and composition studies as it allows the exposure time of UVC to be based upon a relative time in the sun.

Rampant free Radicals: AIBN; Benzoyl Peroxide are used to make polymers from vinyl monomers (small molecules containing carbon – carbon double bonds).The carbon – carbon double bond in a vinyl monomer, has a pair of electrons which is very easily attacked by the free radical. As a model for the production of free radicals in the skin; since the effects of reactive oxygen species (ROS) on squalene has been shown in in previous literature this investigation will determine the effects of other free radicals on skin surface lipids and whether it is possible that the application of skin creams, or bacterial processes may have an effect on the composition of the sebum on the skin.

Intensity of sun that reaches Earth is very low relative to the power of the UVC bulb used for photo induction experiments to compare the relative effects of these two phenomena. The sun has a power of 1360 watts per square meter whereas a 8.14 eV 254nM UVC bulb is used which sees the effects of a long exposure to the sun in a short period of time for our investigation.

6.2.3.2 Results

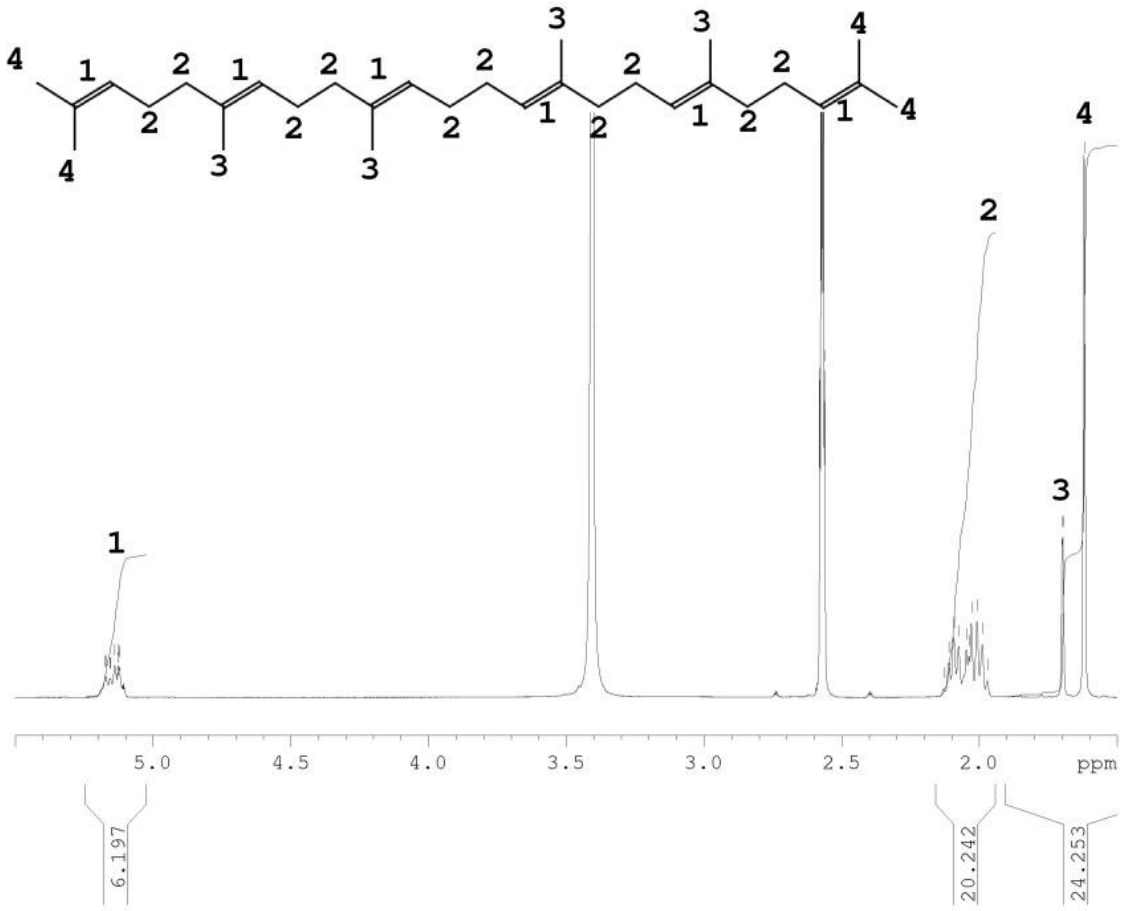

Figure 138 1D NMR spectra showing characterisation of Squalene 0.5% w/w; 256 scans, and same squalene concentration as polymerization experiment samples

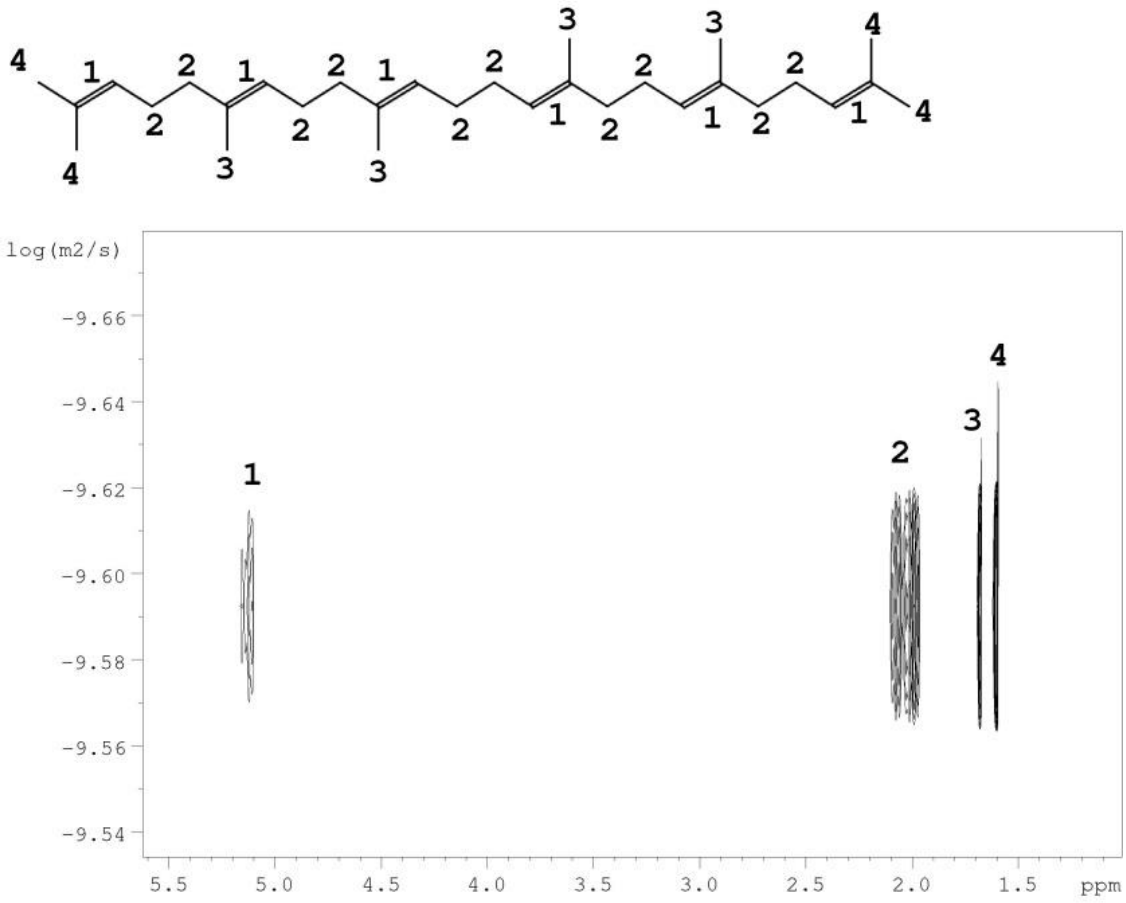

Figure 139 DOSY Spectra characterising relevant cross peaks of squalene and its respective diffusion coefficient

6.2.3.2.1 Experiment 1; Temperature induced initiation of free radicals

In our first experiment decomposition of AIBN and Benzoyl Peroxide to free radicals is achieved thermal decomposition by setting the temperature of the reaction mixtures above that of their half-life at 10 hours; 65 degrees Celsius for AIBN in toluene and 70 degrees Celsius for Benzoyl Peroxide in benzene. 85°C for AIBN and 90°C for Benzoyl Peroxide was used for initiation of free radicals. Below their melting point's; but high enough to allow for the majority of the initiator to be decomposed to their respective free radicals.

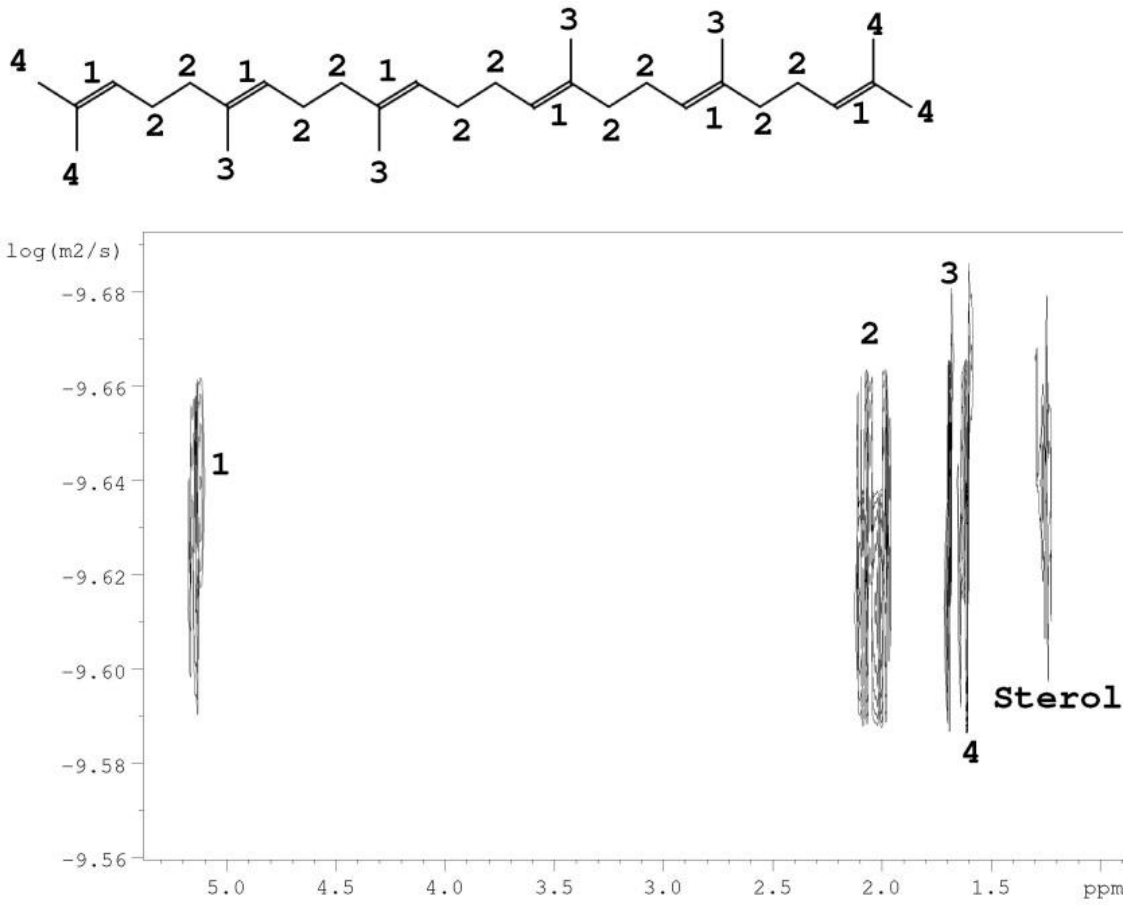

Figure 140 Benzoyl Peroxide/Squalene sample, post polymerization (3 Days) time 11.

Sterol cross peaks formed which demonstrates the intramolecular reduction cascade occurring from free radical initiation but no polymerization reaction as expected.

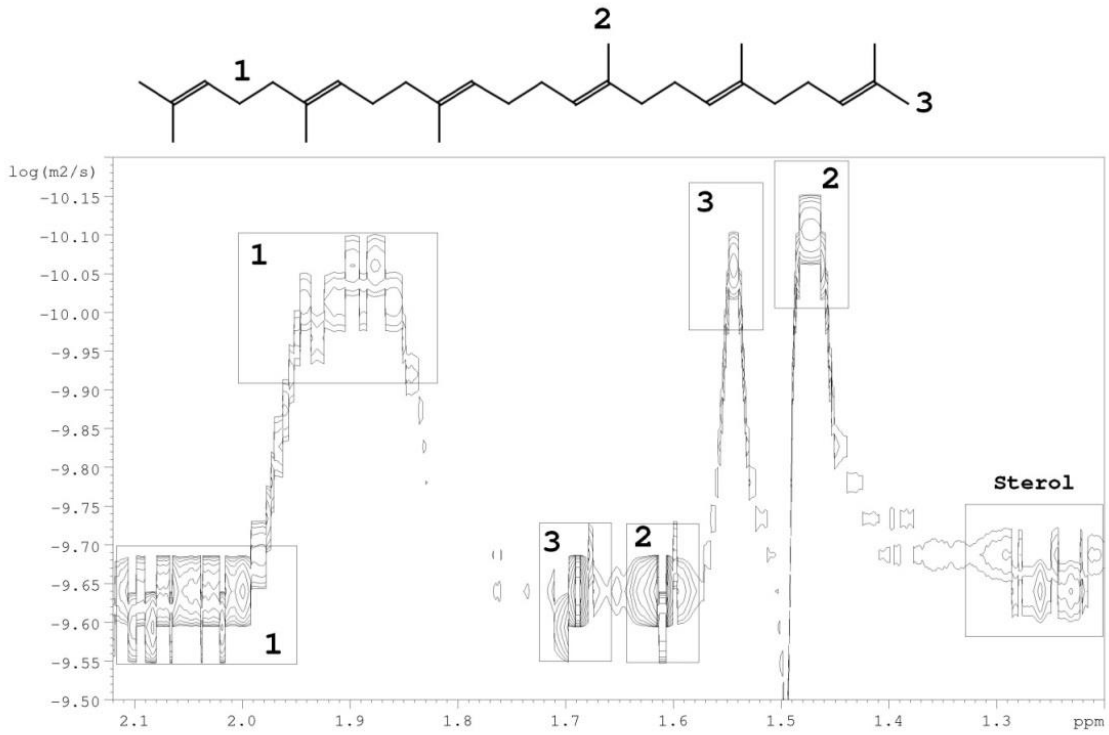

Figure 141 AIBN/Squalene time 13 (3 days), post polymerization

AIBN initiated reaction shows polymerization has occurred to the point of a trimer, as shown in table 15. Like that of Benzoyl Peroxide, the Intramolecular reduction cascade occurs to form a peak characteristic of a sterol. DOSY spectra shows that there are three possible intermediates formed.

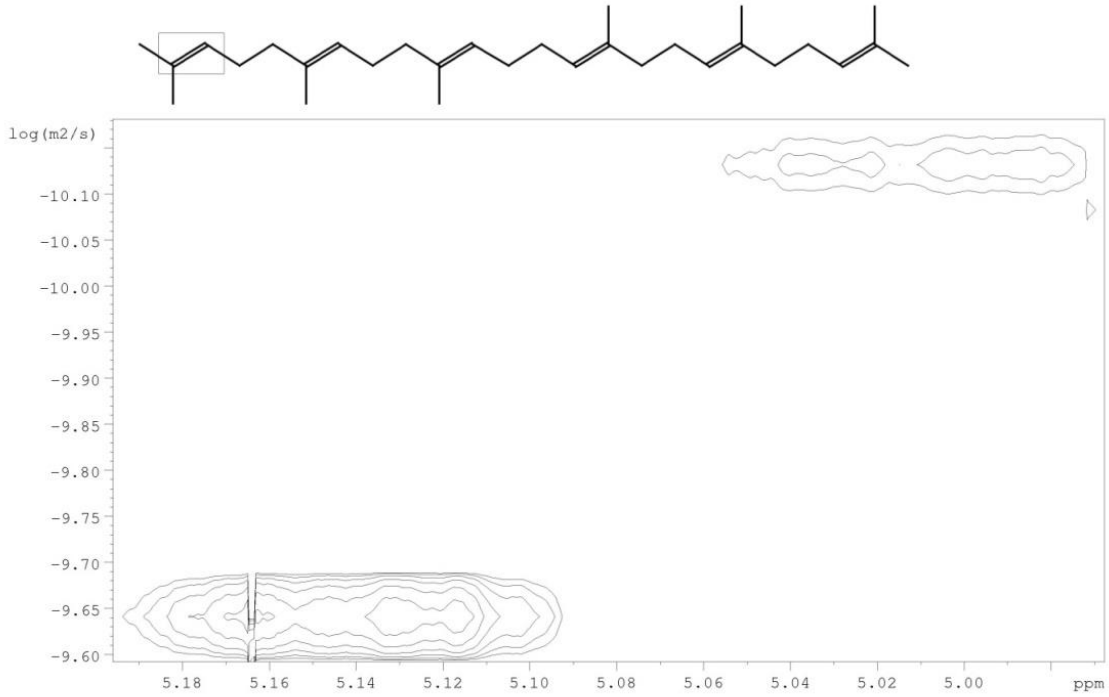

Figure 142 AIBN/Squalene Time 13, covering alkene peaks

Alkene groups have reduced in intensity for the trimer cross peak, suggestive of free radical polymerization varying across the different olefin groups as intensity is not consistent across the cross peak like that of squalene

6.2.3.2.2 Experiment 2; Photo induction, 50mM initiator, in Toluene, in the presence of oxygen

Comparison of Photo-chemical induction of the free radical initiation of squalene polymerization through the decomposition of AIBN and Benzoyl Peroxide to free radicals to thermal decomposition results will demonstrate whether a model system of the sun can illicit the same response as a classical thermal decomposition of free radical initiators.

It has been shown that photochemical decomposition applies a lot more energy for bond breaking than thermal decomposition so it was hoped that this would allow for a faster transformation of squalene to a polymer form.

Samples were made up in toluene so that UVC irradiation would be incident upon a 15% squalene sample; with 50mM of the initiator (AIBN or Benzoyl Peroxide).

Several control experiments were run as well to make sure what was observed was not a decomposition or spontaneous effect of the squalene being exposed to UVC irradiation.

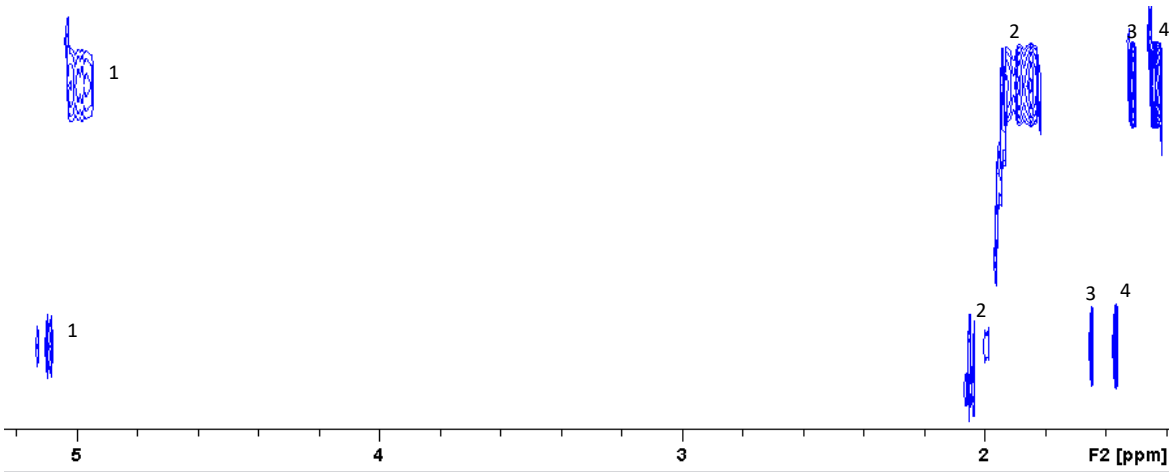

Figure 143 Lines showing squalene peaks at -9.55 log(m²/s) and proposed squalene polymer peaks at -9.83 log(m²/s)

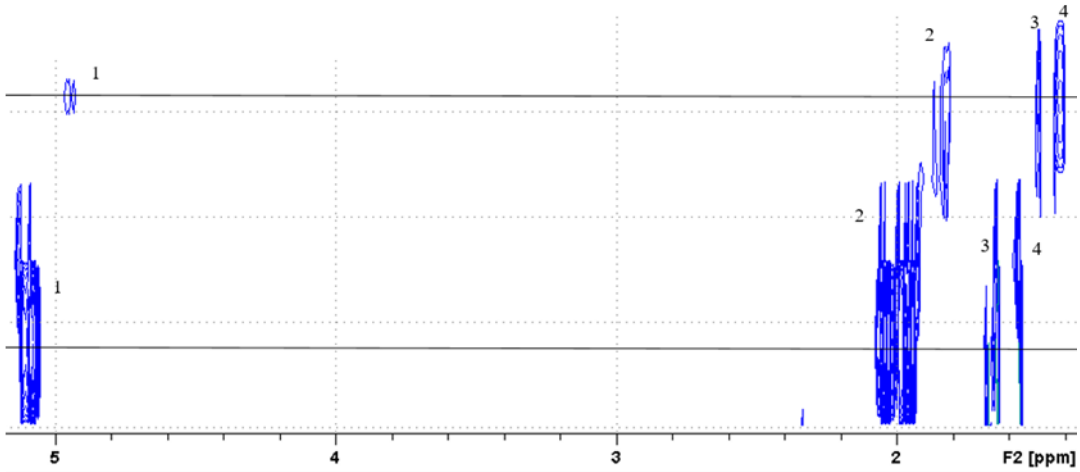

Figure 144 AIBN Squalene and Toluene sample DOSY scan showing two distinct compounds with different diffusion coefficients present in our sample. -9.35 log(m²/s) for squalene and -9.83 log(m²/s) for proposed polymer

6.2.3.2.3 Experiment 3; Photo induction, Benzoyl Peroxide 50mM, run under nitrogen

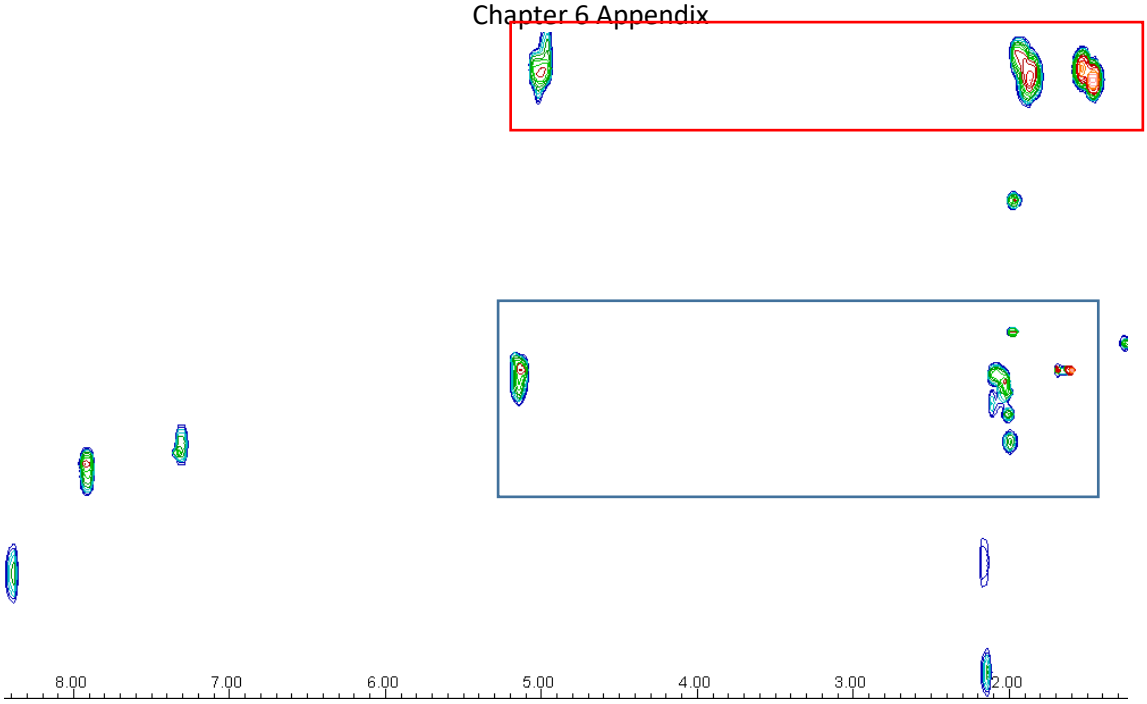

Figure 145 DOSY spectra, analysed in Dynamics centre highlighting the squalene peaks and proposed polymer peaks after 55 mins of UVC exposure on the sample

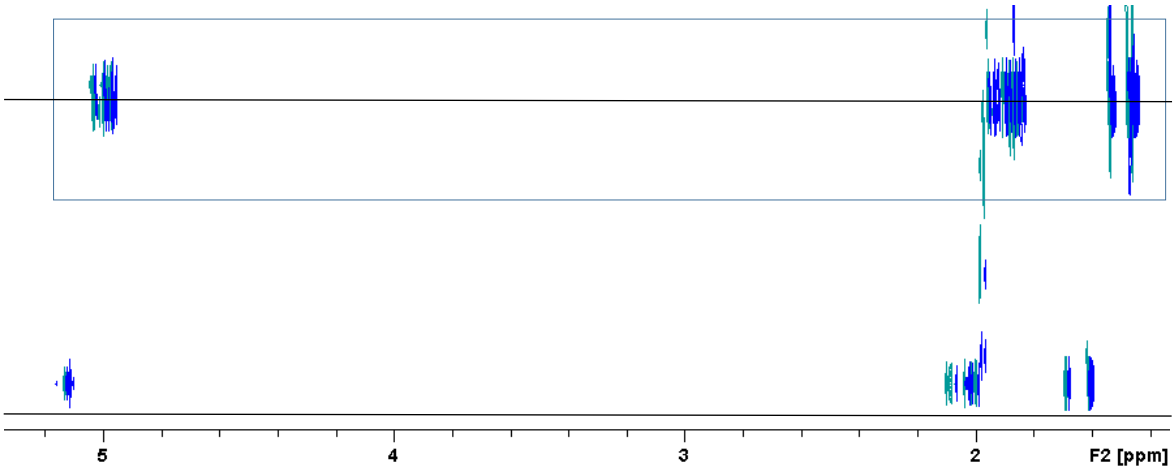

Figure 146 DOSY spectra, analysed in TopSpin highlighting the squalene peaks and proposed polymer peaks after 55 mins of UVC exposure on the sample

Using the software UCC polymer prediction; http://www2.ual.es/NMRMBC automatic calculation of the molecular weight from the calculated diffusion coefficients of our proposed polymer can be done. The calculated value when water was calibrated to was Squalene at a molecular weight of 1992.16 Da and the Squalene oligomer at 22858.18 Da. Determined value when methanol was calibrated to; Squalene 5034.34 Da, Squalene oligomer; 57830.66 Da. This suggests that our oligomer terminates at around 11 monomer units when comparing the ratio of oligomer to monomer unit.

6.2.3.2.4 Assignment and Characterisation of Proposed Polymer

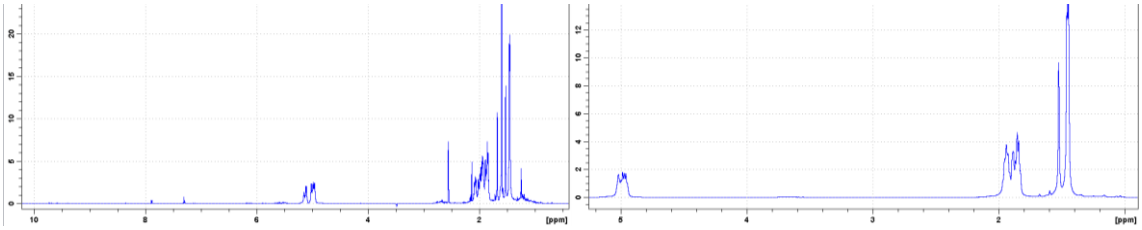

Figure 147 1D Proton of Squalene sample with 50mM Benzoyl Peroxide and 1D Proton with attenuated gradients applied to suppress all peaks apart from polymer peaks in sample

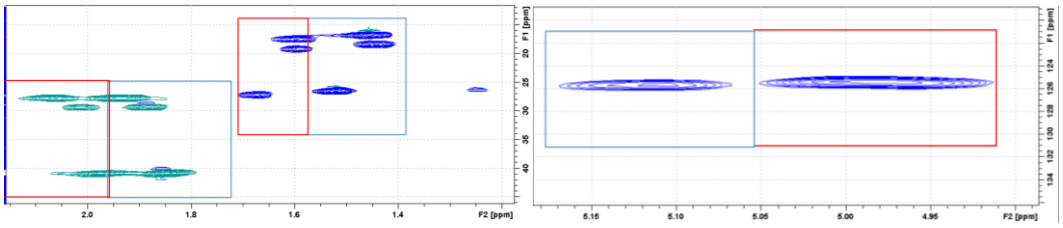

Figure 148 Methyl and CH2's of squalene/oligomer mixture, squalene in red box and proposed oligomer in blue box and Alkene groupsof squalene/oligomer mixture, squalene in red box and proposed oligomer in blue box

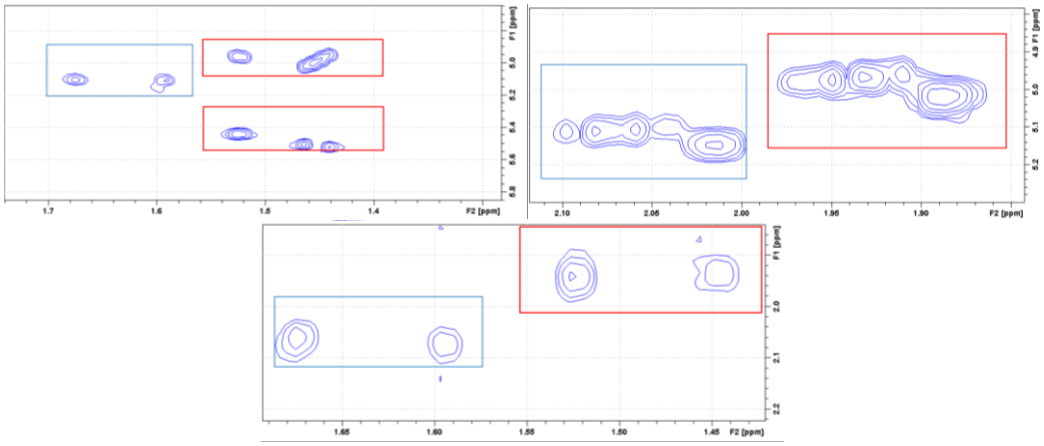

Figure 149 COSY Hydrogen couplings of proposed oligomer shown, shows that the end methyl groups couple to an additional hydrogen environment in the olefin groups which corresponds to our proposed structure. Squalene in blue box and proposed oligomer in red Box. COSY Hydrogen couplings of olefin groups and CH2 chain hydrogens, no observable change in these so this further suggests that the free radical attack occurs at the terminal olefin bonds. Squalene in blue box; proposed oligomer in red box. COSY Hydrogen couplings of terminal methyl groups and chain CH2 hydrogens; showing no new couplings, only the more hydrogenated forms of the same couplings. Squalene in blue box. Proposed oligomer in red box.

6.2.3.2.4.1 PSYCHE

Pure Shift PSYCHE allows us to collapse the multiplicity of peaks and only see the chemical shift of each respective proton; thereby giving the name pure shift. This is useful for mixture analysis and also easier assignment of proton environments as you can see how many protons there are straight away.

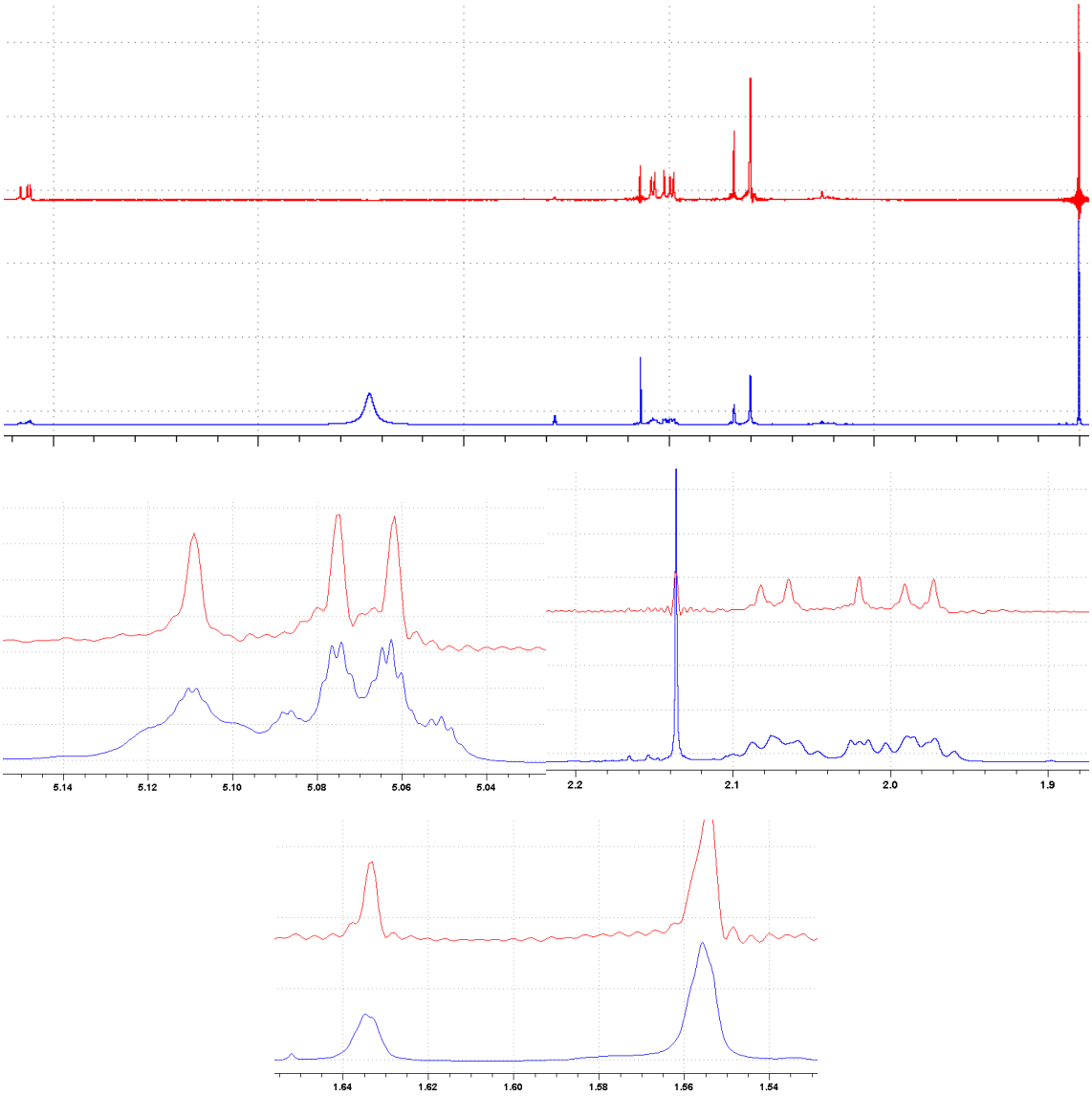

Figure 150 Comparative spectra of squalene with different acquisition methodologies, Red = PSYCHE (with water suppression), Blue = Proton (without water suppression); Whole spectrum of squalene and zoomed in regions

The Olefin and CH2 peaks in the pure shift experiments can easily distinguish the 3 double bond environments present and the 5 CH2 chain environments present within squalene which before with standard proton experiments was very hard to do. This will allow us to determine which of

these environments is being affected by polymerization and give us a greater understanding of the free radical polymerization mechanism.

1D PSYCHE of Squalene and Oligomer mixture

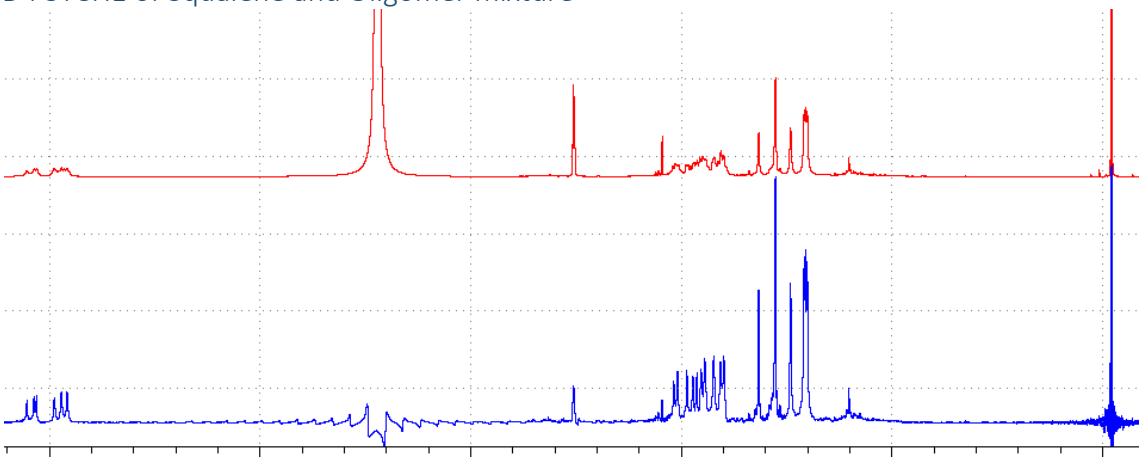

Figure 151 Blue = PSYCHE (with water suppression), Red = Proton (without water suppression); Whole spectrum of squalene and oligomer mixture

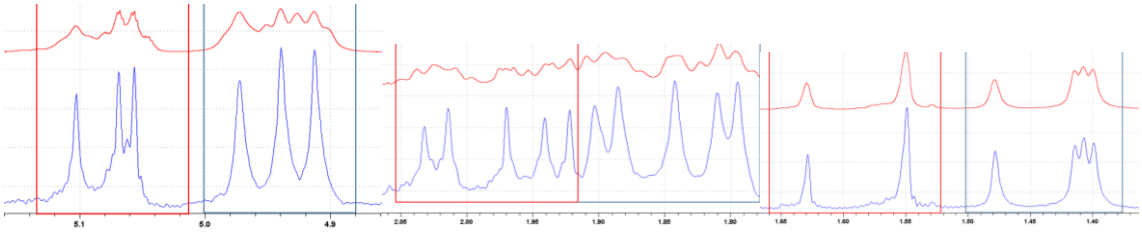

Figure 152 Zoomed in view of squalene peaks (red boxes) and Oligomer (Blue box) for Olefin groups, CH_2 Chain groups and Methyl groups

PSYCHE confirms to us that in the oligomer has three different methyl end group environments rather than being related to splitting; which is coherent with our predicted spectra where methyl groups which are not involved in the free radical polymerization, and two which are present in a monomer that is attached to one or two other monomers. This can also been seen in the HSQC's above.

All the other peaks are equivalent to squalene so propagation must be through retention of the double bonds next to the methyl groups.

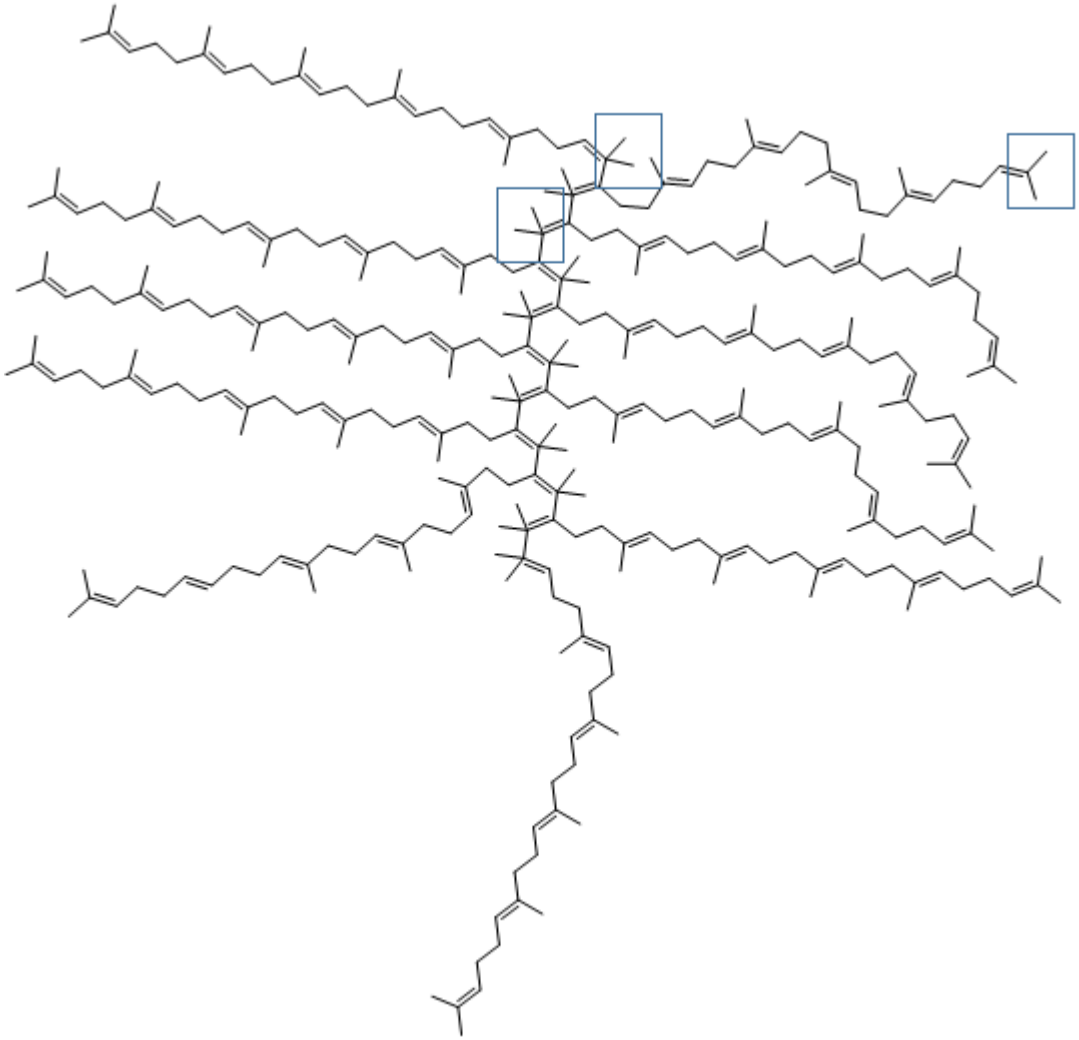

Figure 153 Proposed Squalene Oligomer structure

6.2.3.3 Discussion and conclusion

With initiator (AIBN and Benzoyl Peroxide) concentrations at 50mM, under different experimental conditions, DOSY NMR detects the formation of a molecule with a larger diffusion coefficient.

The new compound has very similiar chemical shifts and coupling as squalene. This insinuates that the nuclei environments of these compounds is very similar to squalene. This suggests from the relationship between diffusion coefficient and molecular weight that compounds are forming that have a greater molecular weight than that of squalene with a very similar structure. The conclusion is that these are most likely oligomers of squalene. The UCC polymer prediction software gives the result of an 11 monomer unit oligomer.

Determining polydispersity of the new compounds becomes more of an issue when looking at the error seen in the diffusion coefficients of the DOSY spectra. In the oxygen excluded experiments

there are two resolved diffusion coefficients present a the diffusion coefficient region of the new compounds. To observe these the contour intensity needs to be measured at a very low signal intensity and is indistinguishable in the other DOSY spectra where it would be expected..

To resolve this issue implementation of PSYCHiDOSY which allows for greater resolution in the F2 dimension through reduction of overlap between peaks; therefore peaks chosen for diffusion analysis are well resolved.

Further DOSY experiments can also be run with more diffusion incremements as a large range in the diffusion coefficents are present within samples. Therefore some compounds in the mixtures will have less accurate diffusion coefficents as there signals are attenuated much faster than others and will have few data points for the fit of the diffusion ccoefficient. 3mm tubes should also be implemented for convection related issues with DOSY results as the larger molecules require shorter D20 times and longer little delta times which in DMSO cause convetion effects to a much greater degree in 5mm tubes but can be greatly reduced in 3mm tubes.

6.3 Experimental

6.3.1 Saturation Transfer Difference Spectroscopy (STD) and STD-TOCSY

Saturation Transfer Difference spectroscopy function through the fact that a weak binding ligand with a binding dissociation constant Kd which range from 10^{-8} mol per litre to Mol per litre. With binding dissociation constants in these range of values exhibits exchange between bound and free states of ligands. The targeted protein or large molecular weight molecule that has large spin diffusing ability, is saturated selectively to produce an on-resonance spectrum through irradiation at a chemical shift region that does not contain resonances for ligand and is exclusively broad protein/large molecule resonance. This on resonance spectrum produces signal intensities labelled Isat which are subsequently subtracted from signal intensities I0 from the recorded off resonance spectrum to produce signal intensities ISTD which produce the difference spectrum. The difference spectrum thus only contains signal intensities which have received saturation transfer from on

resonance protein saturation via spin diffusion through nuclear overhauser effects. Nonbinding small molecules will therefore not experience this nuclear overhauser effect so Isat and I0 intensities will be the same and no peaks will arise. Signal intensities which do arise can then be quantified and gives information on binding and how the small molecule orients itself in the binding pocket of larger molecule/proteins. This means that regions that are closer in proximity to the saturated protein will display larger signal intensities in difference spectra as spin diffusion of saturation is more efficient as nuclear overhauser effects are increase (159).

6.3.2 Syn-Up

6.3.2.1 Sample

For each Physiogel and Syn-Up raw sample, 10mg of sample is dissolved in 660µL of deuterated methanol, spiked with 1mM TSP internal reference and transferred to a 5mm NMR Tube

6.3.2.2 NMR

Quantitative NMR spectra were acquired with 1D 1H NOESY experiments with presaturation applied during the relaxation delay and mixing times. Relaxation time was set to 10s and the number of scans was set to 1024. Automatic processing was done with 2x zero filling of TD, with manual phasing and baseline correction applied.

6.3.3 Synthesis of Deuterated Dodecyl Phosphocholine

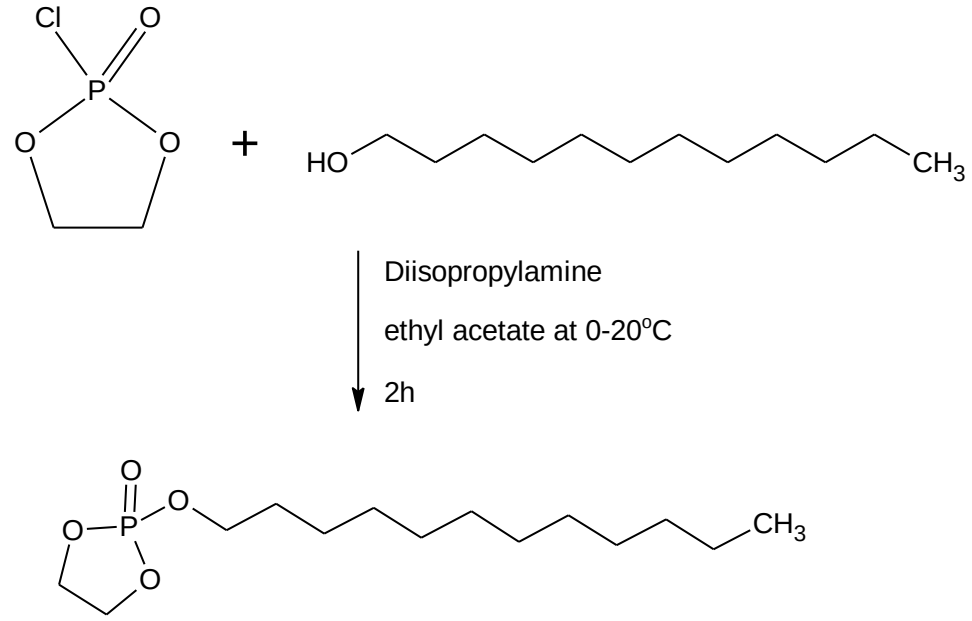

Figure 154 Synthesis step for Dodecylphosphocholine

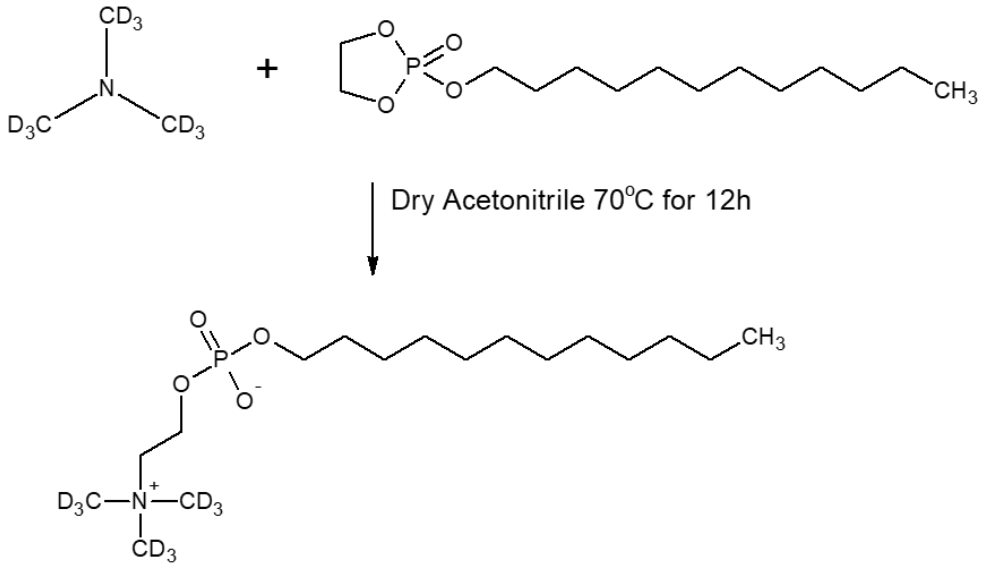

Figure 155 Synthetic pathway for Dodecyl Phosphocholine

6.3.4 Lauric acid Deuteration

These tests were carried out in 20% KOD solution in D_2O 160 ml with palladium Catalyst 10% 2mg, 40ml of NaOD and 10mg anhydride dodecanoic acid stirred for an 8 minute acquisition, broken into two microwave irradiation segments of 4 minutes with additional D_2O/KOD added between

microwave treatments which were set to 40 degrees, microwave power up to 300 watts for 10-30 seconds then down to zero once target temperature was reached for experiment 1 (160). The 2nd and third experiment were carried out in a Parr pressure reactor, instead of a microwave reactor with same sample composition which was loaded into the Parr pressure reactor. The reactor was then degassed by purging with N_2 gas, sealed and heated to 220°C (5 bar) and 250°C (5 bar), for 2nd and 3rd experiment respectively with constant stirring for 3 and 5 days respectively. D_2O was necessary to achieve an efficient H-D exchange, with the rest of the procedure taken from (161)

6.3.5 LL-37 Assignment

6.3.5.1 Samples

LL-37 (human) was purchased from Sigma Aldrich in the lypholised form LL-37 trifluoracetate salt and assayed to >95% by HPLC. Dodecylphosphorylcholine-d_{38} was purchased from Sigma Aldrich with 98 atom % D.

NMR samples were prepared by dissolving LL-37 in an aqueous solution of 10% D2O, 90% H2O) containing 300mM DPC-d_{38} and 20mM phosphate buffer at pH ~3 at a final concentration of 1.5 mM. pH 3 was selected to increase peaks seen in fingerprint region through promotion of NH^+ groups present.

6.3.5.2 NMR

LL-37 and DPC resonances were assigned with COSY,TOCSY and NOESY NMR spectroscopy. 2D STD-TOCSY spectra were recorded with 32 scans. A total of 128 t1 increments were collected in an interlaced mode for the on- and off-resonance spectra. For TOCSY a MLEV-17 spin-lock sequence with a 10 kHz RF field strength and a mixing time of 80 ms was used. Direct Covariance processing was done automatically in TopSpin to give covariance processed spectra with calculation of a square root of covariance matrix (time/freq) (SVD) to increase resolution along the F1 dimension. The selective saturation for STD experiments were targeted at ppm values where respective protein peaks did not overlap ligand peaks ,(30 ppm for off resonance spectra) with 40 Gaussian-shaped pulses (50 ms; 1 ms delay between pulses, $\gamma B1/2\pi$=110 Hz), total saturation time of 4 s.

Enhancement intensity calculation was performed by direct comparison of STD-NMR spectra and reference 1D ^{1}H NMR spectra. The saturated and reference spectra were acquired simultaneously by creating a pseudo-2D experiment. The STD spectra was constructed by subtraction of the saturated spectra from reference spectra performed by phase cycling after manual processing and phasing. The relative STD effect was calculated by (I0−Isat)/I0.

6.4 Appendix References

159. Angulo, J Saturation Ligand-Receptor Binding Affinities from Saturation Transfer Difference (STD) NMR Spectroscopy 2010

160. Miyazawa A, Shimodaira H, Kawanishi Y. Microwave-Assisted Direct H/D Exchange Reactions of Dimetridazole and Metronidazole in Alkaline D2O. Bulletin of the Chemical Society of Japan. 2011 Dec 15;84(12):1368-70.

161. Darwish TA, Luks E, Moraes G, Yepuri NR, Holden PJ, James M. Synthesis of deuterated [D32] oleic acid and its phospholipid derivative [D64] dioleoyl-sn-glycero-3-phosphocholine. Journal of Labelled Compounds and Radiopharmaceuticals. 2013 Jul;56(9-10):520-9.

185. Harner MJ, Frank AO, Fesik SW. Fragment-based drug discovery using NMR spectroscopy. Journal of biomolecular NMR. 2013 Jun 1;56(2):65-75.

186. Lepre CA. Practical aspects of NMR-based fragment screening. InMethods in Enzymology 2011 Jan 1 (Vol. 493, pp. 219-239). Academic Press.

187. Mayer M, Meyer B. Group epitope mapping by saturation transfer difference NMR to identify segments of a ligand in direct contact with a protein receptor. Journal of the American Chemical Society. 2001 Jun 27;123(25):6108-17.

188. Kligman AM, Wheatley VR, Mills OH. Comedogenicity of human sebum. Archives of Dermatology. 1970 Sep 1;102(3):267-75.

189. Oyewole AO, Birch-Machin MA. Sebum, inflammasomes and the skin: current concepts and future perspective. Experimental dermatology. 2015 Sep;24(9):651-4.

190. Motoyoshi K. Enhanced comedo formation in rabbit ear skin by squalene and oleic acid peroxides. British Journal of Dermatology. 1983 Aug;109(2):191-8.

191. Katsuta Y, Iida T, Inomata S, Denda M. Unsaturated fatty acids induce calcium influx into keratinocytes and cause abnormal differentiation of epidermis. Journal of investigative dermatology. 2005 May 1;124(5):1008-13.

192. Mudiyanselage SE, Elsner P, Thiele JJ, Hamburger M. Ultraviolet A induces generation of squalene monohydroperoxide isomers in human sebum and skin surface lipids in vitro and in vivo. Journal of Investigative Dermatology. 2003 Jun 1;120(6):915-22.

193. Ottaviani M, Alestas T, Flori E, Mastrofrancesco A, Zouboulis CC, Picardo M. Peroxidated squalene induces the production of inflammatory mediators in HaCaT keratinocytes: a possible role in acne vulgaris. Journal of investigative dermatology. 2006 Nov 1;126(11):2430-7.

194. Boussouira B, Pham DM. Squalene and skin barrier function: from molecular target to biomarker of environmental exposure. Inskin stress response pathways 2016 (pp. 29-48). Springer, Cham.

6.5 Publications

6.5.1 PSYCHEiDOSY implementation and testing on chemical engineering project

https:/eprints.kingston.ac.uk/id/eprint/43139/

6.5.2 Vitamin D characterisation and quantitation in complex mixtures using novel NMR methodologies

https://eprints.kingston.ac.uk/id/eprint/44416/

6.6 Thesis Supplementary Data

Table 29 BW70 Permeation of topical components

	Niacinamide	Glycerol	Pentylene Glycol	Panthenol	Niacinamide deriv.
1	215.33 ± 2.79	586 ± 6.12	78.26 ± 0.32	82.2 ± 0.65	14.61 ± 0.41
2	145.03 ± 0.83	342.9 ± 0.26	54.73 ± 0.17	55.53 ± 0.076	10.59 ± 0.48
3	156.46 ± 0.57	334.36 ± 6.48	38.53 ± 2.12	47.9 ± 0.46	8.08 ± 0.033
4	57.13 ± 0.79	134.5 ± 1.64	21.5 ± 0.01	20.56 ± 0.65	4.11 ± 0.13
5	44.56 ± 0.14	102.16 ± 1.05	16.6 ± 0.13	14.66 ±0.45	3.5 ± 0.18
6	40.23 ± 0.77	96.5 ± 1.53	17.86 ± 0.80	11.8 ± 0.30	2.78 ± 0.39
7	43.9 ± 0.35	85.1 ± 0.73	17.13 ± 0.16	10.23 ± 0.36	2.98 ± 0.44
8	23.56 ± 0.25	53.1 ± 0.54	12.3 ± 0.2	5.47 ± 0.28	
9	36.6 ± 0.18	71.13 ± 1.02	19.53 ± 0.46	5.86 ± 0.28	
10	23.25 ± 0.035	31.15 ± 0.17	12.65 ± 0.49	4.89 ± 0.039	
11	18.9 ± 0.086	33.63 ± 0.80	11.46 ± 0.25	2.28 ± 0.13	
12	22 ± 0.05	34.53 ± 0.79	12.73 ± 1.02	2.04 ± 0.089	

Table 30 BW Permeation of topical components

	Niacinamide	Glycerol	Pentylene Glycol	Panthenol	Niacinamide deriv.
1	81.53 ± 0.10	936 ± 3.9	19.3 ± 0.30	34.53 ± 0.38	3.84 ±0.018
2	49.73 ± 0.46	119.73 ± 0.40	9.64 ± 0.25	17.26 ± 0.29	2.29 ± 0.24
3	39.7 ± 0.38	100.06 ± 0.41	9.01 ± 0.10	14.7 ± 0.31	2.36 ± 0.23
4	29.86 ± 0.61	73.03 ± 0.53	8.04 ± 0.13	11 ± 0.25	
5	28.7 ± 0.18	61.7 ± 0.58	6.16 ± 0.18	7.78 ± 0.21	
6	28.16 ± 0.80	67.66 ± 1.05	8.58 ± 0.26	7.81 ± 0.17	
7	26.4 ± 0.05	54.96 ± 0.11	7.76 ± 0.16	7.19 ± 0.19	
8	21 ± 0.15	43.43 ± 0.8	6.67 ± 0.24	3.37 ± 0.12	
9	22.56 ± 0.10	36.8 ± 0.76	6.27 ± 0.32	2.37 ± 0.21	
10	23.33 ± 0.19	46.46 ± 0.74	9.28 ± 0.36	2.27 ± 0.14	
11	11.93 ± 0.21	23.86 ± 0.41	6.2 ± 0.22	1.43 ± 0.13	
12	21.46 ± 0.13	32.7 ± 0.28	7.31 ±0.20	2.17 ±0.085	

Table 31 V Permeation of Topical Components

	Niacinamide	Glycerol	Pentylene Glycol	Panthenol	Niacinamide deriv.
1	64.9 ± 0.65	115.5 ± 0.15	24.23 ± 0.14	19.96 ± 0.076	4.69 ± 0.25
2	39.96 ± 0.16	214.4 ±0.25	15.26 ± 0.28	12.53 ± 0.53	3.50 ± 0.16
3	36.9 ± 0.34	68.56 ± 1.01	12.73 ± 0.076	10.40 ± 0.39	1.43 ± 0.15
4	38.6 ± 1.12	53.13 ± 0.45	11.3 ± 0.67	7.11 ± 0.69	
5	21.96 ± 0.28	28.76 ± 0.16	8.46 ± 0.26	6.19 ± 0.56	
6	35.2 ± 0.73	50.56 ± 0.43	14.2 ± 0.05	6.18 ± 0.17	
7	19.76 ± 0.33	25 ± 0.77	8.04 ± 0.03	2.20 ± 0.18	
8	18.43 ± 0.26	23.66 ± 0.25	8.23 ± 0.36	1.37 ± 0.072	
9	20.5 ± 0.39	25.2 ± 0.75	8.64 ± 0.24	1.59 ± 0.07	
10	17.26 ± 0.33	22.1 ± 0.3	8.4 ± 0.085	1.51 ± 0.22	
11	20.9 ± 0.13	24.16 ± 0.45	9.2 ± 0.52	1.22 ± 0.083	

12	11.76 ± 0.26	14.9 ± 0.13	5.14 ± 0.09	1.03 ± 0.056

Table 32 P Permeation of Topical components

	Glycerol
1	743.63 ± 5.62
2	141.06 ± 0.45
3	173.13 ± 0.35
4	129.06 ± 0.39
5	72.26 ± 0.20
6	81.23 ± 0.35
7	85.96 ± 0.93
8	125.6 ± 0.28
9	47.7 ± 0.48
10	89.36 ± 0.25
11	21.76 ± 0.10
12	45.13 ± 1.20

Table 33 AI Permeation of Topical Components

	Glycerol	Pentylene Glycol
1	630.23 ± 3.52	33.56 ± 0.076
2	178.86 ± 0.68	11.46 ± 0.12
3	114.7± 0.86	7.95 ± 0.10
4	24.66 ± 0.28	2.15 ± 0.26
5	69.33 ± 0.64	8.96 ± 0.49
6	78.43 ± 0.71	11.26 ± 0.27
7	45.96 ± 0.37	8.87 ± 0.13
8	26.73 ± 0.21	3.33 ± 0.030
9	24.46 ± 0.10	3.81 ± 0.47
10	15.83 ± 0.076	7.15 ± 0.37
11	17.56 ± 0.15	3.64 ± 0.26
12	24.56 ± 0.076	5.12 ± 0.18

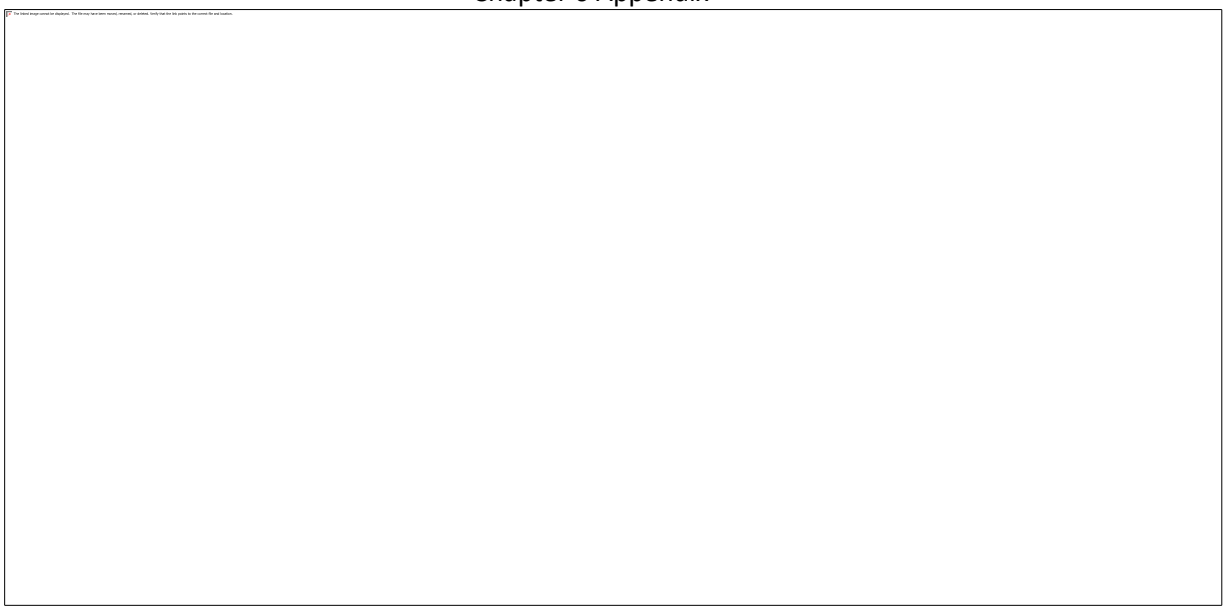

Figure 156 Grouped Bluewater formulation permeation profile data PCA scores plot with PC1 (96%) against PC2 (3%)

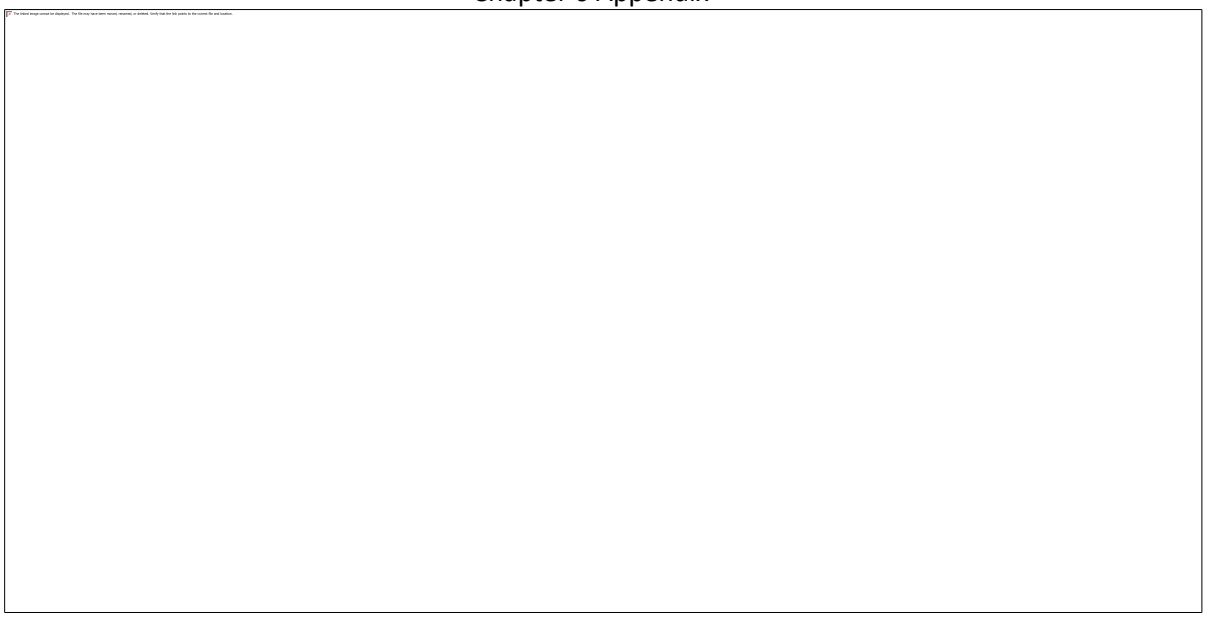

Figure 157 Grouped Bluewater formulation permeation profile data PCA correlation loadings with PC1 (96%) against PC2 (3%)

Figure 158 Grouped BW formulation permeation profile data PCA scores plot with PC1 (96%) against PC2 (7%)

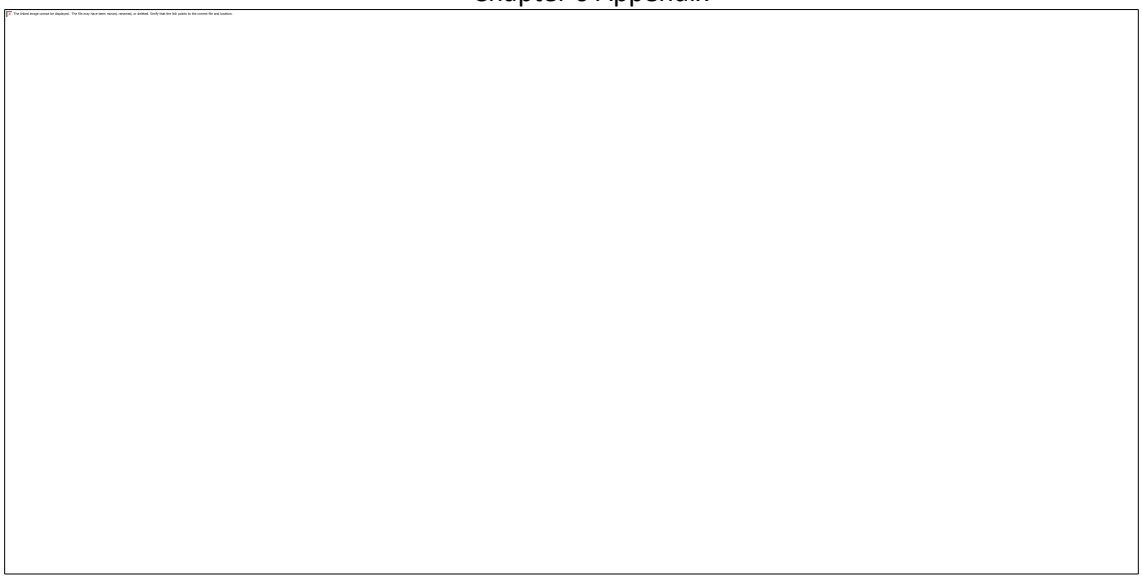

Figure 159 Grouped BW formulation permeation profile data PCA correlation loadings with PC1 (91%) against PC2 (7%)

Figure 160 Grouped BW70 formulation permeation profile data PCA SCORES PLOT with PC1 (89%) against PC2 (8%)

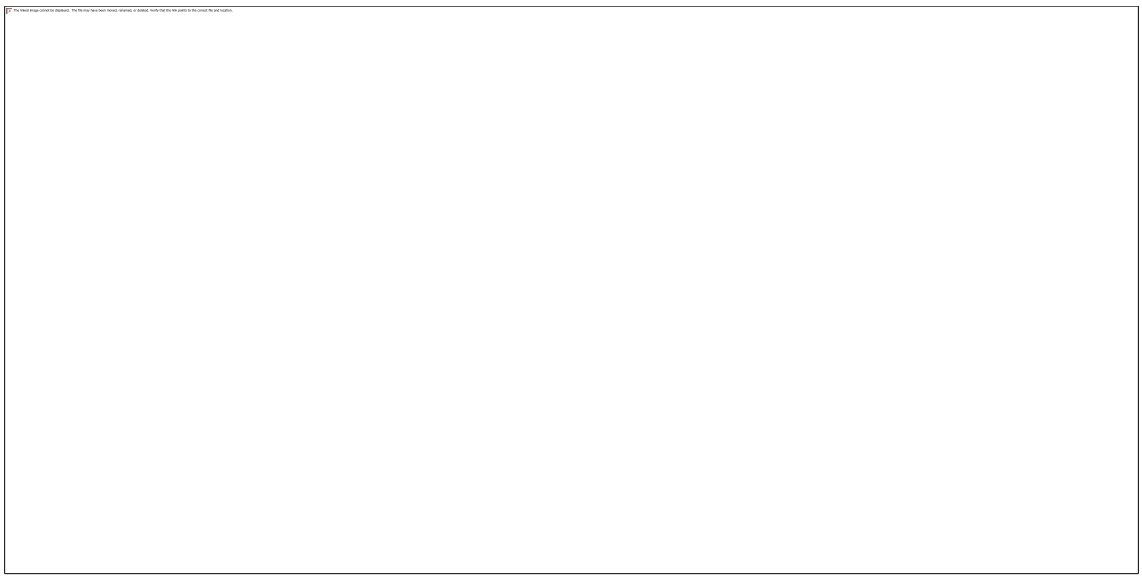

Figure 161 Grouped BW70 formulation permeation profile data PCA correlation loadings with PC1 (89%) against PC2 (8%)

Figure 162 Grouped V formulation permeation profile data PCA scores plot with PC1 (93%) against PC2 (6%)

Figure 163 Grouped V formulation permeation profile data PCA correlation loadings with PC1 (93%) against PC2 (6%)

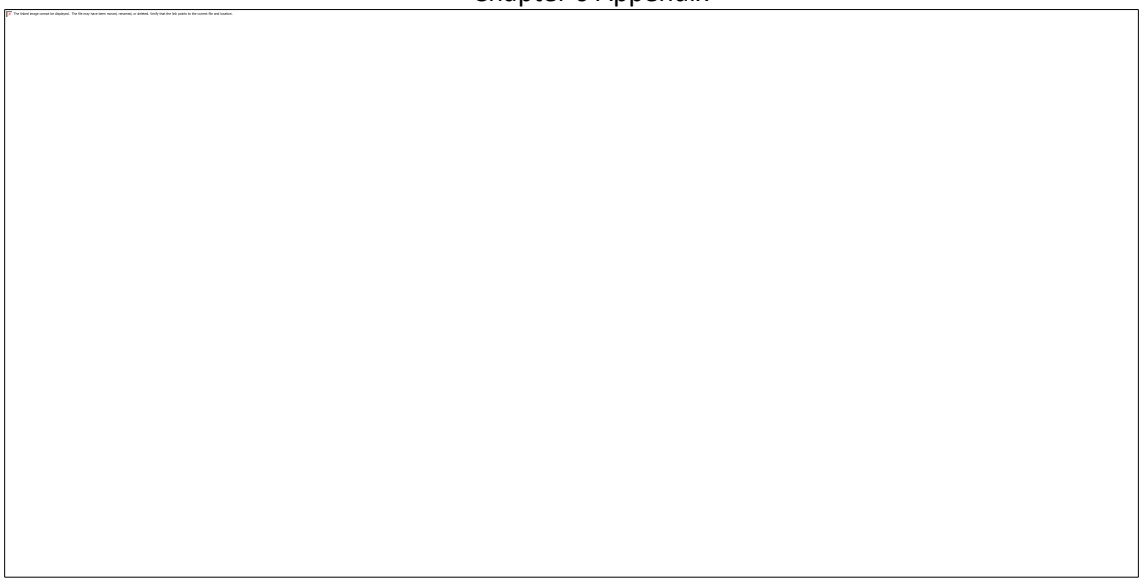

Figure 164 Grouped Bluewater and AI formulations permeation profile data PCA scores plot with PC1 (100%) against PC2 (0%)

Figure 165 Grouped Bluewater and AI formulations permeation profile data PCA correlation loadings with PC1 (100%) against PC2 (0%)

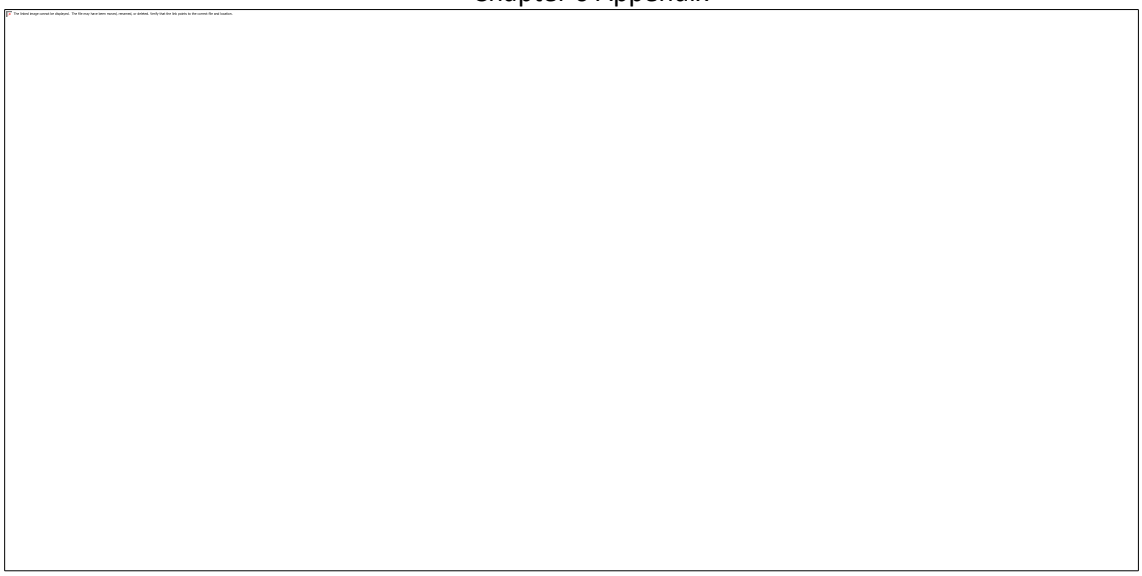

Figure 166 Grouped Bluewater formulations permeation profile and NMF data PCA scores plot with PC1 (93%) against PC2 (6%)

Figure 167 Grouped Bluewater formulations permeation profile and NMF data PCA correlation loadings with PC1 (93%) against PC2 (6%)

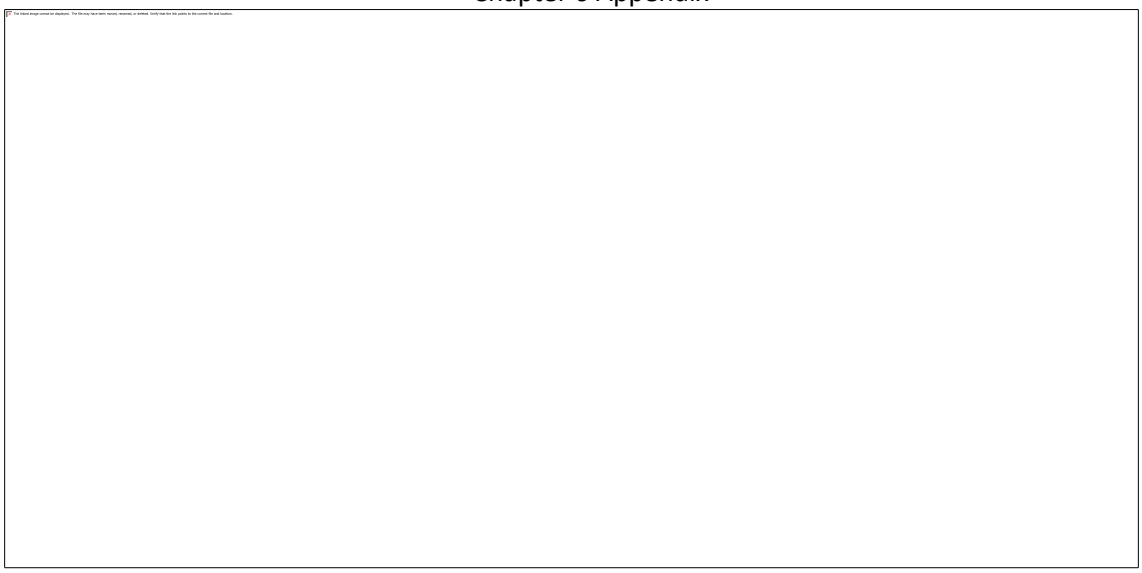

Figure 168 Grouped Physiogel formulations permeation profile and NMF data PCA scores plot with PC1 (99%) against PC2 (0%)

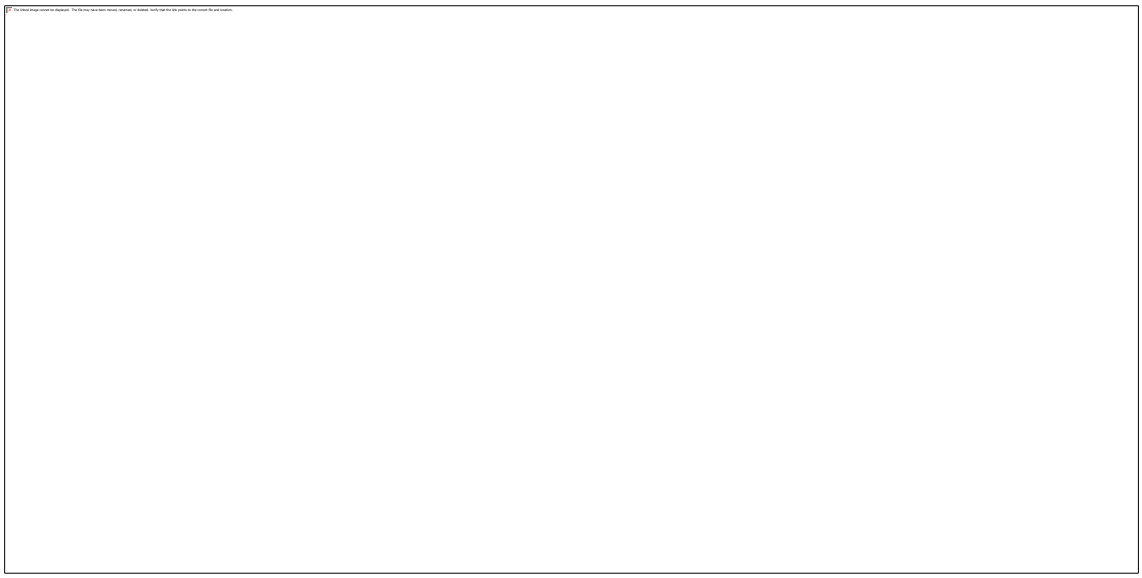

Figure 169 Grouped Physiogel formulations permeation profile and NMF data PCA correlation loadings with PC1 (99%) against PC2 (0%)